Politecnico di Milano

Ph.D. Dissertation

Department of Architecture, Built environment and Construction engineering (DABC)

VIBRATION-BASED STRUCTURAL HEALTH MONITORING OF CIVIL ENGINEERING STRUCTURES: AUTOMATED OPERATIONAL MODAL ANALYSIS AND DAMAGE DETECTION

Gabriele Marrongelli

– 2020 –

“Non è importante quanto vivi, ma come vivi”

N. Toffa

Ad Angelo

che la grinta e l’audacia ti siano sempre amiche e compagne di viaggio
per costruire un futuro ricco di traguardi e soddisfazioni

ABSTRACT

The continuous aging of important and strategic infrastructures that has severely affected the Italian Transport System during the last years and the structural degradation of many historical Italian buildings highlights the need for an adequate strategic plan for the maintenance of the structural integrity of civil structures and the preservation of monumental buildings in our country. In the last decades, these aspects have gained great relevance in Italy because the seismic hazard that adds to the normal deterioration of constructions and makes more difficult the protection and preservation of both modern structures and ancient buildings.

In the last twenty years, many efforts have been made to find appropriate solutions to these issues and an increased interest has been manifested by designers and owners of structures on dynamic tests and vibration–based Structural Health Monitoring (SHM) projects aimed at enhancing the safety of old and new complex constructions. Many efforts have been made to merge available technologies with efficient methodologies and to encourage the development of automatic tools to prevent the occurrence of catastrophic events, especially for those constructions subjected to high seismic risk. In the last years, the efforts in this field have intensified remarkably providing good improvements in the development and application of several techniques mainly devoted to obtaining information about monitored structures in *operational conditions*.

The structural assessment of each investigated system starts with a dynamic test performed to extract the modal parameters (i.e. natural frequencies, mode shapes and modal damping ratios) from the output response collected during the in-service condition and under ambient excitation without measuring the input source. This strategy is defined Operational Modal Analysis (OMA) and implies the use of different techniques to analyze signals recorded during single tests as well as in continuous dynamic monitoring, involving efficient algorithms able to manage and handle a large amount of data and, from them, to extract those meaningful features that are going to be monitored. This task

is not always straightforward, and some calibrations have to be made to clearly obtain the evolution of modal parameters over time.

This work focuses firstly on the implementation of various state-of-the-art algorithms for modal identification. Specifically, two methods in the frequency domain (PP and FDD) and two parametric methods in the time domain (SSI-Cov and SSI-Data) were implemented. Since the parametric techniques are suitable to be automated due to their algebraic nature, they have been adopted in the development of automated tools for OMA purposes. It is worth noting that in OMA applications a lot of time is usually spent on manual analyses, necessary to tune the input parameters implying relevant user interaction. This is in clear contrast with the purposes of permanent dynamic monitoring, which require complete automation. Conversely, the removal of human intervention in OMA methods is still one challenging in this research field.

Accordingly, this Thesis is devoted to providing an improvement in the development of automated tools. Specifically, a first strategy for Modal Parameter Estimation (MPE) based on the interpretation of the stabilization diagrams was implemented with the aim of providing a well-founded array of modal estimates from single test data. The algorithm involves three consecutive sub-routines aimed at: a) removing most of the spurious poles, b) performing the clustering approach and c) improving the accuracy of modal parameters, reducing the uncertainty of the obtained estimates. The efficiency of the presented algorithm was proven using dynamic tests data of a lively footbridge and an ancient masonry bridge. Afterwards, an alternative MPE algorithm based on the construction and the automated interpretation of tri-dimensional stabilization diagrams was developed. The validation of this algorithm was demonstrated with the extraction of the structural modes and the subsequent analysis of short monitoring period of important outstanding infrastructures: the *Infante D. Henrique bridge* in Portugal and the *San Michele bridge* in Italy.

As stated, in the context of vibration-based SHM it is mandatory to develop efficient and robust tools to perform the on-line and automatic processing of large amounts of collected

data, avoiding any user interaction. Hence, in order to complete the implementation of a robust OMA methodology, capable of automatically providing the evolution in time of the monitored features, a new Modal Tracking (MT) procedure was developed and then integrated with both MPE algorithms previously described. In particular, the implemented tool is able to follow the seasonal fluctuations and unexpected variations of the modal features due to extreme environmental conditions. The validation of the tool in the monitoring of two important Italian Cultural Heritage structures (the *Gabbia Tower* in Mantua and the *San Michele bridge*) was proven with excellent results.

Since the structural degradation or the occurrence of damage is often associated with a reduction of the global stiffness in the structure and with a subsequent decrease in frequency values, an accurate characterization of the modal parameters variations (especially natural frequencies) can be a robust way to detect structural problems. Despite this, in the classical SHM approach, damage identification is not always easy because the extracted modal estimates are subject to the effects of environmental factors, which could mask the damage. Therefore, the modal estimates are normally post-processed by routines that minimize the effects of external factors (frequently on the natural frequencies) in order to obtain results that might depend only on structural conditions. This task is performed by applying multivariate regression models and/or principal component analysis models, which should be established using the time evolution of the features under a significant range of variation of environmental and operational factors requiring a long period of training.

The SHM approach developed herein discards the classical approach and performs the structural assessment using the identified modal parameters without removing the external effects on them. The removal of this relevant key-step from the methodology creates a clear distinction between the classical approach and the alternative OMA-based SHM strategy. Thus, a novelty damage detection approach was developed to identify possible structural anomalies thought slight frequency shifts and it was developed with two different strategies, based on: a) the Continuous Segment Analysis (CSA) strategy, defining the undamaged and damaged state of the system with two consecutive segments

of data, and b) the Separate Segment Analysis (SSA) strategy, based on a reference segment of data used as undamaged condition. The validation of the damage strategy was demonstrated using experimental data collected during a seven-month of monitoring of the *Gabbia Tower*. During the monitoring period, the tower was subjected to a far-field earthquake that slightly damaged the structure. The occurred damage was clearly identified by the application of the novelty strategy.

The present work is completed with the application of all implemented algorithms in the continuous assessment of the *San Gottardo bell-tower*. The OMA algorithms were used to perform the continuous identification of the structural modes and the continuous assessment of the tower demonstrating its structural integrity for over two years of monitoring. Furthermore, some damages were simulated to test the sensitivity of the alternative SHM approach in the identification of small damages providing evidence of its usefulness and robustness.

Keywords

Structural Health Monitoring; Operational Modal Analysis; Automated OMA; Continuous Dynamic Monitoring; Modal Parameter Estimation; Modal Tracking; Damage Detection, Masonry Towers, Bridges; Support Vector Machine.

SOMMARIO

L’invecchiamento continuo di importanti strutture strategiche che ha gravemente colpito il sistema dei trasporti italiano negli ultimi anni ed il costante degrado strutturale degli edifici storici mettono in evidenza il bisogno di avere un adeguato piano strategico cha sia finalizzato al mantenimento dell'integrità strutturale delle costruzioni civili ma anche alla conservazione di edifici monumentali del nostro paese. Negli ultimi decenni, questi aspetti hanno acquisito grande rilevanza in Italia, anche a causa della pericolosità sismica del nostro territorio che si aggiunge al normale deterioramento delle costruzioni e rende più difficile la protezione e la conservazione di strutture moderne ed edifici storici.

Negli ultimi vent'anni, sono stati fatti molti sforzi per trovare soluzioni appropriate a questi problemi e un crescente interesse è stato manifestato da progettisti e gestori di strutture riguardo test dinamici e progetti di *Structural Health Monitoring* (SHM) basati su misure di vibrazioni volti a migliorare la sicurezza sia delle costruzioni preesistenti che di quelle più moderne e complesse. Molti progressi sono stati fatti per connettere tra loro le attuali tecnologie con metodologie di analisi sempre più efficaci e per incoraggiare lo sviluppo di strumenti automatizzati per prevenire il verificarsi di eventi catastrofici, specialmente in quelle costruzioni soggette ad alto rischio sismico. Negli ultimi anni, gli sforzi in questo campo si sono intensificati notevolmente favorendo lo sviluppo e l'applicazione di diverse tecniche principalmente orientate al monitoraggio continuo di strutture in *condizioni operative*.

La valutazione strutturale di ogni sistema inizia con un test dinamico che viene eseguito con il fine di estrarre i parametri modali (frequenze naturali, forme modali e coefficienti di smorzamento modale) analizzando direttamente la risposta strutturale raccolta durante le condizioni di servizio, senza dover misurare la sorgente di ingresso e l’eccitazione ambientale. Questa strategia è definita *Operational Modal Analysis* (OMA) ed è eseguita con l’ausilio di diverse tecniche che coinvolgono efficienti algoritmi in grado di gestire grandi quantità di dati, registrati sia durante singole prove che in contesti di monitoraggio continuo, e da essi estrarre le caratteristiche dinamiche più significative da monitorare.

Questo compito non è sempre semplice e l'utilizzo di queste tecniche richiede una elevata esperienza anche per eseguire corrette calibrazioni iniziale ed ottenere una evoluzione significativa dei parametri dinamici nel tempo.

Il lavoro presentato in questa tesi si concentra in primo luogo sull'implementazione di vari algoritmi allo stato dell'arte finalizzati all'identificazione modale. Nello specifico, sono stati implementati due metodi nel dominio della frequenza (PP e FDD) e due metodi parametrici nel dominio del tempo (SSI-Cov e SSI-Data). Poiché le tecniche parametriche sono più adatte all'automazione a causa della loro natura algebrica, esse sono state adottate nello sviluppo di procedure automatiche per scopi OMA. Vale la pena ricordare che normalmente nelle applicazioni OMA viene dedicato molto alle analisi manuali che implicano una rilevante interazione dell'utente soprattutto nelle fasi di tuning per l'ottimizzazione dei parametri di input. Ciò è in netto contrasto con gli scopi del monitoraggio dinamico permanente, che invece richiede un'automazione completa del processo. Al contrario, la rimozione dell'intervento umano nei metodi OMA è ancora una sfida in questo campo di ricerca.

Cosicché questa tesi è principalmente dedicata a fornire un contributo nello sviluppo di strumenti automatizzati per l'identificazione ed il monitoraggio strutturale. In particolare, è stata implementata una prima strategia per la stima dei parametri modali (MPE) basata sull'interpretazione di diagrammi di stabilizzazione con l'obiettivo principale di eseguire l'identificazione di un set consistente di stime modali dall'analisi di singoli test dinamici. L'algoritmo prevede l'uso di tre procedure consecutive volte a: a) rimuovere il maggior numero di poli spuri, b) eseguire un clustering delle stime e c) migliorare l'accuratezza dei parametri modali, riducendo l'incertezza delle stime ottenute. L'efficienza di questo algoritmo è stata dimostrata utilizzando dati di test dinamici di una passerella pedonale ed un ponte in muratura. Successivamente, è stato sviluppato un algoritmo MPE alternativo basato sulla costruzione e sull'interpretazione automatica di diagrammi di stabilizzazione tridimensionali. La validazione di questo secondo algoritmo è stata eseguita attraverso l'estrazione dei parametri strutturali e la successiva analisi di un breve periodo di

monitoraggio di due importanti infrastrutture: il ponte *Infante D. Henrique* in Portogallo ed il ponte *San Michele* in Italia.

Come precedentemente dichiarato, nel contesto del monitoraggio strutturale è necessario sviluppare efficienti e robusti strumenti per eseguire l'elaborazione online e automatica di grandi quantità di dati, evitando qualsiasi interazione dell'utente. Quindi, con il fine di completare l'implementazione di una solida metodologia OMA, in grado di fornire un'accurata evoluzione dei parametri monitorati nel tempo, è stata sviluppata una nuova procedura di *Modal Tracking* (MT) da usare in maniera integrata con entrambi gli algoritmi di identificazione MPE precedentemente descritti. In particolare, la procedura implementata è in grado di tracciare sia le fluttuazioni stagionali che le improvvise variazioni dei parametri modali che possono verificarsi in condizioni ambientali estreme. La validazione di questo strumento è stata dimostrata attraverso il monitoraggio di due importanti strutture che appartengono al patrimonio culturale italiano (la *Torre della Gabbia* a Mantova ed il ponte di *San Michele*) ottenendo ottimi risultati.

Poiché il degrado strutturale o l'insorgenza di un danno è spesso associato a una riduzione della rigidezza globale nella struttura e ad una conseguente diminuzione dei valori di frequenza, un'accurata caratterizzazione delle variazioni dei parametri modali (in particolare delle frequenze naturali) può essere un approccio robusto nell'identificazione di problemi strutturali. Nonostante ciò, nel classico approccio SHM, l'identificazione del danno non è sempre facile perché le stime modali sono soggette agli effetti dei fattori ambientali, che potrebbero mascherare l'occorrenza del danno. Pertanto, le stime modali sono normalmente "post-processate" con routine che riducono al minimo gli effetti di fattori esterni (spesso sulle frequenze naturali) al fine di ottenere risultati che dovrebbero essere dipendenti dalle sole condizioni strutturali. Questo compito viene eseguito applicando modelli di regressione multivariata e/o modelli di analisi delle componenti principali, che dovrebbero essere stabiliti utilizzando l'evoluzione temporale dei parametri modali all'interno di un intervallo significativo di variazione dei fattori ambientali e operativi, richiedendo un lungo periodo di training.

L'approccio SHM qui sviluppato scardina quello che viene definito approccio classico ed esegue la valutazione strutturale utilizzando i parametri modali identificati senza rimuovere gli effetti ambientali esterni. La rimozione di questo importante passaggio chiave dalla metodologia crea una chiara distinzione tra l'approccio classico e la strategia SHM alternativa basata sui parametri OMA. Pertanto, è stato sviluppato un nuovo approccio di *damage detection* per identificare possibili anomalie strutturali attraverso piccole variazioni di frequenza, questo approccio è stato sviluppato con due diverse strategie: a) la strategia CSA (*Continuous Segment Analysis*), che definisce lo stato del sistema non danneggiato e quello danneggiato con due segmenti consecutivi di dati e b) la strategia SSA (*Separate Segment Analysis*), basata su un segmento di dati di riferimento fisso utilizzato per definire la condizione non danneggiata. La validazione della strategia di *damage detection* è stata dimostrata analizzando i dati sperimentali raccolti durante sette mesi di monitoraggio permanente della *Torre della Gabbia*. Durante il periodo di monitoraggio, la torre ha risentito dell'effetto di un lontano terremoto che danneggiò leggermente la struttura. Il danno è stato chiaramente identificato dall'applicazione della *novelty strategy*.

Il presente lavoro si completa con l'applicazione di tutti gli algoritmi implementati nella verifica continua del benessere strutturale della torre campanaria del *San Gottardo*. Gli algoritmi OMA sono stati utilizzati sia per eseguire l'identificazione dei modi e sia per la verifica strutturale della torre dimostrando la sua integrità strutturale per oltre due anni di monitoraggio. Infine, danni strutturali sono stati simulati per effettuare una analisi di sensitività della nuova metodologia nell'identificazione di piccoli danni, a dimostrazione della sua utilità e robustezza.

ACKNOWLEDGMENTS

I present here my sincere gratitude to all who have accompanied me during my PhD journey, family, friends and colleagues that, through their friendship and support, contributed to the achievement of this work.

In particular, I wish to sincerely express my special thanks and gratitude to:

- Professor Carmelo Gentile, for providing all the necessary resources, motivation and suggestions regarding the development of this Dissertation, for his important support concerning the practical applications of the case studies in my research, for his invaluable patience, for encouraging me to participate in important international conferences, for the numerous reviews of this thesis and, most importantly, for the total willingness to support, motivate and guide me throughout my research career;

- Professor Filipe Magalhães, from FEUP (Portugal), for sharing his experience and knowledge, for his important support concerning the application of my work to the Infante D. Henrique Bridge, for our productive discussions held during important conferences and for the interesting suggestions and advice received during all our meetings;

- Professor Alvaro Cunha, from FEUP (Portugal), for inviting me to participate in international conferences, for the motivation and numerous encouragements that he conveyed during our meetings;

- Professor Guido Barbosa, from UFJF (Brazil), for receiving me into his research group for four months, for his hospitality and the generous insights he gave me in the area of artificial intelligence;

- Professor Antonino Morassi and Professor Francesco Clementi, for their support in the review of the final draft of this Dissertation and for their important suggestions allowing me to highlight the main original contributions developed during my PhD career;

- Doctor Elisa Bertolesi, for her great support during my PhD career, for helping me find my enthusiasm during times of intense work and for sharing several interesting ideas during the preparation of this Dissertation;

- Mauro Minutilla, for his great fellowship and understanding, very essential in moments of intense work, and for giving me encouragement and valid points of view about my research perspectives and future;

- Vladimir Moldovan-Coracu, for helping me with the final draft of the thesis, for giving me special advice on my Dissertation and for the very good times we shared in the process of achieving one of the most important goals of my life;

- my best friend Francesco, for sharing a good and sincere friendship, for the laughter and silliness and for helping me take the edge off work;

- my work colleagues Gessica, Silvia, Paolo, Antonello, Zehra, Elisa, Giacomo, Alfredo and all the others, for always being there to help me balance periods of hard work with moments of relaxation during breaks, lunches and extra-curricular activities;

- my friends, including Gian, Filippo, Roberto, Umberto, Alessandro, Carlo, Michele, Salvatore, Marco, Paolo, Daniele, Massimo and all the others, for putting up with me during these years, for their friendship, the delicious meals and the nights of fun we enjoyed together;

- my family, for supporting me during this amazing journey.

CONTENTS

Chapter 1

INTRODUCTION AND ORGANIZATION OF THE THESIS

Contents

1.1 Research context

The catastrophic events that severely affected the Italian transport system during the last year together with the general and widespread uncertainty regarding the vulnerability of ancient historic structures and strategic infrastructures highlighted the need to ascertain the structural conditions and the actual state of preservation of many constructions in our country. Furthermore, the continuous aging and the structural degradation of many ancient buildings in our country emphasizes the need for continuous assessment strategies to preserve the safety condition of such important constructions.

In the last twenty years, many efforts have been made to find appropriate solutions to these issues, which contributed to the significant increase in support and interest manifested by designers and owners regarding dynamic tests and vibration–based Structural Health Monitoring (SHM) projects. This need can be satisfied with the use of several resources aimed at linking engineering skills to the built environment in order to capitalize on the cultural aspects and to enhance the safety of old and new constructions with high level of complexity. In this way, the structural condition can be defined by adopting actual available technologies together with efficient methodologies, in order to prevent the occurrence of catastrophic events.

In the last decades, the efforts in this field have grown remarkably providing good improvements in the development and application of several techniques mainly devoted to obtaining important information about monitored constructions in so-called *operational conditions*.

As is well known, the assessment of the structural condition of each investigated system should start by performing a dynamic test and recording its response, subjected to environmental loads (also defined as response in operational condition) or under different load-scenarios to which the structure is generally subjected during its life-cycle.

In this context, dynamic tests are usually adopted to perform the identification of modal parameters (i.e. natural frequencies, mode shapes and modal damping ratios) of relevant

modes of vibration of the investigated structure but also to characterize the vibration amplitude associated with normal operational conditions or motivated by recreated load scenarios, as for instance tests done on footbridges with crowds trained to walk with a predefined pacing rate or controlled train passages on railway bridges.

The identification of the modal parameters based on experimental data can be classified in two categories: the Forced Vibration Tests (FVT), in which the extraction of the modal parameters is normally performed by adopting controlled excitations and using specific instrumentation (e.g. hammer test in order to define the modal parameter during laboratory tests on small scaled prototypes, or vibrations induced by big shakers, that are used to provide the input excitation for full-scale tests performed on large buildings or on infrastructures). Meanwhile, when the civil engineering structures are tested under environmental and traffic loads, over or nearby the structures, and the modal parameters are extracted using the structural dynamic response under ambient excitation without measuring the input source, this kind of tests are designed as Ambient Vibration Tests (AVT). Furthermore, as ambient excitation is always present in the collected signals, the techniques used to analyze data recorded during a single test can also be adopted for the continuous processing of data series acquired by monitoring systems in the context of continuous dynamic monitoring. The application of these techniques implies the development of efficient algorithms and procedures able to manage and handle a large amount of data and, from them, to extract those meaningful features that are to be monitored. This task is not always straightforward. Moreover, these techniques must provide a correct tracking of the reference features so as to clearly identify the evolution of modal parameters over time.

Since the structural degradation or the occurrence of damage is often associated with a reduction of the global stiffness in the structure and with a subsequent decrease in frequency values, an accurate characterization of the modal parameters variations (especially natural frequencies) can be a straightforward way to detect structural problems. Moreover, a gradual loss of structural properties can also be identified by performing a monitoring of the modal shapes associated with the structural modes. In

fact, the mode shapes can be adopted as reference parameters to identify the occurrence of structural anomalies and, consequently, also to define which part of the structure is affected. In both applications, dynamic tests and health monitoring systems, a crucial step is the accurate identification of modal parameters from measured structural responses. This strategy is defined as the Operational Modal Analysis (OMA) approach and it is performed by using several alternative techniques developed during the last decades.

Despite this observed progress, the OMA methods are still dependent upon strong interaction with expert user in the initial tuning of data inputs as well as during the continuous monitoring process. Nowadays, the removal of human intervention in the definition of the boundary thresholds to make the identification analysis fully automated is still one of the most challenging tasks in this research field.

At this moment, standard algorithms already implemented in commercial software preserve some manual selections of input parameters that have always required an expert user's judgement. These choices make the analysis of data very time-consuming during the very initial phase and they give an implicit uncertainty about the results, which always depend on user sensitivity. On the other hand, the lack of automation in the analysis processing does not allow solving the problem related to the continuous identification of the dynamic parameters. In fact, this issue is particularly evident in the context of developing vibration-based health monitoring systems, where it is mandatory to develop efficient and robust routines to perform an on-line and automatic processing of large amounts of collected data without any user interaction.

Presently, the continuous technological developments allow for the installing of effective monitoring systems, capable of collecting accurate information and easily amending large amounts of data. Therefore, by combining sophisticated equipment with effective processing routines, it is possible to implement a monitoring system capable to perform an on-line monitoring of the structures, but also capable to generate proper alarms in case of occurrence of structural anomalies.

It is worth noting that the identification of any structural anomalies is not always easy because the extracted modal estimates are subject to the effects of the environmental factors that affect their nominal values. In the classical approach, the routines implemented to perform the processing of the data acquired by a monitoring system and aimed at identifying structural changes are not developed only for the automatic identification of the modal parameters but also for the elimination of the environmental and operational effects on the modal features (principally on estimated frequencies).

Therefore, the classical approach to the monitoring process based on OMA features is generally composed by consecutive steps that are briefly summarized as follows:

i) measurement of structural response in operational conditions. This task is performed by using sensors that measure accelerations, velocity variations or displacements,

ii) extraction of the modal parameters estimates adopting powerful techniques that convert the collected time series into relevant dynamic features,

iii) tracking of the time evolution of the modal estimates (i.e. natural frequencies) and any other derived parameters that provide useful information about the healthy state of the investigated structure,

iv) removal or minimization of environmental and operational effects on natural frequencies, in order to obtain results that depend only on structural conditions,

v) development of novelty detection procedures able to recognize possible structural changes and to automatically flag anomalies in the normal behavior.

A clear scheme about the classical strategy for vibration-based SHM system is provided by [Magalhães (2010)] and reported below:

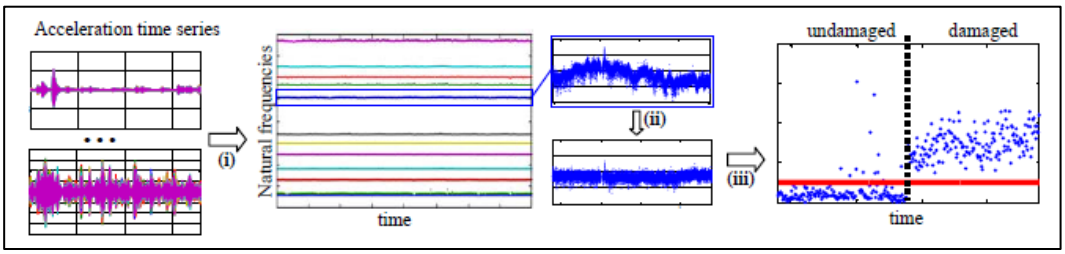

Fig. 1.1 Main processing steps of a classical vibration-based health monitoring system

1.2 Objective and main contributions

The main contributions of this Dissertation can be summarized in a few points aimed at making the application of OMA approach more common and straightforward in the context of SHM purposes. Despite the complexity of these techniques, the developed efforts are principally oriented towards making the use of these experimental tools simpler and more user-friendly, reducing their dependence on human interaction and demonstrating, through practical evidence, their usefulness for the dynamic testing and monitoring process of important structures and infrastructures.

The main objectives achieved in this work are summarized in the following:

i) development and implementation of useful methodology based on frequency domain and time domain techniques capable to efficiently obtain modal parameters estimates from data collected during single dynamic tests;

ii) development and validation of algorithms oriented towards the automatic extraction of modal features from the structural responses continuously collected by the monitoring system, even if composed by a reduced array of sensors;

iii) increase of the automation level of the identification techniques reducing the dependence of the analysis on expert user sensitivity in the beginning and during the monitoring process;

iv) removal of the post-processing performed on the modal estimates (frequently on natural frequencies) to minimize the effects of the environmental and operational conditions;

v) development of an alternative SHM methodology based on the application of pattern recognition models directly on the corrupted modal parameters estimates obtained by the tracking process, without performing any further filtering out of the environmental and operational effects.

To reach these objectives, further improvements have been made in the implementation of the identification methods devoted to making the process less sensitive to human user judgment also during the initial phase of parameters tuning. Furthermore, the continuous

assessment of the monitored structure is performed avoiding any training period normally used in the context of SHM to remove the environmental effects. The aim of the following efforts is definitely devoted to allowing for quasi-real time checking of the structural performance and to increasing the safety of the investigated civil infrastructure and ancient construction from the beginning of the continuous monitoring process.

A simple and clear scheme of the alternative vibration-based SHM approach is given in **Fig. 1.2**, in which the main steps are pointed out.

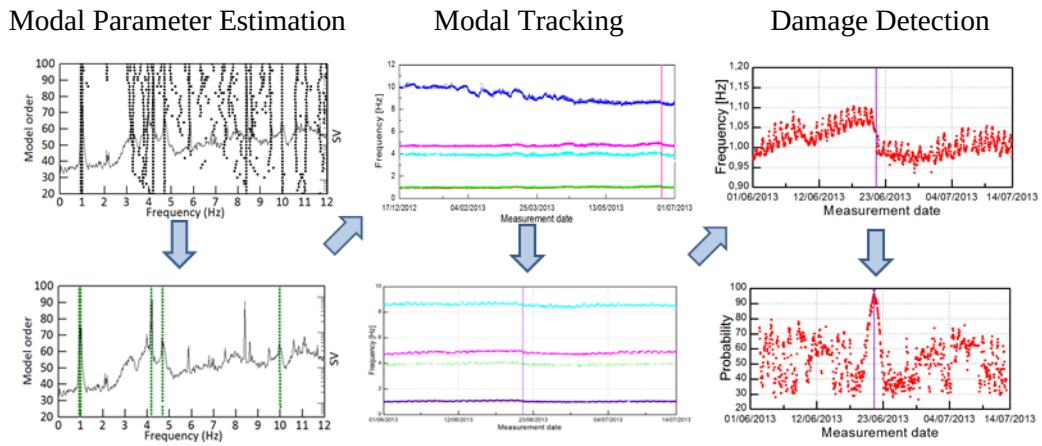

Fig. 1.2 Main processing steps of a classical vibration-based health monitoring system

For clarity purposes, once the installed dynamic monitoring system is fully active, the proposed monitoring software which analyzes the collected data is composed by only two stages: 1) automated identification of the modal parameters and tracking of the evolution in time of the extracted futures 2) continuous assessment of the structure in which the algorithm is able to flag possible damages based on frequency shifts and mode shape variations.

More specifically, the main contributions of this Dissertation are:

i) implementation of four state-of-the-art identification algorithms: Peak Picking (PP), Frequency Domain Decomposition (FDD), Covariance-driven Stochastic Subspace Identification (SSI-Cov) and Data-driven Stochastic Subspace Identification (SSI-

Data) using numerical simulations, and evaluation of the effect of user-defined variables on the accuracy of modal parameter estimates;

ii) development and implementation of a new strategy for Modal Parameter Estimation (MPE) based on a sequence of three key-steps aimed at providing a well-founded array of modal estimates during the single test analysis. The three sub-routines are oriented to: a) removing most of the spurious poles, b) performing the clustering approach and c) improving the accuracy of the modal parameters, reducing the uncertainty of the obtained estimates;

iii) testing and validation of the developed methodology firstly explained by using a simple numerical structure and subsequently validated by adopting experimental data collected during the AVTs performed on a lively footbridge and an ancient masonry bridge;

iv) implementation of an alternative Modal Parameter Estimation algorithm based on the construction and interpretation of tri-dimensional stabilization diagrams also generalized to complex structural modes;

v) validation of the developed algorithm in the analysis of databases collected during the continuous monitoring of important outstanding structures: the *Infante D. Henrique Bridge* in Portugal, and the *San Michele Bridge* in Italy;

vi) development of a new Modal Tracking (MT) procedure capable of following unexpected variations of the modal features due to extreme conditions; testing and validation of the new MT procedure in the context of continuous dynamic monitoring of two important Italian Cultural Heritage structures: a) the *Gabbia Tower* located in the city of Mantua and b) the *San Michele Bridge* that connects the small cities of Paderno and Carlusco d'Adda in the neighborhood of Milan;

vii) development of a new damage detection approach based on the use of pattern recognition models. The algorithm was developed in two different strategies, based on: a) the Continuous Segment Analysis (CSA) strategy, defining the undamaged and damaged state of the system with two consecutive segments of data, and b) the Separate Segment Analysis (SSA) strategy, based on a fixed segment of data used to define the reference undamaged condition of the investigate system;

viii) testing of both damage detection strategies using a simple numerical structure. The algorithm was applied to identify the structural damages in the numerical acceleration time series corrupted by simulated reduction of stiffness;

ix) validation of the damage strategy using experimental data collected during the seven-months of continuous dynamic monitoring of the *Gabbia Tower*. During this period, the tower was subjected to a far-field earthquake that produced a damage in the structure. The occurred damage was clearly identified by the application of the implemented damage detection strategy.

x) continuous assessment of the San Gottardo masonry bell tower with the application of the developed algorithms. Firstly, the OMA algorithms were adopted to perform the continuous identification of the structural modes of the tower for over two years of monitoring, creating a complete database that can be used in the future to test alternative monitoring methodologies. Subsequently, the application of the novelty detection algorithm demonstrates the structural integrity of the construction during the monitoring process.

xi) some damages on the structure have been simulated through frequency shifts in order to test the efficiency of the implemented methodology in the identification of small damages. The robustness of the alternative SHM approach was proved.

1.3 Organization of the Text

This section is aimed at providing the most important information on the topics covered in this Dissertation. Moreover, a brief description of the contents and the focus on the arguments treated in each chapter is given.

Chapter 1 introduces the Thesis with a contextualization of the developed research, followed by the description of the main objectives and contributions provided by the developed work and by the present description of the organization of the text.

Chapter 2 is devoted to providing a brief review of the mathematical models of dynamic systems and the theoretical basis of the modal identification analysis implemented in the time and frequency domain. Subsequently, an overview of the existent algorithms for operational modal analysis is given, followed by a detailed description and implementation of four state-of-the-art identification techniques, such as: PP and FDD, in the frequency domain, and SSI-Cov and SSI-Data implemented in the time domain. A simple academic structure and numerical simulations were used to exploit each implemented method highlighting the main aspects and advantages related to the application of the described methods.

Chapter 3 synthetizes the importance of the automation aspect in the identification process, highlighting the main issues related to the manual extraction of the modal parameters during the analysis of the single dataset or, especially, in the context of continuous dynamic monitoring. Furthermore, the main issues related to the induced environmental and operational effects on the modal parameters estimates are described as well as the capability of the novelty detection strategy developed with the aim to detect possible early structural damage in the investigated constructions.

Chapter 4 is completely dedicated to the description of the proposed methodology consisting of automatically performing the Operational Modal Analysis and the extraction of the modal parameters estimates from a single dataset of recorded time measurements. As will be described, the MPE algorithm can be used in those cases where the identification method involves the construction of stabilization diagrams. The algorithm was tested and validated through applying it to both a lively footbridge and an ancient bridge.

Chapter 5 describes in detail the development of a second Modal Parameter Estimation procedure aimed at reducing the dependence of the automated process on the expert user choices made during the initial setting phase of the parametric methods input parameters. The robustness of the developed methodology is demonstrated by its application to sequences of permanent monitoring concerning two large infrastructures.

Chapter 6 is devoted to describing a new automated Modal Tracking procedure. The performance of the developed strategy is highlighted by its application to data collected during the monitoring process of two case studies. Based on the results obtained, the ability of the procedure in providing the modal parameters evolutions – also in case of high fluctuations (i.e. both natural frequencies and mode shapes) due to high variations of the environmental conditions – is proved.

Chapter 7 is devoted to completing the SHM strategy presenting a new damage detection tool applied to modal parameters estimates obtained by the monitoring process. This algorithm was developed adopting a computational intelligence approach based on a Support Vector Machine (SVM), with the aim of automatically provide the occurrence of structural changes and damages in the investigated structure. This algorithm has been developed in two different strategies (i.e. CSA and SSA strategy) and exemplified by its application to a simple numerical structure. Subsequently, its accuracy was proved using data collected on a real structure.

Chapter 8 focuses on the application of the previously developed automatic modal identification algorithms, exploring their potentiality in the context of SHM. The performance of the proposed methodology is firstly exemplified using data collected during a two-year monitoring period of the masonry tower of the Church of *San Gottardo in Corte* in Milan. Based on the automatic tracking of the natural frequencies, the novelty procedure was applied to a reference monitoring period (10 months) confirming that the structure did not suffer any damages along such period, preserving its current integrity. Subsequently, in order to test the robustness of the algorithm, small structural damages were simulated through frequency shifts on the resulting frequency data. The results obtained by avoiding the removal of environmental and operational effects from the estimates prove the capability of the novelty strategy to reveal slight damages and to detect anomalies in the normal behavior of the structure.

Chapter 9 summarizes the Thesis with conclusions and future developments of the presented strategy pointing out possible developments for OMA–based SHM purposes.

Chapter 2

BACKGROUND AND DEVELOPMENT OF OPERATIONAL MODAL ANALYSIS TECHNIQUES

Contents

2.1 Introduction to Operational Modal Analysis

Experimental identification of the modal parameters has been one of the most interested research topics during the last decades. As well known, this research topic was born inside the laboratories principally oriented to test and analyze small structures under controlled environment, typically for mechanical engineering components. This approach was named Experimental Modal Analysis (EMA) and it is based on the measurement of the structural responses collected under controlled input excitation. For the relation between the applied input forces and the observed output responses the modal parameters could be defined. Since the first practical applications until the present developments, the testing equipment and the processing tools evolved significantly encouraging more interested groups in this research field.

EMA techniques have also been adopted for the identification of modal parameters of Civil Engineering structure over the years, mainly tall buildings, bridges, and dams. But the analysis carried out using EMA approaches required the application of additional measurable dynamic excitation forces that, due to the dimension of the investigated structures, have to be provided by large and expansive devices. Despite the complications due to considerable dimension of the excitation devices and prolonged closure of the in-service condition of the structures, these tests, named Forced Vibration Tests (FVT), have been performed on large infrastructure as bridges and on massive dams.

Consequently, the focus of the research turned on the performance of much practical and economical tests, in which the dynamic excitation provided by large devices was replaced by freely available ambient forces already present during such tests as: micro-tremors induced by ambient excitation as the traffic circulating nearby the structure, wind forces or in-service loads that both directly insist on the investigated structure. This relevant advantage lead to an increased development of equipment and processing tools to perform the dynamic tests and the assessment of important Civil Engineering structures without interrupts their normal operation, which consists of an important

economic benefit for the owners of the infrastructures. Furthermore, the adoption of Ambient Vibration Test (AVT) to characterize the dynamic behavior of the structure allows the definition of the dynamic behavior during in-service operative conditions that's means to obtain realistic results associated to real vibration conditions, with another advantage of highlighting possible anomalies or non-linearity of the structure that could not be obtained using artificially generated vibrations.

Although the economical and practical advantages in the use of AVT compared to FVT, some disadvantages affect this methodology. The first issue is related to the noise content of the signals; in fact, if the input excitation is very low – as happened for Cultural Heritage constructions generally located in the central areas of the cities – becomes mandatory the use of very sensitive sensors with very low noise levels to obtain consistent data in which is possible to extract dynamic properties of the investigate structure. The second issue is related to the modal mass that is not estimated. On the other hand, is equivalent to say that the mode shapes are not unique defined, or they are not scaled in absolute way. Moreover, another issue could be related to the frequency excitation which may not cover all the band of interest, which means that not all modes are well excited by environmental forces.

Despite the aforementioned issues, the identification of the dynamic characteristics in operative condition using AVTs received and increasing attention in the last decades, driving the development of new technological devices and new powerful algorithms to perform the automated identification of the modal parameters and, consequently, to allow the continuous assessment of strategic and important infrastructure only measuring the response in operative conditions. In this way, as the modal information is derived from structural responses during the in-service condition, this process was named Operational Modal Analysis (OMA) or also Output-only Modal Analysis, because the measured outputs. This approach is based on the main hypothesis related to the input excitation that it is always present, and it can not be removed during the tests. The input is replaced by the assumption of a realization of stochastic process (even defined as white noise

process) which has a constant spectrum with constant intensity along the frequency interval of interest. Starting from this assumption many approaches were developed to determine a model that fits the response of the structure and then extract the associated modal feature from the measured data, also called Stochastic System Identification methods.

Afterwards, new techniques have been developed in recent years to deal with those cases in which the frequency excitation may not cover the whole frequency band of interest (i.e., narrow-band ambient excitation) or when the amplitude of the ambient forces is weak, and consequently not all modes are well excited by environmental forces. A possible methodology to overcome these issues is represented by the combining an artificial force applied to the structure with the ambient excitation. In other words, measured input are added to unknown operational forces. This approach is known as Operational Modal Analysis with eXogenous inputs (OMAX).

Many interesting papers regarding this topic are presented in literature, such as: [Guillame et al. (2007); Reynders et al. (2009a); Devriendt et al. (2011)]. The main differences between EMA and OMAX are given by the inclusion of (artificially generated) operational forces in the identified system instead of using only the ambient excitation and assuming that they are noise. In this way, relatively small excitation devices can be used during the dynamic test, checking that the amplitude of the applied artificial forces falls into the range of the ambient excitation. The theoretical background and the application of this approach to civil engineering structures can be found in [Reynders et al. (2009b)], where the efficiency of the OMAX algorithm was demonstrated by its application to data collected in FVTs that involve both large shakers and also small excitation devices. Meanwhile in [Reynders et al. (2011)] the performance of the OMAX algorithm was demonstrated in the modal testing of a two-span steel arch footbridge in operational conditions, with and without using an additional actuator. The system model was fitted by measured signals collected during the FVT of the bridge taking both the measured and the operational excitation into account.

The present work is only focused on the use of Operational Modal Analysis, therefore, in this Chapter, after a brief characterization of the models of dynamic system adopted by identification methods, it is given a deep description of the available OMA algorithms, followed by a detailed description of four of the most used and representative identification methods that are extensively used in Civil Engineering applications.

Among many different dynamic identification techniques based on OMA procedures have been implemented in the last decays, usually classified as non-parametric and parametric methods, which operate in frequency or in time domain, some of them described in the previous Chapter. Then, it will be pointed out the use of modal techniques in the framework of dynamic monitoring purposes in operational conditions.

In this context, the continuously measured data has to be processed automatically and so algorithms to perform an automatic operational modal analysis need to be developed. For this reason, two different approach for automated modal identification based on parametric methods are developed. The efficiency of the tools is demonstrated using data collected during several ambient vibration tests performed on civil structures and Cultural Heritage constructions presented in Chapters 4 and 5. Moreover in Chapter 6 the presentation of an alternative technique of automated Modal Tracking is provided, given special attention on the efficiency of the procedure even in case of structural anomalies and damage of the present case studies.

After a brief overview of other available tools presented in literature, a new methodology for Structural Health Monitoring (SHM) purpose based on pattern recognition models will be presented in Chapter 7. The efficiency of the proposed SHM methodology is then demonstrated on the basic of the continuous monitoring applications presented in Chapter 8, talking profit from the previously presented tools for automatic modal analysis. It is worth to give special attention to the performance of the new methodology for Damage Detection purposes aimed at ensuring the correct monitoring with really sustainable cost, providing a reasonable alarm in case of changes in the normal condition of the structure with a very short delay from the anomaly occurrence.

2.2 Modelling of the dynamic behavior of linear systems

In this paragraph the main concepts concerning the solution of typical vibration problem will be summarized. In particular, several mathematical models used to characterize the dynamic behavior of linear systems will be described. Firstly, the classical formulation of the problem based on the resolution of a system of second order differential equations will be described in detail highlighting its solving in time domain and frequency domain. Subsequently, the state-space model will be presented in detail. Furthermore, the advantages derived by the use of this model in the identification problems will be described in detail as well as the main assumption about the input excitation that constitute the principal steps for the implementation of the output-only identification techniques.

2.2.1 Spatial and modal models

Starting from the basic assumptions of the Structural Dynamic courses, the characterization of a mathematical model that best fits the dynamic behavior of a structural system requires an adequate knowledge about the geometric and mechanical properties of the structural elements belong to the system as well as the actions exerted on the structure itself. The action, variable in time, can be classified as: deterministic or stochastic. In the former, the variation of the input excitation is known, and it is possible to quantify the response of the structure in deterministic way. On the other hand, in the latter case the variation of the actions has to be derived through probabilistic concepts because the statistical uncertainty related to their random nature and the structural responses can be quantified by stochastic response relations.

As usually illustrated in several civil engineering courses, the definition of a mathematical model to study the dynamic response of simulated structures that is strictly depended on the distribution of mass, damping and stiffness. These properties are usually

defined using matrix representation resulting by an initial spatial discretization of the investigate system. Under these assumptions, the behavior of the model is defined by a set of differential equations of equilibrium that are related to the spatial discretization of the finite element structure which characterize the basis of the different models. Such equations can be defined in continuously or discrete time characterizing, respectively, continuous models, in which the response is defined in continuously manner over time, and discrete models, in which the response is obtained after a properly discretization.

Spatial formulation

The equation of motion for linear time-invariant (LTI) multi-degree-of-freedom (MDOF) systems in continuous time can be formulate by:

$$M \cdot \ddot{q}(t) + C \cdot \dot{q}(t) + K \cdot q(t) = F(t) = B \cdot f(t) \qquad (2.1)$$

This expression represents the so-called *Spatial Model* because it models the behavior the dynamic system by the distribution of the mass M, stiffness K and damping C. The solution of the coupled second-order differential equation system (in **Eq. 2.1)** can be solved, in the time domain, using the impulse response functions (IRF) and considering the initial conditions (both displacements and velocities vectors) in the time instant t=0 as follows [$q(t=0)=q_0$] and [$\dot{q}(t=0)=\dot{q}_0$].

In **Eq. 2.1** is assumed the system composed by a planar rigid body, moving in the plane of the body (the *x–y* plane), and subjected to forces and torques causing rotation only in this plane, so M, C and K are [*N*-by-*N*] square matrices, where each single element m_{ij}, c_{ij} and k_{ij} corresponds to the generalized force in the coordinate *i*, when at the coordinate j is introduced an acceleration, a velocity or a displacement with unit value, respectively. Moreover, the vectors $\ddot{q}(t)$, $\dot{q}(t)$ and $q(t)$ contain the accelerations, velocities and displacements referred to each single degree of freedom (SDOF) of the structure. Meanwhile, $F(t)$ is the vector of exciting forces applied to each SDOF and matrix B maps the arbitrary inputs defined by $f(t)$ to the corresponding well-selected

points in which the excitation forces are applied. All functions are expressed in the continuous time domain and referred to the same instant t.

It is worth noting that a major uncertainty of **Eq. 2.1** is related to the damping phenomenon and its modelling. Generally, proportional damping is assumed to describe the observed decaying responses, and it is obtained by a linear relation between the mass (M) and stiffness (K) properties of the system, as described in **Eq. 2.1.** This property was initially proposed by Rayleigh, and it permits the introduction of some simplifications in the mathematical approach of the dynamic system problems allowing their easier resolution without modify the physical meaning of the results. The proportional property between the damping, mass and stiffness distributions of the linear system presented in **Eq. 2.1** is reported in the following equation:

$$C = M \cdot \sum_b a_b \, [M^{-1} \cdot K]^b \, ; \qquad C = \alpha M + \beta K \tag{2.2}$$

The second relation in **Eq. 2.2** represents the *proportional damping* property of the linear system and it defines how the damping matrix can be obtained as linear combination between M and K [Clough and Penzien (1993)]. The Rayleigh damping (C=αM+βK) is a particular case of a general proportional damping formula and it is obtained considering the values b=0 and b=1 in the above expression. The system of coupled second-order differential equations can be solved in the time domain by using the function of the impulsive response function through the application of the Duhamel integral.

This strategy is not convenient because in a MDOF system the dynamic response of each SDOF is related to the motion of the previous and the consequent DOF. This means that the second order equations do not be solved independently, making difficult the solving of the problem. As widely demonstrated during Master's Degree courses, the solution of a dynamic system is generally founded using the so-called *Modal Domain* and switching the problem from time domain in to frequency domain and allowing a faster and easier analysis. This second strategy is more interesting and easier to understand, so it will be introduced and described in the next paragraph.

Now, to explain the main concepts related to the classical representation of the dynamic system in the *Spatial Model*, it is only introduced the analysis of the dynamic response of a simple SDOF oscillator obtained under the hypothesis of deterministic excitation. The dynamic behavior of the structure is described with mass *m*, stiffness *k* and damping *c*, and it is defined by the following equation:

$$m\,\ddot{q}_1(t) + c\,\dot{q}_1(t) + k\,q_1(t) = f_1(t) \tag{2.3}$$

where $q_1(t)$ is the response of the oscillator subjected to an arbitrary force $f_1(t)$, and $\dot{q}_1(t)$ and $\ddot{q}_1(t)$ are the two derivatives (first and second) of $q_1(t)$, respectively. The solution of the time domain equation, considering the initial conditions (displacement and velocity) as null values, can be obtained by using the Duhamel convolution integral:

$$q_1(t) = \int_0^t f_1(\tau)\,h_1(t-\tau)\,d\tau \quad , \qquad t > 0 \tag{2.4}$$

where the function $h_1(t-\tau)$, defined by following relation, is the response of the system in the instant $t-\tau$, caused by a unitary impulse generated in the instant τ.

$$h_1(t-\tau) = \frac{1}{m\,\omega_{1d}}\,e^{-\omega_1\xi(t-\tau)}\,sen[\omega_{1d}\,(t-\tau)] \quad , \qquad t > \tau \tag{2.5}$$

This function defines the dynamic response of a 1-DOF oscillator, that strictly depends on its intrinsic characteristics: mass (m), stiffness (k), natural frequency (ω_1) and damping (ξ). The damped frequency (ω_{1d}) is given by:

$$\omega_1 = \sqrt{(k/m)} \quad \rightarrow \quad \omega_{1d} = \omega_1\sqrt{1-\xi^2} \tag{2.6}$$

It is worth noting that the general damping value *c* in **Eq. 2.3** is related to the known damping coefficient ξ of the system by the following equation:

$$c = 2\,\xi\,m\,\omega_1 \tag{2.7}$$

Solving the problem using the Duhamel integral, means splitting the force acting on the system as a train of impulses, or rather a sequence of impulsive functions, and thus

calculating the response of the system through the sum of the single response due to the action exerted by every single impulsive function.

Regarding the linear-invariant MDOF system described by **Eq. 2.1** the solution is given by the system response $q(t)$ which characterizes the dynamic behavior of the structure under deterministic input. In order to find the solution of the system, N different coupled second-order differential equations might be written and solved simultaneously. A valid alternative to the classical approach based on the *Spatial Model* consists of performing an efficient strategy that permits to convert the system composed by N coupled second-order differential equations into a system of N decoupled equations in which the dynamic behavior is defined by a single DOF and then to solve each SDOF system, separately.

This strategy is called *Modal Analysis* and it is described in detail in the next paragraph. Furthermore, in structural analysis (e.g. Finite Element (FE) analysis) the investigated structure is divided in several elements and the matrices M and K are directly obtained by their geometric and material properties. In general cases, it is impossible to assemble the damping matrix C in the same way as M and K, mainly due at the lack of the reliable constant property of the material that represents the global damping behavior of the structure. So, as mentioned in **Eq. 2.2**, the damping matrix can be modelled following the ordinary way, introducing the proportional damping and, in more general way, the viscous damping.

Anyway, the solution of the system described in **Eq. 2.1** is given starting from the simplest case without considering damping. Because, as it will be demonstrated in the following, the dynamic solution of a linear system with proportional damping is equal to the same system considering the damping equal to zero. Consequently, the proportional damping and the general viscous damping will be also described.

Modal formulation

As mentioned, the modal formulation allows transforming the system of N coupled second-order differential equations into an equivalent system composed by a set of N independent differential equations. This task can be achieved by expressing the vector of the displacements as linear combination of N independent vectors. These vectors are named as *modes of vibrating* and normally indicated with the notation: φ_k. From a mathematical point of view, the vibration modes of a proportional damping system (see **Eq. 2.2**) have similar mode shapes to those modes extracted by a non-damping system with same characteristics in terms of mass and stiffness. Its dynamic behavior is defined by the *homogeneous equation of motion* that can be expressed as follows:

$$M \cdot \ddot{q}(t) + K \cdot q(t) = 0 \tag{2.8}$$

in which the matrices M and K have the same dimensions and values described for the system in **Eq. 2.1** with not null initial conditions [$q(t=0)=q_0 \neq 0$] and [$\dot{q}(t=0)=\dot{q}_0 \neq 0$]). As well-known, the general solution of the system described in **Eq. 2.8** consists of:

$$q(t) = \varphi_k \, e^{\lambda_k \cdot t} \tag{2.9}$$

Applying the theory of the linear systems, the eigenvalues and eigenvectors of the general system described in **Eq. 2.8** can be extracted by the following equation:

$$\lambda_k^2 \, M \cdot \varphi_k + K \cdot \varphi_k = 0 \;\Leftrightarrow\; K \cdot \varphi_k = -\lambda_k^2 \, M \cdot \varphi_k \tag{2.10}$$

By solving the eigenvalue problem, N independent equations can be used to extract the eigenvalues $\left(-\lambda_k^2\right)$ and its corresponding eigenvectors (φ_k). As already stated, the dynamic properties of the system are defined by the eigenvalues (ω^2) and the eigenvectors matrix (Φ). It is demonstrated that the eigenvalues are intimately correlated to the square of the non-damped angular frequencies as follows:

$$\lambda_k = i \, \omega_k \tag{2.11}$$

Meanwhile the eigenvectors are strictly related to the vibration modes of the structure. Moreover, such modes φ_k are usually organized in a matrix Φ – defined as *modal matrix* – in which the eigenvectors correspond to the column of this matrix, as follows:

$$\Phi = [\cdots \quad \varphi_k \quad \cdots] \; with \; k = 1 \ldots N \tag{2.12}$$

Hence, the key issue to decouple the equations of motion lies in the orthogonality property of the modal matrix Φ with respect to the mass matrix and the stiffness matrix. This leads to the fact that the eigenvectors are independent by each other and they do not depend on the external input forces since the frequencies and mode shapes characterize the free vibration problem.

Therefore, the *modal matrix* described in **Eq. 2.12** can be used to perform the separation of the equations of a general non-damped MDOF system described in **Eq. 2.8**. This operation can be performed because each vibration mode is orthogonal to the distribution of the mass and the stiffness and they satisfy the following conditions:

$$\Phi^T \cdot M \cdot \Phi = \begin{bmatrix} \ddots & & \\ & m_k & \\ & & \ddots \end{bmatrix} \quad \Phi^T \cdot K \cdot \Phi = \begin{bmatrix} \ddots & & \\ & k_k & \\ & & \ddots \end{bmatrix} \tag{2.13}$$

Accordingly, pre-multiply the undamped equation of motion (including now the external input) by Φ^T, the modal matrix transforms both square matrices M and K in diagonal matrices; and the resulting diagonal matrices are named as: *modal mass matrix* (M_d) and *modal stiffness matrix* (K_d) where m_k and k_k indicate mass and stiffness associated to the *k-th* DOF, respectively. Furthermore, pre-multiply the **Eq. 2.8** with the modal matrix Φ^T and using the conditions obtained in **Eqs. 2.11** and **2.13**, the non-damped angular frequencies associated to each SDOF of the MDOF system can be extracted by a similar formula used for the free response of a 1-DOF oscillator (see **Eq. 2.6**) as follows:

$$\omega_k = \sqrt{\frac{k_k}{m_k}} \tag{2.14}$$

For general cases (i.e. damped vibration systems) it is necessary to consider the orthogonality property of the vibration modes also related to the damping matrix (C) and to assume "proportional damping" distributed in the whole structure. In this case, the problem can be solved adopting the same strategy used for undamped systems, since the damping matrix is obtained by linear relation between the mass and stiffness matrices:

$$\Phi^T \cdot C \cdot \Phi = \begin{bmatrix} \ddots & & \\ & c_k & \\ & & \ddots \end{bmatrix} = \begin{bmatrix} \ddots & & \\ & 2\xi_k m_k \omega_k & \\ & & \ddots \end{bmatrix} \qquad (2.15)$$

In the previous equation the *modal damping matrix* (C_d) and modal damping coefficients c_k are defined. Again, the second equality of **Eq. 2.15** also means that when the damping is considered proportional, the *modal damping matrix* (C_d) is obtained as linear combination between the *modal mass matrix* (M_d) and the *modal stiffness matrix* (K_d**)**.

Accordingly with the **Eq. 2.9**, a general solution of the free dynamic response of MDOF systems with proportional damping leads to a series of individual equations as follows:

$$\lambda_k^2 + 2\,\xi_k\,\omega_k\,\lambda_k + \omega_k^2 = 0 \qquad (2.16)$$

Solving the *N* expressions of **Eq. 2.16** associated to the liner system of **Eq. 2.8**, *n* different values of λ_k - in which *n=2N* - are provided. Thus, the obtained eigenvalues are related to the non-damped angular frequencies and the damping coefficients as follows:

$$\lambda_k, \lambda_k^* = -\xi_k\,\omega_k \pm i\sqrt{1-\xi_k^2}\,\omega_k \qquad (2.17)$$

In this way, Furthermore, the general solution of the system q(t) expressed in **Eq. 2.1**, can be defined as linear combination of the vibration modes in the *Modal Space*:

$$q(t) = \sum_{k=1}^{N} \varphi_k \cdot \eta_k(t) \qquad (2.18)$$

Considering the superposition of the effects, a general linear equation system with proportional damping can be transformed into a system of independent second-order

differential equations in which the solution is given by a liner combination of *N* independent solutions associated to each singular vibration modes.

$$m_k\,\ddot{\eta}_k(t) + c_k\,\dot{\eta}_k(t) + k_k\,\eta_k(t) = f_k(t) \quad with\ k = 1 \dots N \tag{2.19}$$

in which $\dot{\eta}_k(t)$ and $\ddot{\eta}_k(t)$ are the first and second derivative of the *modal coordinate* $\eta(t)$, m_k, k_k and c_k are the modal components of the modal matrices described in **Eqs. 2.13** and **2.15**, respectively. Meanwhile, f_k is the modal component of the input excitation associated to *k-th* DOF and it is given by the product between the transpose of the each vibration mode φ_k, the resulting vector ($B \cdot f(t)$) of the input excitation and the identity matrix, respectively. This value is defined as follows:

$$f_k(t) = {\varphi_k}^T \cdot [(B \cdot f(t)) \cdot I] \tag{2.20}$$

For clearness, as stated in **Eq. 2.13**, the modal matrix (Φ) is used to transform the mass matrix (M) and the stiffness matrix (K) in diagonal matrices defined as: *modal mass matrix* (M_d) and *modal stiffness matrix* (K_d). Such relation is express by the follows:

$$M_d \cdot \ddot{\eta}(t) + K_d \cdot \eta(t) = f_\eta(t) \qquad with \begin{cases} \eta(t) = \Phi^{-1} \cdot q(t) \\ f_\eta(t) = \Phi^T \cdot [B \cdot f(t) \cdot I] \end{cases} \tag{2.21}$$

Moreover, since the vibration modes are obtained by the resolution of the eigenvalues problem, they can be defined up to a scale factor. Thus, it is usual to scale the modal mass components (with the value $\varphi^T \cdot M \cdot \varphi$) to obtain a *unit modal mass matrix*:

$$\ddot{\eta}(t) + \begin{bmatrix} \ddots & & \\ & \omega_\eta^2 & \\ & & \ddots \end{bmatrix} \eta(t) = \Gamma_\eta(t) \;\rightarrow\; \ddot{\eta}(t) + \omega_\eta^2\,\dot{\eta}(t) = \Gamma_\eta(t) \tag{2.22}$$

in which ω_η^2 corresponds to the square value of the undamped angular frequency associated to each SDOF and $\Gamma_\eta(t)$ is the *participation coefficient* and it identifies the modal component of the input associated to each SDOF after performing the modal mass normalization as follows $\Gamma_\eta(t) = f_\eta(t)/[\Phi^T \cdot M \cdot \Phi]$. Finally, the system in **Eq. 2.8** is decoupled in *N* independent differential equations that can be independently solved.

To conclude this overview, the complete solution of an undamped SDOF system loaded by an arbitrary ZOH input reported in **Eq. 2.3**, can be solved in the time domain adopting the Duhamel integral defined in the *Spatial Space*. After the introduction of the *Modal Model* these relations can be expressed in the *Modal Space* as follows:

$$\eta(t) = \int_0^t f_\eta(\tau)\, h(t-\tau)\, d\tau \ , \qquad t > 0 \tag{2.23}$$

$$h(t-\tau) = \frac{1}{m_k\, \omega_{dk}}\, e^{-\omega_k \xi (t-\tau)}\, sen[\omega_{dk}\, (t-\tau)] \ , \quad t > \tau \tag{2.24}$$

Similarly, to **Eqs. 2.4** and **2.5**, the function $h(t-\tau)$, describes the impulse response function of a SDOF system in the time domain, that defines the output of this system at any time *t* to a unitary impulse generated in the instant τ. In other words, the output response in the Modal Space can be viewed as a filters sum of the input history $f_\eta(t)$, in which the impulse response function is completely defined by the mass (m_k), the natural frequency (ω_k) and the damping ratio ξ_k associated to the SDOF system as follows:

$$\omega_{dk} = \omega_k \sqrt{1-\xi^2} \quad with \quad \xi_k = \frac{c}{2 m_k \omega_d} \quad and \ \omega_k = \sqrt{\frac{k_k}{m_k}} \tag{2.25}$$

Concluding this paragraph, the *Modal Model* admits that the damping distribution along the structure is proportional to the mass and stiffness distributions. Adopting this assumption, the mathematical formulation is simplified. Since the solutions of the linear system with proportional damping is identical to those obtained for the simpler undamped system, the analysis is generally carried out using the simplest problem also applying the orthogonality property of the vibration modes. Besides, this assumption can turn out to be a restricted condition. In fact, for some structures (as Cultural Heritage or damaged structures) the damping is not constant distributed over the structure and this issue can provide several problems in the identification of modal estimates (e. g. the imaginary components of the mode shapes become relevant and the mode shape turn out to be complex).

2.2.2 Frequency response models

Alternatively, the dynamic problem described in **Eq. 2.1** can be solved transferring the problem from the time domain to the frequency domain and avoiding the use of second-order differential equations. In this way, the problem can be solved using simpler algebraic equations applying the Fourier Transform to all terms of the equation.

2.2.2.1 Frequency response models

Recalling the 1-DOF system described in the **Eq. 2.3** the differential equation is transformed in the following algebraic equation:

$$-m\,\omega^2\,Q_1(\omega) + c\,i\,\omega\,Q_1(\omega) + k\,Q_1(\omega) = F_1(\omega) \qquad (2.26)$$

in which the functions $Q_1(\omega)$ and $F_1(\omega)$ are the Fourier transforms functions of $q_1(t)$ and $f_1(t)$. Inspecting the **Eq. 2.26**, it is easy to understand the advantage obtained; in fact, it is possible to write the structural response in the explicit way as follows:

$$Q_1(\omega) = \frac{F_1(\omega)}{-\omega^2\,m + i\omega c + k} = H_1(\omega)\,F_1(\omega) \qquad (2.27)$$

where $H_1(\omega)$ is the Frequency Response Function (FRF) of 1-DOF system. The FRF can also be written in the following form:

$$H_1(\omega) = \frac{1}{-\omega^2 m + i\,\omega\,c + k} = \frac{1/m}{\omega_1^2 - \omega^2 + 2\,i\,\xi\,\omega\,\omega_1} \qquad (2.28)$$

In the convolution of the problem from the time domain to the frequency domain the term $H_1(\omega)$ is the Frequency Response Function (FRF) and it corresponds at the Furrier transform of the impulse response function $h_1(t-\tau)$ of a SDOF (see **Eq. 2.5**). Moreover, dividing numerator and denominator for mass value (m), expressing the natural frequency as $\omega_1 = \sqrt{(k/m)}$ and using equality $c = 2\,\xi\,m\,\omega_1$, the FRF can be re-written in order to highlight some important characteristics:

$$H_1(\omega) = \frac{1/k}{1 + 2i\xi\left[\frac{\omega_1}{\omega}\right] - \left[\frac{\omega_1}{\omega}\right]^2} \qquad (2.29)$$

The FRF above expressed characterizes the dynamic behavior of 1-DOF oscillator describing how the input force is transformed in the response of the system (**Eq. 2.27**).

As depicted in **Fig. 2.1**, the FRF represents a complex function (composed by a real part R and an imaginary part I), through its amplitude $\sqrt{R^2 + I^2}$ and phase $arctg(I/R)$. As can be easily deduced from the **Eq. 2.29**, the amplitude of FRF has its maximum in correspondence of the value $\omega = \omega_1\sqrt{1 - \xi^2}$, that represents a good natural frequency estimation when the damping value is low.

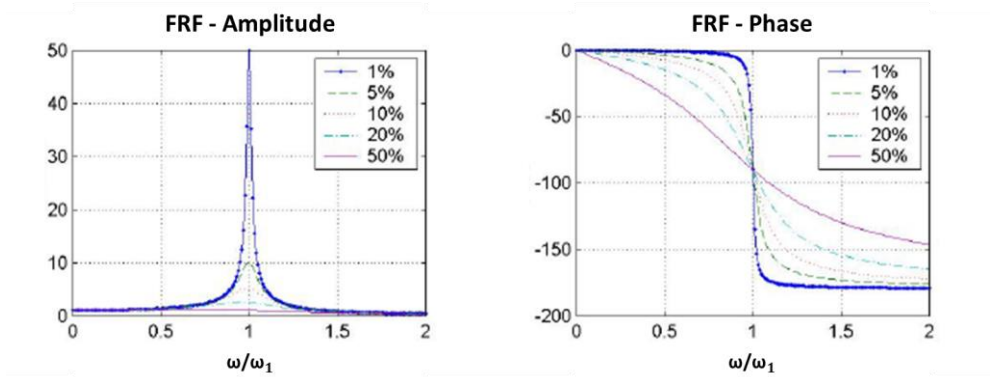

Fig. 2.1. Amplitude and phase of the Frequency Response Function of 1-DOF system

Furthermore, analyzing the **Eq. 2.29**, it clearly appears that if the frequency excitation is quite low in relation to the undamped natural frequency of the system, the FRF tend to be 1/k. This means that the mass inertial and the damping forces are negligible. Thus, the plot of the amplitude presents a quite constant trend and the phase remains close to 0. When the frequency excitation reaches the natural frequency, the response exhibits a maximum peak and the phase jump from 0° to 180° (**Fig. 2.1**), activating the so-called *resonance phenomenon*.

In the region around the natural frequency the damping forces become dominant and the mass moves in opposite phase of the direction of motion. Finally, in case of resonance

(i.e. $\omega = \omega_1$) the response is purely imaginary, and it is mostly related to the damping forces. It also possible to estimate the damping value by the bell-shape of the amplitude plot. The damping coefficients are lower for the sharper graphics of the amplitude.

Following the analogous sequence of steps used for the 1-DOF, applying the Fourier transform to both members of the system of **Eq. 2.1**, the relation between the system's response and the input excitation can be defined using the following matrix expression:

$$Q_N(\omega) = H(\omega) \cdot F_N(\omega) \qquad (2.30)$$

where $\mathrm{Q_N}(\omega)$ and $\mathrm{F_N}(\omega)$ are vectors of [*N*-by-*1*] dimension (*N* is the number of differential equations of the system), that represent the Fourier transforms of each $\mathrm{q_i}(t)$ response and each $\mathrm{f_i}(t)$ excitation, respectively. Otherwise, $\mathrm{H}(\omega)$ is an [*N*-by-*N*] matrix where each $\mathrm{H_{ij}}(\omega)$ component identifies the FRF of the system related to the response at coordinate i subjected to a generalized force applied at coordinate j. The relation among this matrix and the characteristics of the structure is given by the following expression:

$$H(\omega) = [-\omega^2 M + i\,\omega\,C + K]^{-1} \qquad (2.31)$$

Numerical example

To explain in detail the basic concepts that are described in this Chapter, a simple academic structure is adopted as reference example. This system refers to a numerical model that approximates a simple building structure and it consists of 3 DOFs composed by 3 rigid floors each one connected with four columns. The structure is considered rigidly fixed at the base. Each floor is made of steel sheets with a 1 cm of thickness, meanwhile the pillars are made of aluminum sheets with 16 cm of inter-floor height and section dimensions equal to 2 mm x 16 mm. The dimensions of the system are reported in the **Fig. 2.2**. It is worth noting that due to the different bending inertia of the columns, the structure can be approximate by a simpler 2D scheme as reported in **Fig. 2.3** and the analysis can be performed only on one direction of motion, in particular on the most flexible one.

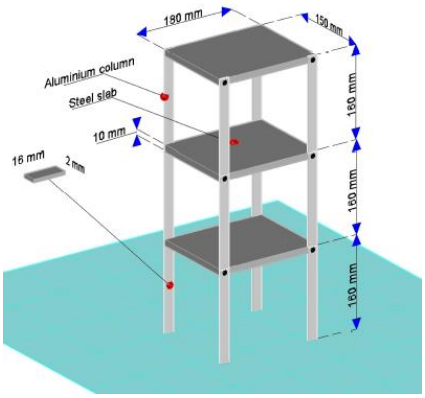

Fig. 2.2. Structural Model

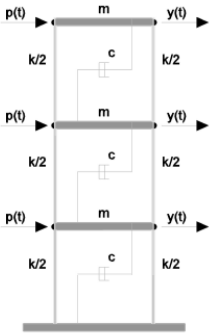

Fig. 2.3. Shear-type model

This approximation means to consider the structure as a shear-type model in which **Eq. 2.1** can be re-written using the following matrix equation:

$$\begin{bmatrix} m & & \\ & m & \\ & & m \end{bmatrix}\begin{bmatrix} \ddot{x}_1 \\ \ddot{x}_2 \\ \ddot{x}_3 \end{bmatrix} + \begin{bmatrix} 2c & -c & \\ -c & 2c & -c \\ & -c & c \end{bmatrix}\begin{bmatrix} \dot{x}_1 \\ \dot{x}_2 \\ \dot{x}_3 \end{bmatrix} + \begin{bmatrix} 2k & -k & \\ -k & 2k & -k \\ & -k & k \end{bmatrix}\begin{bmatrix} x_1 \\ x_2 \\ x_3 \end{bmatrix} = \begin{bmatrix} p_1 \\ p_2 \\ p_3 \end{bmatrix}$$

Using the relations in **Eq. 2.31** and considering the mass of each floor *m* equal to 2,080 Kg (considering 2 kg the weight of the iron plate and 20 grams the weight of each connector between the iron plate and column) the stiffness *k* equal to $4*12EI/L^3$ (in which EI is the inertial bending of the section and L=16 cm is the height of the column), and the damping value equal to $c= \xi \cdot 2 \cdot m \cdot \sqrt{k/m}$. Two different damping values were used: ξ=1% and ξ=5%.

The FRF function of each DOF was defined for 2500 points that means 2500 inverse matrices (as described in **Eq. 2.31**) were calculated with a very high time consuming. From the inspection of Fig. 2.4 and Fig. 2.5 the dynamic characteristics of the system can be easily detected. In fact, as happened for 1-DOF system, the natural frequencies of the MDOF system correspond to the peaks of the amplitude plot (see **Fig. 2.4**) where the phase jumps from 0 to π (see **Fig. 2.5**). Furthermore, the bell-shapes of the amplitude associated to each mode depends on the damping coefficient value. Consequently, preliminary consideration can be done about the damping values. From the amplitude diagrams can be highlighted that the damping value is higher in the third mode than the second mode, because the bell-shape of the FRF of the third mode is smoother than second one. In the same way, the damping of the second mode is higher than one associated to the first mode.

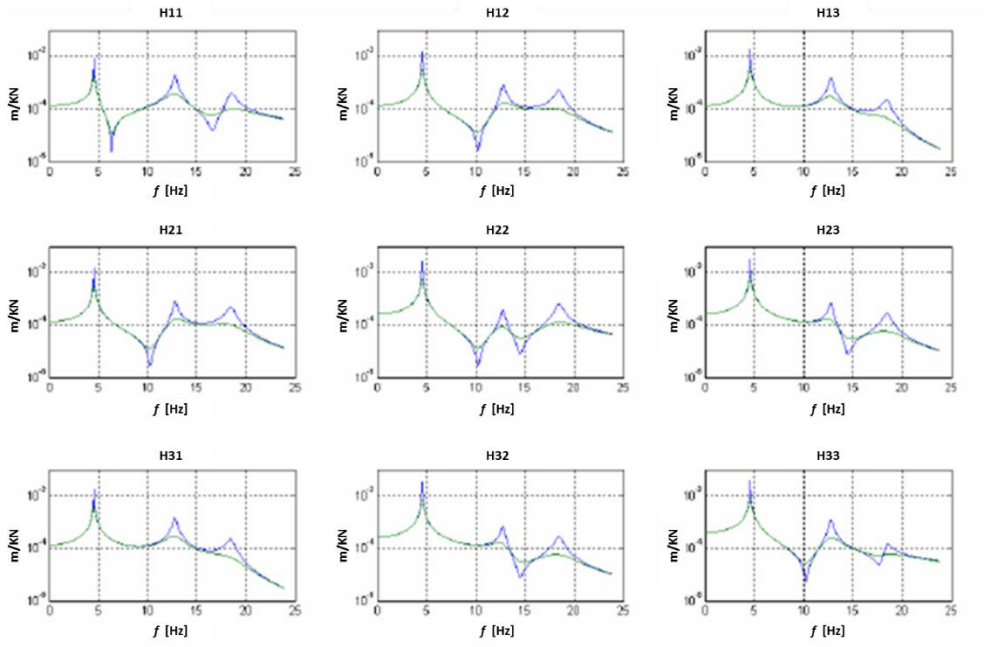

Fig. 2.4. Amplitude values of the FRFs matrix (ξ=1% blue line, ξ=5% green line)

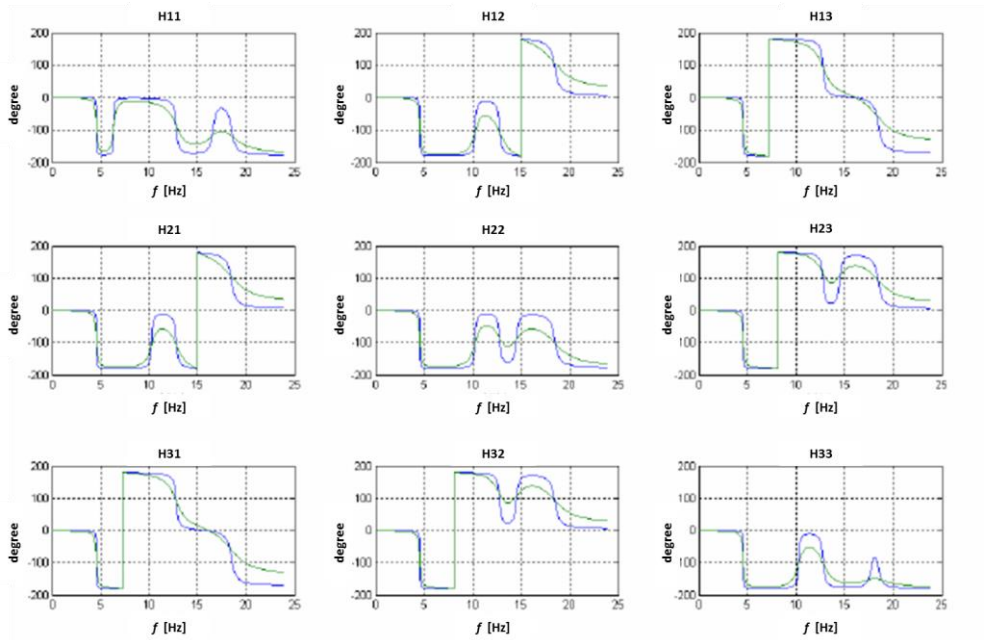

Fig. 2.5. Phase values of the FRFs matrix (blue line if ξ=1%, green line if ξ=5%)

Concluding, is should be highlighted that the construction of the matrix of the FRFs described in **Eq. 2.31** requires a high computational effort because an inverse matrix must be calculated for each frequency value into investigated frequency interval. To overcome this problem, the modal formulation allows to obtain the FRFs exploiting the intrinsic characteristics of the modal model delivering same results through a more efficient way.

2.2.2.2 Frequency response models in the Modal Space

As already stated, the *modal model* is one of the most efficient way to solve the dynamic problem of linear system, because it permits the decoupling of the differential equations that describe the dynamic behavior of the system and maintaining a sort of physical meaning among eigenvalues and eigenvectors on one side with natural frequencies and mode shapes on the other side.

As already stated, the structural response of a general MDOF system expressed in modal coordinates (see **Eq. 2.18**) can be decoupled and solved in the time domain adopting the Duhamel integral, (**Eq. 2.24**). On other hand, an efficient and straightforward approach can be performed transporting the problem in the frequency domain. In this way, the solution of a general linear system expressed by **Eq. 2.30** can be re-written as follows:

$$Q_{\eta k}(\omega) = H_{\eta k}(\omega) \cdot F_k(\omega) \qquad (2.32)$$

where the subscript η of indicates that each component of **Eq. 2.32** is expressed in *modal coordinate* and the subscript k is referred to the number of the coordinate itself. Each term of the FRFs matrix $\mathrm{H_{\eta k}}(\omega)$ in the *Modal Domain* is composed by the FRF expressed by modal parameters defined as follows:

$$H_{\eta k}(\omega) = \frac{1}{\omega_k^2 - \omega^2 + 2\, i\, \xi_k\, \omega\, \omega_k} \qquad (2.33)$$

The vibration modes of the dynamic system can be used to construct the "complete" FRFs matrix in the initial generalized coordinates (e. g. Spatial Model) as shown below:

$$H(\omega) = \Phi \cdot H_{\eta}(\omega) \cdot \Phi^{T} = \sum_{k=1}^{N} H_{\eta k} \cdot \varphi_k \cdot {\varphi_k}^{T} \qquad (2.34)$$

in which H_{η} is a diagonal matrix composed by FRFs calculated in the *Modal Space*, normalized respect to the *modal mass matrix*. As stated, pre- and post-multiply the H_{η} matrix with the *modal matrix* Φ permit to construct the obtained $H(\omega)$ related to each principal mode of the system as described in the following equation:

$$H_{\eta_{(i,j)}}(\omega) = \sum_{k=1}^{N} \frac{[\varphi_i]_k \cdot [\varphi_j]_k}{\omega_k^2 - \omega^2 + 2\, i\, \xi_k \cdot \omega\, \omega_k} \qquad (2.35)$$

It is worth highlighting that the construction of the matrix of the frequency response functions through the modal formulation is much more efficient than that one developed adopting the classical formulation because it involves a reduced number of mathematical operations and it requires a less numerical cost.

Furthermore, the use of the FRFs matrix in the modal domain permits the analysis of the structural response also adopting a limited number of vibration modes. This means that varying the upper limit of the series expressed in **Eqs. 2.34** and **2.35** it is possible to take into account only the contribution of the lower modes which are the most representative of the dynamic behavior of the investigated MDOF system.

Finally, taking into account the response of the system in the *modal space* expressed by **Eq. 2.18** and the relation in the frequency domain described by **Eq. 2.33**, the output response of the MDOF liner system subjected to known excitation forces can be provided by the following formula:

$$Q(\omega) = \sum_{k=1}^{N} \varphi_k \cdot H_{\eta k}(\omega) \cdot F_k(\omega) \qquad (2.36)$$

Numerical example

The simple numerical system previously described was adopted to extract the modal parameters through the *modal formulation*. In this case, too, the damping matrix was constructed respecting the proportionality property with the mass and stiffness distributions. The vibration modes were obtained solving the Eigen-problem expressed by **Eq. 2.10**. Subsequently, the circular frequencies and the natural frequencies were extracted by the relation in **Eq. 2.11**. Meanwhile the damping coefficients related to the principal modes were obtained from the relation expressed in **Eq. 2.7**. so, the amplitude of the FRF associated to each SDOF of the structure in the modal space is depicted in **Fig. 2.6**. The results obtained in the modal space are in agreement with those ones previously obtained using the full FRFs matrix; the natural frequencies can be defined by the abscissa value of the peak of each FRF. It also can be notated that the damping value increases for higher modes.

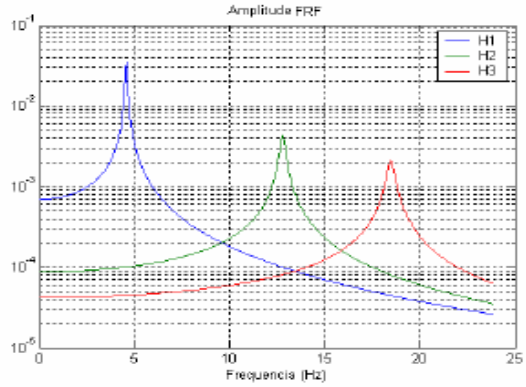

Fig. 2.6. Amplitude values of the FRFs associated to each DOF in the modal space

Table 2.1 summarizes the obtained values of the modal parameters considering the general damping coefficient ξ equal to 1% ($c = 2\xi m\sqrt{k/m}$). In particular are reported also the mode shapes of each mode obtained by the matrix of eigenvectors.

Table 2.1. Frequencies, damping values and mode shapes obtained in the modal spaces

Mode	**Frequency [Hz]**	**Damping [%]**	**Mode Shape**		
			1st	**2nd**	**3rd**
1	4,75	0,45	0.328	0.737	-0.591
2	13,22	1,25	0.591	0.328	0.737
3	19,25	1,80	0.737	-0.591	-0.328

Again, considering the linear time invariant system described in **Eq. 2.1**, the FRF can be also defined as the ratio of the Fourier Transform of the output data $Q(\omega)$ and the Fourier Transform of the input force system $F(\omega)$. In other words, the FRF consists of the Fourier Transform of the impulse response function (IRF) defined by Duhamel integral in **Eq. 2.4**. For a simple system composed by a SDOF system excited by several harmonic inputs with nominal frequency equal to ω_p, the FRF can be expressed as follows:

$$H(\omega) = \frac{Q(\omega)}{F(\omega)} = \frac{1/k}{1 + 2i\xi\left(\frac{\omega_p}{\omega_n}\right) - \left(\frac{\omega_p}{\omega_n}\right)^2} \quad (2.37)$$

Using this notation is also evident that, when the input excitation ω_p approaches the nominal natural frequency ω_n of the system, the entire system is in *resonance* and the phase jumps from the 0 to π, the response is purely imaginary and related to the damping forces. Remarking, the matrix $H_{ij}(\omega)$ can be obtained by the following formula:

$$H_{ij}(\omega) = \sum_{r=1}^{N} H_{ijr} = \sum_{r=1}^{N} \frac{R_{ijr}}{j\omega_p - \lambda_r} + \frac{R_{ijr}^*}{j\omega_p - \lambda_r{}^*} \quad (2.38)$$

where:

$$\lambda_r = -\xi\omega_n \mp j\omega_n\sqrt{1-\xi^2} \quad \text{and} \quad R_{ijr} = \frac{\varphi_{ir}\varphi_{jr}}{j2\omega_{dr}m_r} \quad (2.39)$$

in which the values λ_r are the system poles, or the complex roots of the equations, which provide information about the damped frequencies (imaginary part) and damping ratios (real part), and R_{ijr} are the so-called residuals that contain the mode shape coefficients.

Detailing, the **Eq. 2.38** is the general expression of the FRFs of a MDOF system, and generally called *modal superposition equation* [Bendat and Piersol (1993)], since it sums the contribution of the FRF of each single SDOF system. Furthermore, this matrix is a symmetric matrix, this means that the response measured in the *i-th* point by exciting *j-th* point, is equal to the response measured in the *j-th* point by exciting *i-th* point.

This propriety is intrinsically related to the linear nature of the MDOF system and it provides an important practical information about the mode shape. In fact, considering the symmetry of the matrix $H_{ij}(\omega)$, it is possible to extract the mode shape associated to a specific frequency just knowing one row or one column associated to that defined natural frequency. More specifically, to know the mode shape associated to the first natural frequency of a MDOF system it is enough to know just the first row or the first column of the flexibility matrix $H_{ij}(\omega)$.

Concluding the paragraph, it is worth to highlight that the approach based on frequency response models deserves any problems in case of experimental tests, since it is not adequate to fit experimental data due to the high non-linearity of its inverse problem. Moreover, the dynamic problem referred to experimental data is quite often modelled in the frequency domain using the FRF through the application of the Fourier Transform Function (FTF) that leads to any problems from the time domain into frequency domain.

It is worth mentioning that the FRFs and generally the frequency domain models are suitable for those cases in which the forces acting on the structure could be associated to stochastic realization, such as wind, traffic loads or waves. This condition becomes very important in all those experimental cases where the environmental loads can be treated as stochastic process as well as during the development of an Ambient Vibration Test (AVT) but also in the context of Continuous Dynamic Monitoring (CDM) purposes. Under the hypothesis of stochastic process, the input is not known and, assuming properly statistical conditions, it can be associated to a stationary zero mean Gaussian distributed stochastic process and the system is assumed to be linear and time invariant. Thus, the system response can be described by its correlation function which contain all the dynamic information about the collected random data [Bendat and Piersol (1993)].

From the practical point of view, this relation becomes fundamental for the development of methodologies in the frequency domain. Indeed, the correlation function is used to calculate the power spectral density function through the Fast Fourier Transform (FFT) function in order to identify the frequency content of the recorded experimental data.

In the next paragraph, before to introduce the most powerful methods used for identification problem regard Civil Engineering constructions, the relation between correlation function and power spectral density function will be described in detail, since they represent the core of the most used identification methods also adopted in this Dissertation. This relation describes how the spectral density of stochastic input is related to the spectral density of the measured outputs and how it constitutes the key point of non-parametric frequency domain identification methods.

Such relation is given by FRFs of each SDOF of the representative MDOF system and it works as a linear filter. This means that if the input is assumed a stochastic white noise process then the output is a stochastic process too, scaled by the FRF function which describes the energy content of the system in the bound frequency range. This important passage will be resumed in the next paragraph, but to get a more detailed view, at interested reader is suggested the reading of the following works present in literature: [Bendat and Piersol (1993); Ljung (1999)].

2.2.3 State-space models

As already mentioned in the previous paragraph, in the classical formulation concerning linear-time-invariant (LTI) systems, the solution is obtained separating each differential equation using the orthogonality property of the eigenvectors. This operation is possible only if damping is considered proportional; in fact, under this hypothesis, the modes of a proportional damping structure are equal to those ones obtained in the same non-damped structure. Obviously, this does not happen for real cases where the damping distribution is never proportional to mass and stiffness distribution, and the presence of localized damping might invalidate the hypothesis. The following scheme shows the sequential steps apt to define the stochastic model used to solve identification problem. Hence, the concept of *viscous damping* is introduced, and the dynamic problem is reformulated as a linear combination of independent SDOF system through the use the *state-space-model.*

In this paragraph all fundamental steps to understand the *state-space formulation* are reported, from the general equation of the motion to define the stochastic model used to extract the modal parameters from experimental data collected in operational conditions. Moreover, the state-space model also permits to model the noise content of the signals always present in the experimental tests. The following scheme describes all relevant steps adopted to construct the stochastic state-space model used in the identification problems, since they consist of fundamental steps useful to understand and manage the identification methods based on its implementation implemented in this Dissertation.

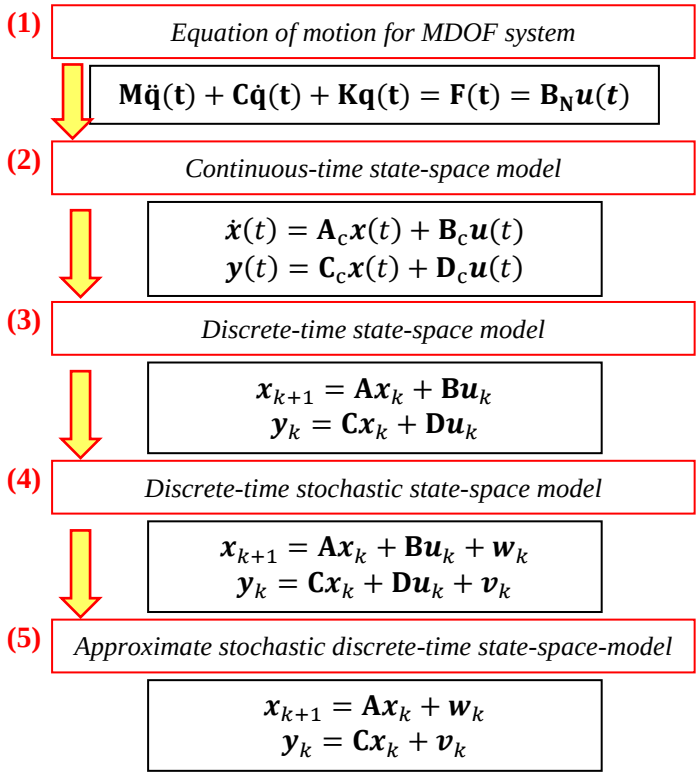

Fig. 2.7. Genesis of the stochastic state-space-model used for general applications

Moreover, this paragraph reports in order: the model in continuous time, the model in discrete time, which considers the discrete nature of collected the time series, and finally the discrete stochastic model. The last model permits to study the structural responses of the dynamic system subjected to unknown input forces and affected by random noise.

2.2.3.1 Continuous-time state-space model

In the state-space formulation, the second order equation of motion of a multi degree of freedom system (MDOF) characterized by *N* degrees of freedom can be expressed as:

$$M \cdot \ddot{q}(t) + C \cdot \dot{q}(t) + Kq \cdot (t) = F(t) = B_N \cdot u(t) \qquad (2.40)$$

where M, C and K are the [*N*-by-*N*] mass, damping and stiffness matrices, respectively, F(t) is the exciting force vector defined by u(t), both at continuous time *t*. The vector q(t) is the solution of the differential equation. It should be noted that, since usually not all the N degrees of freedom of the system are excited, the F(t) vector composed by *N* elements can be replaced by a vector u(t) with dimensions $m<N$ which only takes into account the *m* applied inputs. This input vector u(t) is then multiplied by a [*N*-by-*m*] matrix B_N, mapping the *m* inputs with the *N*-DOFs of the system.

Adopting this formulation, the *N*-dimensional system composed by *N* second-order differential coupled equations can be transformed into an equivalent system of $n=2N$ independent differential equations of the first order. This task can be performed defining the state vector x(t) of *n* components, composed by the vector of displacements q(t) and velocities $\dot{q}(t)$ which depends on the *N*-DOFs of the structure and defining the matrices P and Q as combination of mass, stiffness and damping matrices, as shown in **Eq. 2.41**; finally, the matrix B_N which has dimensions [*N*-by-*m*], is composed of zeros and ones values, mapping the *m*-DOFs of the structure and *N*-DOFs of the numerical model.

$$x(t) = \begin{bmatrix} q(t) \\ \dot{q}(t) \end{bmatrix}; \quad P = \begin{bmatrix} C & M \\ M & 0 \end{bmatrix}; \quad Q = \begin{bmatrix} K & 0 \\ 0 & -M \end{bmatrix}; \quad F(t) = B_N(t) \cdot u(t) \qquad (2.41)$$

Accordingly, the system expressed in **Eq. 2.40** can be substituted by another equivalent system composed by first-order differential equations, which can be re-written in a compact form as follows:

$$P \cdot \dot{x}(t) + Q \cdot x(t) = \begin{bmatrix} B_N \\ 0 \end{bmatrix} \cdot u(t) \qquad (2.42)$$

Considering q(t) as the same generic solution used of the classical formulation, expressed in the **Eq. 2.9**, the solution of the new formulation can be found solving the eigenvalues problem [Peeters (2000)] as shown in the following form:

$$Q \cdot \Psi = -P \cdot \Psi \cdot \Lambda_C \qquad (2.43)$$

The matrices Λ_C and Ψ contain eigenvalues and eigenvectors expressed as follows:

$$\Lambda_C = \begin{bmatrix} \Lambda & 0 \\ 0 & \Lambda^* \end{bmatrix} \ , \ \Psi = \begin{bmatrix} \Theta & \Theta^* \\ \Theta \cdot \Lambda & \Theta^* \cdot \Lambda^* \end{bmatrix} \qquad (2.44)$$

From these equations we can find the relationships that exist between the elements of the aforesaid matrices with the vibrating modes (described by φ_k and λ_k) that characterize the dynamic behavior of the structure (the symbols Λ^* and Θ^* define the complex conjugate values of the obtained eigenvalues and to eigenvectors):

$$\Lambda = \begin{bmatrix} \ddots & & \\ & \lambda_k & \\ & & \ddots \end{bmatrix}; \quad \Theta = [\cdots \quad \varphi_k \quad \cdots] \text{ with } k = 1 \ldots . N \qquad (2.45)$$

In this formulation the matrix Θ that contains the vibration modes does not transform the mass, stiffness and damping matrices, such condition is given by the orthogonality property expressed by the following relationships:

$$\Psi^T \cdot P \cdot \Psi = \begin{bmatrix} \ddots & & \\ & a_k & \\ & & \ddots \end{bmatrix}; \quad \Psi^T \cdot Q \cdot \Psi = \begin{bmatrix} \ddots & & \\ & b_k & \\ & & \ddots \end{bmatrix} \qquad (2.46)$$

These matrices are the *modal matrices*. If the orthogonality conditions were included in **Eq. 2.43**, the resulting matrix Λ_C will be:

$$\Lambda_C = -\begin{bmatrix} \ddots & & \\ & 1/a_k & \\ & & \ddots \end{bmatrix} \cdot \begin{bmatrix} \ddots & & \\ & b_k & \\ & & \ddots \end{bmatrix} \qquad (2.47)$$

As evident the matrix Λ_C is a diagonal matrix in which each component is obtained by the product of the components belong to the diagonal modal matrices previously defined.

State equation

The system described in **Eq. 2.40** can be transformed into an equivalent first-order differential equation system applying some mathematical manipulations. One of the most used possibility is based on the use of so-called *state-space model*. This model is often adopted in Civil Engineering applications because it provides the modal parameters estimations of those structures characterized by a general *viscous damping*. Thus, starting from the **Eq. 2.43** and multiplying both terms for the invers matrix P^{-1} the equilibrium equation (**Eq. 2.40**) can be re-written into so-called *state equation*:

$$\dot{x}(t) = A_C \cdot x(t) + B_C \cdot u(t) \tag{2.48}$$

where $(\bullet)_C$ stands for 'continuous time'. The architecture of the matrices is:

$$\begin{aligned} A_C &= -P^{-1} \cdot Q = \begin{bmatrix} 0 & I \\ -M^{-1}K & -M^{-1}C \end{bmatrix} \\ B_C &= P^{-1} \cdot \begin{bmatrix} B_N \\ 0 \end{bmatrix} = \begin{bmatrix} 0 \\ M^{-1}B_N \end{bmatrix} \end{aligned} \tag{2.49}$$

in which the matrix A_C is a [*n*-by-*n*] square matrix defined as *state matrix* (with *n=2N*), meanwhile B_C is named *input matrix* with dimension [*n*-by-*m*] and x(t) is the *state vector* with dimensions *n*. In this way, recalling the **Eq. 2.47** the relations between the state matrix A_C and the matrices of the eigenvalue Λ_C and the eigenvectors Ψ of the linear system in **Eq. 2.40** can be defined. Thus, pre- and post-multiply both matrices P and Q with the matrix Ψ, such relations are highlighted:

$$\begin{aligned} A_C &= -P^{-1} \cdot Q = -\Psi \cdot diag[1/a_k] \cdot \Psi^{-T} \cdot \Psi^T \cdot diag[b_k] \cdot \Psi^{-1} \\ A_C &= \Psi \cdot \Lambda_C \cdot \Psi^{-1} \Leftrightarrow A_C \cdot \Psi = \Psi \cdot \Lambda_C \end{aligned} \tag{2.50}$$

The last equality in the previous equation proves a very important concept because it demonstrates that eigenvalues and eigenvectors of the matrix A_C are the same values of the eigenvalues and eigenvectors obtained solving the **Eq. 2.43**. This relation says that is possible to extract all modal characteristics of the dynamic system from the matrix A_C.

Again, for clearness, it is worth to remember that the number of elements of the *state vector* indicates the number of independent variables that describe the state of the system, and its dimension corresponds to the double number of DOFs in the referred system. This is due by the fact that the state vector $x(t)$contains the displacement $q(t)$and the velocity $\dot{q}(t)$vectors of the dynamic system.

Observation equation

To complete the *state-space* formulation, another equation must be defined to establish a relation between the outputs of the generalized *N*-DOFs of the system and the values directly measured. In fact, in practical applications it is not possible to measure the structural response associated to all DOFs, so it is usual to refer the collected data to only *l* DOFs on the investigate structure, assuming $l<n$ instrumented points that are generally referred to the displacements, velocities and accelerations associated of such points.

In this way, the so-called *observation equation* establishes the relation among the vector of system response – organized in y(t) – and considering the different contribution of the instrumented sensors, the relation is described in the follows:

$$y(t) = C_a \cdot \ddot{q}(t) + C_v \cdot \dot{q}(t) + C_d \cdot q(t) \qquad (2.51)$$

where y(t) is the measurement vector with dimensions *l*, meanwhile C_a, C_v, C_d with dimension [*l*-by-*N*] are the output location matrices for accelerations, velocities and displacements, respectively. The location matrices are composed by zero or one values to establish the relation between the DOF of the model with those ones measured by installed transducers: accelerometers, velocity and displacement sensors on the structure.

Recalling the **Eq. 2.40** and using the definition of the state vector expressed in **Eq. 2.41**, the matrices C_C and D_C can be re-organize as follows:

$$C_C = [C_d - C_a \cdot M^{-1} \cdot K \quad C_v - C_a \cdot M^{-1} \cdot C_N]$$
$$D_C = C_a \cdot M^{-1} \cdot B_N \qquad (2.52)$$

So, the relationship between the outputs $y(t)$ with the state vector $x(t)$ and the inputs $u(t)$ can be re-written in the compact form as follows:

$$y(t) = C_C \cdot x(t) + D_C \cdot u(t) \qquad (2.53)$$

where C_C is named *output matrix* and D_C is the *direct transmission matrix* with dimensions [*l*-by-*n*] and [*l*-by-*m*], respectively.

State-Space Model

Pacing together the *state equation* (**Eq. 2.48**) and the *observation equation* (**Eq. 2.53**) the *continuous-time deterministic state-space model* of order *N* can be defined as follows:

$$\begin{aligned} \dot{x}(t) &= A_C \cdot x(t) + B_C \cdot u(t) \\ y(t) &= C_C \cdot x(t) + D_C \cdot u(t) \end{aligned} \qquad (2.54)$$

This model allows for establishing the relation between the response of the system y(t) and the deterministic excitation u(t). Important considerations can be made on the A_C matrix; it contains relevant information concerning the fundamental properties of the structure which can be extracted from it. Moreover, the order of the model is defined through the state vector x(t), which contains the displacements q(t) and the velocities q̇(t) of the system. This is the reason way that the order of the state-model is equal to twice the number of DOFs of the structure under analysis.

2.2.3.1.1 State-space model in the Modal Domain

To complete the discussion, the state-space model can be expressed in the *modal domain* introducing the modal coordinate in the state vector as follows:

$$x_m(t) = \Psi^{-1} \cdot x(t) \quad , \quad \Psi = \begin{bmatrix} \Theta & \Theta^* \\ \Theta \cdot \Lambda & \Theta^* \cdot \Lambda^* \end{bmatrix} \qquad (2.55)$$

After some manipulation and considering the decomposition in eigenvalues and eigenvectors of the matrix A_C, the following relations can be obtained:

$$\begin{matrix} {L_C}^T = \Psi^{-1} \cdot B_C \\ V_C = C_C \cdot \Psi \end{matrix} \quad (2.56)$$

Therefore, the state-space model is defined in the modal domain and it called *modal model* and it can be expressed by the system equation reported below:

$$\begin{matrix} \dot{x}_m(t) = \Lambda_C \cdot x_m(t) + {L_C}^T \cdot u(t) \\ y(t) = V_C \cdot x_m(t) + D_C \cdot u(t) \end{matrix} \quad (2.57)$$

An important consideration needs to be highlighted about the physical meaning of the matrix V_C. In fact, the columns of this matrix exactly contain the components of the vibration modes observed by the sensors installed on the structure.

The main advantage of this model is provided by the diagonal values of matrix Λ_C which permits the separation of the contributions of different vibration modes and then to construct a reduced model that takes account only those dominant modes of the structure. A further consideration can be done about structures with proportional damping. In this case the modal model described in **Eq. 2.47** can be simplified adopting a similar model based only on the modal parameters. As it will be shown, this model, obtained by less computational effort, can be used to simulate experimental data. The new model is obtained in the similar way defined in **Eq. 2.57**, introducing a simpler transformation of the modal coordinates in the state vector:

$$x_p(t) = {T_P}^{-1} \cdot x(t) \ , \ T_P = \begin{bmatrix} \Phi & 0 \\ 0 & \Phi \end{bmatrix} \quad (2.58)$$

remarking that the columns of the matrix Φ contain only the components of the vibration modes, which should be real.

Finally, the modal model obtained considering *proportional damping* is defined below:

$$\begin{matrix} \dot{x}_P(t) = A_P \cdot x_P(t) + B_P \cdot u(t) \\ y(t) = C_P \cdot x_P(t) + D_P \cdot u(t) \end{matrix} \quad (2.59)$$

where all matrices can be characterized using by the modal parameters as reported below:

$$A_P = T_P^{-1} A_C \, T_P = \begin{bmatrix} 0 & I \\ -\Omega^2 & -\Gamma \end{bmatrix}$$

$$B_P = T_P^{-1} B_C = \begin{bmatrix} 0 \\ M_m^{-1} \Phi^T B_N \end{bmatrix} \qquad (2.60)$$

$$C_P = C_C T_P = [C_d \Phi - C_a \Phi \Omega^2 \quad C_v \Phi - C_a \Phi \Gamma]$$

$$D_P = D_C = [C_a \Phi M_m^{-1} \Phi^T B_N]$$

obtained considering the following diagonal matrices:

$$\Omega = \begin{bmatrix} \ddots & & \\ & \omega_k & \\ & & \ddots \end{bmatrix} \quad \Gamma = \begin{bmatrix} \ddots & & \\ & 2\xi_k \omega_k & \\ & & \ddots \end{bmatrix} \quad M_m = \begin{bmatrix} \ddots & & \\ & m_k & \\ & & \ddots \end{bmatrix} \qquad (2.61)$$

Numerical example

Using the matrices M, K and C associated to the 3-DOFs the continuous-time matrices A_C, B_C, C_C and D_C are composed as described in **Eq. 2.49**. As stated, all dynamic properties of the system are defined in the state matrix A_C. Thus, the eigenvalues will be extracted from it.

Ac =

	x1	x2	x3	x4	x5	x6
x1	0	0	0	1	0	0
x2	0	0	0	0	1	0
x3	0	0	0	0	0	1
x4	-9014.42	4507.21	0	-2.6854	1.3427	0
x5	4507.21	-9014.42	4507.21	1.3427	-2.6854	1.3427
x6	0	4507.21	-4507.21	0	1.3427	-1.3427

Bc =

	u1	u2	u3
x1	0	0	0
x2	0	0	0
x3	0	0	0
x4	0.4808	0	0
x5	0	0.4808	0
x6	0	0	0.4808

Cc =

	x1	x2	x3	x4	x5	x6
y1	-9014.42	4507.21	0	-2.6854	1.3427	0
y2	4507.21	-9014.42	4507.21	1.3427	-2.6854	1.3427
y3	0	4507.21	-4507.21	0	1.3427	-1.3427

Dc =

	u1	u2	u3
y1	0.4808	0	0
y2	0	0.4808	0
y3	0	0	0.4808

As shown A_C is a [*n*-by-*n*] square matrix with double dimension of the initial system. Applying the *eig* function implemented in the commercial software MatLab, the eigenvalues and eigenvectors of the dynamic system are extracted obtaining the following matrices:

$\Lambda_C =$

-2.180 +	120.95 *i*	0.000 +	0.00 *i*	0.000 +	0.00 *i*	0.000 +	0.00 *i*	0.000 +	0.00 *i*	0.000 +	0.00 *i*
0.000 +	0.00 *i*	-2.180 -	-120.95 *i*	0.000 +	0.00 *i*	0.000 +	0.00 *i*	0.000 +	0.00 *i*	0.000 +	0.00 *i*
0.000 +	0.00 *i*	0.000 +	0.00 *i*	-1.044 +	83.71 *i*	0.000 +	0.00 *i*	0.000 +	0.00 *i*	0.000 +	0.00 *i*
0.000 +	0.00 *i*	0.000 +	0.00 *i*	0.000 +	0.00 *i*	-1.044 -	-83.71 *i*	0.000 +	0.00 *i*	0.000 +	0.00 *i*
0.000 +	0.00 *i*	0.000 +	0.00 *i*	0.000 +	0.00 *i*	0.000 +	0.00 *i*	-0.133 +	29.88 *i*	0.000 +	0.00 *i*
0.000 +	0.00 *i*	0.000 +	0.00 *i*	0.000 +	0.00 *i*	0.000 +	0.00 *i*	0.000 +	0.00 *i*	-0.133 -	-29.88 *i*

$\Psi_C =$

0.0001 +	0.0049 *i*	0.0001 -	0.0049 *i*	-0.0001 -	0.0088 *i*	-0.0001 +	0.0088 *i*	0.0000 -	0.0110 *i*	0.0000 +	0.0110 *i*
-0.0001 -	0.0061 *i*	-0.0001 +	0.0061 *i*	0.0000 -	0.0039 *i*	0.0000 +	0.0039 *i*	-0.0001 -	0.0198 *i*	-0.0001 +	0.0198 *i*
0.0000 +	0.0027 *i*	0.0000 -	0.0027 *i*	0.0001 +	0.0071 *i*	0.0001 -	0.0071 *i*	-0.0001 -	0.0247 *i*	-0.0001 +	0.0247 *i*
-0.591 +	0 *i*	-0.591 +	0 *i*	0.737 +	0 *i*	0.737 +	0 *i*	0.328 +	0 *i*	0.328 +	0 *i*
0.737 +	0 *i*	0.737 +	0 *i*	0.328 +	0 *i*	0.328 +	0 *i*	0.591 +	0 *i*	0.591 +	0 *i*
-0.328 +	0 *i*	-0.328 +	0 *i*	-0.591 +	0 *i*	-0.591 +	0 *i*	0.737 +	0 *i*	0.737 +	0 *i*

As previously stated, the eigenvalues are grouped in pair of complex and conjugated values, as well as the eigenvectors. From the values reported in Λ_C using **Eq. 2.17** it is possible to extract the damping values (ξ_k) and the circular frequencies (ω_k) and consequently the natural frequencies associated to investigated system from the obtained eigenvalues λ_k.

$\mathrm{diag}(\Lambda_C) =$

-2.180 +	120.95 *i*
-2.180 -	120.95 *i*
-1.044 +	83.71 *i*
-1.044 -	83.71 *i*
-0.133 +	29.88 *i*
-0.133 -	29.88 *i*

$$\xi = \begin{bmatrix} 0.0180 \\ 0.0125 \\ 0.0045 \end{bmatrix} \rightarrow \xi = \begin{bmatrix} 1.80 \\ 1.25 \\ 0.45 \end{bmatrix} \ [\%]$$

$$\omega = \begin{bmatrix} 120.935 \\ 83.704 \\ 29.877 \end{bmatrix} \ [\mathrm{rad}] \rightarrow f = \begin{bmatrix} 19.247 \\ 13.322 \\ 4.755 \end{bmatrix} \ [\mathrm{Hz}]$$

It should be noted that in the last three rows of the matrix Ψ_C are located the vibration modes of the structure, each one associated to respective eigenvalues in matrix Λ_C. As demonstrated the modes coincide with those ones obtained in the classical formulation, although eigenvectors are duplicated because they are reported their original values together with their respective conjugates. Furthermore, being the damping matrix proportional to the mass and the stiffness distribution, the resulting modes of the system should be real, as demonstrated by the columns of Ψ_C in which the imaginary part of the components is zero.

Finally, to obtain the observable modal components, the matrix Ψ_C should be multiplied for the matric C_C, as shown in **Eq. 2.56**. In this example all DOFs of the system were designed as reference points, therefore the resulting mode shapes provide the same modal component obtained through the classical formulation, which could differ only by a constant value.

2.2.3.2 Discrete-time state-space model

The models described up to now are all continuous over time. But in real applications, experimental data always have discrete nature, in fact the analog signals recorded by different transducers are converted to digital data by an analog to digital converter (A/D) and then stored and processed by a computer. Therefore, all available information on dynamic systems is always digitalized. However, a discrete time version of the previously presented model is more appropriate to fit experimental data. Therefore, a *discrete-time state-space model* is characterized by the following equation:

$$\begin{aligned} x_{k+1} &= A \cdot x_k + B \cdot u_k \\ y_k &= C \cdot x_k + D \cdot u_k \end{aligned} \qquad (2.62)$$

The continuous time function $x(t)$, $y(t)$ and $u(t)$ are replaced by series of values x_k, y_k and u_k defined in the discrete time instant $k\Delta t$, with $k \in \mathbb{N}$ and Δt is the adopted sampling interval: x_k=$x(k \cdot \Delta t)$.

If the time functions that connect two consecutive discrete samples are assumed to be constant (zero-order-hold assumption, ZOH) [Juang (1994)], the continuous-time model matrices A_C, B_C, C_C, D_C are related with their owns discrete-time matrices A, B, C, D by the following expressions:

$$\begin{aligned} A &= e^{A_c \Delta t} \qquad B = \int_0^{\Delta t} e^{A_c \tau} d\tau \cdot B_c \\ C &= C_c \qquad\quad D = D_c \end{aligned} \qquad (2.63)$$

In the first expression of the equations reported above, the relation between the matrices A_C and A is described. Furthermore, performing the McLaurin decomposition of the second equality, it is possible to relate the model matrix in the discrete time *A* with its corresponding continuous matrix A_C as follows:

$$A = e^{A_C \cdot \Delta t} = I + (A_C \cdot \Delta t) + \frac{(A_C \cdot \Delta t)^2}{2!} + \frac{(A_C \cdot \Delta t)^3}{3!} + \cdots \qquad (2.64)$$

Recalling the **Eq. 2.50** and substituting the eigenvalues decomposition, it can be stated that the eigenvectors of matrix A coincide with the eigenvectors of matrix A_C:

$$A_C = \Psi \cdot \Lambda_C \cdot \Psi^{-1}$$
$$A = e^{A_C \cdot \Delta t} = e^{\Psi \cdot \Lambda_C \cdot \Psi^{-1} \cdot \Delta t} = \Psi \cdot e^{A_C \cdot \Delta t} \cdot \Psi^{-1} = \Psi \cdot \Lambda_D \cdot \Psi^{-1} \quad (2.65)$$

where Λ_D contains exactly the eigenvalues of the *state matrix A* correlated as follows:

$$\Lambda_D = \begin{bmatrix} \ddots & & \\ & \mu_k & \\ & & \ddots \end{bmatrix}; \quad \mu_k = e^{\lambda_k \Delta t} \leftrightarrow \lambda_k = \frac{\ln(\mu_k)}{\Delta t} \quad (2.66)$$

Consequently, it is proven that once a discrete-time state-space model has been identified from experimental data; the modal parameter of the tested structure can be easily estimated. In particular, the natural frequencies and the modal damping ratio are obtained from the eigenvalues of A using **Eq. 2.11**. meanwhile, as it will be demonstrated, the eigenvectors of A coincide with the eigenvectors of A_C.

Numerical example

For the academic structure were calculated the system matrices A and C in the discrete time formulation starting from the matrices A_C and C_C of the continuous model. The new matrices have been obtained after transposing the system from the continuous time to discrete time domain applying the relation in **Eq. 2.63**. This task has been performed using the functions *ss* and *c2d* included in the MatLab and adopting a time variation Δt=0.02. As shown below, after the transformation the matrices A and C have a different design from their corresponding matrices in the continuous time (A_C and C_C); meanwhile, the matrices B and D maintain the same characteristics of B_C and D_C from in continuous model to discrete model.

As stated, all dynamic properties of the investigated system are included in the state matrix A. Therefore, inspecting the eigenvalues of A it can be proved that they are equal to those ones belong to A_C, as described by **Eq. 2.66**. Therefore, using the *eig* function, the following matrices Λ_D and Ψ are derived, in which eigenvalues and eigenvectors of A are reported.

A =

	x1	x2	x3	x4	x5	x6
x1	-0.2062	0.4466	0.1016	0.0102	0.0042	0.0005
x2	0.4466	-0.1046	0.5483	0.0042	0.0107	0.0047
x3	0.1016	0.5483	0.3421	0.0005	0.0047	0.0148
x4	-72.8500	10.4000	16.6200	-0.2279	0.4497	0.1066
x5	10.4000	-56.2300	27.0200	0.4497	-0.1213	0.5563
x6	16.6200	27.0200	-45.8300	0.1066	0.5563	0.3284

B =

	u1	u2	u3
x1	0.0001	0	0
x2	0	0.0001	0
x3	0	0	0.0001
x4	0.0049	0.0020	0.0002
x5	0.0020	0.0051	0.0022
x6	0.0002	0.0022	0.0071

C =

	x1	x2	x3	x4	x5	x6
y1	-9014.42	4507.21	0	-2.69	1.34	0
y2	4507.21	-9014.42	4507.21	1.34	-2.69	1.34
y3	0	4507.21	-4507.21	0	1.34	-1.34

D =

	u1	u2	u3
y1	0.4808	0	0
y2	0	0.4808	0
y3	0	0	0.4808

Consequently, extracting the non-null values from the matrix Λ_D can be highlight that the eigenvalues of the discrete state-space model are grouped in complex and conjugate pair.

Performing the **Eq. 2.66** the modal parameters of the system can be easily defined confirming the relation expressed in **Eq. 2.65**. as shown, the eigenvalues of the state matrix A_C have the same values of A belong to the discrete state-space model.

Λ_d =

-0.718 +	0.63 *i*	0.000 +	0.00 *i*	0.000 +	0.00 *i*	0.000 +	0.00 *i*	0.000 +	0.00 *i*	0.000 +	0.00 *i*
0.000 +	0.00 *i*	-0.718 -	0.63 *i*	0.000 +	0.00 *i*	0.000 +	0.00 *i*	0.000 +	0.00 *i*	0.000 +	0.00 *i*
0.000 +	0.00 *i*	0.000 +	0.00 *i*	-0.101 +	0.97 *i*	0.000 +	0.00 *i*	0.000 +	0.00 *i*	0.000 +	0.00 *i*
0.000 +	0.00 *i*	0.000 +	0.00 *i*	0.000 +	0.00 *i*	-0.101 -	0.97 *i*	0.000 +	0.00 *i*	0.000 +	0.00 *i*
0.000 +	0.00 *i*	0.000 +	0.00 *i*	0.000 +	0.00 *i*	0.000 +	0.00 *i*	0.824 +	0.56 *i*	0.000 +	0.00 *i*
0.000 +	0.00 *i*	0.000 +	0.00 *i*	0.000 +	0.00 *i*	0.000 +	0.00 *i*	0.000 +	0.00 *i*	0.824 -	0.56 *i*

Ψ_d =

-0.0001 -	0.0049 *i*	-0.0001 +	0.0049 *i*	-0.0001 -	0.0088 *i*	-0.0001 +	0.0088 *i*	0.0000 -	0.0110 *i*	0.0000 +	0.0110 *i*
0.0001 +	0.0061 *i*	0.0001 -	0.0061 *i*	0.0000 -	0.0039 *i*	0.0000 +	0.0039 *i*	-0.0001 -	0.0198 *i*	-0.0001 +	0.0198 *i*
0.0000 -	0.0027 *i*	0.0000 +	0.0027 *i*	0.0001 +	0.0071 *i*	0.0001 -	0.0071 *i*	-0.0001 -	0.0247 *i*	-0.0001 +	0.0247 *i*
0.591 +	0 *i*	0.591 +	0 *i*	0.737 +	0 *i*	0.737 +	0 *i*	0.328 -	0 *i*	0.328 +	0 *i*
-0.737 +	0 *i*	-0.737 +	0 *i*	0.328 -	0 *i*	0.328 +	0 *i*	0.591 -	0 *i*	0.591 +	0 *i*
0.328 +	0 *i*	0.328 +	0 *i*	-0.591 +	0 *i*	-0.591 -	0 *i*	0.737 -	0 *i*	0.737 +	0 *i*

From the comparison between the eigenvectors' matrix Ψ_C in the continuous time and the eigenvectors matrix Ψ derived in the discrete time, the columns coincide (differing just for a constant value) and they characterize the same modes.

$\text{diag}(\Lambda_d) = \mu_k =$

-0.718 +	0.63 *i*
-0.718 -	0.63 *i*
-0.101 +	0.97 *i*
-0.101 -	0.97 *i*
0.824 +	0.56 *i*
0.824 -	0.56 *i*

$\rightarrow$ $\lambda_k =$

-2.185 +	120.96 *i*
-2.185 -	120.96 *i*
-1.043 +	83.71 *i*
-1.043 -	83.71 *i*
-0.135 +	29.88 *i*
-0.135 -	29.88 *i*

$\rightarrow$ $\xi = \begin{bmatrix} 1.80 \\ 1.25 \\ 0.45 \end{bmatrix}$ [%]

$\rightarrow$ $f = \begin{bmatrix} 19.247 \\ 13.322 \\ 4.755 \end{bmatrix}$ [Hz]

2.2.3.3 Introduction to stochastic process

In the previously presented modes is assumed that the input time functions are known or using other words, that the input forces can be expressed in deterministic form. Otherwise, in the context of Operational Modal Analysis, the input excitation is unknown, and it is represented by a stochastic process, which also takes into account the noise effects in the model.

A stochastic process is a set of *n* (with n → ∞) time dependent random functions, also designed by realizations, associated to characterize one or several variables. In this way, the characterization of the variables (i.e., a set of excitation forces) can be done through the statistical properties of the realizations themselves. In practical applications, is common to assume that stochastic processes are stationary, ergodic and zero mean. Stationary means that the statistical properties of the processes are constant over time. The zero-mean assumption is valid because the measured time signals are commonly de-trended before being processed. Ergodicity means that the statistical properties (of the measured signals) can be calculated either considering average values over many realizations at a certain time instant or using the average values of just one realization over time. On other words, a stochastic process is called ergodic when statistical averages converge almost everywhere at average times. A necessary condition for ergodicity is therefore stationarity. In particular, the ergodicity of the mean value is obtained when the temporal and the statistical averaged value coincide; meanwhile, in case of correlation, the ergodicity is verified when the statistical auto-correlation and the temporal auto-correlation coincide. For continuous time stochastic process $y(t)$ with n_y components, the correlation matrix can be expresses as:

$$\Sigma_{yy}(\tau) = E[y(t) \cdot y(t+\tau)^T] = \lim_{T\to\infty} \frac{1}{T} \int_{-T/2}^{+T/2} y(t) \cdot y(t+\tau)^T \, dt \qquad (2.67)$$

where $\Sigma_{yy}(\tau)$ is a [n_y-by-n_y] square matrix that depends on considered time-lag (τ). The elements in the diagonal are designed auto-correlations otherwise cross-correlations.

In the context of modal analysis, most of the dynamic identification techniques are directly applied to the correlation functions of the measured structural responses. In fact, the correlation matrix contains all the important information of the random data associated to the time responses of the system. Therefore, for discrete time signals the correlation function is only defined for $t \geq 0$, the integral is replaced by a series of sum:

$$\Sigma_{yy}(\tau) = E[y_k \cdot {y_{k+\tau}}^T] = \lim_{n_t \to \infty} \frac{1}{n_t} \sum_{t=0}^{n_t-1} y_k \cdot {y_{k+\tau}}^T \qquad (2.68)$$

The left term of the equation is referred to the expected auto-correlation function of the time signals $y(t)$. In fact, E[•] is the expected value operator, which provides the average value when the realizations of the stochastic process approaches infinite, and y_k is the value of $y(t)$ at the time instant $k \cdot \Delta t$.

Hence, the auto-correlation function provides a measure of the similarity and the common properties between the original signal with its time-shifted version. In other words, it provides the correlation of the time signal with its own past and future values. For stationary processes, the auto-correlation depends only on the time-shift and gives the information about how quickly the process changes respect to the time. Moreover, an infinite number of samples is not available in real applications; thus, an estimate of the correlation is obtained by limiting the series to a finite number of samples. In the similar way it is estimated the cross-correlation function. This function provides the information about the correlation degree of two different time signals *y* and *x*:

$$\Sigma_{yx}(\tau) = E[y_k \cdot {x_{k+\tau}}^T] = \lim_{n_t \to \infty} \frac{1}{n_t} \sum_{t=0}^{n_t-1} y_k \cdot {x_{k+\tau}}^T \qquad (2.69)$$

Concluding, the correlation function describes how an instantaneous observation depends upon previously occurring observations. Furthermore, due to zero mean assumption of the time signals, in the applications of modal analysis the covariance functions coincide with the correlation functions. Therefore, in the signal processing, it is common to use indistinctively both terms: correlation and covariance.

2.2.3.4 Stochastic discrete-time state-space model

As already mentioned, when structures are subjected to a non-deterministic excitation, the responses can not be predicted, and it is convenient to characterize the excitation through the use of probabilistic concepts and to idealize it through a stochastic process. In general cases, experimentally collected data are always affected by noise, which can not be measured individually, but it has been taken into account in the models, adding a stochastic component that represents it. Therefore, noise has to be considered in the discrete-time state-space model (see **Eq. 2.62**) including two statistical components. The obtained model is referred as *stochastic discrete-time state-space model*:

$$\begin{aligned} x_{k+1} &= A \cdot x_k + B \cdot u_k + w_k \\ y_k &= C \cdot x_k + D \cdot u_k + v_k \end{aligned} \qquad (2.70)$$

where vectors w_k and v_k represent two stochastic processes due to noise content in the signals. Specifically, the former it is due to modeling inaccuracies and the latter is due to measurement noise due to sensor inaccuracy. Further consideration should be done in order to explain exactly the final stochastic model used in the identification problems. In fact, it should be noted that both these immeasurable vectors are assumed to be zero-mean realizations of stochastic processes with the following covariance matrices:

$$\begin{aligned} &E\left(\begin{bmatrix} w_p \\ v_p \end{bmatrix} \begin{bmatrix} w_p^{\mathrm{T}} & v_p^{\mathrm{T}} \end{bmatrix}\right) = \begin{bmatrix} \mathrm{Q} & \mathrm{S} \\ \mathrm{R} & \mathrm{S}^{\mathrm{T}} \end{bmatrix} \\ &E\left(\begin{bmatrix} w_p \\ v_p \end{bmatrix} \begin{bmatrix} w_q^{\mathrm{T}} & v_q^{\mathrm{T}} \end{bmatrix}\right) = 0 \;\; p \neq q \end{aligned} \qquad (2.71)$$

where p and q are two arbitrary time instants. Since the correlation matrices of the processes w_k and v_k are assumed to be zero for any time delay $\tau = q - p$ different from zero, each new observation is independent from the previous ones. Such random stochastic process is defined as *white noise* process. In the context of vibration tests and OMA techniques, the excitation acting on the structure is not measured and the discrete vector u_k is unknown. Thus, a further approximation can be done assuming white noise excitation. Under this hypothesis, the unknown excitation is included in the noise terms to define the *approximate stochastic discrete-time state-space model* as follows:

$$\begin{aligned} x_{k+1} &= A \cdot x_k + w_k \\ y_k &= C \cdot x_k + v_k \end{aligned} \qquad (2.72)$$

where the terms w_k and v_k are slightly different than the quantities already introduced in **Eq. 2.70**, they represent the effect of noise indeed the model under the assumption that the inputs are also realizations of white noise processes. Thus, vectors w_k and v_k are now representing the effect of unknown inputs, modelling inaccuracies and measured noise. It is worth noting that the system expressed in **Eq. 2.72** is an approximation of the reality that has consequences on the results of the identification methods. This aspect will be deeply discussed during the development of the most used identification techniques in the next paragraphs.

2.2.3.5 Properties of the stochastic model

For clearness, some properties of the *stochastic state-space model* presented in **Eq. 2.72** must be explain in order to highlight the main properties of the identification techniques based on its development [Van Overschee and De Moore (1996), Inman (2006)].

First, the basic assumption is that the state vector x_k can be represented as a stationary stochastic process, this means that the expected mean values of the states (expected means that it is theoretically related to an infinite number of samples) is zero. Moreover, the expected covariance matrix in instant time $\tau=0$ is independent of the time instant k, implying that the matrix A is a stable matrix (or rather it evolves within a certain bound related to a specific range of the response for all time instants k), and it can be defined by the n-dimensional matrix Σ. This information can be resumed as follows:

$$E[x_k] = 0\,, \qquad \Sigma_{xx_k} = E\left[x_k \cdot x_k^T\right] \qquad (2.73)$$

Furthermore, regarding the vectors w_k and v_k in **Eq. 2.70**, they are also assumed as zero means realization of stochastic process with the covariance matrix expressed in **Eq. 2.71**.

In addition, since these vectors are independent from the state vector, their expected values are zero, as described in the following equation:

$$E\left[x_k \cdot w_k^T\right] = 0 \quad , \quad E\left[x_k \cdot v_k^T\right] = 0 \tag{2.74}$$

Taking in to account the above properties and the relations in **Eqs. 2.72**, **2.73** and **2.74** it can be obtained the following relation for *discrete-time stochastic state-space models*:

$$\begin{aligned} \Sigma_{xx_{k+1}} &= E[x_{k+1} \cdot {x_{k+1}}^T] \\ &= E[(A \cdot x_k + w_k) \cdot (A \cdot x_k + w_k)^T] \\ &= A \cdot E[x_k \cdot {x_k}^T] \cdot A^T + E[w_k \cdot {w_k}^T] \\ &= A \cdot \Sigma_{xx_k} \cdot A^T + Q \end{aligned} \tag{2.75}$$

This relation is also called the *Lyapunov equation* for the state covariance matrix, which confirms the stability of the state matrix A. on other words, it means that the energy associated to the state in the instant *k* converge to the energy of the state in the successive instant *k+1*, and this is true for any time instant *k*. Furthermore, it is possible to define the output covariance matrices of the response $y(t)$. In discrete time, the output covariance matrix can be written as:

$$R_i = \Sigma_{yy_i} = E\left[y_{k+i} \cdot y_k^T\right] \tag{2.76}$$

where *i=1, ..., p+q* is an arbitrary value of the time-lags, generally *p+1=q*.

By considering the model in **Eq. 2.72**, and the properties in **Eqs. 2.71**, **2.73** and **2.74**, Σ_{yy_0} is defined as:

$$\begin{aligned} R_0 = \Sigma_{yy_0} &= E\left[y_k \cdot y_k^T\right] \\ &= E[(C \cdot x_k + v_k) \cdot (C \cdot x_k + v_k)^T] \\ &= C \cdot E[x_k \cdot {x_k}^T] \cdot C^T + E[v_k \cdot {v_k}^T] \\ &= C \cdot \Sigma_{xx} \cdot C^T + R \end{aligned} \tag{2.77}$$

In the same way, the use of previous equations allows to write the definition of the covariance matrix Σ_{xy} between the next state and the reference output as:

$$\begin{aligned} G = \Sigma_{xy} &= E\left[x_{k+1} y_k^T\right] \\ &= E[(A \cdot x_k + w_k) \cdot (C \cdot x_k + v_k)^T] \\ &= A \cdot E[x_k \cdot {x_k}^T] C^T + E[w_k \cdot {v_k}^T] \\ &= A \cdot \Sigma_{xx} \cdot C^T + S \end{aligned} \tag{2.78}$$

Finally, using some mathematical manipulations, as described in [Bernal (2008)], and exploiting the discrete-time state equation as follow:

$$\begin{aligned} &x_1 = A \cdot x_0 + w_0 \\ &x_2 = A \cdot x_1 + w_1 = A \cdot (A \cdot x_0 + w_0) + w_1 = A^2 \cdot x_1 + A \cdot w_0 + A \cdot w_1 \\ &\vdots \\ &x_{k+1} = A^i \cdot x_k + A^{i-1} \cdot w_k + A^{i-2} \cdot w_{k+1} + \cdots + w_{k+i-1} \end{aligned} \tag{2.79}$$

And post-multiplying by ${x_k}^T$ and considering the covariance matrix calculated between different time instant *k*, the relation obtained is:

$$E[x_{k+1} \cdot {x_k}^T] = A^i \cdot E[x_k \cdot {x_k}^T] = A^i \cdot \Sigma \tag{2.80}$$

By substituting **Eq. 2.80** in **Eq. 2.77** and considering **Eq. 2.78**, after any mathematical simplification it is possible to re-write the output covariance matrix (see **Eq. 2.76**) as:

$$\begin{aligned} R_i &= C \cdot A^{i-1} \cdot G \\ R_{-i} &= G^T \cdot \left(A^{i-1}\right)^T \cdot C^T = {R_i}^T \end{aligned} \tag{2.81}$$

This last property is very important because it constitutes the solution of the stochastic identification methods based on state-space models. Since it relates the output covariance sequence, which can be estimated by the experimental data, with the state matrix *A*, and from this one to identify the modal parameters of the structure, as it will be demonstrate in the next paragraph. Finally, the property expressed in the last equation can be defined also using the modal parameters obtained the following relation:

$$\begin{aligned} \Lambda_i = R_i &= C \cdot A^{i-1} \cdot G \\ &= C \cdot \Psi^T \cdot \Lambda^{i-1} \cdot \Psi^T \cdot G \\ &= V \cdot \Lambda^{i-1} \cdot G_m \end{aligned} \tag{2.82}$$

in which G_m plays the role of the modal participation matrix in input-output models.

2.2.4 Auto-spectra and cross-spectra functions

The models presented in the previous paragraphs have been developed adopting the main hypothesis of stochastic process of the input excitation with normal distribution and zero mean value (i.e., $p \rightarrow$ N (0, σ)). This property is very common in many natural phenomena, also confirmed by the Central Limit theorem which describes that the sum of a considerable number of independent random variables, each one composed by its own independent distribution, tends to a Gaussian distribution. Moreover, if the stochastic process is stationary and ergodic, the auto-correlation function is independent from the time instants t_i and t_j but it depends only on the time interval $\tau = t_j - t_i$.

Consequently, the stochastic process can be defined by a realization of the process $(x_e(t))$ which depends only on this time-lag. So, auto-correlation function is defined as:

$$R_{xx}(\tau) = \lim_{T\to\infty} \frac{1}{T} \int_{-T/2}^{+T/2} x_e(t) \cdot x_e(t+\tau) \quad dt \qquad (2.83)$$

It is worth to mentioning that the auto-correlation function tends to zero in relation to the irregularity of the time series involved, more irregularity of process means faster decay of the function. For clarity, the auto-correlation functions associated to zero mean stationary stochastic processes are symmetrical functions with maximum value in the origin $(\tau = 0)$ in which the ordinate is given by the standard deviation of the process.

The auto-correlation function can be transposed in the frequency domain through the use of the *Fourier Transform* obtaining the so-called a*uto-spectrum function*:

$$S_{xx}(\omega) = \int_{-\infty}^{+\infty} R_{xx}(\tau) \cdot e^{-i\cdot\omega\cdot\tau}\, d\tau \qquad (2.84)$$

The auto-spectrum function quantifies the distribution of the energy content associated to the signal in terms of frequencies. In fact, the area underlying the function represents the total energy content of the signal. Furthermore, for white noise signals the energy value is

given by just its variance value. The concepts considered for the definition of the auto-correlation and auto-spectrum functions defined in the **Eqs. 2.83** and **2.84**, can be also adopted to define the cross-correlation and the cross-spectrum functions:

$$R_{x_1x_2}(\tau) = \lim_{T\to\infty} \frac{1}{T} \int_{-T/2}^{+T/2} x_{1e}(t) \cdot x_{2e}(t+\tau) \quad dt \tag{2.85}$$

$$S_{x_1x_2}(\omega) = \int_{-\infty}^{+\infty} R_{x_1x_2}(\tau) \cdot e^{-i\cdot\omega\cdot\tau}\, d\tau \tag{2.86}$$

The cross-spectra function, also called *cross-spectral density function*, can be obtained using an alternative way. Applying the Fourier Transform to the realization of the stochastic process, as defined in the following expression:

$$S_{x_1x_2}(\omega) = \lim_{\substack{T\to\infty \\ n\to\infty}} \frac{1}{n} \sum_{e=1}^{n} \frac{F_{T,e}[x_1(t)]^* \cdot F_{T,e}[x_2(t)]}{T} \tag{2.87}$$

The term $F_{T,e}[x_1(t)]$ is the Fourier Transform of the realization x_e associated to the process $x_1(t)$ in the interval [-T/2, T/2]. This expression can also be used to calculate the auto-spectrum function considering $x_2 = x_1$. It is worth to highlight that the auto-spectrums are functions with real components because they are obtained from the multiplication between a complex number for its complex conjugate. Meanwhile, the cross-spectrums are complex functions as evident.

In case of different processes associated to several physical phenomena that maintain the characteristics of stationarity and ergodicity, is possible to define a vector stochastic process. In this case, the scalar function of the auto-correlation is substituted by a correlation matrix in which the diagonal elements define the auto-correlations and the extra-diagonal ones are the cross-correlations. Grouping different stationary stochastic processes into vector $y(t)$, the correlation matrix can be defined by the follows:

$$R_y(\tau) = E[y(t) \cdot y(t+\tau)^T] = \lim_{T\to\infty} \frac{1}{T} \int_{-T/2}^{+T/2} y(t) \cdot y(t+\tau)^T \, dt \qquad (2.88)$$

In order to estimates the modal parameters of a dynamic system using only its output, special attention deserves the output-spectrum, which obviously depends on the input spectrum and on the characteristics of the dynamic system. Therefore, if the initial hypothesis on the input is verified and it is assumed as white noise process, their continuous-time correlation matrix function is given by:

$$R_y(\tau) = R_y \cdot \delta(\tau) \qquad (2.89)$$

In which R_y in a [n_i-by-n_i] constant matrix and $\delta(\tau)$ is the Dirac delta function that has the following properties:

$$\begin{gathered} \delta(\tau) = 0 \quad if \quad t = 0 \\ \delta(\tau) = 0 \ \text{elsewhere} \\ \int_{-\infty}^{+\infty} f(t)\delta(t-a)dt = f(a) \end{gathered} \qquad (2.90)$$

Consequently, due to the property of the $\delta(\tau)$ function, the input spectrum is a constant matrix equal to R_y. This implies that the spectrum is "flat", which means that the energy associated to the input signal is uniformly distributed along the frequency axis. In the following equation is summarized the main concept previously described. In fact, the relation between the stochastic excitations and the output responses of the structure subjected to random actions can be expressed by relation between the spectrum of the output response S_{yy} and the input spectrum S_{uu} as follows:

$$S_{yy}(\omega) = H(\omega) \cdot S_{uu}(\omega) \cdot H^H(\omega) \qquad (2.91)$$

When the input is assumed to be a white noise process, the output spectrum of the system only depends on the system transfer function H(ω) and on the constant matrix R_p:

$$S_{yy}(\omega) = H(\omega) \cdot R_p \cdot H^H(\omega) \qquad (2.92)$$

Moreover, if the input signals can be defined using white noise process and they are also statistical independent, the cross-correlation are zero and the constant matrix becomes a diagonal matrix. In this case, recalling the **Eq. 2.35** reported below:

$$H_{i,j}(\omega) = \sum_{k=1}^{N} \frac{[\varphi_i]_k \cdot [\varphi_j]_k}{\omega_k^2 - \omega^2 + 2\, i\, \xi_k\, \omega\, \omega_k} \qquad (2.93)$$

the contribution provided by a general *k-mode* on any elements of the output spectrum can be calculated using the following expression:

$$S_{q_{(i,j)}}{}^{k}(\omega) = \sum_{k=1}^{N} \frac{[\varphi_i]_k \cdot [\varphi_j]_k}{\omega_k^2 - \omega^2 + 2\, i\, \xi_k\, \omega\omega_k} \cdot R_p \cdot \frac{[\varphi_i]_k \cdot [\varphi_j]_k}{\omega_k^2 - \omega^2 + 2\, i\, \xi_k\, \omega\, \omega_k} \qquad (2.94)$$

This formula turns be very interesting because it divides the contribution of each mode for the spectrum system and it also defines the relation between the output spectra matrix with the modal properties of the structure. Taking into account the modal composition of the transfer function (see **Eq. 2.38**), it is possible to express the output spectrum as a superposition of the different contributions of the structural modes, as shown below:

$$S_{yy}(\omega) = \sum_{k=1}^{N} \frac{\varphi_k \cdot {g_k}^T}{i\omega - \lambda_k} + \frac{{\varphi_k}^* \cdot {g_k}^H}{i\omega - \lambda_k} + \frac{{g_k}^* \cdot {\varphi_k}^T}{-i\omega - \lambda_k^*} + \frac{{g_k}^* \cdot {\varphi_k}^H}{-i\omega - \lambda_k^*} \qquad (2.95)$$

This equation was introduced in [Peeters (2000)] and it defines the output spectral matrix and the structural modes and the vector g_k, called operational reference vector, in which take place the modal participation. As it proved in [Peeters (2000)], this vector is not depended on the characteristic of the *k-mode*, but it depends on all modal parameters, on the input location and on the input correlation matrix.

Again, the modal decomposition of the output spectrum shows that four different poles (λ_k,$-\lambda_k$, λ_k^* and $-\lambda_k^*$) can be extracted for each structural mode. This disadvantaged can be avoided recurring to the use of the *Positive* or *Half-Spectrum* function that it can be easily obtained from the correlation matrix limiting the Discrete Fourier Transfer (DFT) function only to positive time-lags:

$$S_{yy}^{+}(\omega_j) = \frac{R_{yy}(0)}{2} + \sum_{k=1}^{j} R_{yy}(k\,\Delta t)\; e^{-i\omega_j k \Delta t} \qquad (2.96)$$

As it is demonstrated, for instance in [Cauberghe (2004)], the modal decomposition of the Positive Spectrum is given by:

$$S_{yy}^{+}(\omega) = \sum_{k=1}^{N} \frac{\varphi_k \cdot {g_k}^T}{i\omega - \lambda_k} + \frac{{\varphi_k}^* \cdot {g_k}^H}{i\omega - \lambda_k} \qquad (2.97)$$

As can be noted, this equation has the same structure as the modal decomposition of the transfer function, or the FRF (see **Eq. 2.38**); thus, all the previously described models can also be adopted to define the positive spectrum matrix. It is worth highlighting that this approximation on the input excitation as a stochastic process with zero-mean value is essential for theoretical implementation of the "output-only" identification methods, being based only on the measured responses of the investigated structure. It is worth noting that if the white noise assumption is not respected and the input contains some dominant frequency components, such values will result as poles of the state matrix *A* and it will not be possible to distinguish the frequencies associated to such components from the natural frequencies of the system.

Numerical example

The simulation of experimental data consists of a useful task to understand the concepts related to the state-space model and, in particular, to characterize the response of the system subjected to non-deterministic input excitation. Moreover, the simulation of experimental data also permits to define the performance of different identification methods comparing different obtained results with the exact solution of the problem, characterizing the level of accuracy of each technique by statistical properties of the results. Furthermore, the easily creation of numerical responses also allows the testing of the robustness of identification method related to more specific cases: tests with high level of noise, symmetric structures with closely spaced modes or structures with no-proportional damping.

Therefore, the continuous state-space models are adopted to simulate experimental data, since to evaluate the response of the system in continuous time requires only the definition of the interval period of time Δt (sampling period). However, the use of continuous model demands that the response of the system to external excitation should be obtained in analytic way. In most of real applications is not possible to extract the response in continuous time, being necessary to solve this problem evaluating the response using discrete models. In this way, some routines have been developed in order to create artificial responses of the system and to simulate experimental data which will be used to calibrate the implemented algorithms presented in the next Chapters. Therefore, a procedure apt to create numerical accelerations referred to a simple academic structure will be used to exemplify the application of different identification methods based on OMA approach.

The first step of the developed procedure consists of the definition of the different matrices of the continuous time state-space model. Theses ones can be directly obtained by the mass, stiffness and damping matrices after some simple mathematical manipulations (see **Eq. 2.49**). Moreover, in the particular case of structure with proportional damping, the same matrices can be obtained from the modal properties of the system itself (see **Eq. 2.60**).

Consequently, once the substitution of the state matrices from continuous time domain to discrete time domain has been performed, applying the expression in **Eq. 2.63**, the response of the structure can be obtained using series of input excitation artificially created and applying the relation defined in the **Eq. 2.62**. this last task is performed adopting the function *dlsim* present in the toolbox of MatLab. Follow this way, three different excitations have been created and applied to obtain the time series of horizontal accelerations related to the simple 3-DOFs stricture. It is worth noting that the response has been obtained forcing each DOF of the system with an external input. Each input force was configured as stochastic process characterized by a zero mean Gaussian distribution (i.e., $p_i \rightarrow$ N (0, σ), with σ=1),

To represent the inputs time series of 5 minutes long have been created, adopting a sampling frequency equal to 50 Hz. Each excitation is described by a zero mean normal distribution (defined by using *randn* function), and each model matrix has been obtained by mass, stiffness and damping matrix. In the following are reported the acceleration time series of the output responses associated to the three levels of the structure, in the time domain, as well as the frequency domain representation.

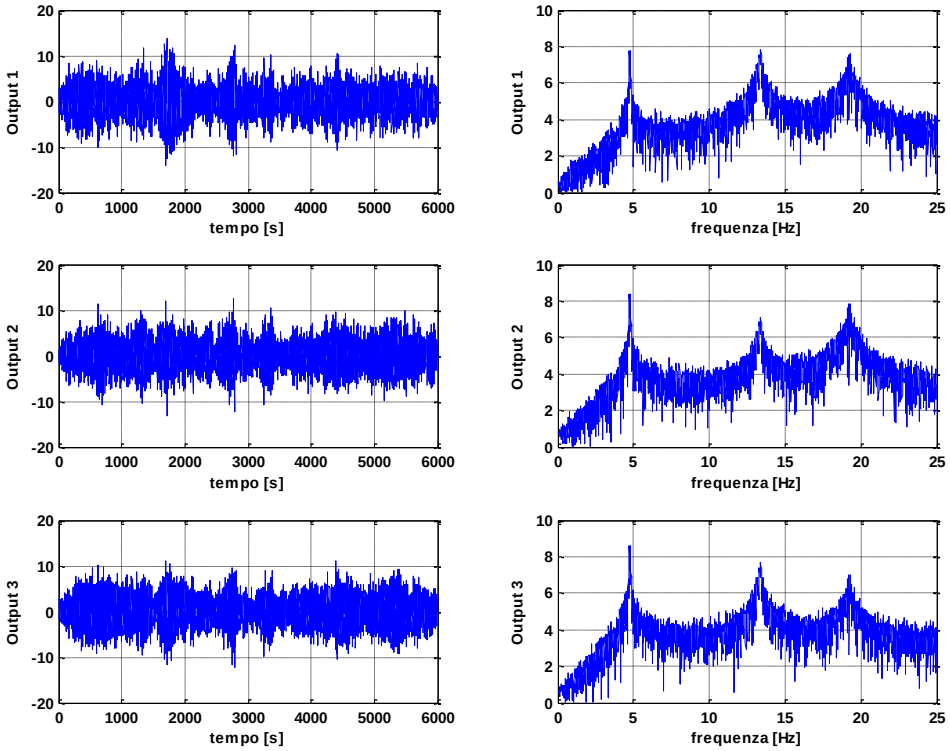

Fig. 2.8. Simulated output responses of the 3 system, in the time and frequency domain

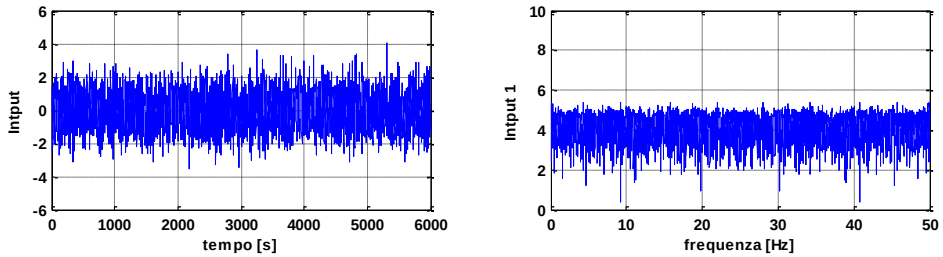

Fig. 2.9. Characterization of the simulated excitation in the time and frequency domain

Furthermore, is also reported the representation of the input excitation applied to each mass of the structure. It should be noted as the spectra content of the input signal (in the frequency domain representation) is uniformly distributed, as expected. This information remarks the fact that the peaks of the spectral function associated to each response (then natural frequencies) are depended only on structural conditions of the structure being the content of

the input "flat" within investigated frequency interval. Again, to perform this simple simulation, the noise content has not been introduced to corrupt the output signals. Meanwhile, the noise it will be added to the vectors of structural response in the further applications to validate the identification methods implemented in the next Chapter.

Before to complete this paragraph and to describe the principal techniques used in the Operational Modal Analysis process, some observations should be done about the main assumption about the stationarity property of the input signals. As proved, for Civil Engineering structures, this hypothesis is generally respected under certain initial conditions, as: micro-tremors, wind, waves and light traffic loads which constitute the normal operating conditions of the structure. On the contrary, the stationarity is compromised when the characteristics change over time due to particular environmental and/or operational conditions, such as: earthquakes, impacts, train passages or strong atmospheric turbulences as well as any occurred damages. For these cases, some methods described in literature provide interesting approach to face this problem: [Hammond and White (1996); Antoni (2009); Feldman (2011)].

In practical applications the white noise assumption is not always strictly respected. In fact, carried out in the frequency domain some spikes of the spectrum reveal that some low frequency components hold higher energy. Most of the stochastic techniques tend to be quite robust and do not provide incorrect solution indeed such violations. Conversely, in case of the presence of harmonic component in the recorded signal could lead to improper analysis described by a clear peak on the spectrum. These situations are more common in mechanical engineering or civil engineering structure that suffer some rotating and oscillation effects induced by close vibration machines. This problem is normal faced taking into account that the harmonic components are non-damped modes, hence sharp peaks that appear in the spectrum are clearly distinguishable and they can be easily removed. As described in some interesting papers present in literature that propose possible methods to remove the harmonic disturbance during the analysis performed with OMA procedures [Dion et al. (2012); Devriendt et al. (2009); Pintelon et al. (2008); Randall et al. (2013)].

2.3 Output-only modal identification techniques

The identification of the dynamic characteristics of the structures can be performed following two paths: by relating the output response of the structure to the corresponding artificial input excitation also measured, or by analyzing only the structural response and establishing initial hypotheses about the nature of environmental excitement. As already stated in the introduction of this Chapter, for dynamic tests of Civil Engineering structures, the second approach is used to be the most followed because it involves substantial advantages avoiding the use of very heavy equipment whose transport and installation involve a very high economic cost. Since the environmental excitation is composed by simultaneous contribution of several factors: micro-tremors, wind, traffic loads above or near the structure, it is usual to admit that the action acting on the structure can be represented as a white noise process. Under this assumption, the methods aimed at identifying the modal parameters of a structural system from dynamic response only are known as *output-only identification techniques*.

Four methods have been implemented during the development of this Dissertation, that will be presented in this section: i) the Peak Picking (PP), ii) the Frequency Domain Decomposition (FDD), iii) the Covariance-based Stochastic Subspace Identification (SSI-Cov) and iv) Data-driven Stochastic Subspace Identification (SSI-Data) method, respectively. In order to facilitate and clarify the development of each method a short view of the literature is given in the beginning of each subsection. Then, to better understand the used approach and the reading of the results, the procedures are explained performing the analysis using a simple academic structure composed by a few DOFs system. For more details about dynamic identification techniques of civil structures an interest reader is addressed to excellent scientific journal papers and conference proceedings reported in the follows: [Juang and Pappa (1985), Bendat and Piersol (1993); Van Overschee and De Moor (1996); Guillame et al. (1999); James et al. (1992); Brinker et al. (2001); Peeters et al. (2004); Peeters et al. (2005); Devriendt and Guillame (2008); Magalhães and Cunha (2011); Cabboi et al. (2017)].

The description of the identification methods is made considering two groups: the methods in the frequency domain (based on the spectral estimation of the structural response) and the time domain methods (based on the correlations or on the projections of the collected output responses).

2.3.1 Pre-processing and estimates

Reference channels

Most of output-only modal identification techniques start with the construction of a data matrix which organizes and contains all the information about the output responses of the investigate structure; the construction of such matrix consists of the basic step of each identification method and it is composed by two type of data: by the cross-correlations, or alternatively, by the spectral estimates of recorded signals, and it could have a square dimension if all recording channels are used as reference outputs and it contains all the cross-correlations or the cross-spectra between all measured outputs. Otherwise, this matrix can be reduced adopting only a few available channels as reference ones. In this way, the reduction of the size matrix leads to a faster execution and a less time consuming in data analysis due to a lower required computational afford.

Correlation function

The definition of correlation function of a discrete time signal was already presented in **Eq. 2.68**. As obvious, during dynamic tests and even for continuous monitoring only a finite number of samples can be recorded. So, only an estimation of the correlation ($\hat{R}$) can be get. Considering this limitation, the correlation function is estimated as:

$$\hat{R}_j^{ref} = \frac{1}{n_t - j} \sum_{k=0}^{n_t-j-1} y_k \cdot y_{k+j}^{ref^T} \quad \text{with} \quad j = 1,2, \dots j_m \tag{2.98}$$

where $\hat{R}_j^{ref}$ is a [n_o-by-n_r] matrix, with n_o is the number of the all output channels and n_r represents the number of the selected reference outputs. In additions, n_t represent the total number of collected samples and $j_m \cdot \Delta t$ is the maximum time-lag of the correlation functions. To clarify, $\hat{R}_j^{ref}$ represents the estimates of the correlation matrix R_j adopting the reference outputs in which R_j is a simplification of the notation $R_{yy}(\tau = j \cdot \Delta t)$. The calculation of the correlation matrix (**Eq. 2.98)** is very time consuming. However, same accuracy can be obtained adopting a high-speed FFT- based approach, [Oppenheim and Shafer (1975)], implemented in the Signal Processing Toolbox of MatLab.

Spectra function and Positive Spectra

Recalling the cross-spectra functions between two stochastic realizations are obtained by applying the Fourier Transform to the output response signals (see **Eq. 2.87**). As stated for the correlation function (see **Eq. 2.98**), it is only possible to calculate an estimate of the spectra due to the limit number of the recorded samples $(\hat{S})$ as follows:

$$\hat{\mathrm{S}}_{x_1x_2}(\omega) = \frac{X_1(\omega)^* \cdot X_2(\omega)}{N\,\Delta t} \qquad (2.99)$$

where X(ω) is an estimation of the realization obtained applying the DFT. The series (see **Eq. 2.87**) in which $n \to \infty$ disappear, the total acquired points is defined by N and the length of the temporal segment in which the signals are collected is defined by $N \cdot \Delta t$. So, the Fourier Transform is substituted by the Discrete Fourier Transform (DFT). Due to the discrete nature of the acquired signals, the spectrum estimates are affected by two typical errors: the *leakage* error, that is directly due to the discretization process of the time series, specifically due to the discontinuity between the points of the discretized signal; and the *aliasing* error, that is related to the energy content in the discretized signal which is larger than the same signal defined in continuous time. So that the simple estimate of the spectra directly, obtained by application of the **Eq. 2.97** to a discretized process with a finite duration, produces unacceptable errors that must be mitigated.

Part of the error can be minimized dividing the entire time response into shorter segments and perform the estimate of the spectra applying **Eq. 2.99** to shorter intervals. Hence, the error related to the estimates is reduced, but the use of a high number of short segments leads to a decreasing of the variance in the average estimate and, therefore, to a general worsening of the leakage error. This condition affects also the frequency resolution of the signal that it is not acceptable. Since the linkage error is due to the discontinuity and the finite length of the discretized series, it can be minimized performing a "windowing" of the signals. Several approaches are discussed in the reference book [Maia and Silva (1997)]. In this case only *periodogram* approaches is reported.

The Periodogram approach, also known as Welch estimator [Welch (1967)], calculates the spectra function directly from the collected time series involving the following steps: 1) dividing the output response records in n_b segments y_b in which all segment have the same length (n_b), 2) performing a windowing of the segments adopting the *Hanning window* (see **Eq. 2.100**), 3) calculating the DFT of the "windowed" signals and, 4) extracting the estimates after the averaging the resulting values with 50% of overlapping.

$$\begin{aligned} w(t) &= \frac{1}{2}\left[1 + cos\left(\frac{2\pi t}{T}\right)\right], \quad |t| \leq T/2 \\ w(t) &= 0 \qquad\qquad\qquad\quad , \quad |t| > T/2 \end{aligned} \tag{2.100}$$

The application of the Hanning window with an overlapping of 50% does not modify the energy contribution of the truncated time series. In fact, as shown in **Fig. 2.10**, the sum of a series of Hanning window with an overlap of 50% leads to a horizontal line in the overlapping area. Hence, the frequency content is not modified.

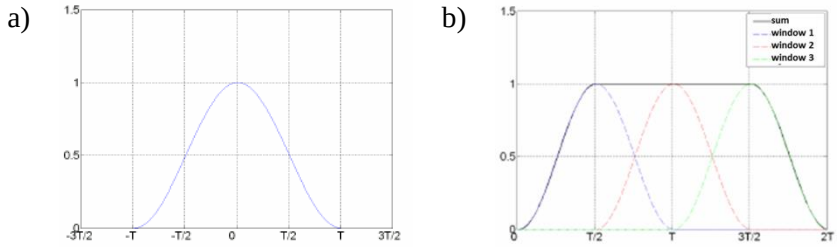

Fig. 2.10. a) Hanning window, b) overlapping of 50% between Hanning windows

In the reference book [Bendat and Piersol (1980)], several methods used to estimate the spectra functions and their errors are described in detail. Meanwhile, in [Brandt et al. (2004)] main aspects related to these methods are exploited.

To estimate the spectra functions in the contest of ambient vibration test in which all channels are considered as reference ones, it is usual to organize the auto-spectra and the cross-spectra into a *spectral matrix* ($\hat{\mathrm{S}}$) in which the diagonal elements correspond to the auto-spectra function calculated using the structural response recorded by the *i-th* sensor in the *i-th* DOF of the structure. Otherwise, the extra diagonal elements of the matrix correspond to the cross-spectra estimates related to the output responses measured by the *i-th* sensor in the *j-th* DOF and vice versa. If the measured of the output responses were recorded in the same time the matrix is a [n_o-by-n_o] square matrix, in which n_o is the number of the transducers installed on the structure. The spectra matrix is also defined as *power spectra density matrix*, and it can be express in the compact form as follows:

$$\hat{S}_{yy}(\omega) = \frac{Y(\omega)^* \cdot Y(\omega)^T}{n\,\Delta t} \tag{2.101}$$

where $Y(\omega)$ is a column vector with the number of elements equal to the number of instrumented points in which are contained the FFT of the $y(t)$ recorded set of responses. In case of multi-setups tests, it is also possible to estimates a "reduced" PSD matrix with [n_o-by-n_r] dimensions, in which n_r corresponds to the number of reference channels used for all measurements. Therefore, the PSD matrix can be estimates as follows:

$$\hat{\mathrm{S}}^{ref}{}_{yy}(\omega) = \frac{Y(\omega)^* \cdot Y^{ref}(\omega)^T}{n\,\Delta t} \tag{2.102}$$

where $Y^{ref}(\omega)$ corresponds to a vector with n_r dimension composed by the FFTs of the responses collected in the reference DOFs common for all setups.

A developed routine, implemented in MatLab code, was used to simulate the output responses and to calculate the spectra estimates of the simple academic system composed by 3-DOFs, already described in the previous paragraph.

Numerical example

As reported in the previous paragraph, a simple share-type composed by 3-DOFs has been used to simulate a series of numerical responses of the system subjected to random excitation with a zero mean Gaussian distribution (white noise). The acceleration time series were collected on all levels of the structures when the input forces acting on the same DOFs of the structure. In this example, all the DOFs were selected as reference channel and the sample frequency adopted to collect the output response was set at 50 Hz. Each recorder time series is 5 min long (15000 sampled values) and the Hanning window (**Eq. 2.100**) was used to estimate the spectra matrix. Starting from the simulated accelerations, the power spectral density matrix was calculated varying the length of segments. The use of different length of the trunked segments involves the definition of different spectra estimates with different accuracy. In **Fig. 2.11** the estimations of the auto-spectra $\hat{S}_{33}(\omega)$ is reported highlighting the differences between the resulting estimates varying the length of the trucked series.

Detailing four different length of the Hanning window were adopted to estimate the spectra. In **Fig. 2.11** the plots of the estimates obtained using a number of points equal to 512, 1024, 2048 and 4096 are reported. As shown, the estimate obtained with low resolution (512 points) seems to be more regular but it provides an estimate with lower accuracy because the high number of segments. This produces a general worsening of the leakage error that affects also the frequency resolution ($\Delta f = 0.0976$ Hz). Otherwise, the estimate obtained with higher number of points (4096 points) has a more irregular trend but the associated estimates is more accurate also providing a higher frequency resolution ($\Delta f = 0.0122$ Hz).

It is worth noting that the spectral estimations reported in **Fig. 2.11** have been calculated using the simulated output responses without include the noise in the measurements. Therefore, the irregularity of the spectra is only related to the estimation error. In order to represent a real condition test, in Chapter 4 and Chapter 5 the modal parameters of the simple 3-DOF system are extracted including the noise content in the measurements. In this context, the best results can be obtained taking into account both inaccuracies related to the frequency resolution and to the induced error. Moreover, to mitigate the error effect, the length of the acquisition signals should be long enough to permit the use of a high number of values and to get a fair compromise between uncertainty and frequency resolution.

Estimate n° 1

L → length of the segments = 512 points
Δf → frequency resolution = 0.0976 Hz
T → time of each Segment = 10.24 sec
n°→ number of segments 2928

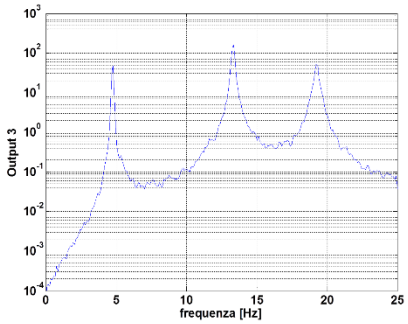

Estimate n° 2

L → length of the segments = 1024 points
Δf → frequency resolution = 0.0488 Hz
T → time of each Segment = 20.48 sec
n°→ number of segments 1462

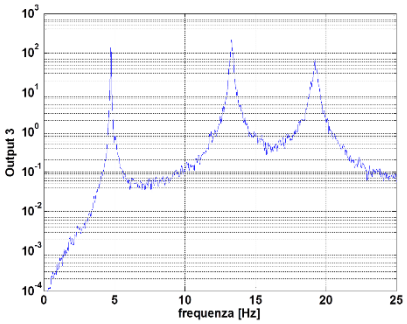

Estimate n° 3

L → length of the segments = 2048 points
Δf → frequency resolution = 0.0244 Hz
T → time of each Segment = 40.96 sec
n°→ number of segments 732

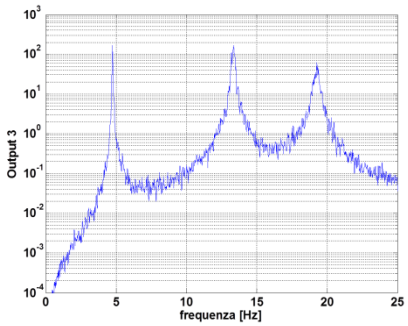

Estimate n° 4

L → length of the segments = 4096 points
Δf → frequency resolution = 0.0122 Hz
T → time of each Segment = 81.92 sec
n°→ number of segments 366

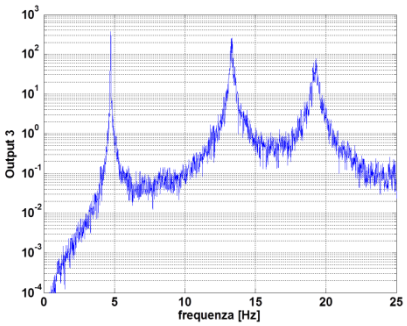

Fig. 2.11. Spectra estimations obtaining using a different windowing

2.3.2. Identification methods developed in the frequency domain

In the context of OMA applications in Civil Engineering structures and Cultural Heritage constructions, as: bridge, viaducts, dams, buildings and towers, the main assumption on the input excitation permits to represent the structural behavior through mathematical models establishing a relation between output spectra matrix and modal parameters.

In this section a brief overview of two important frequency domain identification techniques is presented. In particular, the *Peak Picking* method and the *Frequency Domain Decomposition* algorithm are described. The first one corresponds to the oldest developed method to extract the modal parameters, but due to its simple implementation and its user-friendly approach it is still used for faster analysis during dynamic tests. The second one was firstly presented in [Brinker et al (2000)] and even if it is based on the main concept of the Peack Picking method, some improvements were implemented allowing the separation of closely spaced modes and solving the problem related to the identification of the modal damping ratio.

2.3.2.1 Peak Picking method

The first identification technique described in this section is the Base Frequency Domain (BFD) method, also known as the Peak Picking (PP) method. It is the simplest and most popular used approach to estimates the modal parameters in Civil Engineering applications. This method is based on the analysis of the output responses collected when the structures are subjected to environmental forces. Currently, it is one of the most used methods because its easy implementation and interpretation of the results that maintain a clear physical meaning.

The theoretical basis of this method was firstly introduced in [Bendat and Piersol (1980)], meanwhile the development for practical applications was performed in [Felber (1993)]. The practical implementation of this technique encouraged the use of the modal parameters to determine the dynamic characteristics of different kind of structures mainly performing ambient vibration tests, as demonstrate in [Felber and Cantieni (1996)].

The PP method is a frequency domain identification method that permits to estimate the natural frequencies though a visual inspection of the pecks of the spectrum magnitude plotted on a magnitude vs. frequency diagram. This method provides good estimates of

the modal parameters when two initial conditions are respected; a) the natural frequencies of to the structural modes are well separated, b) the modes are slightly damped. In fact, the definition of the correct estimates of the natural frequencies are obtained under the assumption of well-separated resonant modes. Otherwise, this technique could fail to provide a reasonable set of modal parameters associated to the resonant modes. To better understand the previous assumption, it is worth remarking that nearby each natural frequency value, the dynamic response of the structure is essentially conditioned by the contribution of one resonant mode. Therefore, it is possible to say that: in the neighborhood of the natural frequencies, the dynamic behavior can be approximated at the single contribution of the resonant mode in that frequency. This means that near the resonant frequency the structural response can be simulated by a 1-DOF oscillator model characterized by the same frequency and the same damping value of the resonant mode.

This hypothesis is even more reliable if the frequencies associated to the structural modes are not closely spaced. Otherwise, the method is not able to separate the contributions of different modes [Bendat and Piersol (1980)]. This is the main limitation of this method. The PP method is principally used to extract fast information about the dynamic characteristics of the investigated structures, and it is mainly used to provide resonant frequencies and the mode shapes associated to the structural modes. To better understand, this method is exploded using a MDOF system already used in the previous paragraph.

Identification of the natural frequencies

As already mentioned in the previous paragraphs (see **Eq. 2.92**), the spectral matrix of a MDOF system subjected to white noise random excitation can be estimated starting from the FRFs matrix (see **Eq. 2.93**). This strong relation is obtained because the spectral function of a white noise excitations is constant, and it is not depended by other factors:

$$S_q(\omega) = H(\omega) \cdot R_p \cdot H^H(\omega) \tag{2.103}$$

As stated, the elements of the FRFs matrix have maximum values in the correspondence of the damped resonant frequency values that generally correspond to good estimations

of the natural frequencies when the damping values are low. A this point a further information needs to be pointed out, in fact from the **Eq. 2.103** it is evident that each spectral function belong to the spectra matrix have maximum peaks in correspondence of the same frequencies values, because the white noise nature of the input. Therefore, it is possible to extract the natural frequencies of the system just performing the analysis of the auto-spectra function (also defined power spectral density function) as follows:

$$PSD_i(\omega_k) = \sum_{k=1}^{N} PSD_i(\omega_k) \tag{2.104}$$

In order to ensure the identification of the natural frequencies during the analysis of data recorded in a single setup, as well as in multi-setups during the any dynamic tests, a practical implementation of the Peak Picking method was firstly realized by Felber in [Felber (1993)]. In which it is suggested the use of the *averaged normalized power spectrum density* (ANPSD) of all measurement points, that means averaging the diagonal elements of the spectrum matrix $S_{yy}^{+}(\omega)$. In fact, the analysis of only one spectrum (one element in the diagonal of the spectrum matrix) is not enough to identify all resonant frequencies, because the reference DOF could stay on the node of one or more vibration modes and therefore the identification of the mode is not permitted. So, the strategy developed in [Felber (1993)] implies the identification of the resonant frequencies estimating the auto-spectra of all registered signals. Consequently, the average value of the normalized PSD associated to each DOF is performed to define the *averaged normalized power spectrum density* (ANPSD) as reported in the following equation:

$$ANPSD(\omega) = \frac{1}{l}\sum_{i=1}^{l} NPSD_i(\omega) = \frac{1}{l}\sum_{i=1}^{l}\left[\frac{PSD_i(\omega)}{\sum_{i=1}^{N} PSD_i(\omega)}\right] \tag{2.105}$$

in which *l* is the number of instrumented DOFs and $NPDS_i$ are the normalized spectrum associated to each DOF obtained by **Eq. 2.104**. This strategy was very efficient and became one of the most important bases in the OMA analysis because it relates the modal parameters estimations with the energy content associated to each DOF of the structure.

Numerical example

The numerical acceleration series were used to calculate the NPSD associate to each DOF of the share-type model. Consequently, the ANPSD has been defined using the Eq. 2.104. For clearness, it is worth mentioning that all estimates have been obtained using the parameters previously defined for the *Estimation n°2* (1024 points for each segment).

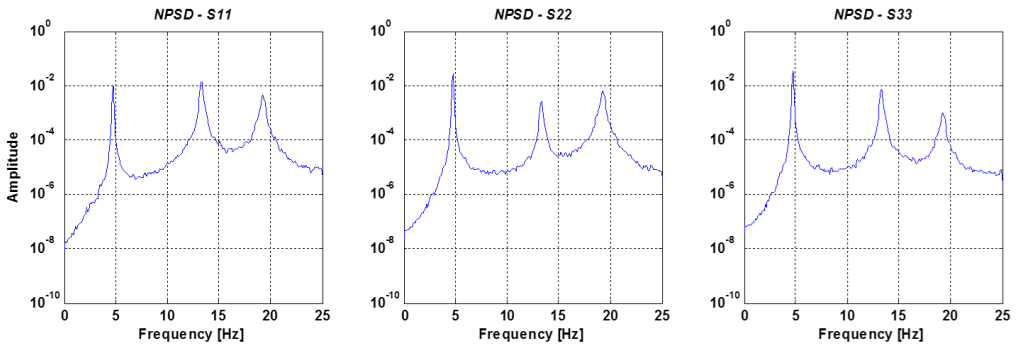

Fig. 2.12. Normalized auto-spectra associated to each DOF of the structure

From the inspection of each obtained NPSD all the resonant frequencies of the numerical structure are well defined. This means that the measurement points are not located on the node of the vibration modes. Then, after averaging the NPSDs, the natural frequencies of the structure are obtained selecting the peak values of the ANPSD. Hence, the experimental values are compared with the theoretical ones as reported in the **Table 2.2**.

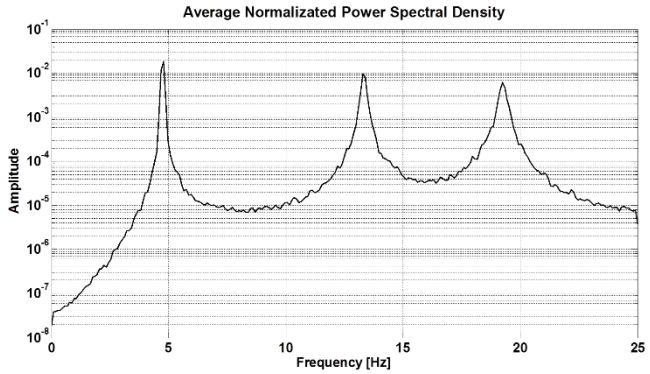

Fig. 2.13. Average Normalized Power Spectral Density (ANPSD) function.

Table 2.2. Comparison between natural frequency estimates and theoretical values

Mode	Theoretical values	Experimental values	Error
1	4.755	4.736	0.40 %
2	13.323	13.28	0.32 %
3	19.252	19.22	0.16%

From the comparison between the natural frequencies obtained by the application of the ANPSD function and the theoretical values, the scatter values are less than 1%.

Identification of vibration modes

From the relation that describes the FRFs matrix in modal domain expressed by **Eq. 2.34**.

$$H(\omega) = \Phi \cdot H_\eta(\omega) \cdot \Phi^T = \sum_{k=1}^{N} H_{\eta k} \cdot \varphi_k \cdot {\varphi_k}^T \tag{2.106}$$

in which $H_\eta(\omega)$ is a diagonal matrix that depends by the modal parameters as follows:

$$H_\eta(\omega) = diag\left[\frac{1}{\omega_k^2 - \omega^2 + 2\, i\, \xi_k\, \omega\, \omega_k}\right] \tag{2.107}$$

if the natural frequencies are well-spaced and the values of the damping coefficients are low, the diagonal elements of the matrix $\mathrm{H_\eta}$ have very high values in the nearby of the resonance frequencies. This means that in the proximity of a natural frequency ω_k, the value of the *k* element of H_η can be approximated to the contribution of the *k-th* mode in that frequency as follow:

$$\mathrm{H_\eta(\omega_k)} = \varphi_\mathrm{k} \cdot \frac{1}{\omega_\mathrm{k}^2 - {\omega_\mathrm{k}}^2 + 2\,\mathrm{i}\,\xi_\mathrm{k}\,\omega_\mathrm{k}\,\omega_\mathrm{k}} \cdot {\varphi_\mathrm{k}}^\mathrm{T} = \varphi_\mathrm{k} \cdot \mathrm{c_1} \cdot {\varphi_\mathrm{k}}^\mathrm{T} \tag{2.108}$$

This means that the component in *k-th* position of the FRFs matrix is given by a scalar complex value c_1 that depends on the natural frequency ω_k, on the damping value ξ_k and on the mode shape φ_k. Consequently, introducing the relation obtained in **Eq. 2.108** into **Eq. 2.103**, the spectra is defined as:

$$S_y(\omega_k) = \varphi_k \cdot c_1 \cdot {\varphi_k}^T \cdot R_u \cdot \varphi_k \cdot c_1^* \cdot {\varphi_k}^T = c_1 \cdot c_1^* \cdot \varphi_k \cdot c_2 \cdot {\varphi_k}^T \tag{2.109}$$

in which c_2 is a constant scalar value that is obtained by a vector product between $\varphi_k{}^T$ (vector 1-by-n), R_u (matrix n-by-n) and φ_k (vector n-by-1). Pacing together the three coefficients in the Eq. 2.108, the relation can be re-written as follows:

$$S_y(\omega_k) = c_3\ \varphi_k \cdot \varphi_k{}^T \tag{2.110}$$

this relation reveals an important consideration about the value of the spectra estimates, in fact, this equation says that from a column of the spectral matrix it is possible to know the configuration of the mode associated to that specific natural frequency value ω_k, and vice-versa. This relation is very important because once a reference DOF is selected, the element in the *ref* position of the *ref* column of the S_y matrix can be calculated as:

$$S_y(\omega_k)_{(ref,ref)} = c\ \left(\varphi_{ref}\right)_k \cdot \left(\varphi_{ref}\right)_k{}^T \tag{2.111}$$

in the same way the other components are defined as:

$$S_y(\omega_k)_{(j,ref)} = c \cdot \left(\varphi_j\right)_k \cdot \left(\varphi_{ref}\right)_k{}^T \tag{2.112}$$

From the ratio between **Eq. 2.111** and **Eq. 2.112** the *pseudo transfer function* is defined:

$$T_{j,ref} = \frac{S_y(\omega_k)_{(j,ref)}}{S_y(\omega_k)_{(ref,ref)}} = \frac{\left(\varphi_j\right)_k}{\left(\varphi_{ref}\right)_k} \tag{2.113}$$

which is a complex number and it permits to estimate, in the instrumented DOFs, the components of the structural modes in a selected natural frequency ω_k. in this way it is possible to characterize the dynamic behavior of a structure adopting just two reference sensors. Moreover, due on the complex nature of the cross-spectra, the transfer functions are complex numbers in which the amplitude is related to the components of the *i-th* and the *ref-th* selected modes, meanwhile the phase should be equal to 0° or 180° if the *i-th* component is in phase or in opposite phase respect to the same component of the reference DOF. For clearness, phase=0° means that the displacement of the component of the *i* and *ref* DOF are in the same direction, otherwise they move in the opposite direction when phase=180°.

Numerical example

The auto-spectra defined in the previous example have been used to estimate the vibration mode of the simple academic structure. In addition, for the definition of the modes the displacement of the highest floor was selected as reference DOF. In Fig. 2.14 the cross-spectra and the associated transfer functions related to the third column of the spectra matrix are depicted. The last two diagrams represent the auto-spectra value S_{33} and the transfer function T_{33} obtained considering the displacement of the third floor as reference degree. The other diagrams represent the cross-spectra and the relative transfer functions expressed by amplitude and phase components.

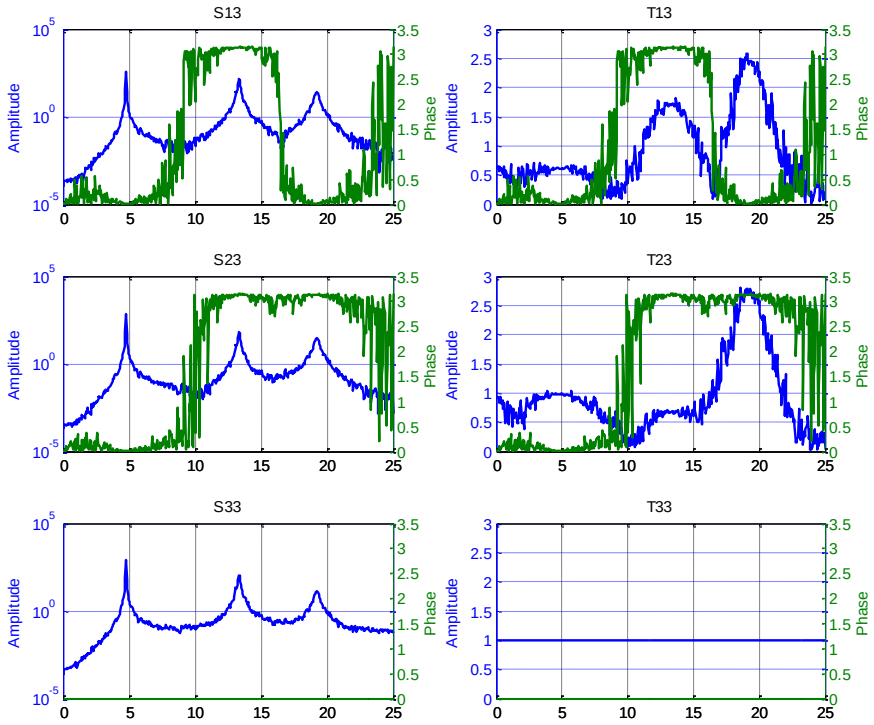

Fig. 2.14. Cross-spectra end auto-spectra function (3rd column of spectra matrix) associated to the 3rd DOF of the system and associated transfer functions

Finally, when the PP method is applied to identify the mode shapes, instead of estimate spectrum $S_{yy}^{+}(\omega)$, only the spectrum between the reference sensor and the other ones are

calculated. This reason is that only one column (or row) of the spectrum matrix is enough to obtain the mode shape estimates. Moreover, *coherence functions* can assist the selection of the natural frequencies, because it tends to 1 nearby the resonant damped frequencies. The phase angles of the cross-spectra functions are also useful for determining the damped natural frequencies since the phase angle should be either 0° or 180° in the corresponding nodes of the mode shape. An interested reader is referred to [Felber (1993)] in which the procedure for extracting modal parameters using PP method is detailed.

Ending, in **Fig. 2.15** the amplitude and phase variation of the transfer functions considering the displacement of the third floor as reference DOF are reported. Detailing, the amplitude and the phase were determined for the modal configurations.

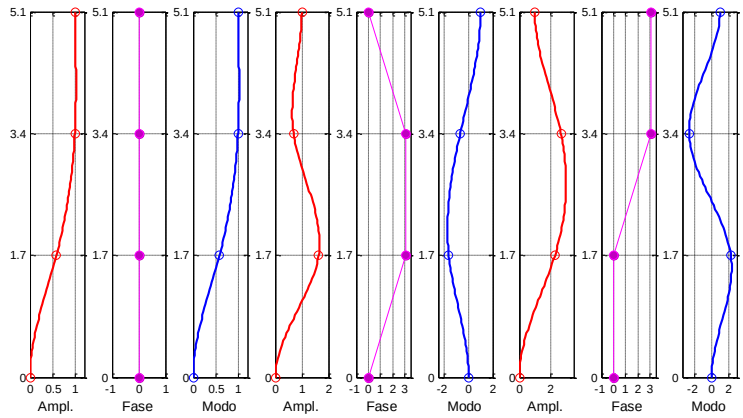

Fig. 2.15. Extracted mode shapes of thee identified modes: amplitude (red color) phase (magenta) and final mode shape (blue) of each mode are depicted

To conclude the presentation of this identification technique in the frequency domain, it is worth mentioning that the mode shapes obtained using the transfer functions do not exactly coincide with the theoretical modes, but they are defined as *operational deformation modes*. This is due on the fact that such modes are not obtained by a representative model that approximates the structural behavior, but they are obtained from a relation of the responses measured in different DOFs of the structure. Furthermore, in case of closely-space modes, this technique could not provide the contributions associate to the different modes, and the resulting operational deformation modes represent just a combination of the real ones.

2.3.2.2 Frequency Domain Decomposition method

The *Frequency Domain Decomposition* (FDD) technique was first proposed in [Brincker et al. (2000); Brincker et al. (2001)] and an important improvement has been published in [Brincker et al. (2009)]. The FDD method was developed in order to remove some limitation in the identification problem provided by the Pick Peaking technique: such as: a) difficulty in the detection of the spectrum peaks, b) separation of closely spaced modes, c) the estimation of the modal damping ratio with higher accuracy.

It is worth noting that the basic concepts of the FDD method had already been adopted in the analysis of structures excited by ambient inputs as [Prevosto (1982] and for the extraction of modal parameters from the FRF in the form of *Complex Mode Indication Function* (CMIF) [Shih et al. (1989)]. The basic concepts behind FDD have already been proposed in the past by [Shih et al. (1989)], Brinker introduced the concept of Modal Domain improving the identification of the modal parameters of the existing procedure. Nevertheless, respect to classic spectral analysis this procedure shows any improvements mainly related at evaluation of the mode shapes and the possibility of identifying closely spaced modes with higher confidence.

The FDD method is a frequency domain non-parametric method based on the construction and the factorization of the output spectrum matrices calculated with the Welch method [Welch (1967)]. The strategy behind this procedure is the identification, at each spectral line, of the contribution of each vibration mode from the total available spectral magnitude that are contained at that corresponding frequency. In other words, this method can detect the contribution of the different modes in the same frequency.

To easily understand the basic concepts at the base of the FDD method, it is needed to remind the theory of the modal analysis. Remarking, the general response $y(t)$ of a vibrating structure can be obtained as superposition of n vibration modes (each one characterized by its mode shape ϕ_i), expressed by means of the modal coordinates η_i:

$$y(t) = \phi_1 \cdot \eta_1(t) + \phi_2 . \eta_2(t) + \cdots + \phi_n \cdot \eta_n(t) = [\Phi] \cdot \{\eta(t)\} \tag{2.114}$$

By recalling the definitions provided at the beginning of this Chapter, and computing the value of the correlation function as follows:

$$\begin{aligned} R_{yy}^{+}(\tau) &= E[q(t+\tau) \cdot q(t)^T] = E[\Phi \cdot \eta(t+\tau) \cdot \eta(t)^T \cdot \Phi^T] \\ &= [\Phi] \cdot \Sigma_{\eta\eta}^{+}(t) \cdot [\Phi]^T \end{aligned} \tag{2.115}$$

where $R_{\eta\eta}(\tau)$ indicates the correlation function in the modal coordinate in the time domain. By applying the FTT to **Eq. 2.114**, the spectral matrix $S_{\eta\eta}(\omega)$ is obtained:

$$S_{yy}(\omega) = [\Phi] \cdot S_{\eta\eta}(\omega) \cdot [\Phi]^H \tag{2.116}$$

in which $S_{yy}(\omega)$ is defined as complete output spectrum matrix. By recalling the basic assumptions of the modal analysis, specifically the orthogonality property of the mode shapes contained in the *modal matrix* Φ and the hypothesis on the input excitation as white noise stochastic process well distributed over the structure, then the modal coordinates can be considered as uncorrelated [Brinker et al. (2001); Peeters (2000)]. Therefore, the correspondent power density spectral matrix $\boldsymbol{S}_{\eta\eta}(\omega)$ is diagonal.

Looking at **Eq. 2.114** and taking into account the conditions previously mentioned, the power spectral density matrix can be factorized in terms of Singular Values (SV) performing the Singular Value Decomposition (SVD) method. In order to clarify the characteristic of this algorithm, the main steps are reported below.

Singular Value Decomposition

Singular Value Decomposition (SVD) is an algorithm that permits the decomposition of a generic matrix $A \in \mathbb{C}^{n \times m}$ (with $n>m$) as product of three matrices as follows:

$$A = [U] \cdot [S] \cdot [V]^H \quad \text{with} \quad S = \begin{bmatrix} S_1 \\ 0 \end{bmatrix} \tag{2.117}$$

where $U \in \mathbb{C}^{n \times n}$ and $V \in \mathbb{C}^{m \times m}$ are matrices containing the right and left singular vectors of matrix A. $S \in \mathbb{C}^{n \times m}$ is a rectangular matrix and from this one is extracted contains the diagonal matrix $S_1 \in \mathbb{C}^{n \times n}$ in which the non-null SVs are organized in decreasing way. The number of non-null SV defines the rank of the matrix A and also define the number of

columns, or rows, linearly independent. Moreover, SVD is related to the definition of the eigenvalues and eigenvectors of the matrices A^TA and AA^T. In fact, the eigenvalues of A are equal to the positive root square of the eigenvalues of A^TA and AA^T, the columns of the matrix U contain the eigenvectors of A^TA, meanwhile the columns of the matrix V contain the eigenvectors of A^TA and AA^T. If A is a complex matrix, the equality is still valid but the transposition operation $(\bullet)^T$ has to be replaced with the complex conjugation operation $(\bullet)^H$. Furthermore, when a general matrix A is real and symmetric or complex and Hermitian (that means $A^H=A$) its SVs coincide with the eigenvalues and U and V are the same matrix. Therefore, the previous equation is replaced as follows:

$$A = [U] \cdot [S] \cdot [U]^H \qquad (2.118)$$

in which U, V and $S \in \mathbb{C}^{n\times n}$ and S is a diagonal matrix and it only contains non-null SVs. In this way, the definition of the SV can be obtained as a particular case of the general application commonly used for rectangular matrices.

As already stated, the FDD method was firstly introduced in [Brinker et al. (2000)] in which the application of the SVD to the spectrum response matrix leads to a sum of different spectral power density functions related to each 1-DOF oscillators that have the same frequencies and the same damping coefficients of the modes of the structure. The results provided by this procedure can be considered highly reliable if the following basic assumptions [Brinker et al. (2000); Brinker et al. (2001)] are fulfilled: 1) the excitation is a white noise, 2) the mode shapes are orthogonal, and 3) the investigated structure is lightly damped. If such hypothesis is not satisfied, the SVD must be considered approximate. Nevertheless, the obtained results are still more accurate than those provided by traditional techniques. Some steps need to be performed before applying the FFD method for modal parameter estimation. The first step consists of the estimation of the *half positive spectral matrix*, named S_{yy}^{+}, based on the output measurements. From mathematical point of view, this method was implemented performing the *Singular Value Decomposition* (SVD) of the S_{yy}^{+} at each discrete frequency point ω_i. Hence, the spectral matrix of the output can be formally re-written for the generic discrete frequency ω according to the SVD formulation:

$$S_{yy}^{+}(\omega) = [U(\omega)] \cdot [S_n] \cdot [U(\omega)] \tag{2.119}$$

Due on the fact that $S_{yy}^{+}(\omega)$ is a complex and Hermitian matrix, the matrix U defined in the **Eq. 2.117** coincide with the matrix U and the SVD operation can be carried out using the expression defined in the **Eq. 2.118**. The matrix U is a square matrix of singular vectors and S_n is a diagonal matrix composed by n SVs (n corresponds to the instrumented points and to the dimension of the $\mathbf{S}^{+}$ matrix) that appear in descendent order. Such SVs coincide with the amplitude of each spectrum, defined for each discrete value of ω, of the SDOF oscillators in the correspondence of the investigated frequency.

In more details, the performance of the SVD to the S_{yy}^{+} matrix allows the decomposition of the spectral matrix as a combination of auto-spectral density functions, each one corresponding to a SDOF. In this way, the first singular value contains in its ordinate of the auto-spectra related to the dominant mode in that specific frequency. This means that it is possible to identify the dominant mode looking at the peaks of the first SV, because the other SVs, that represent the contribution of the other modes at the same frequency value, are negligible. Hence, every dominant *k-th* mode can be detected by the bell-shaped described by the first SV of S_{yy}^{+} nearby the corresponding peak.

If there are not close spaced modes, the graphical variation of the first SV throughout the frequency values contains the most important segment of auto-spectrum of all SDOFs in the nearby the resonant frequency, which are necessary to explain the behavior of the structure. In this way, the plots of the remaining SVs should tend to zero.

On the contrary, in case of closely spaced modes, the decomposition of the spectral matrix, in the nearby of a resonant frequency, presents several SVs with significant values equal to the number of modes that are present in the neighbors of that frequency. Hence, the first column (or row) of the matrix U still contains the configuration of the dominant mode for every frequency value, but the configurations of the other modes can be estimated by other columns of the matrix U and the frequency values might to be evaluated in the correspondence of the maximum values of other SVs. This latter

situation yields to some identification difficulties, even more evident in case of automation of the process, that still deserve more research efforts to be solved.

Once the resonant peak (or the natural frequency) is defined, the mode shape associated at dominant mode is obtained taking the first singular vector u_1 of the matrix U. The contributions of other modes provided by other SVs should be negligible. It is worth remarking that the singular vector is an estimation of the associated mode shape:

$$\hat{\phi} = u_1 \tag{2.120}$$

Numerical example

The numerical accelerations of the 3-DOFs system have been used to test the performance of the developed FDD technique, implemented in MatLab environment. In the developed approach, the natural frequencies values are not extracted through selecting the local maxima of the SVs of the spectral matrix but using the Welch method. They were used segments with shorter length (1024 points) to extract the spectra estimate affected by lower noise averaging a higher number of estimates. In this example the adopted frequency resolution was equal to 0.0488 Hz. **Fig. 2.16** shows a typical plot of the singular values of the spectral matrix $S_{yy}^{+}(\omega)$ obtained for a simple numerical system already described. As highlighted, the first singular value is significantly larger than others and the typical "bell-shapes" of the modal peaks associated to the natural frequencies are well defined.

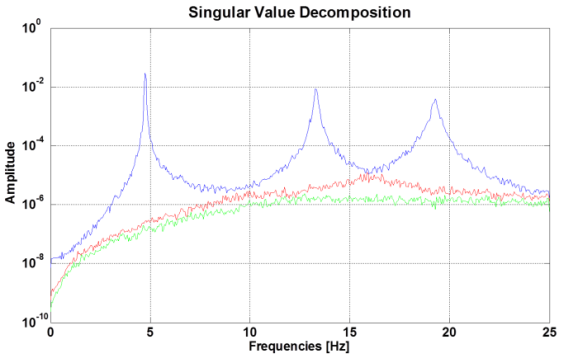

Fig. 2.16. Plot of the first SV lines obtained applying the FDD identification method

2.3.2.3 *Enhanced Frequency Domain Decomposition* method

The main limitation of the FDD technique is represented by the high inaccuracy related to the damping estimation. To overcome this issue, an improved version of the algorithm was proposed by Brincker in [Brincker et al. (2001)], the *Enhanced Frequency Domain Decomposition* (EFDD) method. This improvement was principally developed to estimate the damping value with more accuracy. Moreover, the natural frequency and the modal configuration can be extracted with lower uncertainty defining an interval frequency range in which the frequency peak of the first singular values is dominant.

A good operating strategy consists of detecting the *modal domain* around the resonance peak, defining the auto-spectral density of the dominant SDOF system in that domain.

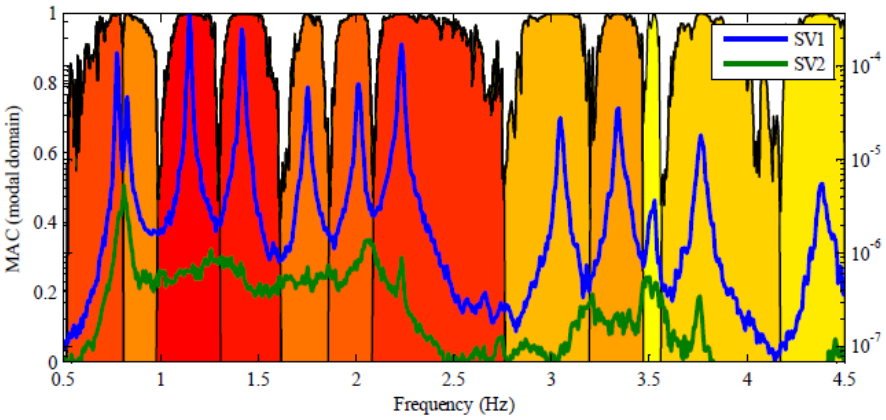

Fig. 2.17. Typical modal domains associated to structural modes [Magalhães et al. (2010)]

Follow this way, using the correlation between the singular vector associated to the resonance peak and the singular vectors associated to other values around such peak, it is possible to define the modal domain related to that specific resonant mode. The correlation between such vectors is defined through the Modal Assurance Criterion (MAC) [Allemang and Brown (1983)].

$$MAC = \frac{(\phi_1^T \cdot \phi_2)^2}{(\phi_1^T \cdot \phi_1)(\phi_2^T \cdot \phi_2)} \tag{2.121}$$

The MAC index is an indicator of consistency between two mode shapes. Its value ranges from 0, corresponding to orthogonal mode shapes, and 1, in case of similar mode shapes that only differ of a scale factor, respectively. If the MAC values calculated between the vector of the resonant peak and each other one associated to the values around the resonant peak are close to 1, then all these points can be included in the modal domain. Obviously, a threshold of the MAC value needs to be fixed in order to define the modal domain associated to each resonant frequency [Brinker et al. (2001)]. Otherwise, those singular vectors with lower correlation degree, in term of MAC value, are discarded from the modal domain.

Once the modal domain is defined for each resonant peak, the estimation of the mode shape is performed averaging all the singular vectors that belong to the identified modal domain. Therefore, when similar singular vectors are selected for a given modes, the segment of auto-spectrum may be re-converted to the time domain using the inverse FFT function. Then, the modal damping ratio of the investigated mode could be extracted from the auto-correlation function applying simple concepts of structural dynamic and considering the structure composed by 1-DOF system.

In fact, once the modal domain has been defined, the bell-shaped auto-spectrum (of the SDOF model) can be converted back into the time domain separating the contribution of one single mode. The auto-correlation function of a SDOF system excited by white noise is proportional to its impulse response, defined as [Clough and Penzien (1993)]:

$$h(t) = ce^{-\xi_k \omega_k t} \sin(\omega_k t) \tag{2.122}$$

where c is a constant and ξ_k and ω_k represent the damping ratio and the circular frequency, respectively. Therefore, it is possible to estimate the damping ratio of the SDOF system by fitting the impulse response to the auto-correlation function or computing the logarithmic decrement of the normalized SDOF auto-correlation function.

This procedure became very popular in the Civil Engineering community principally due to its user-friendly approach capable to provide useful information with relevant physical meaning strictly related to the dynamic behavior of investigate structure.

Nevertheless, some disadvantages of this method should be pointed out. The first one consists of the strong dependence of the modal parameters on the frequency resolution, that affects the correct identification. Other conditions that may lead to any difficulties in the identification process are the low value of the signal-to-noise ratio or the presence of closely spaced modes. In these circumstances, the estimated of the mode shape might differ from the correct one because in structural dynamics the orthogonality between mode shapes is related to mass and stiffness matrices, meanwhile the SVD algorithm leads to singular vectors whose orthogonality is defined by the geometrical nature of the problem. So, in the latter case, high uncertainty could affect the mode shape estimate.

2.3.3 Identification techniques implemented in the time domain

The Stochastic Subspace Identification (SSI) methods, described in [Van Overschee and De Moor (1996); Peeters et al. (1999); Peeters (2000)] are parametric identification techniques developed in the time domain. In both cases, the modal parameter identification is performed adopting a discrete-time state-space representation (see **Eq. 2.72**), and on the identification of the system matrix A which contains all the dynamic features of the investigated system. Mainly, two subspace algorithms are usually adopted in OMA applications: the Covariance-driven SSI (SSI-Cov), as described in [Peeters et al. (1999)], [Peeters (2000)] based on the construction of the correlation matrix, and the Data-driven SSI (SSI-Data) introduced in [Van Overschee and De Moor (1996)] based on the projection of the recorded response time series.

2.3.3.1 Covariance-driven Stochastic Subspace Identification method

The Covariance-driven Stochastic Subspace Identification (SSI-Cov) method is a parametric technique developed in time domain that identifies a stochastic state-space model from the output covariance matrix (or correlation, if the signal is ZOH) starting from the output responses collected on the structure. The algorithm presented in this section correspond to the version described in [Peeters et al. (1999); Peeters (2000)] in which the possibility of using the covariance functions between l pre-selected output references instead all r available channels is described. The choice of the reference channels is related to the redundancy of information provided by the sensors themselves on the structure. In fact, if the sensors are not located on a node of the mode and they are positioned in symmetrical position respect to the expected modes, they might provide the same information in terms of frequency and damping ratio. Under this condition, some recorded points can be omitted for the construction of the correlation matrix.

Furthermore, as already previously mentioned, when a dynamic test is performed in "multi-setups" configuration, the structural responses in the instrumented DOFs are measured at different times. Some of these DOFs must be measured in all setups, and they constitute the so-called *reference sensors* that become the reference channels in the application of the identification method. Therefore, for each acquisition instant k, two vectors have to be defined: y_k^{ref}, column vector containing the accelerations measured at l reference DOFs, and y_k, column vector containing the response measured at all r instrumented DOFs, at each time-instant k.

As previously stated, the SSI-Cov method addresses the dynamic identification problem adopting the state-space model to fit the behavior of the investigated structure, under the hypothesis of white noise excitation and linear time-invariant property of the representing system. This task is performed estimating the system matrix A, the output matrix C and the model order n from the output responses [Peeters et al. (1999)], as also described in the practical application reported in [Magalhães et al. (2008)].

The first step of this method consists of defining the covariance matrix of the output $y(t)$. Recalling the equation defined in **Eq. 2.76**, and referring the correlation function to the reference channels as reported below:

$$E\left[y_{k+i} \cdot {y_k^{ref}}^T\right] \tag{2.123}$$

The correlation functions are evaluated for positive time-lags varying its value from $1\Delta t$ to $(2i\text{-}1)\Delta t$ represented by $\mathrm{R}_1^{\mathrm{ref}}$ to $\mathrm{R}_{2\mathrm{i}-1}^{\mathrm{ref}}$ and organized into [$n_0 i$-by-$n_r i$] blocks to construct the following Toeplitz matrix:

$$T_{1|i}^{ref} = \begin{bmatrix} R_i^{ref} & R_{i-1}^{ref} & \dots & R_1^{ref} \\ R_{i+1}^{ref} & R_i^{ref} & \dots & R_2^{ref} \\ \vdots & \vdots & \ddots & \vdots \\ R_{2i-1}^{ref} & R_{2i-2}^{ref} & \dots & R_i^{ref} \end{bmatrix} \tag{2.124}$$

Where n_0 is the number of the selected outputs and n_r corresponds to all channels. Recalling the factorization property in **Eq. 2.81**, the Toeplitz matrix (**Eq. 2.124)** can be expressed as:

$$T_{1|i}^{ref} = \begin{bmatrix} CA^{i-1}G^{ref} & CA^{i-2}G^{ref} & \dots & CA^0G^{ref} \\ CA^iG^{ref} & CA^{i-1}G^{ref} & \dots & CA^1G^{ref} \\ \vdots & \vdots & \ddots & \vdots \\ CA^{2i-2}G^{ref} & CA^{2i-3}G^{ref} & \dots & CA^{i-1}G^{ref} \end{bmatrix} \tag{2.125}$$

Eq. 2.125 reveals that the information in the system defined by $\mathrm{T}_{1|\mathrm{i}}^{\mathrm{ref}}$ could appear redundant (as the first covariance block term $\mathrm{R}_1^{\mathrm{ref}}$ contains all dynamics information on the system) but the single block alone is not sufficient to solve the identification problem. Hence, the Toeplitz matrix can be decomposed in the product of the following matrices:

$$T_i = \begin{bmatrix} C \\ C \cdot A \\ \dots \\ C \cdot A^{i-1} \end{bmatrix} \cdot \begin{bmatrix} A^{i-1} \cdot G^{ref} & \dots & A \cdot G^{ref} & G^{ref} \end{bmatrix} = O_i \cdot \Gamma_i^{ref} \tag{2.126}$$

In the second equality the *observability matrix* $\mathrm{O_i}$ and the *controllability matrix* $\Gamma_{\mathrm{i}}^{\mathrm{ref}}$ are defined. The first matrix is composed by a column of i blocks with [n_0-by-n_r] dimension; the second one is formed by a row of i blocks with [n_r-by-n_r] dimension.

From the computational point of view, the factorization of the Toeplitz matrix can be performed by using the SVD algorithm as follow:

$$T_i = U \cdot S \cdot V^T = [U_1 \quad U_2] \cdot \begin{bmatrix} S_1 & 0 \\ 0 & 0 \end{bmatrix} \cdot \begin{bmatrix} V_1^T \\ V_2^T \end{bmatrix} = U_1 \cdot S_1 \cdot V_1^T \tag{2.127}$$

In which, as well-known the matrices U and V are orthonormal matrices and S is a diagonal matrix composed by positive SVs in descending order. For clarity, the index 1 is associated to non-zero singular values, which defines the rank of the decomposed matrix, which, in this case, coincide with n (assuming $n<i\cdot n_r$), the maximum dimension of the state-space model and then the maximum rank of the matrix A.

Comparing **Eq. 2.126** and **Eq. 2.127** it comes out that the observability and the controllability matrices can be obtained splitting the outputs of the SVD into two parts:

$$\begin{aligned} O_i &= U_1 \cdot S_1^{1/2} \\ \Gamma_i &= S_1^{1/2} \cdot V_1^T \end{aligned} \tag{2.128}$$

Considering the structure of the matrices presented in **Eq. 2.128**, once the latter have been obtained, the identification of the state-space model through the matrices A and C is quite straightforward solved. In fact, matrix C can be extracted from the first n_0 lines of the observability matrix O_i. The most efficient and robust procedure to obtain matrix A is based on the shift structure of the observability matrix [Kung (1978)]. Thus, A is the solution of a least squares problem expressed by the following equation:

$$\begin{bmatrix} C \\ CA \\ \cdots \\ CA^{i-2} \end{bmatrix} \cdot A = \begin{bmatrix} CA \\ CA^2 \\ \cdots \\ CA^{i-1} \end{bmatrix} \Leftrightarrow \bar{O} \cdot A = \underline{O} \tag{2.129}$$

$$A = \begin{bmatrix} C \\ CA \\ \cdots \\ CA^{i-2} \end{bmatrix}^{\dagger} \cdot \begin{bmatrix} CA \\ CA^2 \\ \cdots \\ CA^{i-1} \end{bmatrix} \Leftrightarrow A = \bar{O}^{\dagger} \cdot \underline{O} \tag{2.130}$$

$$\text{where} \quad \overline{O} = \begin{bmatrix} C \\ CA \\ \vdots \\ CA^{i-2} \end{bmatrix}, \quad \underline{O} = \begin{bmatrix} CA \\ CA^2 \\ \vdots \\ CA^{i-1} \end{bmatrix} \tag{2.131}$$

where $\overline{O}$ contains the first *l·(i-1)* lines of O_i and $\underline{O}$ contains the last *l·(i-1)* lines of O_i. The symbol $(\bullet)^{\dagger}$ represents the Moore-Penrose pseudo-inverse operational function, which is used to solve the least squares problems of an overdetermined system of equations, minimizing the sum of the squared errors of the individual equations.

Subsequently, as referred in the previous paragraph, the modal parameters can be easily extracted from matrices A and C, performing the eigenvalue decomposition of the obtained system matrix A. In fact, recalling the **Eq. 2.66**, the natural frequencies f_k and modal damping ratios ξ_k can be extracted from the eigenvalues of the matrix A (i.e., μ_K), after removal the poles with negative imaginary component, as described below:

$$\lambda_k = \frac{ln\,(\mu_k)}{\Delta t} \Rightarrow f_k = \frac{|\lambda_k|}{2\pi}\,; \qquad \xi_k = -\frac{Re(\lambda_k)}{|\lambda_k|} \tag{2.132}$$

where Abs(•) and Re(•) are the absolute value and the real part value of the complex number (•).

Concluding, the mode shapes ϕ_k are evaluated by multiplying the output matrix C and the corresponding eigenvectors ψ_k of the matrix A, as shown below:

$$V = \mathrm{C} \cdot \Psi \;\Leftrightarrow\; \phi_k = \mathrm{C} \cdot \psi_k \tag{2.133}$$

It is worth noting that the eigenvectors of the matrix A are organized in a [n_0-by-n] dimensional matrix, which contains the columns of the observable components of the mode shapes. Due on the fact that the solutions of the state-space model are described by complex conjugate pairs, only the columns associated at eigenvectors associated to the eigenvalues with positive imaginary component are selected to extract the mode shape. In this way, a state-space model of order *n* provides *n/2* possible solutions.

Furthermore, in the context of practical applications, SSI-Cov outputs are based on estimates of the output correlation matrices that are calculated using a limited number of samples. Hence, possible non-linear behavior of the structure (modelling inaccuracies) together with the noise content in the collected signals do not permit the exact definition

of the state-space model. Indeed, the system matrix A and the output matrix C together with the relative modal parameters must be considered also as estimates.

In addition, the SVD of the Toeplitz matrix does not permit the identification of *a priori* model order. Moreover, the higher singular values theoretically should be equal to zero but in practice they present residual values because the noise content and the inaccuracy. Several applications on real structures have also shown that is even not possible to identify any gap between consecutive singular values that permit to obtain reasonable estimates of the most adequate model that best fits the dynamic behavior of the system.

The most efficient way currently used in practical applications to overcome this issue is defining the modal parameters through using several models with increasing orders (within a previously fixed interval) defined in conservative way. The interval of the order is defined choosing the upper limit much higher that two times the number of the expected physical modes within the investigate frequency range. Subsequently, the best model (and then the model order) is chosen to estimate the correct modal parameters.

This strategy can be accomplished in effective way, because the SVD of the Toeplitz matrix, that consists of the most demanding operation, has only performed once and all corresponding singular values are defined during this operation. So, when the maximum model order is defined (during the initial tuning of the input parameters) the Toeplitz matrix is constructed and the SVD of the complete Toeplitz matrix is performed. At this point the strategy consists of extract the modal parameters defining models with successively increasing orders until reach the maximum available order. Thus, models with increasing order are estimates selecting increasing number of singular values to calculate the observability and controllability matrices.

It is worth highlighting that the use of high model orders leads to a comparison of numerical modes (also called noise or spurious modes) that do not have physical meaning and they are mainly related to the noise content in the collected records.

At this point the separation of the physical modes from spurious modes plays an important role in the identification process. One of the most efficient strategy to overcome this problem is given by the construction of the so-called *stabilization diagram*. This diagram consists of a graphical tool in which the modal estimates (principally natural frequencies) provided by all state-space models defined for increasing order are reported. The inspection of the stabilization diagram (natural frequency vs. model order diagram) allows the identification of stable alignments composed by so-called *stable poles* that maintain consistency in terms of modal parameters for increasing model order.

Therefore, all poles that appear for increasing model order with consistent natural frequency, mode shape and damping ratio values are considered as stable and are likely to be physical. Meanwhile, those poles that are spread out on the diagram and appear only in some models are classified as spurious and they should not be considered for the estimation of the modal parameters.

Numerical simulation

The numerical acceleration time series of the shear-type model (3-DOFs system) have been used to test the performance of the developed SSI-Cov technique, implemented in MatLab environment. Since all DOFs were considered as reference sensors (n_r), the numerical series were organized in a block Hankel matrix and for each record the correlation functions were defined using the *xcorr* function belong to the MatLab toolbox. Thus, the three-dimensional correlation matrix with [n_r×n_r×(2i-1)] dimension, in which n_r represents the number of the reference sensors and i is the time-lag value, was defined. Then the Toeplitz matrix with [$n_r i$×$n_r i$] dimension was constructed by reshaping the correlation matrix. The parameter i (time-lag) limits the maximum model order (n_x) of the stochastic space models: n_x=i×n_r. Since, the maximum order was fixed at 30, being the reference channel equal to 3, the time-lag has to be set equal to i=30/3=10, which it also consists of the minimum values necessary to define the state-space model with 30 order.

From performance of the SVD (see **Eq. 2.118**). of the $T_{1|i}^{ref}$ (see **Eq. 2.125**), performed for the application of the SSI-Cov identification technique, 30 solutions can be obtained. The SV values are depicted in **Fig. 2.18** (after scaling them by using the maximum value).

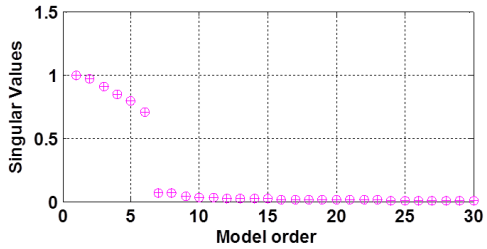

Fig. 2.18. Singular values obtained by applying the SVD technique to the Toeplitz matrix

As shown in **Fig. 2.18**, the dynamic behaviour of the numerical structure is well defined by a state-space model of order 6. This is confirmed by the main jump between the 6th and the 7th SV. In fact, the obtained value obtained for higher model order can be considered as residuals. It is worth noting that this result was expected by the fact that the system is composed by three DOSF and all DOF have been used as reference outputs; so, the state-space model that best fit this system has an order twice of its reference DOFs.

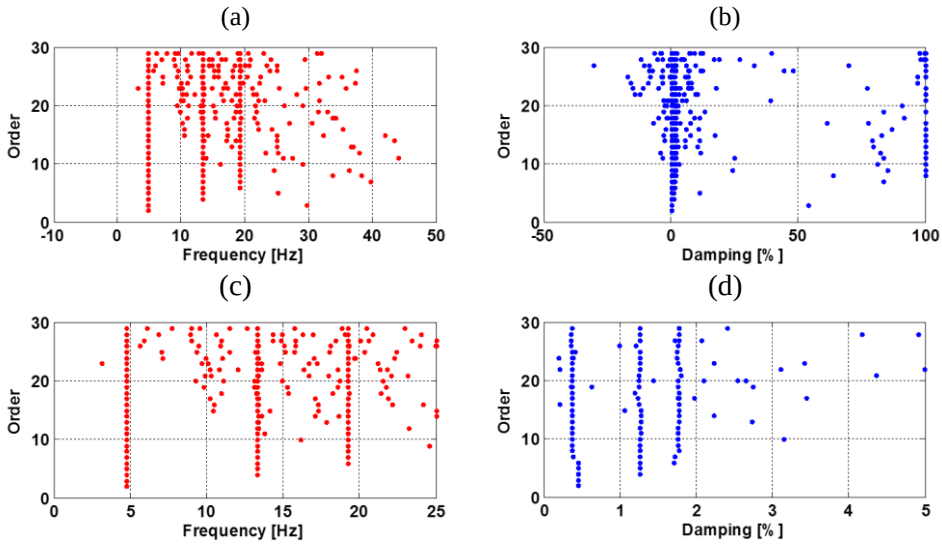

Fig. 2.19. Stabilization diagrams: a) natural frequencies and b) modal damping ratios; zoom of the c) stable natural frequency and d) stable damping ratio values

Consequently, the further step performed by the SSI-Cov technique consists of constructing the system matrix A adopting the **Eq. 2.130** and estimating the natural frequencies and the modal damping ration of the system using the relations in **Eq. 2.132**. Then, the relative natural frequencies and damping ratio values are extracted and reported on the stabilization diagram as depicted in **Fig. 2.19**.

In the diagrams of **Fig. 2.19** are reported all frequencies and damping ratios estimates (stable and unstable) obtained referred to a model order between 2 and 30. Inspecting both diagrams reported in **Fig. 2.19**(a and b), it is not easy to detect those values that maintain consistency in term of modal parameters (i.e., natural frequencies and modal damping) for increasing model order. Meanwhile after zooming the diagrams, **Fig. 2.19**(c and d), the stable alignments are quite evident. Accordingly to the results reported in **Fig. 2.19**, as well as the SV values depicted in **Fig. 2.18**, a state-space model with order equal to 6, fit well enough the dynamic behavior of the numerical system. Therefore, the natural frequencies and the damping ratios associated to the selected model are reported below:

Table 2.3. Comparison between the theoretical values and the extracted modal estimates.

Modes	Theoretical		Experimental	
	Freq. [Hz]	Damp. [%]	Freq. [Hz]	Damp. [%]
1	4.755	0.45	4.756	0.49
2	13.323	1.25	13.318	1.32
3	19.252	1.80	19.245	1.83

Again, the matrix V defined by the **Eq. 2.133** is composed by complex conjugate vectors which represent the mode shapes associated to the solution of the selected model. Therefore, this matrix is composed by 6 columns because the solutions of the model, but in fact they represent 3 complex conjugated structural modes. The amplitude and the phase values of the extracted modes are reported in the **Table 2.4**.

Table 2.4. Identified vibration modes extracted using the SSI-Cov technique

Mode 1			Mode 2			Mode 3		
Amplitude	Phase	Mode	Amplitude	Phase	Mode	Amplitude	Phase	Mode
9.166	1.542	0.445	17.156	3.111	-1	12.544	0.017	0.803
16.505	1.543	0.802	7.691	3.114	-0.448	15.619	3.119	-1
20.590	1.543	1	13.785	0.032	0.803	6.952	0.019	0.445

Meanwhile the graphical configuration of the mode shapes, normalized through the maximum floor displacement, are reported in **Fig. 2.20**.

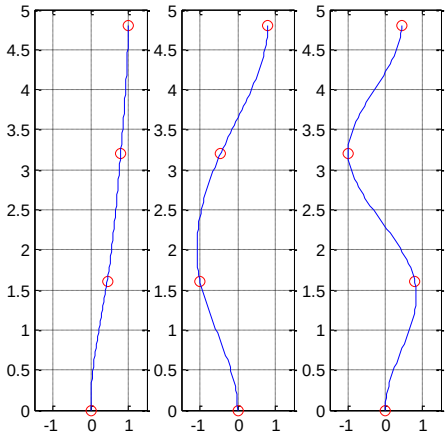

Fig. 2.20. Identified mode shapes of the 3-DOFs system

Concluding, it is worth highlighting that all components of each identified mode are "in phase" or "in opposite phase", this means that all components move in the same direction or with a difference phase equal to π, at same time. This information indicates that all modes are real. This result was expected because the acceleration time series have been simulated respecting the hypothesis of the proportional damping of the damping matrix between the mass ad stiffness distributions.

2.3.3.2 Data-driven Stochastic Subspace Identification method

Alternatively, the system model can be identified using the Data-driven Stochastic Subspace Identification (SSI-Data) method [Van Overschee and De Moor (1996)] [Ljung (1999)] estimating the state-space model directly using the collected response time series avoiding the construction of the outputs covariance matrix. This last step is replaced by projecting the row space of "future" outputs into the row space of "past" of the outputs previously organized in a Hankel matrix.

This identification method was implemented in two different programs: MACEC [(Branden et al. (1999)] and ARTeMIS (SVS 2004). The program MACEC is a "toolbox" developed in MatLab code in the University of Leuven. Meanwhile, ARTeMIS is a commercial program implemented by research group in the University of Aalborg.

The good quality of the results obtained by the application of this last program has motivated its increasing use in the dynamic identification of civil engineering structures. Nowadays, due to the easy interpretation and the good accuracy of the results, ARTeMIS is generally used for preliminary modal parameters identification of AVTs.

In this subsection, the fundamental steps of this time-domain identification method are illustrating referring to the algorithm presented in [Peeters (2000)] previously introduced in the textbook [Van Overschee and De Moore (1996)]. The efficiency of this version was initially confirmed by several applications in Civil Engineering structures described in [Peeters and De Roeck (2001)].

In this paragraph the main concepts related to the non-stationary Kalman Filter are succinctly described in order to justify the implementation of the identification method. Consequently, the main steps related to the development of the SSI-Data technique as: 1) organization of the collected responses into a Hankel matrix, 2) estimation of the observability matrix in two consecutive time-instants, and 3) extraction of the modal parameters after the definition of the system matrix A and the output matrix C, will be describes in detail.

Kalman filter

It is mandatory to mention that the *Kalman filter* plays a fundamental role on the developed of this method. For clearness, the description of the algorithm will not be done following the classical approach and introducing the Kalman Filter concepts, very important for the mathematical approach but very difficult to understand even for expert engineering with a normal background in the structural dynamic. In this way, the main

concepts related to Kalman Filter are succinctly described referred to the implementation of the SSI-Data method.

The objective of the no steady Kalman filter is to provide an optimal estimation of the vector state x_{k+1} using the outputs responses and the statistical properties of the matrices A, C, R_0 and G described in the previous paragraph. The estimate of the state vector $\hat{\mathrm{x}}_{\mathrm{k+1}}$ is obtained applying the expressions of the **Eq.** 2.134 in recursive way considering the observation of the outputs up at time instant *k*, the initial state estimate $\hat{\mathrm{x}}_0$=0 and the initial covariance of the state estimates $\mathrm{P}_0 = \mathrm{E}\left[\hat{\mathrm{x}}_\mathrm{k}\hat{\mathrm{x}}_\mathrm{k}^\mathrm{T}\right] = 0$

$$\begin{gathered}\hat{x}_{k+1} = A \cdot \hat{x}_k + K_k \cdot (y_k - C \cdot \hat{x}_k) \\ K_k = (G - A \cdot P_k \cdot C^T) \cdot (R_0 - C \cdot P_k \cdot C^T)^{-1} \\ P_{k+1} = A \cdot P \cdot A^T + (G - A \cdot P_k \cdot C^T) \cdot (R_0 - C \cdot P_k \cdot C^T)^{-1} \cdot (G - A \cdot P_k \cdot C^T)^T\end{gathered} \tag{2.134}$$

in which K and P are the *Kalman filter gain matrix* and the *Kalman state covariance matrix*, respectively. The interested reader could find more information in the following references [Ljung (1987), Juang (1994), Overschee and De Moor (1996)].

The estimates of the *state vectors* of the Kalman filter $\hat{x}_i$ can be subsequently organized to form the Kalman filter $\hat{X}_i$ state sequence, used in the SSI-Data algorithm, defined as:

$$\hat{X}_i = (\hat{x}_i \;\; \hat{x}_{i+1} \ldots \hat{x}_{i+N+1}) \in \mathbb{R}^{n \times N} \tag{2.135}$$

Such sequence can be written as linear combination of the past output measurements and it is generated by a bank of non-steady Kalman filters working in parallel on each column of the block Hankel matrix of past outputs Y_p. This consideration implies that the bank of Kalman filters can be determined directly from the outputs data [Juang (1994), Overschee and De Moor (1996)].

Factorization and Projection matrix

The first task in the SSI-Data technique consists of organizing the output measurements into the block Hankel matrix (H) (a matrix being constant along its anti-diagonal elements) of [2i-by-N] dimension; which 2i defines the number of the block-rows and N is the number of the columns. The value of i remarks the time-lag concept introduced for SSI-Cov method, and from a statistical point of view the number of columns should be $N\rightarrow\infty$. In practical application this value is chosen in order to use all available data in the projection phase and it is set as $N=j-(2i-1)\rightarrow j-2i+1$ where j is the number of all sampling points of the collected response. However, if l defines the number of available channels the dimensions of the Hankel matrix are $2il \cdot N$ can be subdivided into two submatrices of the "past" Y_p^{ref} and "future" Y_f part.

For clearness, from this point the notation and the description of the procedure will not referred to the reference sensors; this does not involve any modification of the algorithm but only a minor computational cost due to a smaller number of rows used for the construction of the "past" submatrix. By the way, in this Thesis this procedure is implemented to be used in the context of continuous monitoring process in which all installed sensors are normally used as references ones.

Before explaining the identification algorithm, the data reduction and smoothing procedures used to divide the experimental signals in to "past" and "future" part are introduced. As stated, in experimental data, only discrete samples of time signals y_k (k=0,1…N, N→∞) are available, therefore once the sensors configuration placed at certain nodes of the structure are defined, the discrete samples of the output responses y_k can be described as sample matrix as follows:

$$y_k = [y_m^n] = \begin{bmatrix} y_1^n \\ y_2^n \\ \vdots \\ y_l^n \end{bmatrix} = \begin{bmatrix} y_1^0 & y_1^1 & \cdots & y_1^N \\ y_2^0 & y_2^1 & \cdots & y_2^N \\ \vdots & \vdots & \ddots & \vdots \\ y_l^0 & y_l^1 & \cdots & y_l^N \end{bmatrix} \tag{2.136}$$

where y_m^n refers the n^{th} ($n=0,1,2...N$) samples points from the m^{th} ($m=1,2...l$) available sensor. Once the data are organized in this way, the Hankel matrix can be construct dividing the data in a "past" Y_p and "future" Y_f section as described in the follows:

$$H_{0|2i-1} = \frac{1}{\sqrt{N^*}}\begin{bmatrix} y_0 \\ y_1 \\ \vdots \\ y_{i-1} \\ y_i \\ y_{i+1} \\ \vdots \\ y_{2i-1} \end{bmatrix} = \frac{1}{\sqrt{N^*}}\left[\begin{array}{cccc} y_0 & y_1 & \cdots & y_{N-1} \\ y_1 & y_2 & \cdots & y_N \\ \vdots & \vdots & \ddots & \vdots \\ y_{i-1} & y_i & \cdots & y_{i+N-2} \\ \hline y_i & y_{i+1} & \cdots & y_{i+N-1} \\ y_{i+1} & y_{i+2} & \cdots & y_{i+N} \\ \vdots & \vdots & \ddots & \vdots \\ y_{2i-1} & y_{2i} & \cdots & y_{2i+N-2} \end{array}\right] = \begin{bmatrix} Y_{0|i-1} \\ \hline Y_{i|2i-1} \end{bmatrix} = \begin{bmatrix} Y_p \\ \hline Y_f \end{bmatrix} \qquad (2.137)$$

where $H \in \mathbb{R}^{2il \times N^*}$ is a symmetric matrix since the components are constant across the anti-diagonals. The number of block rows *i* is a user defined index which is theoretically larger than the maximum order of the system. It is noted that $H_{0|2i-1}$ consists of *2li* block of rows since each block includes *l* (number of output measurements). The number N^* is typically equal to all number of samples *N* defined in the previous equation reduced by *2i-2* elements, which implies the all samples of the collected signal are used in the organization of the matrix.

The subscripts of $Y_{0|i-1}$ $Y_{i|2i-1}$ indicate the first and last block-element in the first column of the *H* matrix used to define the *past* and *future* matrices dimension. Such matrices are obtained by splitting the *H* matrix in two sub-matrices of *i* block rows each.

A second step of the identification algorithm consists of another division obtained omitting the first block-row from the "future" matrix $Y_{0|2i-1}$ and adding this block-row as the last one in the "past" matrix $Y_{0|i}$ which can be explained as follows:

$$H_{0|2i-1} = \frac{1}{\sqrt{N^*}}\begin{bmatrix} y_0 \\ y_1 \\ \vdots \\ y_i \\ y_{i+1} \\ y_{i+1} \\ \vdots \\ y_{2i-1} \end{bmatrix} = \frac{1}{\sqrt{N^*}}\left[\begin{array}{cccc} y_0 & y_1 & \cdots & y_{N-1} \\ y_1 & y_2 & \cdots & y_N \\ \vdots & \vdots & \ddots & \vdots \\ y_i & y_{i+2} & \cdots & y_{i+N-1} \\ \hline y_{i+1} & y_{i+2} & \cdots & y_{i+N} \\ y_{i+2} & y_{i+3} & \cdots & y_{i+N+1} \\ \vdots & \vdots & \ddots & \vdots \\ y_{2i-1} & y_{2i} & \cdots & y_{2i+N-2} \end{array}\right] = \begin{bmatrix} Y_{0|i} \\ \hline Y_{i+1|2i-1} \end{bmatrix} = \begin{bmatrix} Y_p^+ \\ \hline Y_f^- \end{bmatrix} \qquad (2.138)$$

This operation allows the estimation of the system matrices of the adopted state-space model. Accordingly, Once the data are well organized, the next step of SSI-Data procedure is the projection of the row space of the *future outputs* into the row space of the *past outputs*. Namely, the projection is defined as follows:

$$\mathcal{P}_i = \left[\frac{Y_{i|2i-1}}{Y_{0|i-1}}\right] = \frac{Y_f}{Y_p} = Y_f Y_p^T \left(Y_p Y_p^T\right)^\dagger Y_p \tag{2.139}$$

In which, as already defined, the $Y_{i|2i-1}$ and $Y_{0|i-1}$ are the blocks matrix that contain the *future* and the *past* outputs, respectively. The main motivation behind this projection is that it retains all the information in the *past* that are useful to predict the *future*.

From **Eq. 2.139** it is clear how the notions of projection and covariance are closely related as they both aimed at removing the (uncorrelated) noise. However, the products $Y_f Y_p^T$ and $Y_p Y_p^T$ are block Toeplitz matrices that contain the covariance between output signals. Moreover, the projection matrix is also equal to the product of the extended observability matrix O_i and the Kalman filter state sequence $\hat{X}_i$.

$$\mathcal{P}_i = O_i \cdot \hat{X}_i \tag{2.140}$$

This relation is based on the main theorem of SSI method and a good proof can be find in the appendix proved in [Van Overschee and De Moor (1996)]. Should be also highlighted that **Eq. 2.139** is just a definition and the projection can not be computed straightforward. In fact, for practical applications such operation is numerically computed by using the *QR-factorization* of the H matrix as described in [Peeters et al. (1999)].

$$H_{0|2i-1} = \left[\frac{Y_p}{Y_f}\right] = R \cdot Q^T \tag{2.141}$$

The QR factorization can be viewed as a compression data step. In fact, the H matrix, composed by a very large number of columns, is decomposed and compressed in a smaller lower triangular matrix R which contain all information regarding the system.

Without going deeper in the numerical implementation details, the QR factorization is a simple tool used to easily calculate the projection matrix:

$$H_{0|2i-1} = \begin{matrix} l \\ li \\ l(i-1) \end{matrix} \updownarrow \begin{matrix} \begin{pmatrix} R_{11} & 0 & 0 \\ R_{21} & R_{22} & 0 \\ R_{31} & R_{32} & R_{233} \end{pmatrix} \cdot \begin{pmatrix} Q_1^T \\ Q_2^T \\ Q_3^T \end{pmatrix} \\ \begin{matrix} \leftrightarrow & \leftrightarrow & \leftrightarrow \\ li & l & l(i-1) \end{matrix} \end{matrix} \begin{matrix} \updownarrow \\ \updownarrow \\ \updownarrow \\ \leftrightarrow \\ N \end{matrix} \begin{matrix} l \\ li \\ l(i-1) \end{matrix} \tag{2.142}$$

Substituting the **Eq. 2.142** in **Eq. 2.140**, the projection matrix $\mathcal{P}_{\mathrm{i}}$ is expressed by the product of R and Q submatrices as follows:

$$\mathcal{P}_i = \begin{pmatrix} R_{21} \\ R_{31} \end{pmatrix} \cdot Q_1^T \tag{2.143}$$

Similarity, the subsequent Projection matrix $\mathcal{P}_{\mathrm{i}-1}$ is computed by alternative expression of the *future* outputs Y_f^- and the past outputs Y_p^+, both obtained as the **Eq. 2.138**:

$$\mathcal{P}_{i-1} = \begin{pmatrix} R_{31} & R_{32} \end{pmatrix} \cdot \begin{pmatrix} Q_1^T \\ Q_2^T \end{pmatrix} \tag{2.144}$$

Finally, the factorization property applied to the projection matrices pays a crucial role in the SSI-Data technique because the computational cost of the QR factorization is very time consuming. Otherwise, once the projection matrices $\mathcal{P}_{\mathrm{i}}$ and $\mathcal{P}_{\mathrm{i}-1}$ are available, the system matrices and the modal parameters can be easily estimated. As detailed in [Overschee and De Moor (1996)], the main theorem of the SSI methods states that the projection $\mathcal{P}_i$ can be factorized as the product of the previously defined observability matrix (see **Eq. 2.126**) and the Kalman filter state sequence (**Eq. 2.135**):

$$\mathcal{P}_i = \begin{bmatrix} C \\ CA \\ \vdots \\ CA^{i-1} \end{bmatrix} \cdot [\hat{x}_i \;\; \hat{x}_{i+1} \dots \hat{x}_{i+N+1}] = O_i \cdot \hat{X}_i \tag{2.145}$$

On the other side, the singular value decomposition of the obtained prediction matrix is:

$$\mathcal{P}_i = U \cdot S \cdot V^T = \begin{bmatrix} U_1 & U_2 \end{bmatrix} \cdot \begin{bmatrix} S_1 & 0 \\ 0 & 0 \end{bmatrix} \cdot \begin{bmatrix} V_1^T \\ V_2^T \end{bmatrix} = U_1 \cdot S_1 \cdot V_1^T \tag{2.146}$$

The matrix $\mathcal{P}_i$ has order *n*, since it results from the multiplication of a matrix with *n* columns (O_i) by a matrix with lines (X_i), so the number of different non-zero values resulting from its decomposition is also equal to *n* and it denotes the order of the model and it defines the dimension of the matrix A. Therefore, comparing **Eqs. 2.145** and **2.146**, the matrices O_i and X_i can be factorized as follow:

$$\begin{aligned} O_i &= U_1 \cdot S_1^{1/2} \\ \dot{X}_i &= O_i^{\dagger} \cdot \mathcal{P}_i \end{aligned} \tag{2.147}$$

In order to identify the matrices A and C, another projection has to be defined, shifting one block row down from *past* to *future* outputs of the Hankel matrix (**Eq. 2.140**):

$$\mathcal{P}_{i-1} = \frac{Y_f^{-}}{Y_p^{+}} = O_{i-1} \cdot \dot{X}_{i+1} \tag{2.148}$$

The new projection can be decomposed similarly to the form described in **Eq. 2.145**:

$$\mathcal{P}_{i-1} = \begin{bmatrix} C \\ CA \\ \vdots \\ CA^{i-2} \end{bmatrix} \cdot [\hat{x}_i \ \hat{x}_{i+1} \dots \hat{x}_{i+N}] = O_{i-1} \cdot \hat{X}_{i+1} \tag{2.149}$$

From this equality it is easy to obtain the sequence of the Kalman filter state $\hat{X}_{i+1}$:

$$\hat{X}_{i+1} = O_{i-1}^{\dagger} \cdot \mathcal{P}_{i-1} \tag{2.150}$$

Follow this way, the Kalman filter state sequences $\hat{X}_i$, $\hat{X}_{i+1}$ are computed using output data only. Using the sequence of vectors state a system with more equations then unknown variables is obtained. So, the system matrices can be determined from the following overdetermined set of linear equations, obtained by stacking the state-space model for time instants *i* to *i+N-1*:

$$\begin{bmatrix} \hat{X}_{i+1} \\ Y_{i|i} \end{bmatrix} = \begin{bmatrix} A \\ C \end{bmatrix} \hat{X}_i + \begin{bmatrix} W_i \\ V_i \end{bmatrix} \tag{2.151}$$

where $Y_{i|i}$ is a Hankel matrix with only one block row and W_i, V_i can be treated as the residuals of an optimization problem. Since the Kalman state sequences and the outputs

are known, and the residuals are uncorrelated with $\dot{X}_i$, the set of equations can be solved for A and C in a least square sense:

$$\begin{bmatrix} A \\ C \end{bmatrix} = \begin{bmatrix} \hat{X}_{i+1} \\ Y_{i|i} \end{bmatrix} \hat{X}_i^{\dagger} \tag{2.152}$$

The identification problem is now theoretically solved: based on the outputs, the system order n and the system matrices A and C are identified. Natural frequencies f_k and mode shapes $\boldsymbol{\phi}_k$ can be obtained following the same procedure previously described for the SSI-Cov technique.

Furthermore, there are some variations of the method that can be useful to extract the modal parameters from the time series. In fact, for the algorithm presented, no matrix weighting was performed. However, in the more general formulation of the SSI-Data identification method, two weighting matrices W_1 and W_2 are considered, which are multiplied by the value of the data to be decomposed into singular values:

$$\bar{\mathcal{P}}_i = W_1 \cdot \mathcal{P}_i \cdot W_2 \tag{2.153}$$

This weighting operation introduces a transformation of state vector coordinates, such as those described in this Chapter, to control similar template arrays, which lead to identical identification results of the process. The SV resulting from each variant have different meanings. For example, those resulting from the CVA variant can be interpreted as the cosines of the principal angles between two vector spaces: the vector space generated by the lines of the matrix Y_f and the vector space generated by the lines of the matrix Y_p.

Table 2.5. The variant weighting matrices in: PC - main component, CVA - canonical analysis

Variation	$\mathbf{W_1}$ **(il · il)**	$\mathbf{W_2}$ **(N · N)**
UPC	I	I
PC	I	$\mathrm{Y_p^T} \cdot (\mathrm{Y_p} \cdot \mathrm{Y_p^T})^{-1/2} \cdot \mathrm{Y_p^T}$
CVA	$(\mathrm{Y_f} \cdot \mathrm{Y_f^T})^{-1/2}$	I

Numerical Example

The SSI-Data technique was also applied process the experimental data previously used for other identification methods. The time–lag value adopted in the previous analysis (using the SSI-Cov technique) was maintained in conservative way to construct the block Hankel matrix. Thus, the parameter *i* was set equal to 10. The first step of the SSI-Data is to gather the output measurements into row blocks to construct the Hankel matrix with dimension equal to $2il \times N^*$, in which N^*corresponds to all number of samples *N* menus *2i+1* element (i.e., (120×45961]). Once the Hankel matrix was computed, the projecting of the row space of the future outputs onto row space of the past outputs was realized using the QR function. Thus, the Projection matrix P_i (**Eq. 2.145**) was created. Consequently, the second projection shifting a row-space-block is performed to obtain the second Projection matrix P_{i-1} (**Eq. 2.149**). Therefore, once both Projection matrices (in the initial step-time (P_i) and in the second step-time (P_{i-1}) have been performed, the state sequence of $\widehat{X}_i$ (see **Eq. 2.147**) and $\widehat{X}_{i+1}$ (see **Eq. 2.150**) can be easily defined. Consequently, the system matrices *A* and *C* referred to the stochastic state-space model are obtained using the **Eq. 2.152**.

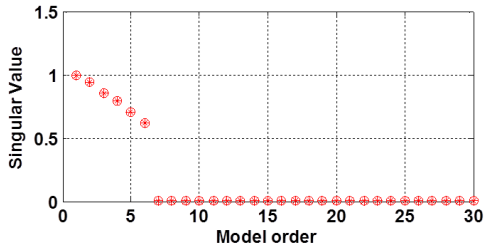

Fig. 2.21. Singular values obtained from the application of the SVD algorithm to the projection matrix (P_i)

As for the SSI-Cov method, is not easy to estimates the order of the model that best fit the experimental data, even for numerical data. Then, a stabilization diagram is constructed by identifying different state-space model. In **Fig. 2.22**(a and b) the solutions related to a state-space models with an increasing order are reported.

As shown, it is not straightforward to define the stable estimates and a manual investigation is required to identify those alignments composed by stable estimates that maintain

consistency in terms of modal parameters. Thus, a zoom of the investigation interval of frequency and modal damping is performed in **Fig. 2.22**(c and d).

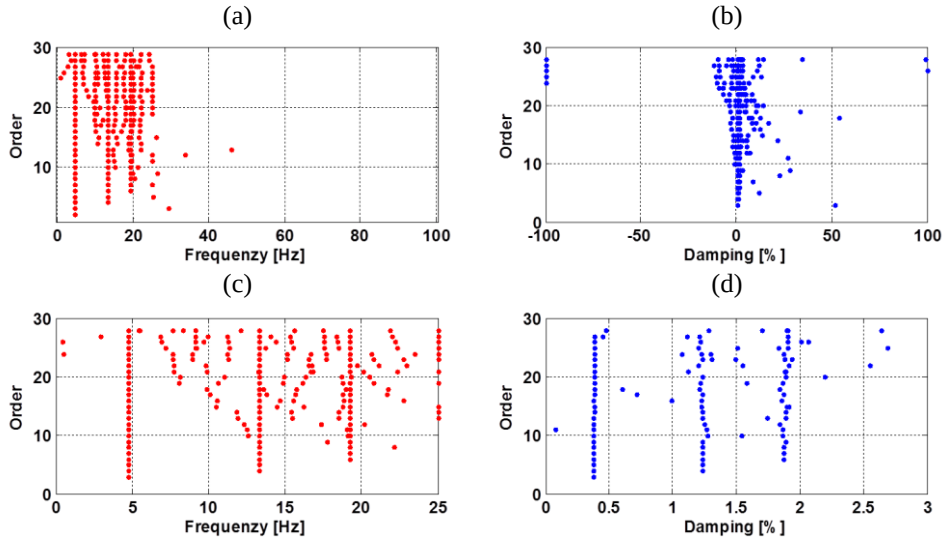

Fig. 2.22. Stabilization diagrams: a) natural frequencies and b) modal damping ratios; c) and d) zoom of both diagrams in the interval of investigation

As can be easily noted, the structure composed by 3-DOFs is well represented by a state model of order equal to 6, (see **Fig. 2.21**). Hence, the modal parameters computed for the order *n=6* have been selected and reported in the following table.

Table 2.6. Natural frequencies, modal damping ratios and mode shapes configuration of the 3-DOFs system

Modes	Theoretical		Experimental		Mode Shape		
	Freq. [Hz]	Damp. [%]	Freq. [Hz]	Damp. [%]	1	2	3
1	4.755	0.45	4.756	0.515	0.444	1	-0.796
2	13.323	1.25	13.328	1.289	0.802	0.444	1
3	19.252	1.80	19.237	1.738	1	-0.803	-0.446

Finally, the mode shapes configurations were obtained from the eigenvectors associated to the selected state-space model with order 6 and they are reported in **Fig. 2.23**. As expected, the mode shapes obtained by applying the SSI-Data technique coincide with those ones previously obtained using the SSI-Cov method.

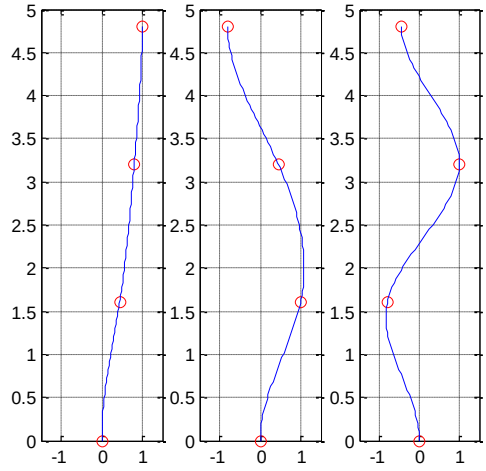

Fig. 2.23. Mode shapes associated to the three natural frequencies extracted by the selected state-space model with order equal to 6 applying the SSI-Data technique.

Furthermore, in **Fig. 2.24** are reported the mode configuration of the 3-DOF system using the polar plot representation. As expected, the 3 mode are real since the mode shape components move in-phase (deviation phase equal to 0°) or in out-of-phase (with a deviation phase equal to 180°).

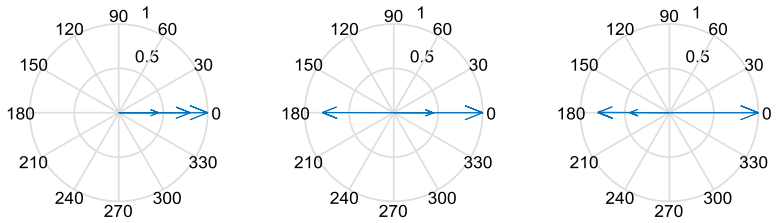

Fig. 2.24. Polar plot configuration of the extracted modes of the numerical structure

It is worth remarking that for a complete system identification procedure also the matrices R_0 (**Eq. 2.77**) and G (**Eq. 2.78**) need to be identified together with the system matrices A and C. However, the identification of the full state-space matrices A, C, G, R_0 in the SSI-Data technique leads to post-processing procedure including spectrum analysis, modal decomposition and prediction errors. For more detail to an interested read is suggested the paper [Peteers (2000)] in which an application of such analysis is reported.

2.4 Conclusions

In this Chapter, the main theoretical concepts of linear-time-invariant systems have been provided to understand the main fundamental concepts behind the dynamic analysis useful to characterize the dynamic properties of the structures. Consequently, the implementation of the most used output-only identification techniques as: PP, FDD, SSI-Cov and SSI-Data methods have been described in detail because they consist of the fundamental milestones of the strategies developed in this Dissertation.

First of all, several mathematical models that are normally used to characterize the dynamic behavior of linear time-invariant systems have been presented; the classical and the modal formulation have been described to define deterministic and stochastic continuous models, in the time and frequency domain. Subsequently, the use of the state-space model allowed the generalization of the identification problem to the structure with non-proportional damping, in both deterministic and stochastic implementation. Finally, the main hypothesis of white noise realization was introduced allowing the development of the stochastic state-space model that consists of the basic step-tool in the implement of the output-only identification methods.

Consequently, four different modal identification techniques used to characterize the dynamic behavior of the structures subject to environmental actions have been implemented. The focus was on those methods that have receive most interest from the Civil Engineering community; as: the Peak Picking (PP), the Frequency Domain Decomposition (FDD) and the Subspace Identification method based on the correlation functions (SSI-Cov) and the other one based on the projection of the collected time series (SSI-Data). These techniques have been implemented in MatLab environment in order to fully manage of the different mathematical operations adopted in the identification process and to understand the physical meaning of the obtained results. Moreover, the application of the developed techniques to a simple structural model (composed by a few DOFs) was useful for testing the efficiency of the implemented algorithms.

The Peak Picking method is the most common used identification technique because its easy implementation and interpretation of the results. For this reason, it is the first reference method adopted in Structural Dynamics courses and also one of the most used in Civil Engineering applications. Due to its easy implementation, this method has some important limitations that lead to possible incorrect results in the case of modes with similar frequency (closely spaced modes) and in those cases where the coefficient of the damping ratio is high (highly damped modes). therefore, this method is very adequate to carry out primary analysis and obtain fast information about the investigate structure.

The FDD method, in its most used developed version, solves the main problems related to the PP method. In fact: it is capable to estimates modes with very close frequency and solves the problem of estimating the modal damping coefficient by using the Enhanced-FDD (EFDD) method. It is worth noting that this last technique – as well as other frequency domain methods – is affected by the error associates to the Finite Discrete Fourier Transform (leakage error) which generally overestimates the damping value.

The SSI-Cov method is the first parametric method developed in time domain that lead to the estimation of the state-space model though the correlation function of the collected time series. This method it is not commonly used because its difficult implementation, and also the concepts related to the estimation of the system matrices in the stochastic model. Otherwise, the advantage of this identification method consists of a good estimate of results obtained with low computational cost.

The SSI-Data method is the last technique and developed in the MatLab environment. Like the previous one, also this method is based on the use of a state-space model, but its implementation requires a higher computational cost than the SSI-Cov method, although this effort is compensated by a better numerical behavior. It is worth remarking that this method has been implemented in the well-known commercial software ARTeMIS, developed by the research group of the University of Aalborg.

Chapter 3

STRUCTURAL HEALTH MONITORING BASED ON OPERATIONAL MODAL ANALYSIS

Contents

3.1 Introduction to Structural Health Monitoring

Structural Health Monitoring (SHM) is generally defined as a multi-disciplinary process involving: (a) the repeated or continuous measurement of the response of a structural system through arrays of appropriated sensors; (b) the extraction from measured data of features, which are representative of the health condition and (c) the statistical analysis of these features to detect any novelty or abnormal change in the investigated system.

In the last decades, the SHM strategy based on vibration monitoring and operational modal analysis (OMA, i.e. the identification of modal parameters from output-only measurements) has received increasing attention in the field of Civil Engineering structures. The raising scientific and practical interest on dynamic monitoring and vibration-based SHM has many motivations, such as: (a) the ageing of existing structure and infrastructures and the preservation of Cultural Heritage, (b) the increasing complexity of new constructions (where the implementation of monitoring system is usually convenient because it is possible to amortize the costs within the construction process); (c) the technological advantages, allowing relatively cheap installation of monitoring systems exhibiting fully computer-based operation; (d) the possibility of assessing the health of the structure from the analysis of its dynamic response to operational and/or ambient excitation.

In this context, after the definition of the dynamic by applying the techniques described in the previous Chapter, the structural response in operational conditions might be collected and analyzed in continuous way.

The implementation of continuous dynamic monitoring directly led to the development of procedures capable to efficiently process data collected by dynamic monitoring systems in order to obtain accurate evolution of the modal parameters over time. For this reason, the development of routines able to analyze large amount of data collected during the continuous monitoring process become mandatory, as well as the automation of the OMA techniques described in Chapter 2.

The availability of new tools performing the automatic identification of the modal parameters represents a milestone for the automation of the identification process. Basically, this task is aimed at mimicking the choice of an expert used takes during the analysis of data recorded during dynamic tests or during the process of each single dataset collected in the contest of permanent monitoring of the structure.

Once the baseline set of modal parameters has been estimated, those parameters are used as reference features to perform the comparison in the tracking process over time. Natural frequencies are the most used parameters adopted as sensitive features in many damage detection applications. On the other hand, they are subjected to external factors that produce periodic variations could mask the occurrence of damage. Thus, the subsequent challenge task consists of the removal of environmental and/or operational effects that affect these features. Nowadays, several approaches have been implemented and applied in order to remove such effects (i.e. Principal Component Analysis, Auto Regressive Models with exogenous input, etc.) under operational conditions, but the damage identification is still a challenging task, as demonstrated in several publishes present in the literature.

In this Chapter a brief overview of the main steps needed to perform a correct assessment of Civil Engineering structures is given, highlighting the main differences between the procedures available in the literature and the approach to SHM adopted in this Dissertation. Subsequently, a brief introduction and the main issues related to the automation of the identification process, mainly oriented to those parametric method based on the construction and interpretation of stabilization diagram are pointed out. Furthermore, the description of different methods nowadays adopted to remove environmental and operational effects on modal parameters (typically the natural frequencies) is also reported in this Chapter. Finally, the outcomes of selected example regard SHM purpose based on OMA parameters are discuss in the end of this Chapter.

3.2 Classical approach and alternative strategy for SHM

In the context of development of vibration-based health monitoring system, there is an increased need of efficient and robust algorithms capable to manage huge quantity of data and to perform an automatic processing of large amounts of continuously recorded data. The recent technological developments have already permitted the installation of efficient and reliable dynamic monitoring systems on large infrastructures capable to provide accurate and relevant information about their dynamic characteristics.

The installation of dynamic monitoring systems on important civil infrastructures in the last decays encouraged huge economical efforts in this research field, driving the development of innovative equipment and robust methodologies that are used to convert large amount of data coming from permanent monitoring into relevant information about structural condition of the monitored constructions. The technological advance and the continuous improvements in the automation of the analysis process have also allowed the assessment of the heath state and the normal behavior of these infrastructures providing a reliable alarm in case of abnormal changes or occurred damages.

Within a Structural Health Monitoring purpose, the processing of the data collected by dynamic monitoring system are automatically analyzed in order to monitor the normal behavior of the investigated structure that comprehends not only the continuous identification of modal parameters but also the removal of environmental and operational effects on extract parameters (normally natural frequencies). In this way, the whole process is composed by four different steps:

1) the recording of the structural responses through the use of different type of sensors (i.e., accelerometers, seismometers, etc.) installed on the structure;
2) identification of the modal parameters applying different algorithms capable to provide the evolution in time of the most meaningful parameters selected for the continuous monitoring process.

3) elimination of the environmental and operational effects on the modal parameters (mainly performed on the natural frequency) that could mask the occurrence of small structural changes or damages;
4) definition of an opportune approach or labels and design of any threshold values or confidence intervals to monitor the resulting features that now are not sensitive to external factors, but they depend only on structural changes.

A clear scheme about the classical strategy for vibration-based health monitoring system is provided by [Magalhães (2010)] and reported below:

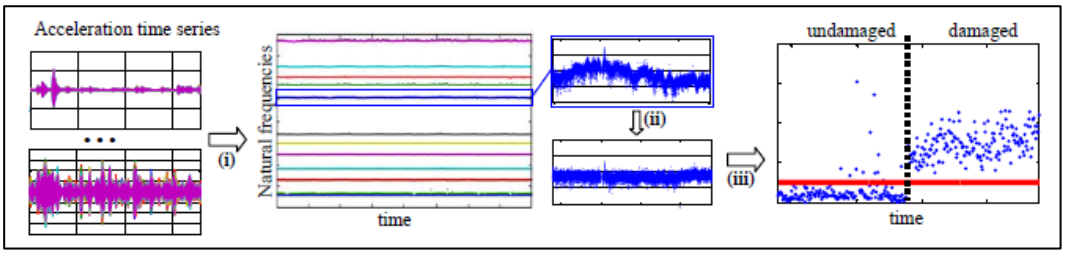

Fig. 3.1. Main processing steps of a classical vibration-based health monitoring system

Some remarks on the procedures available in the literature on the above steps 2-4 are described n the following subsections.

As discussed in the introduction of this Dissertation, the development of processing tools to fully automated the identification analysis in operational conditions is still a challenge task. Over last years, the performance of several full-scale testing over the world and the constantly improving of existent processing tools demonstrate the usefulness of this approach in the monitor of the health state and the vulnerability condition in several type of constructions. Moreover, the practical evidence convinced the owners and the commitments of Civil Engineering structures and Cultural Heritage buildings about the economical relevance of the dynamic testing and permanent monitoring based on OMA.

Efforts are also required in order to define a new strategy of SHM which is one on the main goals of this Dissertation. In more details, the contribution herein developed consists of the following steps:

1) Developing and implementing automated OMA procedures capable of extracting accurate estimates of the dynamic characteristics from a single recorded dataset. Improving the efficiency of the developed algorithms reducing the human interaction in the initial tuning phase and during the analysis of the data.
2) Finalizing the develops OMA procedures to the complete automatization of the continuous monitoring process by proposing a novel modal tracking strategy, which is based on adaptive reference values and adaptive rejection thresholds.
3) Implementing a damage detection strategy (based on automated OMA results and pattern recognition methods) that does not require the removal of environmental and operational effects from the damage sensitive features. The novelty damage detection approach has been exploited using natural frequencies, but, in case of investigated structures with widespread monitoring systems, it might be based on the analysis of mode shapes variations as well as complexity indices.

A schema of the approach herein proposed is shown in **Fig. 3.2**. It can be observed that, once the dynamic monitoring is activated, only two steps are conceptually required: 1) automated identification of the modal parameters and tracking of the evolution in time of the extracted futures 2) analysis of the automatically identified modal parameters aimed at detecting the onset of possible structural anomalies or damages.

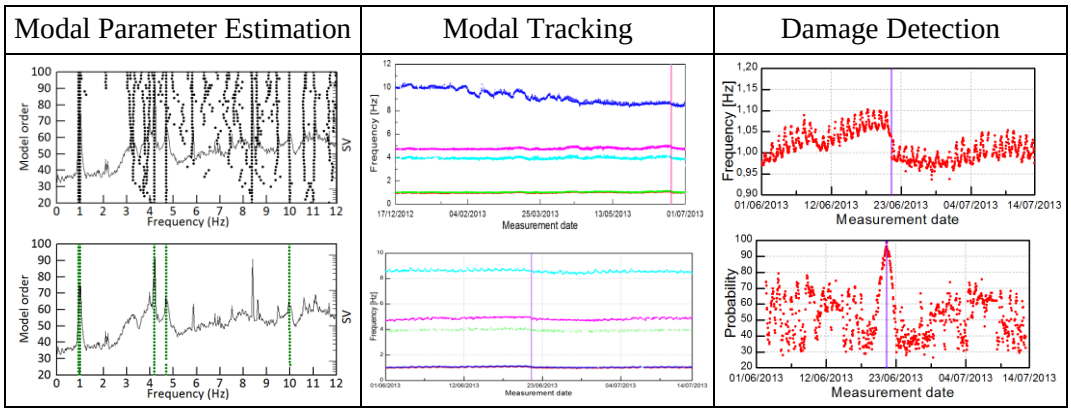

Fig. 3.2. Alternative approach for vibration-based Structural Health Monitoring system

In the next subsection, a brief introduction about the automation of the identification process is given, focusing on techniques that involve the use of stabilization diagrams. Meanwhile, the detailed description of the developed tools to perform the automated identification of the modal parameters is given in Chapters 4, 5 and 6. Furthermore, Chapter 7 focus on the damage detection strategy presented in this Dissertation.

Finally, in order to provide a clear information about classical SHM approach, the main statistical methods used for the elimination of the environmental and operational effects on modal parameters together with some well-known SHM applications on real structures are given in the end of this Chapter.

3.3 Automated OMA algorithms

The increasing diffusion of long-term dynamic monitoring systems for structural assessment as well as the success of different damage detection algorithms are driving the strong interest of the last decades towards automated procedures of output-only modal identification.

The papers available in the literature on automated monitoring of structure, includes the following: [Andersen et al. (2007), Magalhães et al. (2009), Peters et al. (2009), Cross et al. (2013), Gentile et al (2015)] for large infrastructures, but also [Saisi et al. (2015), Ubertini et al. (2016)] for Cultural Heritage buildings.

The large attention currently received by SSI-methods probably depends on the fact that these procedures are apt to accurately identify weakly excited and closely space modes and are especially suited to be automated. The SSI procedures can be implemented in two classic forms: covariance driven (SSI-Cov) and data driven (SSI-Data). Various strategies have been implemented for the SSI outputs interpretation [Magalhães et al. (2008), Reynders at al. (2011), Ubertini et al. (2013)], considering that two main parameters affect the obtained results: a) n, the maximum order of the stochastic model;

b) *i*, the time-lag index used to define the number of output block rows used to build the Toeplitz block matrix (SSI-Cov), or the size of the block Hankel matrix (SSI-Data).

All the techniques presented in the previous Chapter require an initial "tuning" of the input parameters in order to perform a correct identification of the modal parameters. As already declared, the definition of such inputs - for both parametric and non-parametric methods - is not always straightforward and it needs a strong intervention of an expert user. This aspect is very crucial in the context of single identification tests as well as for the continuous monitoring and it deserve special attention. In the following Chapters main issues strictly related to the identification of the modal estimates and to the continuous monitoring of these modal estimates will be addressed in detail providing some significant solutions valued by excellent outcomes.

The automation of the SSI algorithms usually involves the interpretation of the stabilization diagrams [Peeters et al. (1999)] focusing on four important aspects: a) conception of identification algorithm capable to deliver clearer stabilization diagrams, b) characterization of additional criteria to make well-founded the selection of stable alignments on stabilization diagrams, c) development of efficient strategy aimed at automatically processing the information present on stabilization diagrams.

3.3.1 Stabilization diagrams

The concept related to the stabilization diagram is already introduced in Chapter 2, it consists of a graphical tool in which the modal estimates (principally natural frequencies) provided by all state-space models obtained for increasing order are reported. The stabilization diagram was firstly introduced by [Peeters (2000)] and it is normally used coupling with any parametric procedure (i.e. SSI-Cov and SSI-Data) as well as p-LSCF method in the output-only version presented [Peeters and Van der Auweraer (2005)].

As already stated, when the state-space model that represent the dynamic of the system under analysis has been defined, the modal parameters of the system can be easily extracted from the matrices A and C. First, the eigenvalue of A (μ_k), which are the poles of the discrete-time state-space model, have to be related to the poles of the continuous-time model (λ_k). Then the poles with positive imaginary component are used to obtain natural frequencies (f_k) and the modal damping ratios (ξ_k), as follows:

$$\lambda_k = \frac{\ln(\mu_k)}{\Delta t} \Rightarrow f_k = \frac{|\lambda_k|}{2\pi} \; ; \quad \xi_k = -\frac{\mathrm{Re}(\lambda_k)}{|\lambda_k|}$$

Furthermore, the multiplication of the matrix C by the matrix with eigenvectors of A provides a matrix which contain in its columns the observable components of the mode shapes. Furthermore, due to the existent of complex conjugate pair, only the columns associated to the eigenvalues with positive imaginary parts are selected. In this way, the state-space model of order n provides modal parameters for $n/2$ modes.

In practical application is not possible to know *a-priori* the model that best fit the dynamic response of the investigated structure, because the modelling inaccuracies, due to possible non-linear behavior of the tested structure, or the noise content that always contaminates the collected signals. Therefore, the derived state-space model matrices together with the obtained modal parameters have to be considered also estimates. Furthermore, the SVD of the Toeplitz matrix (SSI-Cov), as well as the Projection matrix (SSI-Data), does not permit the exact identification of the model order, because the higher singular values that theoretically should be zero in practice present residual values (as shown in § 2.4.2). Furthermore, for applications on real structures, it is not even possible to identify any gap in the consecutive singular values and to estimate the most adequate model order. Hence, in common practice the most appropriate way to overcome this problem is to overestimate the models using order with a selected interval, in which the maximum value should be much higher than two times the number of expected physical modes within the investigated frequency range and subsequently select the best model by the analysis of the corresponding modal parameters estimates.

In **Fig. 3.3** is reported the construction of the stabilization diagrams obtained by the application of the SSI-Cov method to a dataset collected on the *Infante D. Henrique bridge* [Magalhães et al. (2009)].

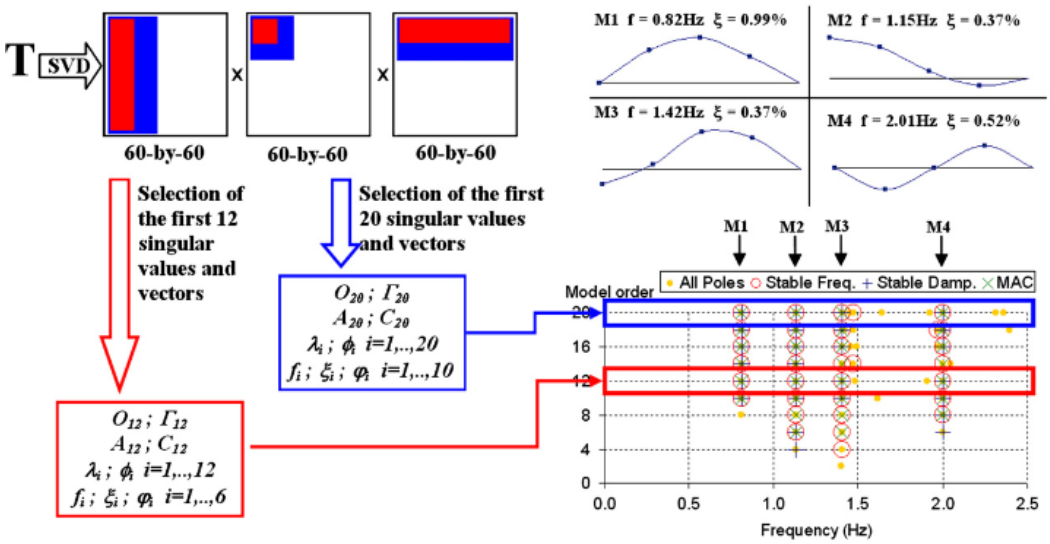

Fig. 3.3. From the Toeplitz matrix to stabilization diagrams, selection of the best model order and extraction of the modal estimates (SSI-Cov) [Magalhães et al. (2009)]

As described in **Fig. 3.3**, because the SVD of the Toeplitz matrix is the most demanding calculation task of the SSI-Cov method, it is only performed once. This means that the maximum order of the stochastic models needs to be fixed a-priori, taking into account the relation between the row-blocks of the Toeplitz matrix and the maximum time-lag of the correlation matrix used in this technique. Then, the SVD of the complete Toeplitz matrix is calculated. Consequently, models with successively increasing order (starting from the lowest one) are estimating by selecting successively increasing number of singular values and vectors obtained by the estimation of the observability and controllability matrices, as reported in the example in **Fig. 3.3**.

All obtained solutions are reported on the diagram. However, the use of high model orders leads to the comparison of numerical modes (also called spurious poles or noise

modes), which have no physical meaning and they are strictly related to the noise content of the signals and model inaccuracies. Therefore, separation between physical mode and spurious poles is a crucial step of the identification algorithm. In this way, the most popular approach to achieve that is based on the creation and the interpretation of stabilization diagrams (**Fig. 3.3**).

As shown, in this diagram the modal parameters estimates provided by all models are reported (in the *x-axis* the natural frequency of the mode estimates; in the *y-axis* the order of the model), allowing the identification of the modal parameters that are *stable* for model of increasing orders. Hence, modes that appear in most of these models generally maintain consistent frequency, mode shape and damping, they are called *stable poles* and are likely to be physical. Meanwhile, those poles that are spread out on the diagram and appear only in some models are classified as spurious and they should not be considered for the estimation of the modal parameters.

In the following paragraph are reported the most used criterion to remove the spurious poles from the stabilization diagrams and the useful approach oriented to deliver clearer diagrams in which identify the dynamic characteristics of the investigated system.

3.3.2 Single criterion check

Concerning the definition of additional criteria used to separate physical poles from spurious ones, several works have been published in the literature aimed at providing solutions for this issue. For example, the procedure implemented by [Pappa et al. (1998)] for the ERA models uses the Consistent Mode Indicator applicable in the context of input-output tests (i.e., data collected during Hammer tests). Or as proposed in [Verboven et al. (2001)] in which the automated modal identification approach is based on the frequency-domain maximum likelihood and the estimation of the physical modes is based on the uncertainty of such estimates. Meanwhile, as described in [Verboven el al. (2002)], the complexity component associated to the modal vector is a useful criterion to

detect spurious poles, in which modes with high complexity are conceivability associated to noise modes and they are considered spurious. Some others additional criteria used to detect and remove spurious poles from stabilization diagram in [Scionti at al. (2003)] or in the most recent paper [Reynders at al. (2011)] that highlights the usefulness of some parameters related to the complexity of the modal vector for OMA approaches.

Once most of all spurious poles are removed from stabilization diagram, the subsequent step is aimed at detecting the set of modal estimates related with the same model. In the manual identification, the simplest approach to extract the modal parameters consists of the choice of the model order the best represent the dynamic characteristics (in terms of modal parameters) of the investigate system instead analyzing a wide range of model order.

Nowadays this approach is not recommendable because several reasons: a) the choice of the order of the stochastic model that best fit the dynamic behavior of the structure requires a strong interaction performed by an expert user; b) the manually selected set of modal parameters is always depended on user's sensitivity and could be affected by human errors; c) it can happened that the selected model does not contain all structural estimates, or otherwise d) noise modes could be selected together with other structural estimates; and e) there is not guarantee that the set of modal estimates provided by that model order is the best one. Moreover, in the context of continuous monitoring the manual identification of all datasets continuously collected requires a very intensive (and expensive) human effort that does not allow a permanent monitoring of the structure.

For these reasons, the most straightforward way for the interpretation of the data on the stabilization diagram is to develop an automated procedure capable to mimic the decision that an expert analyst takes during its examination. Several approaches can be adopted to reach this task but the best way to group poles with same characteristics is given by the application of the clustering algorithm. Several clustering approaches are described in the literature and their efficiency are related to the type of data that to be grouped. Thus, in

the next paragraph an overview of the main characteristics of the clustering approaches present in literature will be described.

It is worth highlighting that some clustering procedure can be performed without the removal of spurious poles from the stabilization diagram. As described in [Magalhães et al. (2009)] OMA analysis was performed on full-scale structures estimating the modal parameters without a pre-filtering of spurious poles obtaining satisfactory results. Obliviously, the time consuming to scanning all poles without removal of numerical estimates increases and some spurious poles can be grouped with physical estimates affecting the mean values. Moreover, in case of limited number of sensors the discrimination between different mode shapes could be not always guaranteed. For this reason, in order to obtain a better performance, a pre-filtering of noise modes is always suggested.

3.3.3 Clustering approaches applied to stabilization diagrams

As stated in Chapter 2, the stabilization diagram is a graphical tool which helps the analyst in the identification of the dynamic characteristics of the structure under investigation. In fact, the solution provided overestimating the state-space model are reported on the diagram in which the solutions with physical maintain consistency in term of modal estimates for increasing model order. As reported in many papers present in the literature, the first step to perform the automation of the process consists of recognize the stable poles on the diagram and extract the modal parameters grouping all poles that share similar performing, in fact, a clustering process.

The clustering procedures based on the interpretation of stabilization diagrams are suitable to handle outputs produced by any parametric identification techniques that provide estimates in terms of natural frequencies, mode shapes and modal damping ratios [Magalhães et al. (2009); Reynders et al. (2011)]. These procedures are mainly devoted to recognizing stables poles on the stabilization diagram that maintain consistency in

terms of natural frequency, mode shape and modal damping [Peeters (2000)]. Subsequently, since the damping ration has higher scattering, it has lower weight than other parameters in the discrimination of spurious poles from physical ones, then it is generally not considered for the characterization of the estimates.

In the context of OMA, the most popular way to group stable poles is to measure the distance between all the pairs of estimated poles. This operation is possible because stable estimations are normally grouped in high density areas whereas noise modes are much more scattered. Such property permits the construction of the hierarchical tree as also well described in [Reynders at al. (2011)]. But, in order to obtain representative structural modes, such procedure needs to be stopped using a so-called cut-level that usually depends on the expected number of modes. There is not a theoretical theory to know *a-priori* the maximum threshold to cut the branches of the hierarchical tree and it is still a user-defined parameter which required some initial test to be tuned. Since this approach in based on the assumption that spurious poles have higher scattering than stable poles. So, it should be easy distinguishing between clusters composed by physical poles and clusters that contain numerical estimates [Magalhães et al. (2009)].

In order to avoid the introduction of many parameters to remove most of poles without physical meaning, it could be possible to define into the clustering procedure the number of maximum available clusters to construct the hierarchical tree. Such information can be easily obtained performing a faster analysis (using the FDD method) to identify the number of principals expected modes selecting the visible peaks of the first singular value. This strategy is a well-founded way in case of slender structures and well excited constructions where the environmental excitation produces visible resonant frequencies. On other hand, it is worth mentioning that this strategy can fail in case of simple monitoring system (composed by a limited array of sensors) and/or in case of low signal/noise ratios of the collected data. Then, this option is not adopted in the development of the automated algorithms of this Dissertation.

As it will be demonstrating the next Chapters, the clustering process is one of the most important steps within identification processes based on OMA parameters. The very first clustering approaches have been implemented using tolerance values checking the variability of the modal parameters for increasing model order of the state-space model.

The check is generally performed on the variation of the natural frequencies, damping ratios and mode shapes (using MAC index and comparing mode shapes estimates obtained for consecutive model order). This approach is quite effective, and it is also implemented in well-known commercial software used for dynamic tests and OMA analysis. The main disadvantage of this approach is related to the number of the tolerance values that need to be tuned requiring a strong human interaction during the analysis.

It is worth highlighting that the automated identification of the stable poles on stabilization diagram is still a challenging task. The application of consecutive checks on the modal parameters associated to each pole (SSI-output) might increase the quality of the results in more demanding application with, for instance, higher level of noise, if some additional criteria are used in the classification of the stable poles. Unfortunately, the use of additional criteria has the disadvantage of require a more user defined parameter that, as evident, does not allow the correct automation of the process.

A first improvement was given by clustering approach proposed by [Magalhães et al. (2009)]. The main contribution is provided by the new metric adopted to group poles with same modal characteristics, reducing the number of user-defined tolerance values to only one distance threshold. Otherwise, the clustering approach defined by Magalhães is based on only two defined parameters: a) the maximum distant threshold among poles within the same cluster and b) the number of expected structural modes. This means that also this approach requires an important choice of the expert user during the analysis phase. Alternatively, to the definition of the number of structural modes, a-posteriori cut level can be used to remove noise modes. As demonstrated, noise clusters are much smaller of the physical ones, and accordingly at many experimental results a reasonable cut level can be set as one third or one fourth of the number of elements within the

highest cluster that stand out on the stabilization diagram. This solution is also suggested by [Ubertini et al. (2013)]. A further improvement in the clustering approach was given by the contribution described in [Cabboi et al. (2017)]. The main original aspect of the new procedure consists of a well-founded improvement of the previous metric in which the distant threshold is not applied to pair of estimates to construct the hierarchical tree but each representative cluster is constructed adopting a reference point obtained averaging the estimates that fall inside the cluster itself. In this way, the reference point is continuously updated when a new pole is englobing in the cluster providing more accurate estimates. Follow this strategy the extraction of the structural modes is automatically performed without define the number of expected modes, but the cutting level is still required. So, the resulting clusters are kept on (or removed) if the number of elements is more (or less) than one third of the highest cluster. Once a group of consistent structural modes are identified, the most representative values are extracted averaging all modal estimates belonging to each detected cluster.

The clustering strategy proposed in [Cabboi et al. (2017)] is robust and it is aimed at interpreting the information on the stabilization diagram with a great improvement related on the reduction of the human intervention. In fact, the introduction of the average process that continuously adapt the representative reference point of the clusters is a useful strategy that gives more stability to the whole process.

On other hand, as stated by the authors, the main issues of such automated procedure are related to the definition of the best inter-cluster distance threshold. In fact, if such threshold is short the cluster that defines the structural mode can be split in two minor clusters and might be removed from the results, otherwise if the distance is very high some spurious modes can fall inside the cluster and affect the modal estimates. For these reasons, to obtain accurate results become mandatory to perform an initial tuning of this parameter. Moreover, such procedure can fail in case of simple monitoring system composed by a low number of instrumented points, because the most weighted criterion to separate different poles is given by the MAC index, and if the number of sensors are really limited there is not a properly discrimination between close spaced modes.

It should be pointed out the all methodologies devoted to identification of the modal parameters needed of an initial tuning of the input parameters. This setting firstly depends on the geometrical and mechanical characteristics of the instrumented structure and, consequently, on the engineering judgment of the analyst during the investigation process. In order to avoid the strictly correlation of the classification criteria to the case study or to the analyst's sensitivity, in the OMA methodology that will be proposed in the next Chapter the use of user-defined parameters is drastically reduced.

3.4 Environmental/operational effects on modal parameters

Any SHM strategy is developed in order to automatically detect, locate and assess the possible presence of damage on the monitored structure. Normally, when the damage occurs, a general loss of stiffness of the construction can be highlighted. This situation corresponds to an irreversible modification in the structural dynamic behavior that interests the global system under analysis.

Unfortunately, in practical applications several issues can significantly complicate the damage detection process. Among these, the most relevant are the effects due to external factors, mainly related to environmental and operational variations, that affect the monitored features. Moreover, the changing environmental and operational conditions (i. e., temperature, wind, traffic loads, etc.) can lead to such relevant variations on the modal parameters that could mask the changes due to occurred damage.

Many papers present in literature report practical examples describing the effects of external factor on modal parameters. Daily fluctuations of the first natural frequency due to temperature variations were observed during the monitoring of the Alamosa Canyon bridge [Farrar et al. (1997)]. The results highlighted that environmental factors could lead to variations of the eigenfrequencies around 5% of the nominal values. Approximately the same variation was detected for the first two natural frequencies of the Z24-bridge in Switzerland [Peeters and De Roeck 2001]. Otherwise reduction of the modal frequencies

of 2-3% due to the change in mass and to the traffic loads were identified on the Tamar bridge in Southwest England [Cross et al. 2013]. Effects of the external factors on the dynamic characteristics of Civil structures have also been analyzed in interesting publications as [Sohn (2003); Ramos et al. (2010); Magalhães et al. (2012)].

As it is well described in the previous papers, all those variations due external factors must be understood and accounted in order to manage results that depend only on structural conditions and to perform a robust assessment of the monitored structure. So, in this way, if all external effects on the modal parameters can successfully be minimized and removed, any variation in the monitored features will be due to structural changes, [Cross et al. (2013)].

To remove the effects of environmental and operational factors, an intensive and detailed analysis should be carried out in order to know the correlations of such effects on the controlled features. A first possibility is reproducing the relationship between external variables and controlled dynamic features. This class of algorithm are referred as *input-output models*.

The major drawback of these methods is related to the choice of what external factors have to be measured to define the correlation between them and controlled features. This selection is not always straightforward and sometimes the measurement of the chosen external factors is not even possible. To overcome this problem, some further methods have been developed in order to remove the external factors without the need to measuring any inputs; these models are known as *output-only methods*. Some important works that describe the application of the output-only techniques to removal external factor effects are present in literature. Most of them are based on decomposition of the covariance matrix of the controlled features, monitored over a long time with changing (but unmeasured) external conditions [Kullaa (2004); Yan et al. (2005a); Deraemaeker et al. (2008)]. Moreover, other application of output-only methods, based on the direct decomposition of time series with the extracted features or on the use of neural networks are present in literature as for instance in [Vanlanduit et al. (2005); Sohn et al. (2003)].

3.4.1 Input-output methods

The development of the input-output models is aimed at defining a linear regression relation among obtained features (i.e. natural frequencies) and external factors (environmental or operational) that are continuously measured through structural responses. Such models can be classified in two distinct groups that are strictly depended on how the input variables affects the features. In the first case, the relationship between inputs and detected features is only defined through data collected simultaneously, then the model is essentially governed by a *static regression model*. Most of times a static relation is not enough to describe the characteristics between external factor and obtained estimates, however it can be enhanced by taking into account also the influence of external factors measured at previous time instants. In this case the model id defined by a *dynamic regression model*.

For both groups of input-output methods, several data-sets need to be used to define the relation between inputs and outputs of the defined model, It is mandatory to understand the influence of each factor on the resulted feature in order to properly calibrate the parameters governing the method. Once the model is defined, it can be used to predict the values of the controlled features when the measured external factors are known (static method) and also the output at previous time instants (dynamic method).

In this way, when external factor and previous outputs are known it is in principle possible to estimate the controlled features and to detect possible variation due to structural conditions (e.g. the occurrence of damage).

3.4.1.1 Multiple Regression Analysis

Multiple Regression Analysis is a statistical technique that can be used to analyze the relation between a single dependent variable and one or more independent (predictor) variables, with the objective of predict the single dependent value using independent variables whose values are known in advance. In the context of Structural Health

Monitoring, it is consisting of the simplest method available to establish a model relating observed environmental or operational factors with estimated natural frequencies. Moreover, the established relation (model) is used, in an initial phase, for understanding the influence of each predictor (input of the model) and the dependent variable (output of the model) and then to predict futures values of the dependent value when the predictors are known. Each independent variable is weighted by the regression analysis procedure to ensure maximum prediction from the set of independent variables. The weights denote the relative contribution of the independent variables to the overall prediction.

When a regression relationship is established between the dependent variable and a single predictor, the regression problem is referred to as *simple regression*:

$$y = \theta_0 + \theta_1 x + \varepsilon \tag{3.1}$$

where y is the dependent variable, x is the predictor, θ_0 and θ_1 are the parameters of the regression relationship, respectively referred to as intercept and regression coefficient. So, ε is the difference between actual and predicted values of the dependent variable, called *prediction error* or *residual*. Nonetheless, the need to model curvilinear effects can arise in some applications. In such cases, it is possible to adopt transformations of an independent variable that add a nonlinear component for each additional the independent variable. Such relationships are known as *polynomials*:

$$y = \theta_0 + \theta_1 x + \theta_2 x^2 + \varepsilon \tag{3.2}$$

Meanwhile, when two or more independent variables are used to predict the dependent variable, the problem is referred as *multiple regression*:

$$y = \theta_0 + \theta_1 x_1 + \theta_2 x_2 + \cdots + \theta_n x_n + \varepsilon \tag{3.3}$$

The relationships in **Eqs. 3.1** and **3.3** have been established to reproduce a linear dependence between predictors and dependent variable. If two or more independent variables are involved, multivariate polynomials can be defined using the following form:

$$y = X\theta + \varepsilon \tag{3.4}$$

where y is a [n-by-1] column vector containing the n measures (y_k) of the dependent variable (y), X is a [n-by-p] matrix that connects n dependent values of the corresponding p selected predictors, θ is a [p-by-1] column vector formed by the p parameters weighting the contribution of each independent variable, ε is the [n-by-1] column vector of the prediction errors (ε_k) that account for measurement errors of the element of y and for the effects of other variables not explicitly considered in the model.

Moreover, it is assumed that the last term in **Eq. 3.4** has the following properties:

$$\begin{gathered} E[\varepsilon] = 0 \\ Cov[\varepsilon] = [\varepsilon \cdot \varepsilon^T] = {\sigma_\varepsilon}^2 \cdot I \end{gathered} \tag{3.5}$$

where $E[\bullet]$ is the expected value operator, and $[\bullet]^T$ means transpose and I represent the identity matrix n-by-n. the relations in **Eq. 3.5** represent that the mean value of ε is zero and that the errors are independent and also their valiance (${\sigma_\varepsilon}^2$) is constant.

In order to accurately reproduce the experimental estimates of the dependent variables and simulate their future values, it is very important to perform a good selection of the input parameters that lead to the best association between measured features and values $\hat{y}_k$ provided by the model. Therefore, when the independent values have been selected the subsequently step consists of characterizing the model through the definition of the θ_k parameters. Their estimation can be achieved by using the Least Squares (LS) method, minimizing the sum of the squared errors and estimating the model parameters θ as:

$$\hat{\theta} = (X^T X)^{-1} X^T y \tag{3.6}$$

It should also be noted that, in system identification, it is usual to normalize input and output data so that the origin of the x and y axes lies at the "center of gravity" of the data points and the slope of the line of regression corresponds to the correlation coefficient [Newland (1993)]. This is achieved by removing the mean value from each measurement x_k and y_k and dividing the results by the variable's standard deviation as follows:

$$\tilde{x}_k = \frac{x_k - \bar{x}}{\sigma_x} \qquad \tilde{y}_k = \frac{y_k - \bar{y}}{\sigma_y} \tag{3.7}$$

As the LS method minimizes the sum of the squares of the equation errors, a first quality criterion is the value of the Loss Function (LF):

$$LF = \frac{1}{N}\sum_{k=1}^{N} \varepsilon_k^2 \tag{3.8}$$

where N is the total number of samples and the prediction errors are obtained as the difference between experimental and estimated values of the output variable:

$$\varepsilon = y - \hat{y} \tag{3.9}$$

It is the most used criterion to firstly obtain a quality indicator of the model accuracy. Alternatively, another important indicator adopted for testing the quality of the model is referred to as coefficient of determination R^2 defined as [e.g. Johnson & Wichern 1992]:

$$R^2 = 1 - \frac{\sum_{k=1}^{N} \hat{\varepsilon}_k{}^2}{\sum_{k=1}^{N}(y_k - \bar{y})^2} = \frac{\sum_{k=1}^{N}(\hat{y}_k - \bar{y})^2}{\sum_{k=1}^{N}(y_k - \bar{y})^2} \tag{3.10}$$

As reported in the previous formula, the coefficient of determination is defined by the ratio value between two variances. Therefore, it can be stated that R^2 provides the percentage of the total variation in the experimental outputs y_k explained by the predictors. If the coefficient of determination tends to zero, then the selected independent variables have no influence on the output, whereas when R^2 tends to one the variation of y_k is completely explained by the predictors.

In the context of SHM, regression analysis is one of the most used available technique adopted to correlate the observed external factors (predictors) and the dependent values. identified natural frequencies (dependent variables). Temperatures measured on the structure and amplitude of excitation (i.e. induced by traffic loads) are the environmental and operational factors typically selected as predictors because of their significant influence on the fluctuations of the natural frequencies (dependent variables).

It is worth mentioning that, in practical applications, regression models can be used in two different forms: static and dynamic form. As previously described, static models establish a relationship only between simultaneously measured data and may not be able to accurately reproduce the effects of common dynamic processes. In this kind of applications, the use of dynamic regression models, accounting for the influence of inputs measured at previous time instants, seems to be more feasible.

A dynamic regression relationship is established between the dependent variable at time k and values of a single predictor at current time k as well as at *(p-1)* previous time instants. Therefore, for dynamic regression models, **Eq. 3.1** can be specified as:

$$y_k = \theta_0 + \theta_1 x_k + \theta_2 x_{k-1} + \cdots + \theta_p x_{k-(p-1)} + \varepsilon_k \tag{3.11}$$

whereas matrix X of **Eq. 3.3** assumes the form:

$$X = \begin{bmatrix} x_1 & \cdots & x_{1-(p-1)} \\ x_2 & \cdots & x_{2-(p-1)} \\ \vdots & \ddots & \vdots \\ x_n & \cdots & x_{n-(p-1)} \end{bmatrix} \tag{3.12}$$

Dynamic regression models, in turns, can be viewed as special ARX models.

3.4.1.2 ARX models

Among the dynamic identification methods described in the literature, as well detailed in [Ljung (1999)], ARX models are probably the most widely used algorithm to estimates the output system features from independent variables. ARX models consist of an Auto-Regressive output and an eXogeneous input part. Its equation can be defined by considering an output and an input variable designated y_k and x_k, respectively, and an error term ε_k defined in a general time instant k. So, it can be expressed as follows:

$$y_k + a_1 y_{k-1} + \cdots + a_{n_a} y_{k-n_a} = b_1 x_{k-n_k} + b_2 x_{k-n_k-1} + \cdots + b_{n_b} x_{k-n_k-n_b+1} + \varepsilon_k \tag{3.13}$$

It should be noted that in **Eq. 3.11** only one input (e.g. temperature), one output (e.g. natural frequency) and the error that takes into account the effects of non-modeled inputs and measurement noise were considered. Moreover, the **Eq. 3.13** can be easily generalized to the case of multiple inputs by replacing b_k and x_k with corresponding row and column vectors, respectively.

Detailing the **Eq. 3.13** it is worth highlighting that ARX models are characterized by three model orders: the auto-regressive order n_a (corresponding to the number of the considered past measures of the dependent variable), the exogenous order n_b (corresponding to the number of previous model inputs considered) and the pure time delay between input and output n_k. Orders n_a and n_b determine the number of model parameters: a_i (i = 1, …, n_a), b_j (j = 1, …, n_b). It should be noted that classic static regression models represent a particular class of ARX models, obtained with the specific selection of parameters: n_a=0, n_b=1, n_k=0. As shown in the **Eq. 3.13** the static regression model can be defined as ARX010 model:

$$y_k = b_1 x_k + \varepsilon_k \tag{3.14}$$

As reported in the excellent publication [Ljung (1999)], the ARX (see **Eq. 3.14**) can also be written using a different form:

$$a(q)y_k = b(q)x_k + \varepsilon_k \tag{3.15}$$

In which a new relation is introduced as follows: $q^{-1}y_k = y_{k-1}$, and where $a_{(q)}$ and $b_{(q)}$ are two polynomials defined as:

$$\begin{aligned} a(q) &= 1 + a_1 q^{-1} + \cdots + a_{n_a} q^{-n_a} \\ b(q) &= b_1 q^{-n_k} + b_2 q^{-n_k-1} + \ldots + b_{n_b} q^{-n_k-n_b\mp 1} \end{aligned} \tag{3.16}$$

Moreover, **Eq.3.14** can be associated to the general expression typically used to define linear input-output models and it can be manipulated to obtain the following formula:

$$y_k = H(q,\theta)x_k + W(q,\theta)\varepsilon_k \tag{3.17}$$

where θ is the vector grouping the modal parameters, H is the transfer function and W is the noise model. Comparing **Eq. 3.15** to **Eq. 3.17**, the variables can be expresses as:

$$\theta^{\mathrm{T}} = (a_1 \dots \; a_{n_a} \; b_1 \dots \; b_{n_b})$$
$$H(q,\theta) = \frac{b(q)}{a(q)}, \quad W(q,\theta) = \frac{1}{a(q)} \tag{3.18}$$

As previously described for the case of multiple regression analysis, the parameters of ARX models can be easily estimated by applying a LS method. Therefore, it is convenient to re-write the ARX model expressed in the **Eq. 3.13** using a matrix form:

$$y_k = \varphi^{\mathrm{T}}\theta + \varepsilon_k \tag{3.19}$$

where $\boldsymbol{\varphi}^{\mathrm{T}} = \left[-y_{k-1} \; \dots \; -y_{k-n_a} \; x_{k-n_k} \; \dots \; x_{k-n_k-n_b+1}\right]$ is a row vector grouping the past measures of dependent variables and predictors.

Concluding the treatment of the ARX models, it is should to remark that considering N measured values of output and input variables, it is possible to write **Eq. 3.19** for each of the N samples. Hence, the ARX problem can be described by the same matrix equation (2.88) obtained for the multiple regression analysis introducing the following vectors:

$$y = \begin{pmatrix} y_1 \\ y_2 \\ \vdots \\ y_N \end{pmatrix} \in \mathbb{R}^N, \qquad X = \begin{pmatrix} \varphi_1^T \\ \varphi_2^T \\ \vdots \\ \varphi_N^T \end{pmatrix} \in \mathbb{R}^{N\times(n_a+n_b)}, \qquad \varepsilon = \begin{pmatrix} \varepsilon_1 \\ \varepsilon_2 \\ \vdots \\ \varepsilon_N \end{pmatrix} \in \mathbb{R}^N \tag{3.20}$$

where the estimates $\widehat{\boldsymbol{\theta}}$ of the model parameters are still obtained by solving the considered system of equations using the LS method, according to **Eq. 3.6**.

Concluding, it should be noted that when multiple input candidates and choices of the model orders n_a, n_b, n_k are available, several different ARX models can be identified from the data and the same quality criteria described in the previous paragraph can be used to compare the fitting skills of the different detected models.

3.4.2 Output-only methods

As previously stated, the correct selection of those external factors that maintain the most relevant influence on the controlled modal parameters is often difficult and not always straightforward. In addition, in the context of continuous dynamic monitoring, the continuous measurement of such factors could be not always available or achievable leading to a relevant problem in the definition of the relationship between external factor and monitored parameters. This problem can be easily bypassed adopting the so-called *output-only models.* Adopting this strategy, the major drawback related to environmental and operational effects can be removed without the knowledge of the external factors is not required.

In this subsection two classes on output-only methods used to remove the effects of environmental and operational factors on monitored features extracted from data collected by a dynamic monitoring system installed on the structure are described. In detail, this task is performed through the decomposition of a covariance or correlation matrix of the time variation of the structural features over a reference period of time (named *training period*). The first group is composed by the Principal Component Analysis (PCA) method, that are described and applied in several papers and works present in literature, such as: [Kullaa (2004); Yan et al. (2005a)], as well as important application on large infrastructures [Deraemaeker et al. (2008); Magalhães et al. (2012)] of ancient constructions; and the Factor Analysis (FA) method that is based on the same principle as detailed in [Johnson and Wichern (1992)].

3.4.2.1 Principal Component Analysis

Principal component analysis (PCA) was firstly introduced in the 1980's [Johnson and Wichern (1992)] and it consists of a multivariate statistical tool performing a linear transformation of data defined into an original coordinate system to a new less dimensional coordinate system. PCA is typically used where is convenient to reduce the dimension of the problem, by replacing a group of correlated variables with a new

smaller set of independent variables, designated as principal components [Deraemaeker et al. (2008)]. Basically, the goal of PCA is to find an [n-by-n] orthonormal matrix T (in which T^T=T^{-1}) which allows the coordinate transformation described as follows:

$$x = T \cdot y \tag{3.21}$$

in which y is a vector of n original variables, T is the *transformation matrix* that applies a rotation of the original coordinate system and x is a vector composed by n variables that are independent on each other. The coordinate transformation performed by matrix T lead to a set of variables (x – the Principal Components) with important properties: all variable are independent between each other and the covariance matrix of x is diagonal and full rank and their variance is organized in decreasing manner from x_1 to x_n. Therefore, the contribution of the first PC is the most relevant to explain the variability of the initial dataset. Meanwhile, most of the last ones represent smaller variances and they could be ignored because they do not explain the variability of the original variables y.

So, starting from the relationship described in **Eq. 3.21** and the properties of matrix T, it is possible to re-write the relation between the original variables (y) and the PC (x) as:

$$y = T^T x \tag{3.22}$$

The covariance matrix Σ_{yy} of y (which coincides with the correlation matrix of y if each variable is ZOH) can be related to the diagonal covariance matrix Σ_{xx} of x as follows:

$$\Sigma_{yy} = E[y \cdot y^T] = E[T^T x \cdot x^T T] = T^T \cdot \Sigma_{xx} \cdot T \tag{3.23}$$

The singular value decomposition (SVD) of Σ_{yy} provides the following relationship:

$$\Sigma_{yy} = U \cdot \Lambda \cdot U^T \tag{3.24}$$

where Λ is a diagonal matrix composed by elements λ_j provided in descending order and they correspond to the eigenvalues of the covariance matrix Σ_{yy}. The matrix U is an orthonormal matrix in which the columns correspond to the eigenvector of the covariance

matrix Σ_{yy}. It is worth mentioning that each *j-th* column is the eigenvector corresponding to the *j-th* eigenvalue of the covariance matrix Σ_{yy}.

Thus, the outputs of the **Eq. 3.24** can be used to obtain the transformation matric ($T=U^T$) and the variance of the component of x from the elements in the diagonal of Λ ans since the SVD algorithm provides the singular value in descending order, the first element of Λ coincides with the variance of x_1.

Therefore, as mentioned before the main goal of the PCA technique is reducing the dimensions of the problem, considering only the first *p* eigenvalues out of the *n* ones collected in Λ relevant to explain the variability of the original components of y, the matrix Λ can be split in two parts: Λ_1=diag(λ_1, λ_2, … λ_p) a diagonal matrix composed by the first *p* singular values and Λ_2=diag(λ_{p+1}, λ_{p+2}, … λ_n) a diagonal matrix with the remain singular values on the diagonal which are not relevant to explain the variability of the original data *y*.

Theoretically, the value of p should be selected by looking for a gap in the diagram of the eigenvalues. But in practical applications, a clearly drop does not frequently occur, so, the choice of *p* is usually based on the definition of ratio *I*:

$$I = \frac{\sum_{i=1}^{p} \lambda_i}{\sum_{i=1}^{n} \lambda_i} \tag{3.25}$$

in which the value of the ratio I defines the percentage of the variability of the original variables y that is explained by the first *p* components of x. Therefore, once a threshold value of *I* has been chosen (e.g. 0.95), the value of *p* can be easily found.

Once *p* has been chosen, the set of PCs x_j can be obtained applying the **Eq. 3.21** using the matrix $\hat{T}$ built from the first *p* columns of *U* (taking into account that $T=U^T$). Hence, with the selection of the PCs, those features with a non-significant contribution on the variability of the original dataset (e.g. random errors in the identification of natural frequencies) are removed keeping into account just the effects due to relevant factors. At

this point, the reduction of the dimension of the problem has already achieved and the application of the statistical tool is ended.

In the context of Structural Health Monitoring purposes, a further step is usually performed in order to re-map the selected $\hat{x}$ components in the original space of y. Thus, this task consists of transforming the selected ẋ PC back to the original coordinate system, by means of the reduced T matrix ($\hat{T}$) as reported in the following equation:

$$\hat{y} = \hat{T}^T \cdot \hat{x} = \hat{T}^T \cdot \hat{T} \cdot y \tag{3.26}$$

If the re-mapped values are removed from the original variables as follows:

$$\varepsilon = y - \hat{y} \tag{3.27}$$

the obtained features ε (residual) will not be affected by the factors modeled by the PC.

In full-scale applications of Structural Health Monitoring purposes on Civil Engineering structures and Cultural Heritage contractions based on OMA features, the removal of the effects due to environmental and operational factors are often carried out on the natural frequency estimates extracted by the continuously collected structural responses. In this way, the vector $\boldsymbol{y}$ that denotes the features in the original space has many components as the number of the most meaningful estimated frequencies of the structure. Moreover, the covariance or the correlation matrix is estimated from the evolution in time of these features during a period that should be sufficiently large to contain the full effects of the environmental and operational factors on the frequency estimates, that should be corresponding to at least one year of continuous monitoring in which the state of the structures is assumed to be "healthy".

As previously stated, these two conditions are strongly binding for the correct application of this output-only method in the context of OMA-based SHM purposes. Furthermore, the correct monitoring of the structure is guaranteed only is case any fundamental conditions are verified: 1) the correct automation of the continuous monitoring process of the structure without considerable loss in the tracking of frequency estimates, 2) a full

year of continuous monitoring intended for the training period of the methodology, and 3) no occurrence of structural anomalies or damage during the training period.

Concluding the description of this output-only method is should be highlighting that the dimension reduction of the problem achieving with the application of the PCA is aimed at keeping the effects of the relevant factors (as for example the temperature) and eliminating the effects due to secondary factors, as could be due to the random error in the identification of the natural frequencies. Then, the difference obtained between the observed features and the re-mapped values lead to those features that are insensitive to the factor modelled by the PCs.

Therefore, the application of the transformation expressed in the **Eq.3.26**, using $\hat{T}$ matrix obtained from the observed data associated to the *reference state* (or *training period*), to new observations and the calculation of the residuals (**Eq. 3.27**) provides the new (components of) features that enhance the environmental/operational effects that are present in the new observation but they are not observed in the training period. Consequently, the post-processing of these new features can be performed to demonstrate to detect structural anomalies in the normal behavior of the structure that might justify the occurrence of a damage.

The efficiency of this methodology is proven along the years by excellent papers present in literature, using data produced by numerical simulations [Yan et al. (2005a)], or by its application to data collected by monitoring system installed in a footbridge [Hu et al. 2009)], or using data collected on the Infante D. Henrique bridge in Porto [Magalhães et al. (2012)] or also using data continuously collected on masonry towers as documented in [Ubertini et al. (2017)] and [Gentile et al. (2016)]. Furthermore, an extension of PCA to non-linear cases was proposed and applied to data collected on the Z-24 bridge as reported in [Yan et al. (2005b)] and also using a local-PCA approach applied to monitoring data as reported in [Comanducci et al. (2016)].

3.4.2.2 Factor Analysis

Factor Analysis (FA) is a multivariate statistical tool concerned with explain the covariance relationship among many variables in terms of a few random quantities called factors [Johnson and Wichern (1992)]. It can be considered as an extension of the PCA as both are based on the decomposition of the covariance matrix, but in this second case the method is based on a more elaborate model in which the factors are unobservable.

As described for PCA, the estimate observed features that are normally expressed by natural frequencies can be defined by the sum of two components:

$$y = f(f_1, f_2, f_3, f_4, \dots) + \varepsilon \tag{3.28}$$

where y is a vector of *n* components (the extracted natural frequencies), f is a function that depends on environmental/operational factors, f_i are the external factors and they can be selected as: f_1 the temperature, f_2 the humidity, f_3 traffic loads, f_4 the wind, …) and ε is a vector that quantify the influence of abnormal occurrences on each component of y. Instead of trying to identify the function f it can be decomposed in two mappings as reported below:

$$f(f_1, f_2, f_3, f_4, \dots) = L[NL(f_1, f_2, f_3, f_4, \dots)] \tag{3.29}$$

a first general mapping, that might be non-linear (NL), transforms the environmental and operational factors into a set of unobservable factors (represented by x), using for instance a regression analysis, which are related with the estimated features by a linear mapping. In this way, the relation between n observable features (the natural frequencies) and p unobservable factors can be expressed by the following equation:

$$y = L \cdot x + \varepsilon \tag{3.30}$$

in which *L* is a *n*-by-*p* matrix, the elements of the matrix are designed *factor loadings*, the components of x are named *common factors* and the components of ε are called *specific factors*. It is worth noting that the expression in **Eq. 3.30** is similar to that one used for

multivariate linear regression, but in this case the x components are not measured. Again, for the factor model are assumed the following properties:

$$\begin{gathered} E[y] = E[x] = E[\varepsilon] = 0 \\ E[x \cdot x^T] = I \\ E[\varepsilon \cdot x^T] = 0 \\ E[\varepsilon \cdot \varepsilon^T] = \Psi \\ \text{where } \Psi = \begin{bmatrix} \psi_1 & 0 & \cdots & 0 \\ 0 & \psi_2 & & 0 \\ \vdots & \vdots & \ddots & \vdots \\ 0 & 0 & \cdots & \psi_n \end{bmatrix} \end{gathered} \tag{3.31}$$

taking into account the properties defined above, the following equation for the covariance matrix of the observations can be established:

$$\begin{aligned} \Sigma &= E[y \cdot y^T] = E[(L \cdot x + \varepsilon) \cdot (L \cdot x + \varepsilon)^T] \\ &= E[L \cdot x \cdot x^T \cdot L + L \cdot x \cdot \varepsilon^T + \varepsilon \cdot x^T \cdot L^T + \varepsilon \cdot \varepsilon^T] \\ &= L \cdot E[x \cdot x^T] \cdot L^T + E[\varepsilon \cdot \varepsilon^T] \Leftrightarrow \Sigma = L \cdot L^T + \Psi \end{aligned} \tag{3.32}$$

In the first instance FA defines the matrices *L* and that fit a set of *n* observation of y. There are two algorithms to reach this task: the principal factors method and the maximum likelihood method.in this section, due to its similarity to the principal components, only the first algorithm will be presented. Meanwhile, for the description of the second algorithm the interested reader is referred to the classical book [Johnson and Wichern (1992)].

As described in **Eq. 3.24**, the covariance matrix of the observed features can be decomposed using the SVD algorithm and the L matrix is defined as:

$$\begin{gathered} \Sigma = U \cdot S \cdot U^T = [U_1 \quad U_2] \cdot \begin{bmatrix} S_1 & 0 \\ 0 & S_2 \end{bmatrix} \cdot \begin{bmatrix} U_1^T \\ U_2^T \end{bmatrix} \approx U_1 \cdot S_1 \cdot U_1^T \\ \hat{L} = U_1 \cdot \sqrt{S_1} \end{gathered} \tag{3.33}$$

Remarking, as described for the PCA, the covariance matrix of the observable features has been approximated considering only the contribution of the lower SV and neglecting the contribution of its last *n-p* values that are less representative of the variance of y. The

number of the relevant SV that are considered can be estimated using the formula expressed in **Eq. 3.33**. Apart the factor scale $\sqrt{s_i}$, the factor loadings of the *i-th* common factor coincide with the coefficients of the *i-th* principal component of the data (this result is obtained considering $E[\varepsilon \cdot \varepsilon^T] = 0$). Therefore, this simple version of the Factor Analysis is equivalent to the application of the Principal Component Analysis.

Going deeper in the description of the Factor Analysis, it is possible to obtain a more accurate factor model including specific factors in order in its development. In fact, recalling the relationship described in **Eq. 3.23**, the diagonal elements of $\Sigma - L \cdot L^T$ can be by the correlation matrix of the specific factors (being $\widehat{\Psi} = diag(\Sigma - \hat{L} \cdot \hat{L}^T)$), in which *L* is estimates through **Eq. 3.24**. Furthermore, it is possible to improve the model following a recursive way to estimate the matrix L. These steps can be summarized as:

1) Application of the SVD algorithm to the correlation matrix estimated by the data:
   $\Sigma = U \cdot S \cdot U^T$
2) Selection of the first *p* SVs and estimation of the matrix *L*:
   $\hat{L} = U_1 \cdot \sqrt{S_1}$
3) Estimation of the correlation matrix of the specific factors $\widehat{\Psi}$:
   $\widehat{\Psi} = diag(\Sigma - \hat{L} \cdot \hat{L}^T)$
4) Estimation of the product matrix $\hat{L} \cdot \hat{L}^T$:
   $\hat{L} \cdot \hat{L}^T = \Sigma - \widehat{\Psi}$
5) Application of the SVD algorithm using the new estimate for $\hat{L} \cdot \hat{L}^T$:
   $\hat{L} \cdot \hat{L}^T = U \cdot S \cdot U^T$
6) Repetition of the steps 2-5 in a consecutive way until the estimate for L convergence.

Therefore, given L and Ψ, the estimates of the common factors (x), also called *factor scores*, can be easily performed. Different formulations are available, as primarily detailed in [Johnson and Wichern 1992] that differ on the way the minimization of the specific factors. In the present demonstration a simple last squares procedure is provided:

$$\hat{x} = (L \cdot L^T)^{-1} \cdot \hat{L}^T \cdot y = (S_1)^{-1/2} \cdot U_1^T \cdot y \tag{3.34}$$

The resolution of a least squares problem in which the squared errors (ε_i^2) are weighted by the inverse of their variances ($1/\Psi_i$), providing the following factor scores:

$$\hat{x} = \left(\hat{L}^T \cdot \hat{\Psi}^{-1} \cdot \hat{L}\right)^{-1} \cdot \hat{L}^T \cdot \hat{\Psi}^{-1} \cdot y \tag{3.35}$$

Alternatively, as described in [Johnson and Wichern (1992)], the use of the regression method leads to the following equation:

$$\hat{x} = \left(I + \hat{L}^T \cdot \hat{\Psi}^{-1} \cdot \hat{L}\right)^{-1} \cdot \hat{L}^T \cdot \hat{\Psi}^{-1} \cdot y \tag{3.36}$$

As stated in the introduction of this section, the main goal of the Factor Analysis is to detect the variable x that are insensitive to the environmental and operational conditions then they can be used as features for damage detection. Therefore, is the normal behavior of the structure changes and if such change could be detected by modal parameters variations, the factor model established using data recorded during the training period cannot explain the variations of the observed variable (typically natural frequencies) over the reference stage. Hence, these changes remain in the specific factors (ε_i), which can be used as damage features. Furthermore, as described for the PCA method, also the factor model should be constructed using data that contain the full range of operational and environmental conditions (typically one year).

3.5 Detection of structural anomalies

In the context of SHM purposes based on OMA applications, the use of the models described in the previous paragraph permits the removal of the environmental and operational effects on the estimates allowing to obtain modal parameters no longer affected by the effect of external factors. Therefore, any variation of the obtained features can be related to only structural conditions. Follow this way, the presence of anomalous occurrences and possible damages on the investigated structure can be detected investigating the evolution in time of the obtained environment-independent features.

A useful strategy adopted for damage detection purpose consists of exploring the trend of the modal parameters after the removal of the external factors, in terms of:

1) prediction error ε_k between experimental estimates and predicted values (obtained after removal of environmental and operational effects) of the modal frequencies;
2) depurated experimental frequencies, computed as:

$$\hat{f}_i(T_k) = \bar{f}_i + \varepsilon_{ik} \tag{3.37}$$

where $\bar{f}_i$ is the mean value of the original *i-th* frequency during the reference period.

3.5.1 Control chart analysis

The most used alternative approach consists of using a statistical tool defined by a *control chart*. It consists of a graphical plot where the variation in time of data is represented along with user-defined variation limits. Normally, the use of the control chart is associated to a previous application of pre-described model apt to removal the environmental effects from the modal frequency estimations. Then, the variation in time of the monitored variables due to structural conditions is checked by means of horizontal lines designated *control limits* and computed from the experimental samples only when the process is assumed to be under control (during a training period when the structure is assumed as undamaged). In this way, any observation falling outside the control limits

has to be considered the result of unusual behavior of the structure that depends on structural anomaly (e.g. the occurrence of damage).

In the context of SHM purposes for continuous assessment applications the control charts are normally used according to two different approaches. In the farmer case they are used to monitor the stability of a sample observations. This means that a checking is performed on all the samples to verify if the control limits extracted from several available observations is respected. In the latter case, control charts can be used to define a safe control region to check the quality of future observations. This requires the definition of an interval reference period (training period) where the process is assumed to be in control (no damage occurred in this period) and the properties of data collected during this time interval are taken into account to define the control region. It is worth to highlighting that this second approach is the more adequate to be implemented in a permanent monitoring system, where one of the main goals is to check if each new observation, continuously obtained by the analysis of each collected dataset, lies within a previously defined "safety" region.

Furthermore, one of the most frequently used control charts is the $\bar{X}$-chart (or X-bar chart) this is composed by checking each new observation using three defined horizontal lines: the center line (CL), the upper control limit (UCL) and the lower control limit (LCL). Where CL is positioned at the mean of the sample and it is defined by all observations, indicated with $\bar{\bar{\boldsymbol{x}}}$, whereas the values of UCL and LCL are respectively given by adding and subtracting three times the sample standard deviation σ to the mean value $\bar{\bar{\boldsymbol{x}}}$ and they define the limits of the safety region.

$$\begin{aligned} CL &= \bar{\bar{\boldsymbol{x}}} \\ UCL &= \bar{\bar{\boldsymbol{x}}} + 3\sigma \\ LCL &= \bar{\bar{\boldsymbol{x}}} - 3\sigma \end{aligned} \tag{3.38}$$

Concluding, if the total sample is divided into subsamples of size m, σ can be computed as the sample standard deviation divided by $\sqrt{m}$. Moreover, the three standard deviation

value is used assuming a normal distribution of the feature that is being controlled and it corresponds to a confidence interval of 99.7%.

Furthermore, in case of SHM approach in which the observations are obtained by the analysis of the structural responses collected by dynamic monitoring systems, x_k is referred to the generic observation at time t_k of a one-dimensional feature after the removal of the operational and environmental effects. The associated feature can be referred to as Novelty Index (NI) [Worden and Manson (2000)] and is defined starting from the prediction error (ε) and using either the Euclidian norm:

$$NI_k^E = \|\boldsymbol{\varepsilon}_k\| \tag{3.39}$$

or the Mahalanobis norm:

$$NI_k^M = \sqrt{\varepsilon_k^T \cdot \left(\Sigma_{yy}\right)^{-1} \cdot \varepsilon_k} \tag{3.40}$$

where Σ_{yy} is the covariance matrix of the measured feature y and both the Euclidian and Mahalanobis indices are assumed to be normally distributed. It should be noted that when more than one feature is to be monitored, multivariate control charts can be applied. In fact, after the definition of a safety region based on the results of the training period, future observations can be checked by following two methodologies: i) the check is continuously performed for each new provided observation or ii) the check is executed only when a set of new observations is available. In this paragraph, only the multivariate control chart designated *Shewhart T* is covered [Montgomery (1997)], meanwhile alternatives approaches are described and detailed in [Johnson and Wichern (1992); Kullaa (2003)].

The formula expressed in the **Eq. 3.41** characterizes the *Shewhart T* control chart. When each future observation x (a vector with p components) is extracted, the T^2*-statistic* parameter is obtained as follows:

$$T^2 = \frac{n}{n+1}(x - \bar{\bar{x}})^T S^{-1}(x - \bar{\bar{x}}) \tag{3.41}$$

where n is the number of observations collected during the reference period, $\bar{\bar{x}}$ is the process average and S is the covariance matrix (both calculated from the observations available during the reference period). Moreover, the LCL (lower limit) is set equal to zero, whereas the UCL (upper limit) is defined as:

$$UCL = \frac{(n-1)p}{n-p} F(\gamma) \tag{3.42}$$

where F (γ) denotes the γ percentage point of the F distribution with p and (n-p) degrees of freedom. Otherwise, when future observations are checked by using subgroups with r observations of x, the T^2-statistic value is calculated as:

$$T^2 = r(\bar{x} - \bar{\bar{x}})^T S^{-1} (\bar{x} - \bar{\bar{x}}) \tag{3.43}$$

where $\bar{x}$ is the subgroup average, $\bar{\bar{x}}$ and S are the process average and the covariance matrix, respectively, computed during the reference period. The LCL is set equal to zero whereas the UCL is defined as:

$$UCL = \frac{p(m+1)(r-1)}{mr-m-p+1} F(\gamma) \tag{3.44}$$

where p is the dimension of the variable (components of each individual observation of x), m is the number of subgroups collected during the reference period and $F(\gamma)$ denotes the γ percentage point of the F distribution with p and (mr-m-p+1) degrees of freedom.

In the last decades, control charts have been successfully adopted for damage detection approach in several SHM practical applications. Due to its easy implementation and to the clear reading of the graphical results control charts approach have received an increasing attention in the continuous assessment of Civil Engineering structures. One of the most interesting contribution is given by the interesting work [Hu et al. (2015)] in which control charts have been successful used for the detection of progressive damage over 13 years of continuous monitoring of the Westend bridge in Berlin.

In that case of studies, after the application of a polynomial regression model that allowed to remove the effects of temperature from the identified natural frequencies, the

X-bar control chart was adopted to detect possible structural modifications and anomalies over time. In **Fig. 3.4** the results obtained by the damage detection strategy application can be observed. The Novelty Index, represented by the solid colorful lines, gradually increases over year and the upper limit are continuously scattered out. Such outcomes suggest that the behavior of the investigated bridge is changing, and the bridge is subjected to some structural modifications between 2000 and 2013. As reported in the work, from an engineering point of view, a possible motivation of this modification can lie in the variation of strain measured in the main pre-stressed cable on the east web that is gradually decreasing from the end of 2000 to the end of 2013. From a first consideration, the progressive loss of strain is suggested by a detected slight drop of the natural frequencies. Subsequently, this aspect is coming out from the continuous increasing of the ratio of mean of NI over time that is dramatically reach the UCL values previously defined.

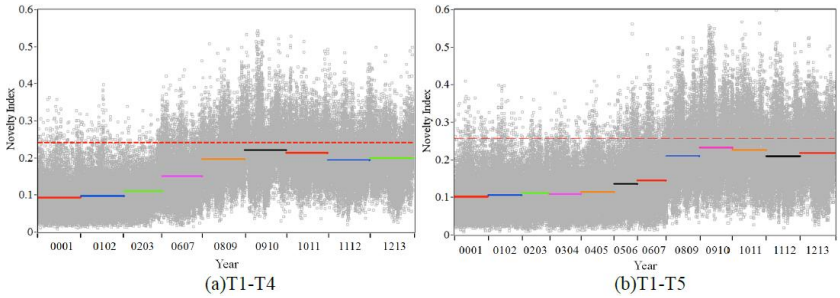

Fig. 3.4. Variation of NI considering four and five temperature sensors.

The control chart approach is also successful used for the detection of possible numerically structural damage scenarios simulated on a representative Finite Element Model (FEM) of the Infante D. Henrique bridge in Porto [Magalhães et al. (2012)].

As reported in the paper, *Shewhart T charts* were used after the combined application of a dynamic regression model and PCA on simulated data of a numerical model calibrated using experimental data obtained by the permanent monitoring system installed on the bridge since the end of 2007. Such approach was used to detect the effects of four different numerically simulated damage scenarios. It is worth mentioning that subgroups

of consecutive observations with 48 elements were selected, corresponding to one day of monitoring, to check the occurrence of possible damage in the structure. Finally, from the results reported in **Fig. 3.5** is possible to appreciate the robustness of the developed strategy capable to detect the occurrence of several damages located in different position over the structure. As reported in the graphics, in all four damage scenarios, most points lay outside of the previously defined control region when the damage was occurred.

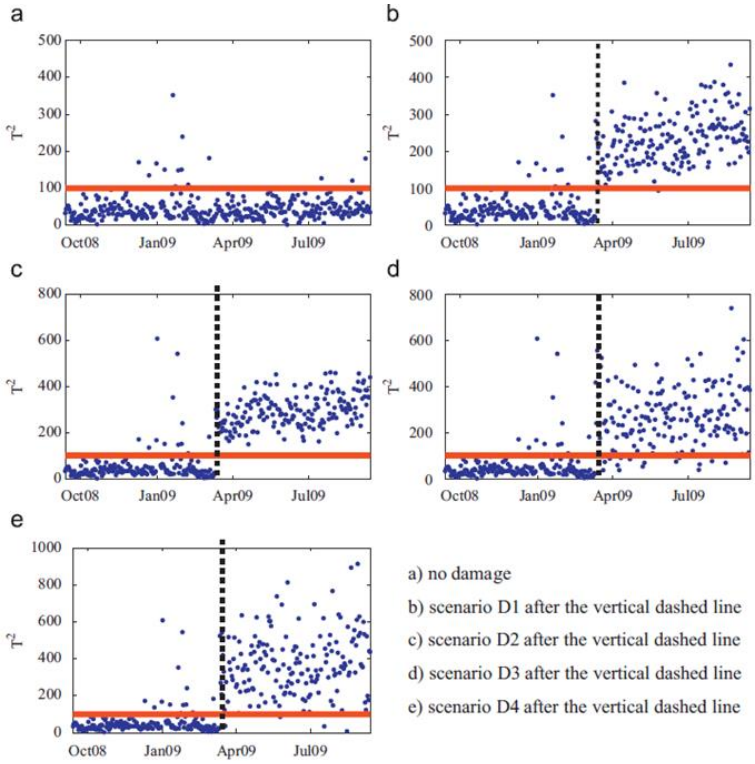

Fig. 3.5. Control charts associated to four damage scenarios in the Infante D. Henrique bridge

3.5.2 Pattern recognition models

Support Vector Machines (SVM) are popular techniques that belong to that class of method called Pattern recognition methods. Such techniques are normally used for classification problems based on forming decision boundaries that separate data into different classes. Many interesting papers and excellent books present in literature describe these techniques and their application in different research fields. Interesting reading of the main concept related to SVMs can be obtained from [Schölkopf et al. (2000), Tax and Duin (1999)], otherwise for a deeper analysis the author suggests the excellent book [Bishop (2006)].

These techniques belong to that class of methods used for classification problems called *domain-based novelty detection* that requires the definition of a boundary margin based on training data. Typically, they are not sensitive to specific sampling or density of the target class because they describe the target using a boundary, or a *domain*, and not through the class density. This means that the boundary, or better to say the novelty boundary, is not detected by all data-points of the input data, but it is determinate through the location of those data that lie closest of the boundary itself (normally detected in a transformed space), called *support vectors*. Hence, the distribution of the data-point that are not support vectors are not included in the identification of the decision boundary, as demonstrate in [Tax and Duin (1999), Hu et al. (2003)].

Originally, the SVM models were developed because ideally suited for binary pattern recognition, used to perform the classification of data linearly separable. Hence, through adopting support vectors these techniques can separate and classify the input data constructing and maximizing the separating margin between two classes. Since the introduction of the original idea, described in the next Section 6.2, several improvements have been implemented to make the algorithm more robust and efficient. As the Robust Support Vector Machines (RSVMs) algorithm, developed to address the overfitting problem caused by the noise in the training dataset [Hu et al. (2003)]. Or the strategy developed by [Schölkopf et al. (2000)] in which the novelty boundary condition is

defined through a kernel obtained transforming the input data from the original space into feature space. In this development the margin is a sort margin that allows the fall outside of same data points from the "normal" class. Another approach, the Support Vector Data Description (SVDD) method, proposed by [Tax and Duin (1999)], defines the novelty boundary adopting hyperspheres with minimum volume the cover all (or almost all) the "normal" class.

Moreover, some extension of the SVDD approach have recently been proposed [Wu and Ye (2009)] to improve the margin boundary using small spheres and large margin. Or using some slack variable and set of hyperspheres with different centers and radii [Le et al. (2011)]. In the last decades, large amount of works presents in the literature has been produced on the use of SVM methods for classification and novelty detection problems, some of them are shown below in order to provide a more accurate view of these applications in very different fields [Manevitz and Yousef (2002), Sotiris et al. (2006), Li (2008), Li et al. (2011)].

Over the years, different algorithm based on SVM algorithm have been implemented and improved aimed to satisfy most disparate classification problems in several research fields. This trend has interested also the Civil Engineering field, addressing special attention to application regarding damage assessment. Hence, during the past years, several methods of novelty procedure for SHM purposes have been proposed in literature. In general, most of these methods consist of evaluating some indexes or indicators that permit to detect any possible anomalies and damages on the structure, possible locations and even the extension of the damaged regions [Yan et al. (2007)], determining if in the structure is present an abnormal behavior associating a probability of "*true detection*" (probability of detect the damage in the structure when it is affectively present in the mechanical system.

On other hand, in SHM approaches for civil engineering structures the first step consists of detecting the occurrence of anomalies in the normal structural behavior, and subsequently localize such anomalies in the structure. For this purpose, several studies

have been performed using statistical tests and pattern recognition approach based on comparison of data extracted by healthy and damaged conditions [Zhang (2007), Iwasaky et al. (2004)]. These approaches are efficient and useful when the structural response can be obtained with high level of confidence. Moreover, these methods proved to be effective when relatively small sets of data are used for the training and testing phases, however large number of features and input data lead to hard time consuming [Chun et al. (2005)]. A proposed strategy to detect possible anomalies was described in [Guo (2006)]. From the results obtained by the application of this methodology was demonstrated how the loss of information can lead to an incorrect classification providing false alarms for damage detection. Many other techniques have been developed to detect several damage scenarios using modal parameter estimation, as described in [Trendafilova and Heyleno, (2003)] where an unsupervised learning classification algorithm was developed and used to detect several structural damage states through the natural frequencies extracted by vibration responses of a cantilever bean.

SVM algorithms are aimed at separating two different classes using a discrimination function which is automatically computed during the classification process of the training datasets. Within the context of SHM and damage detection of civil engineering structures [Sohn et al. (2002)], two classes of data are assumed over time, corresponding to undamaged and damaged condition. Hence, in order to simplify the discussion about the proposed patter recognition algorithm some explanations have to be done: the SVM has to distinguish data belonging at two different classes, if it fails the classification means that data are not separable, then they belong to the same class and, consequently, the structural damage is not identified. On the contrary, the successful detection of two classes implies that a structural anomaly or an instantaneous damage occurred in the monitored system. Although SVM algorithms are normally used for two-class classification problems, extension to multi-classes classification can be done but this aspect will not be treated in this thesis, because the proposed procedure for SHM purpose is developed following a binary condition: absence or presence of damage and no other states are allowed.

The SVMs are generally based on a geometric approach, consisting of the construction of an optimal separating surface – a hyper-plane – which divides the data population in two groups with different statistical characteristics. The hyper-plane is equidistant from the two classes defining a margin zone between them. Similarly, to Neural Network classification, the input data are supposed to belong to different classes and the outputs consist of the target binary vectors (labels) corresponding to each class. In case of linear separable data, the SVM algorithm searches the optimal solution to classify the data by maximizing the distance between the hyper-plane and the extreme values of the two classes, so called *Support Vector*.

Moreover, in order to exemplify and simplify the behavior of the SVM algorithm, the basic assumptions are described in Chapter 6. Furthermore, the processes used to define the optimal separation surface and the margin zone between the classes are exemplified and described in detail.

3.6 Selected examples of SHM based on OMA

Among the important and interesting application regarding the SHM of Civil Engineering structures present in literature, two important case studies are reported here in detail.

Westend bridge

The first author's proposal concerning application of OMA-based SHM on large infrastructure is represented by Westend bridge (see **Fig. 3.6**) in Berlin, Germany. The results provided by continuous monitoring of the bridge over fourteen years (between 2000 and 2013) is reported in the interesting papers [Hu et al. (2015); Hu et al. (2018)].

The bridge was built in 1963 and it is composed by a curved pre-stressed concrete box girder bridge divided into eight spans varying from 5.0 m to 38.0 m, with a whole length of 242.0 m. An integrated permanent monitoring system was initially installed in 1994

with the main purposes of continuously recording the structural dynamic responses of the bridge under normal operational conditions. The permanent system was modified and updated several times and currently it consists of 32 sensors including accelerometers, vertical velocity sensors, temperature sensors, strain gauges, inclination sensors and position sensitive devices. The continuous dynamic monitoring started on March 2000 and it continuously provides the structural responses of the bridge subjected to environmental and operational loads with a sampling frequency equal to 128 Hz.

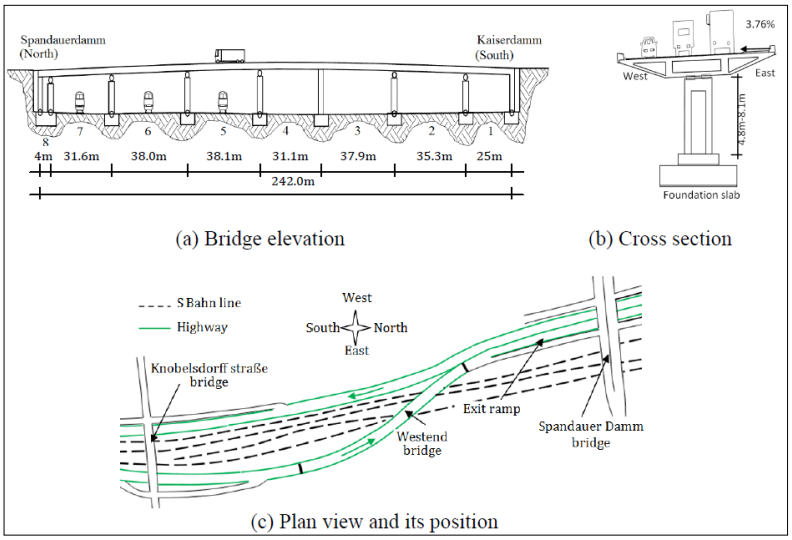

Fig. 3.6. The Westend bridge in the A100 highway in Berlin

From the first inspection of the temperature measurements collected and the five natural frequencies evolutions obtained by the tracking process over the year, a clear dependency of the frequency on temperature is proved by the obvious annual fluctuations reported in **Fig. 3.7**. Furthermore, from a deeper analysis of the correlation between independent variables (i.e. temperature recorded by all 5 sensors) and the obtained features (i.e. natural frequencies) shown in **Fig. 3.8**, a slight non-linear influence of the temperature on the identified modal frequencies was observed.

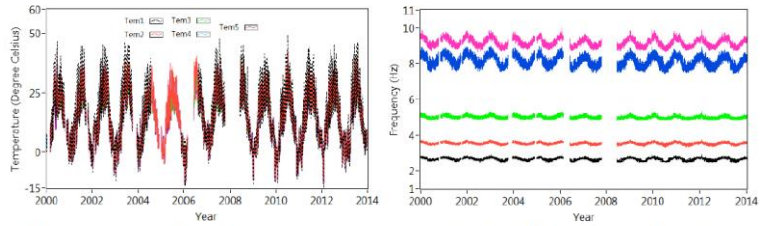

(a) Temperature measured in different positions (b) Estimated frequencies in different modes

Fig. 3.7. Variation of temperature measurements and estimated natural frequencies from 01/01/2000 to 31/12/2013

Furthermore, the implementation of a polynomial regression relationship established between extracted natural frequencies and measured temperature allowed to successfully remove the operational and environmental effects and carry on the damage detection process on environment-independent features.

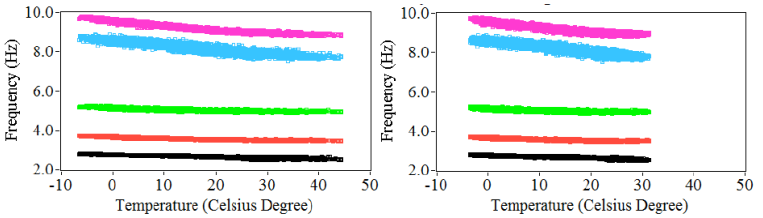

(a) Effect of temperature recorded by T1 on the identified frequencies in 2013 (b) Effect of temperature recorded by T4 on the identified frequencies in 2013

Fig. 3.8. Effect of temperatures on the estimated frequencies

Infante D. Henrique bridge

A further important example of SHM based on OMA approach is referred to the case study of Infante D. Henrique bridge over the Douro River in Porto, Portugal (**Fig. 3.9**), in which a permanent monitoring system is installed for the continuous dynamic assessment purpose of the bridge since September 2007. The structure, opened to traffic in 2004, consists of a rigid pre-stressed concrete box girder supported by a thin reinforced concrete arch that spans 280 m between abutments.

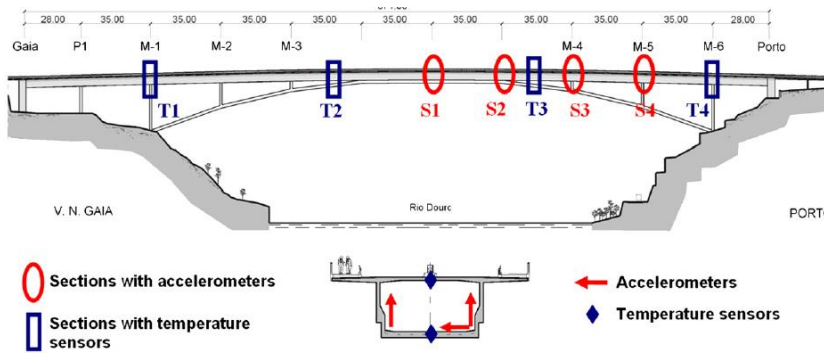

Fig. 3.9. Position of the accelerometers and temperature sensors

The dynamic behavior of the bridge has been continuously monitored since September 2007 using a system composed by twelve accelerometers disposed in four instrumented sections as reported in **Fig. 3.9**. The monitoring of the structure is completed by an independent static system, installed during the construction of the bridge and comprising temperature sensors embedded in the concrete. The modal identification was performed using an automated OMA technique (developed within the DynaMo software) applied to data continuously collected by permanent system over the years.

From the obtained results provided by the continuous dynamic monitoring process a clear yearly fluctuation of the natural frequencies is highlighted. Moreover, from the comparison of the evolution of the natural frequencies with the time trend of the corresponding temperatures the predominant effect of this factor on the frequency variation is established Furthermore, a second factor exhibiting relevant influence on the natural frequencies was the amplitude of the excitation, related to daily and weekly traffic intensity.

The different methodologies adopted to remove environmental and operational effects were calibrated using data collected during the first year of monitoring, whereas data acquired during the second year were used to assess the quality of the forecasts of the methods.

An interesting application, where multiple linear regression and PCA were adopted in sequence in order to remove the effects of environmental and operational factors, is described in [Magalhães et al. (2012)].

In particular, a multiple dynamic regression model was used to remove the effects of the measured environmental and operational factors, whereas PCA was applied to eliminate the residual correlation between natural frequencies due to the influence of unknown common features. This application will be described in detail in the following §0.

At first, three static regression models were implemented considering an increasing number of predictors (from two to five). The results, presented in **Fig. 3.10**, proved the best model to be the one where all the five predictors were used: temperature recorded in two different sections, accelerations recorded in two different sections (lateral in one case and vertical in the other) and the damping ratio of one natural mode to indirectly take into account the effect of traffic jams over the deck.

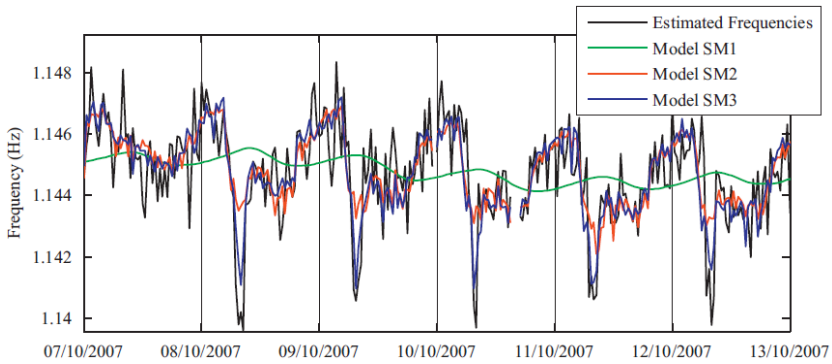

Fig. 3.10. Comparison between experimental and predicted results using static regression models

A second phase involved the adoption of dynamic regression models to further reduce the differences between forecasts and observations. In this context, it was assumed that the frequencies observed at time *t* was also dependent on temperatures measured at previous time instants. Therefore, temperatures referred to 6, 12, 18 and 24 hour-time delays were also considered as predictors. Again, the model providing the best results was the one accounting for all the considered input variables, with slight but not negligible improvements with respect to the static methods.

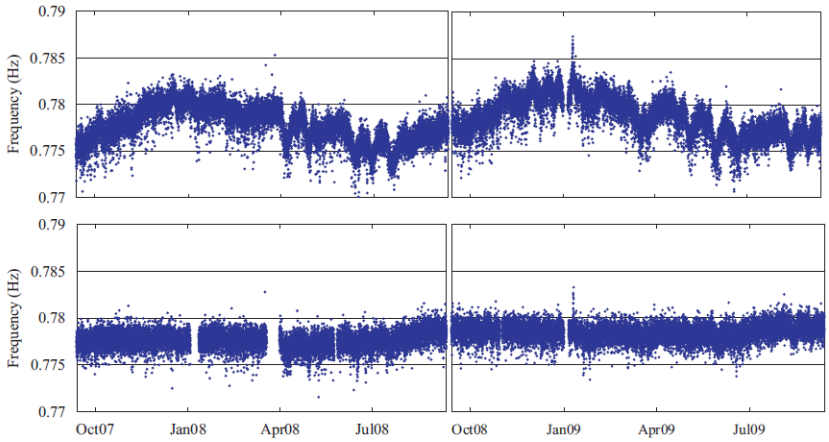

Fig. 3.11. Time evolution of the first natural frequency before and after the application of the dynamic regression model

Finally, in order to test the damage detection skills of the dynamic method, some damage scenarios were simulated adopting a tuned numerical model of the structure and reducing the vertical bending inertia of different elements. It was observed that, after adopting the dynamic model to remove the influence of the factors with greater importance, the natural frequencies of the structure were still correlated with each other (meaning they were still affected by common factors). Therefore, the PCA was used to minimize the effect of the less relevant factors that were not monitored (e.g. humidity, wind, etc.). The obtained results proved the effectiveness of the adopted statistical tools, allowing to detect the effects of damage producing frequency variations smaller than 0.4%.

3.7 Conclusions

This Chapter was devoted to the description of two alternative approaches for Structural Health Monitoring (SHM) purposed based on modal parameters extracted by structural responses continuously recorded by dynamic system installed on investigated structure measured during normal operation. A comparison between the classical SHM approach with the new developed strategy based on pattern recognition models is given detailing

the advantages and disadvantages of both developments. As described, the successful application of the former approach depends on of two crucial tools: algorithms for the automated identification of modal parameters and algorithms for the elimination of environmental and operational effects on modal parameters. Meanwhile, the latter approach is mostly based on the efficiency and robustness of those algorithms apt to only perform the automated identification of the modal parameters.

Due to their importance for the estimation of the modal parameters for SHM purposes, special emphasis about the development and application of such algorithms on data collected during single Ambient Vibration Test or in the context of Continuous Dynamic Monitoring is given in the following Chapters. On the contrary, a deeply description of the main approaches used to eliminate the effects of environmental and operational variables on modal parameters (normally natural frequencies) is provided in this section. Among different techniques developed to remove the external factors effects, two main classes can be defined: the input-output methods and the only-output methods.

As already mentioned, the removal of environmental and operational effects is generally carried out on the natural frequency estimates which are affected by these factors. This is the first limitation of the classical OMA-based SHM purposes that tends to be avoided in the development of this Dissertation trying to keep on also the mode shape variation during the continuous monitoring of the structure as observed parameter.

Nevertheless, in the first case (e.g. input-out methods) it is considered that all the variables with relevant influence on the natural frequencies can be measured. In this case, it is possible to establish regression models between observable variables (the estimated natural frequencies) and the measured operational and environmental factors using data recorded in a reference period (training period) during which the structure is assumed to be undamaged.

On the other hand, in the second case (i.e. output-only methods) the removal of the external factors effects on the natural frequency estimates is carried out adopting multivariate statistical tools as Principal Component Analysis (PCA) and Factor Analysis

(FA) involving the use of implicitly models that define a sort of (linear and/or non-linear) relationship between environmental and operational variables and natural frequencies. Following this approach, the measurements of environmental and operational parameters is avoided. It is worth to highlighted that not all the damages that could be detected using regression models for instance are detectable adopting the output-only methods. In fact, this alternative strategy can be applied after a previous investigation of the linear combination between the observable variables during the training period. This hypothesis affects the strategy making possible the detection of the damages that produce changes on the natural frequencies which are orthogonal to the changes due to environmental or operational factors.

In the end of this Chapter an overview of the main reference about pattern recognition models and Support Vector Machine model that constitutes the main step of the new SHM strategy is given in detail. Thoroughly, the new strategy does not require a large period of time which contains the full range of operational and environmental variations typically used in the classical SHM approaches, making this strategy attractive and economically advantageous for the continuous monitoring of large infrastructures as well as ancient constructions.

Finally, the development of the automated modal parameters estimation (MPE) tools that involve the construction and the interpretation of the stabilization diagrams will be deeply described in the next Chapters. In particular, the first automated MPE algorithm is described in Chapter 4. Moreover, a generalization of the automated algorithm to complex modes and its main improving that avoid the initial tuning of the input parameters of the parametric methods is discussed in Chapter 5. The automated Modal Tracking (MT) procedure is fully described in Chapter 6 with its application on data collected on two important European bridges.

Chapter 7 is completely devoted to the description of the new SHM approach and damage detection procedure that consists of the most important contribution provided by this Dissertation.

Chapter 4

DEVELOPMENT AND IMPLEMENTATION OF AUTOMATED MODAL PARAMETER ESTIMATION ALGORITHM USING 2D STABILIZATION DIAGRAMS

Contents

4.1 Introduction

The increasing diffusion of long-term dynamic monitoring systems for structural assessment as well as the success of different damage detection algorithms are driving the strong interest of the last decades towards automated procedures of output-only modal identification. Nowadays, different approaches of automated procedures apt to identify modal parameters in operational conditions have been developed, often based on the Stochastic Subspace Identification (SSI) methods. The main objective is to automatically estimate modal parameters using of investigated structures just the structural response measured under ambient excitation for big infrastructures [Andersen et al. (2007), Magalhães et al. (2008), Peters et al. (2009), Cross et al. (2013), Gentile et al (2015)] and Cultural Heritage buildings [Saisi et al. (2015), Ubertini et al. (2016)].

The large attention currently received by SSI-methods probably depends on the fact that these procedures are apt to accurately identify weakly excited and closely space modes and are especially suited to be automated. Presently, SSI procedures can be implemented in two classic forms: covariance driven (SSI-Cov) and data driven (SSI-Data). Various strategies have been implemented for the SSI outputs interpretation [Magalhães et al. (2009), Reynders at al. (2012), Ubertini et al. (2013)], considering that two main parameters affect the results: a) *n*, the maximum order of the stochastic model; b) *i*, the time-lag index used to define the number of output block rows used to build the Toeplitz block matrix (SSI-Cov), or the size of the Hankel matrix (SSI-Data).

In this Chapter, an identification algorithm of Modal Parameter Estimation (MPE) for OMA purpose aimed at obtaining the modal estimates from the collected structural responses has been developed. This algorithm consists of the application of a new automated identification procedure based on the adoption of a SSI method in which its outputs (poles), obtained for increasing model order, are used to construct the well-known graphical tool called stabilization diagram [Peeters and De Roeck (1999); Peeter (2000)].

4.2 Proposed method of automated modal identification

4.2.1 Automated Modal Parameter Estimation procedure

The identified algorithm described herein consists of three "key-steps" which are subsequently applied to the stabilization diagram obtained from the application of a parametric method with the aim to easily detect the stable alignments composed of stable poles that maintain consistency in terms of modal parameters for increasing order of the state-space model. In the present application, the collected data are analyzed using the SSI-Cov method which is strictly correlated to the covariance matrix of the time series collected during each single test. Afterwards, the modal estimates are extracted by each pole (i.e., SSI output) solving the eigen-value problem. Thus, the estimates of the resonant frequencies are reported on the stabilization diagram.

The procedure implemented herein is aimed at automatically identifying the modal parameters applying a series of subsequent tasks to the stabilization diagram [Reynders at al. (2012)]. As previously stated, the MPE algorithm is composed of three steps:

1) Pre-filtering, i.e. the removal of certainly spurious poles that are detected by applying three single-mode validation criteria. As usual, validation criteria considering the physical consistency of damping ratios and the complexity of mode shape components have been adopted;
2) Clustering, i.e. the process of detecting and grouping all the poles of the stabilization diagram that share same characteristics in terms of modal parameters. This step ideally corresponds to the inspection of the stabilization diagram, carried out by an expert user in a manual approach, to identify the alignments of stable poles;
3) Post-processing, i.e. the removal of possible replications of the structural modes and outliers in order to conceivably increase the accuracy of the modal estimates.

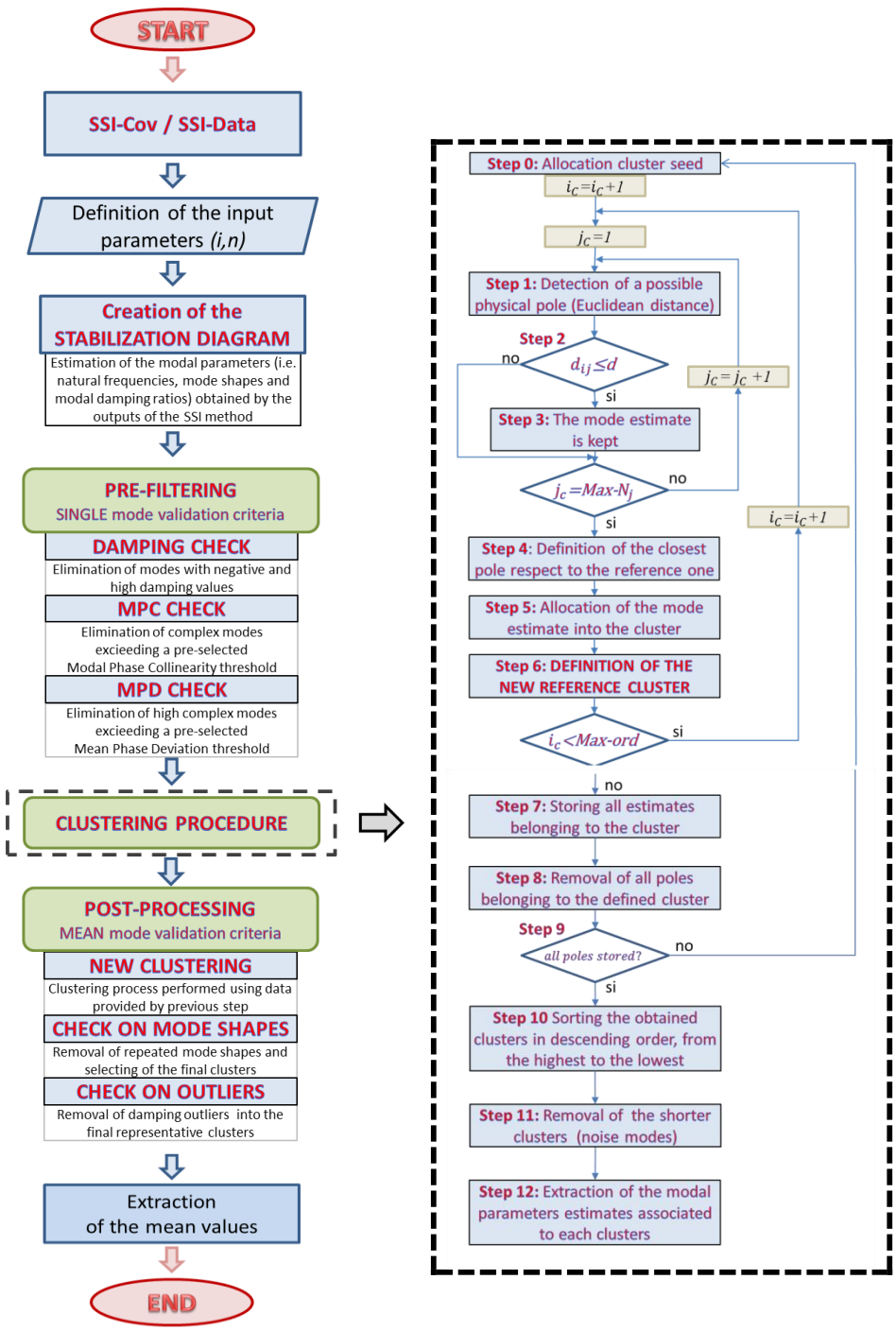

Fig. 4.1. Flowchart of the proposed methodology

4.2.2 Pre-filtering

Pre-filtering is the first part of the developed algorithm and it is composed of a series of applications of different single-mode validation criteria aimed at detecting and removing most of spurious poles from the stabilization diagram. In fact, as well known, the quality of the stabilization diagram can be compromised by poor signal-to-noise ratio of the data, even more evident in case of a simple monitoring system composed of a few sensors. In addition, the choice of high model order, used for detecting weakly excited modes, contributes to the formation of spurious modes which is related to the noise content present in the signal and numerical inaccuracies. Therefore, the application of modal validation criteria is used to reject spurious poles, cleaning the stabilization diagram and consequently speeding up the automatic interpretation of the chart during the clustering process.

In particular, the first discrimination between spurious poles and physical ones is performed using a pre-selected damping ratio threshold. In fact, in normal operating conditions the behavior of the structure is strictly stable, and the structure is lightly damped. Thus, the damping ratio corresponding to a structural mode should be positive [Pappa et al. (1993)]. On the other hand, highly damped modes (for instance, with a damping ratio larger than 10%) are not realistic and conceivably associated with the noise content of the signal [Reynders et al. (2012), Cabboi et al. (2015)]. Therefore, poles associated to negative damping ratio or high damping (i.e., damping exceeding a 10% of threshold, which seem a conservative value for Civil Engineering structures under ambient and/or operational excitations) are discarded.

Subsequently, because in operational modal analysis the identified structural mode shapes are complex vectors, further single-mode validation criteria aimed at quantifying the complexity degree of the mode shape components could be adopted to evaluate whether the estimated poles correspond to physical or spurious modes. In fact, when a structural system is proportionally damped, the mode shape components lie on a straight line of the complex plane. Hence, the covariance between the imaginary and real part or

the angle deviation of the mode components could be used to define a measure of the mode complexity and then the physical meaning associated of each extracted pole.

In this way, the first single-mode validation criterion used to measure the complexity of the mode shapes related to the identified poles is the Modal Phase Collinearity (MPC). This index provides an estimation of the correlation value calculated between the imaginary and real part of each mode shape component. Moreover, it tends to unity in case of real modes. Otherwise it tends to zero for high complex modes.

The description of this criterion can be found in [Pappa et al. (1993)] and its well-founded application is performed in [Reynders et al. (2012)]. Following the description reported in [Reynders et al. (2012)], the MPC can be defined as a correlation index that evaluates the linear relation between the real (*Re*) and imaginary (*Im*) part of the identified modal vector φ_r. Hence, if the imaginary part is strongly correlated to the real part, the MPC value is close to the unity indicating the mono-phase behavior of the mode shape. This usually occurs for real modes. Otherwise, in complex modes this value tends to zero as much as the complexity of the mode. The MPC is calculated as follows:

$$\mathrm{MPC_r} = \frac{\|\mathrm{Re}(\tilde{\varphi}_\mathrm{r})\|^2 + \left[\mathrm{Re}\left(\tilde{\varphi}_\mathrm{r}^\mathrm{T}\right)\mathrm{Im}(\tilde{\varphi}_\mathrm{r})\right]\left[2(\varepsilon_\mathrm{r}^2+1)\sin^2(\alpha_\mathrm{r})-1\right]\varepsilon_\mathrm{r}^{-1}}{\|\mathrm{Re}(\tilde{\varphi}_\mathrm{r})\|^2 + \|\mathrm{Im}(\tilde{\varphi}_\mathrm{r})\|^2} \qquad (4.1)$$

where each unknown coefficient is calculated as described in the following equations:

$$\begin{aligned} \tilde{\varphi}_{kr} &= \frac{\sum_{k=1}^{N}\varphi_{kr}}{N} \\ \varepsilon_r &= \frac{\|Im(\tilde{\varphi}_r)\|^2 - \|Re(\tilde{\varphi}_r)\|^2}{2[Re(\tilde{\varphi}_r^T)Im(\tilde{\varphi}_r)]} \\ \alpha_r &= arctan\left(|\varepsilon_r| + sign(\varepsilon_r)\sqrt{1+\varepsilon_r^2}\right) \end{aligned} \qquad (4.2)$$

To clarify, if the structure is proportionally damped, the mode shape components of the single modes lie on a straight line in the complex plane. In other words, this means that the real part and the imaginary part exhibit a correlation index (MPC) equal to 1. However, in OMA application, the resulting structural mode shapes are generally

complex vectors in which the imaginary part of the components are always (with a certain degree) correlated to the real part, indicating a kind of mono-phase behavior. Mono-phase behavior means that all the instrumented points of the investigate structure vibrate exactly in-phase or out-of-phase. In such case, the covariance matrix between the real and imaginary part of the mode shape vector has only one non-zero eigenvalue. Otherwise, in case of complex modes in which the two parts are completely uncorrelated, the eigenvalues of the correlation matrix are more than one and they will be approximately with same value.

Another single-mode validation criterion, used for detection of noise modes in automatic modal identification analysis, is the Mean Phase Deviation (MPD). This index [Pappa et al. (1993), Verboven et al. (2002)] is a statistical indicator and it is used to define and quantify the mean deviation of each mode shape component from the mean phase of the identified mode. In other words, the MPD can be computed as the angle provided by scalar product between the best straight line that characterize the mode shape in the complex plane (i.e. the straight line associated with the large component) and every single (weighted) component. This indicator tends to zero degree in case of real modes.

Therefore, as reported in [Reynders et al. (2012)], the MPD is a statistical indicator that measures the phase scatter (in degree) of the identified modal vector through the phase deviation of each modal component from the mean phase. In case of real structural modes, in which the imaginary parts of the components are strictly related to their real parts, the value should tend to 0 [Heylen et al. (2007)]. Defining the mean phase as reported in the following equation:

$$MP_r = \frac{\sum_{k=1}^{N_0} |\varphi_{kr}| \cdot \alpha_{kr}}{\sum_{k=1}^{N_0} |\varphi_{kr}|} \tag{4.3}$$

in which φ_{kr} is the weighted factor, and it is the k^{th}element of the r^{th} identified mode shape, and α_{kr} is its phase angle; N_0 indicates the number of the modal vector components. MP_r is the mean phase of the of the identified mode φ_r. Thus, the mean phase deviation (MPD) of the identified modal vector is defined below:

$$MPD_r = \sqrt{\frac{\sum_{i=1}^{N_0} |\varphi_{kr}| (\varphi_{kr} - MP_r)^2}{\sum_{i=1}^{N_0} \varphi_{kr}}} \tag{4.4}$$

Generally, in the literature the MPD is alternatively used to the MPC (because they are both index used to quantify the mode shape complexity for proportionally damped structures) or, as reported in the recent paper [Cabboi et al. (2017)], it is suggested to combine the two criterion to reduce the two parameters to a one indicator of complexity. On the contrary, because the information provided by the two indices (i.e. MPC and MPD) is not completely equivalent, in the proposed methodology the two criteria have been performed in a consecutive way. This strategy is aimed at removing most of spurious poles from the stabilization charts to make easier the automated identification of the stable alignments in the subsequent step.

It is worth noting that the mode complexity depends on various factors, such as identification issues (related to ill excited modes, noise content) or measurements errors (linkage error and synchronization problems) or also to the non-linear behavior of the structure (in case of non-proportional damping). Therefore, assuming good conditions, the choice of the thresholds is mainly related to the expected characteristics of the investigated structure and it requires a previous knowledge of the equipment used for the tests and also the state of preservation of the structure under investigation. Otherwise, if such information is not available, complexity thresholds can be safety selected in order to remove certain spurious poles related to noise modes and deliver a clearer stabilization diagram for the subsequent clustering process.

The cleaning action exerted by the *pre-filtering* routine is exemplified in **Fig. 4.2**. Specifically, **Fig. 4.2**(a) schematically shows the results obtained by applying the SSI method for increasing model orders (i.e., from 4 to 30). As already described in Chapter 2, a stochastic state-space model is used to fit the dynamic behavior of the investigated structures. Each solution of the stochastic model, called *pole*, is defined in terms of eigenvalue and eigenvector which are strictly related to the modal parameters of the structure, being the eigenvalue associated to the modal frequency and damping ratio and

the eigenvector being used to estimate the corresponding mode shape. afterwards, in **Fig. 4.2**(b) the resulting poles obtained after the application of the first single mode validation criterion to SSI outputs, are reported.

In order to provide a intuitively exemplification of the cleaning actions exerted by application of the selected complexity thresholds on the solutions of the stochastic model (poles), the performance of each complexity validation criterion (i.e., MPC and MPD) is reported in the following **Fig. 4.2**(c) and **Fig. 4.2**(d), respectively.

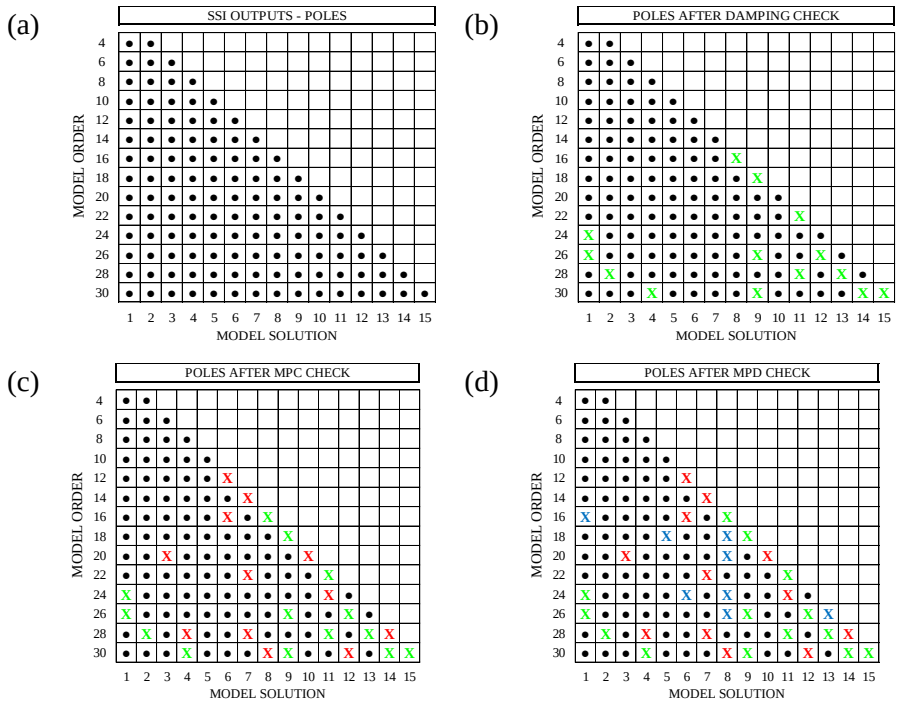

Fig. 4.2. Cleaning action exerted by the pre-filtering: (a) SSI output; (b) after the damping check; (c) after the MPC check and (d) after the MPD check (the "X" mark indicates the removed poles).

4.2.3 Clustering procedure

As described in the previous Chapters, the use of output-only stochastic models was revealed a winner strategy in the context of OMA analysis. In fact, the stable solutions of the state-space model present high consistency for increasing order allowing for an easy identification of the modal features. Once most of noise and spurious poles have been removed through the pre-filtering, a clustering procedure needs to be applied to group all those poles that have same characteristics in terms of modal parameters.

The clustering procedure developed herein is mainly inspired to the procedure described in [Cabboi et al. (2017)] introducing some variations to better define the reference points during the construction of the representative clusters.

As demonstrated by several OMA applications, a popular way to group similar poles is to measure the Euclidean distance among all pairs of estimated poles: this operation can be performed because stable poles are generally grouped in high density areas whereas noise modes are much more scattered. According to [Peeters and De Roeck (1999), Magalhães et al. (2009)], the distance among pairs of estimates is calculated checking their similarity in terms of natural frequencies and corresponding mode shapes into a hierarchical clustering method. This approach turned out to be very effective for the modal identification of recent constructions as well as for permanent monitoring purposes using system with diffused sensors: in such instances, the generation of a high quantity of noise modes is avoided and an easier detection of the structural ones is allowed.

On the other hand, applying the same strategy to ancient buildings and masonry constructions, in which the monitoring system is composed of a limited number of sensors and the recorded responses are generally characterized by a less signal/noise ratio, the identification process could not be always straightforward and also lead to important issues. Taking into account these considerations, the clustering process herein adopted is based on the definition and on the use of a reference point inside each cluster. To clarify, it is worth highlighting that the clustering process presented herein uses the concepts of fixed reject distance (see e.g. Magalhães et al. (2009)) and the reference pole

(see Cabboi et al. (2017)) to group all those poles with same characteristics. The metric used in the clustering procedure is described the follow equation:

$$d_{i,ref} = \frac{|f_{i,ref} - f_{i,j}|}{f_{i,ref}} + 1 - \frac{|\varphi_{i,ref}^{H} \cdot \ \varphi_{i,j}|^2}{\left[\left(\varphi_{i,ref}^{H} \cdot \varphi_{i,ref}\right) \cdot \left(\varphi_{i,j}^{H} \cdot \varphi_{i,j}\right)\right]} \tag{4.5}$$

where:

- $d_{i,ref}$ represents the inter-cluster distance, defined as the distance between each candidate pole and the reference pole of the cluster (update to *i-th* order);
- $f_{i,ref}$ and $\varphi_{i,ref}$ are the mean frequency and mean mode shape of the reference pole, which are updated with the increased dimension of the cluster;
- $f_{i,j}$ and $\varphi_{i,j}$ are the modal parameters (natural frequency and mode shapes) corresponding to the current pole.

The operator $|\bullet|$ is the absolut value, meanwhile $[\bullet]^H$ corresponds to complex conjugate operator. In order to clarify the nomenclature used **Eq. 4.5**, the subscripts associated to each parameter in the formula correspond to the *j-th* solution of the stochastic model defined by *i-th* model order.

The procedure is repeated in order to scan all available poles on the stabilization diagram and it is stopped only when all poles have been checked and grouped into clusters. The clustering procedure consists of the following steps:

1) Allocation of the *cluster seed*. The first reference point of the first cluster is associated to the pole with the lowest natural frequency value of the lowest order;
2) Checking of the similarity between the reference point and the poles obtained for increased orders is evaluated using **Eq. 4.5** and if the Euclidean distance does not exceed a pre-selected inter-cluster threshold, the current pole is kept on;
3) Detection of the closest pole among the previously detected ones;
4) Selection and inclusion of the closest pole (in term of distance) into the cluster;
5) Definition of the new reference cluster point (in terms of mean natural frequency and mean modal shape) using all poles present into the cluster;
6) Repetition of the points 2)-5) until checking the poles in the highest model order.

A graphical representation of the generation of the first cluster is described in **Fig. 4.3**. Specifically, starting from the resulting poles provided by the pre-filtering routine (**Fig. 4.3**(a)), the allocation of the first seed is performed (**Fig. 4.3**(b)), then the formula in **Eq. 4.5** is cursively applied for increasing model order (**Fig. 4.3**(c)) to reach the available estimates in the highest order (**Fig. 4.3**(d)). Therefore, when the poles in the highest order are scanned and possibly grouped, the first representative cluster is completed and all poles already assigned to the cluster are not considered in the process anymore.

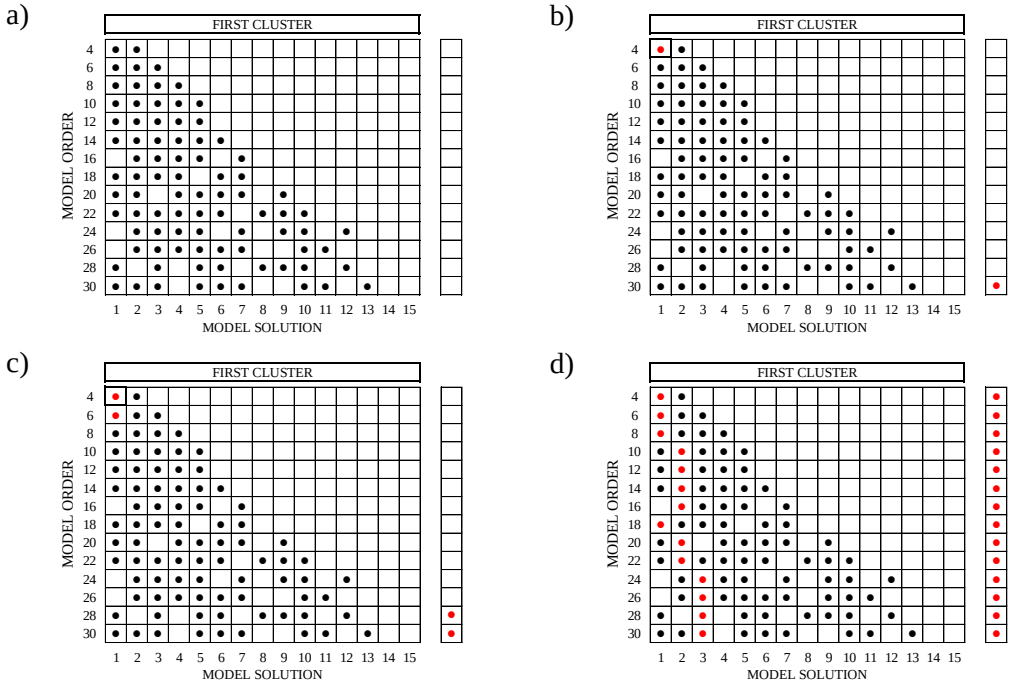

Fig. 4.3. First cluster generation: a) available poles provided by pre-filtering. b) allocation of the cluster seed, c) linking between estimates of consecutive order and d) final cluster.

Subsequently, the steps 1)-6) are recursively repeated to group all available poles with same dynamic characteristics into different representative clusters as depicted in **Fig. 4.4**. Hence when all poles are allocated and grouped, as it is customary, the shorter clusters (i.e., the clusters containing a number of elements lower than one third or one fourth of the elements present in the largest cluster) are considered as noise modes and discarded, as illustrated in **Fig. 4.4**(f).

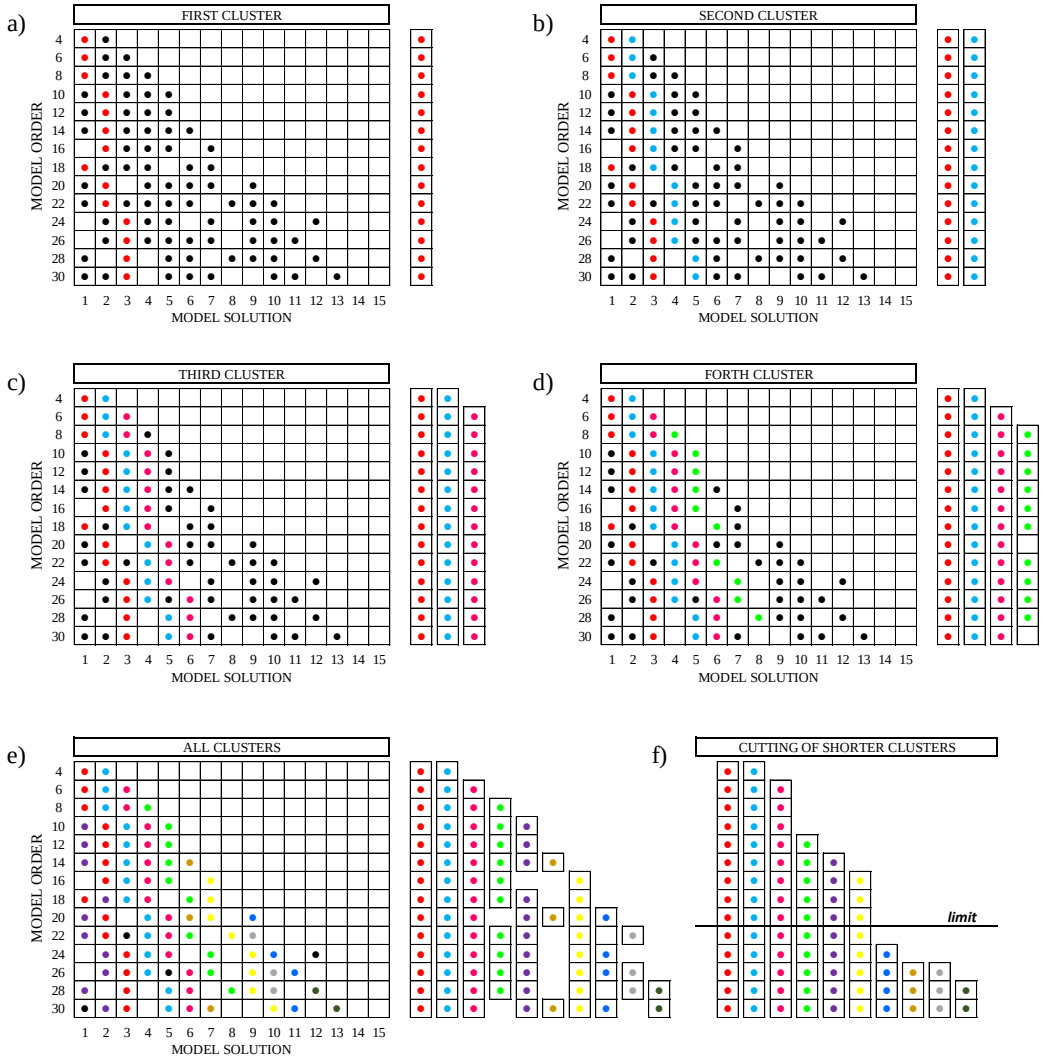

Fig. 4.4. Clustering procedure: a) creation of the first, b) the second, c) the third and d) the fourth cluster, e) allocation of all available poles and 7) removal of the shorter clusters (noise modes).

Finally, in the end of the clustering procedure, only the clusters standing above the limit are not removed and saved for the next subroutine. Moreover, the mean modal estimates extracted by resulting clusters, become the set of reference estimates of the next key-step of the developed tool.

3.2.4 Post-processing

The last subroutine of the proposed MPE algorithm is aimed at checking the consistency of the results delivered by the clustering process and at improving the accuracy of the modal estimates by applying simple statistical rules. The post-processing is composed of three different *checks* applied in consecutive way:

1) The first check is performed on the modal estimates provided by clustering algorithm. This task is achieved performing a further clustering process in order to amend some possible inaccuracies occurred during the construction of the clusters in the previous step, as loos of estimates in beginning of the cluster generation.
2) The second check is performed on the resulting mode shapes estimates in order to remove possible replications of the structural modes mainly related to the model inaccuracy.
3) The third check consists of an application of simple statistical tool to remove the extreme values of the clusters and to extract estimates with less uncertainty.

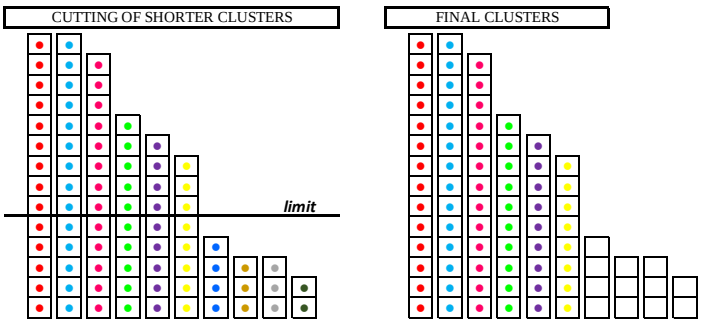

Fig. 4.5. Resulting clusters used to define the centroids and the related inter-cluster distanced used for the post-processing routine.

In more details, the first check of the post-processing is performed through a new (non-hierarchical) clustering approach in which the task of the procedure is reached without providing any user-defined distance thresholds. The characterization of the new clusters is automatically performed by the procedure itself using the statistical properties of the distribution of the estimates within each (previous) resulting group.

To better explain, the pairs of mean values (natural frequency and mode shape) obtained by the previous clustering tool are now used as centroids to construct new clusters inspired to an agglomerative approach. Furthermore, the inter-cluster distance associated to each centroid is now defined by the real distribution of poles inside each selected cluster.

The aim of the present check is to amend possible inaccuracies occurred at the beginning of the cluster generation (such as loss of poles belonging to the cluster or, conversely, outliers fallen into the cluster) and consequently reduce the dependence of the identified modes on the user-defined input parameter (i.e., inter-cluster threshold) that needs to be tuned in the very beginning of the identification process. In other words, the checking is performed to improve the accuracy of extracted modal parameters estimates, generally highlighted by a decreased standard deviation. It is further noticed that, since the reference values have been already defined, the computational cost of the second clustering is drastically reduced.

It is worth highlighting that in the context of automated processing this subroutine tends to solve the main issue related to the initial tuning of the inter-cluster threshold. In fact, as it will be shown in the applications on real structures, it could happen that numerical modes appear between the structural ones during the investigation analysis. This situation could happen when some numerical modes maintain a sort of consistency for increasing order forming groups of poles with considerable number of elements that are not removed by the cluster cut-level.

Normally, such modes are manually removed from the results requiring a user intervention. The aim of the post-processing is to avoid the manual operation mimicking once again the choice of an expert analyst and providing a more robust set of structural modes.

To clarify the role of the second clustering, the main steps are reported here below:

1) The post-processing receives as input the system matrices of poles obtained after the removal of spurious and noise modes (i.e., after pre-filtering), together with the mean values and standard deviations of the obtained clusters (i.e., after clustering).
2) Starting from the cluster with the highest number of elements, a new agglomeration is performed in the sub-routine using the mean value of natural frequency and mode shape associated to each selected cluster as centroid of the group.
3) The Euclidean distance between the centroid and all available poles is calculated for each model order, starting from the lowest order to reach the highest available one.
4) If available, only one pole for each model order is associated to the reference centroid.
5) Once the pole has been associated to the centroid, it is removed from the available ones and it is kept into the new cluster.
6) The steps 2)-5) is repeated in order to use all available centroids provided by the clustering procedure

It is worth remarking that following this strategy, the distance thresholds associated to the representative centroids have different values and each value is equal to four times the standard deviation relates to the poles distribution into the clusters previously obtained.

Subsequently a check on the mode shapes is performed and aimed at identified any possible replications of the physical modes in the stabilization diagram. In fact, as pointed out in [Cabboi (2013)], a stable alignment could split in two close alignments which refer to the same structural mode.

As described in Chapter 2, this situation is typically related to a numerical inaccuracy due to an incorrect choice of the input parameters of the SSI methods (i.e., the time-lag value for the SSI-Cov method or the number of row-block in the SSI-Data method). The procedure is developed to amend this issue and it is able to detect clusters representing the same mode (i.e. clusters in which both the natural frequency and the mode shape are very close) and then to remove the replication.

To reach this task a square matrix composed of MAC values calculated between all resulting mode shapes associated to the modal modes that come out from the new clustering is constructed. Then, the modes shapes detected by MAC values higher than a threshold value (usually is adopted a fixed limit of MAC index equal at 0.95) are selected. Among possible replications, the modal vector exhibiting lower MPC is considered as replication and removed from the final set of results.

Finally, the last check is aimed at limiting the scatter possibly affecting the modal damping ratios. The removal of the outliers is performed by applying a simple statistical tool based on the box-plot rule. The box-plot graphically shows the results obtained using three quantities: lower quartile (Q1) median quartile (Q2) and upper quartile (Q3). In order to remove the outliers, the lower and the upper quartile are estimated, and the inter-quartile range is defined as IQR=Q3-Q1. Subsequently, all poles falling outside the two limits Q1-(1.5IQR) and Q3+(1.5IQR) are defined as outliers and removed. Indeed, the extreme values are removed to improve the mean modal damping values, thus obtaining more stable and accurate prediction of this parameter [Marrongelli et al. (2017)].

The final outputs of the proposed MPE procedure are the mean values of the modal estimates (mean natural frequency, mean mode shape and median modal damping ratio) and the geometric mean value extracted considering the distribution of the MPC and MPD values associated to each pole belonging to each resulting cluster.

4.3 Application of the MPE algorithm to numerical data

The efficiency of the proposed algorithm was initially checked using a simple academic system composed of five degrees of freedom. All the geometrical characteristics of the numerical structure are described in the numerical example described in Chapter 2.
For clearness, a 5-DOFs structure is used along the thesis for doing simulation and for validating the proposed algorithms, in the context of modal parameter estimation (MPE) and also for continuous dynamic monitoring process and subsequently it is also adopted for the validation of the damage detection adopted for the SHM purpose.

4.3.1 Description of the academic structure composed of 5-DOFs

The simulated structure consists of a 2-dimensional scheme composed of five masses, five spring and dashpots (see **Fig. 4.6**), as reported below:

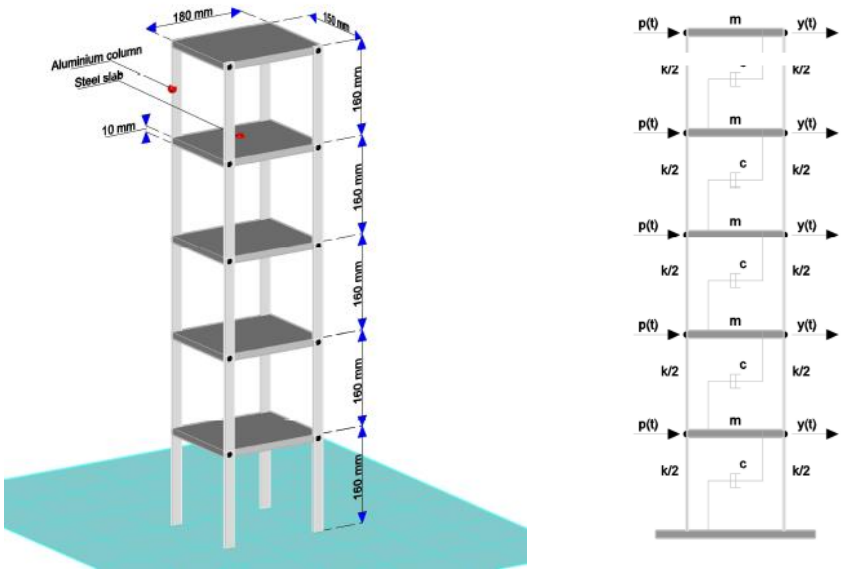

Fig. 4.6. Scheme of the 5-DOFs system used to exploit the developed algorithms. Tri-dimensional representation and two-dimensional scheme

The values chosen for matrices M, D and K (see **Eq. 2.1**) are the following:

- M is equal to the diagonal matrix with five rows and columns;
- K is a square tri-diagonal matrix with same values in the extra diagonal positions;

```
M=[ m  0  0  0  0;          K=[ 2*k  -k   0   0   0;
    0  m  0  0  0;              -k  2*k  -k   0   0;
    0  0  m  0  0;               0  -k  2*k  -k   0;
    0  0  0  m  0;               0   0  -k  2*k  -k;
    0  0  0  0  m];              0   0   0  -k   k];
```

- D is built assuming Rayleigh damping by means of

  $D = \xi \cdot 2m \cdot \sqrt{(k/m)}$ with ξ=0.01 (1%).

- In real structure not all DOF can be measured. In this case, the external excitation was applied only on the masses 1,3 and 5.

```
Bf=[ 1  0  0  0  0;
     0  0  0  0  0;
     0  0  1  0  0;
     0  0  0  0  0;
     0  0  0  0  1];
```

The matrices M, D, K and B_f are used to construct the system matrices A and C of the stochastic state-space model. Thus, numerical acceleration time series have been generated adopting the following inputs:

- Sampling frequency f_s=50 Hz (sampling period Δt=0.002 s).
- Total duration of signals, 1800 s (N=90000 time steps).
- $u(t_k) \rightarrow N(0,1)$. Gaussian distribution input force applied to all the DOF by mean of matrix B_f (B_f is a column vector composed of ones)

  $M\ddot{q}(t_k) + D\dot{q}(t_k) + Kq(t_k) = B_f u(t_k)$, k=1,2,…,N.

  where $t_k = \{0, \Delta t, 2\Delta t, \dots, k\Delta t, \dots, (N-1)\Delta t\}$.

- The observed values $y(t_k)$, k=1,2,…,N are the sum of the structure response at selected DOF, $C_a\ddot{q}(t_k)$, and a sensor Gaussian noise $a(t_k)$ with variance equal to the 20% of the largest acceleration response variance, σ^2:

  $y(t_k) = C_a\ddot{q}(t_k) + a(t_k)$, $a(t_k) \rightarrow N(0, \Sigma^2)$,

  $\Sigma^2 = \sigma^2 I_{n_0 \times n_0}$, $\sigma^2 = 0.20\max\left(\frac{1}{N}\ddot{q}(t_k)^T\ddot{q}(t_k)\right)$

At this point the SSI-Cov method was applied to identified the modal parameters of the academic structure from the simulated acceleration, and the results are shown in the Table 4.1 the space order used has been n_s=10, twice the number of expected modes.

Table 4.1. Theoretical and identified modal estimates of the numerical structure

Mode	f_{th} [Hz]	$\hat{f}_{10}$ [Hz]	ξ_{th} [%]	$\hat{\xi}_{10}$ [%]
1	3.195	0.28	3.195	0.28
2	9.327	0.83	9.324	0.96
3	14.702	1.31	14.715	1.29
4	18.884	1.68	18.907	1.96
5	21.536	1.92	21.554	1.78

In this example, the theoretical system order is known in advance, and good modal parameters have been obtained using this order. This information can be visualized also on the stabilization diagram in which all modes of the structure can be defined at the model order equal to 10.

In case of real structure is impossible to known in advance the system order of the stochastic model that best fits the dynamic behavior of the investigated structure. In this way two different problem can be pointed out: the underestimation or the overestimation of the correct model order.

As well known, in case of underestimation of the model order, the identification method can compute wrong modes, as for example the model fits the response due to two closed modes with only one. Meanwhile, in case of overestimation, the identification method forces the model to compute a number of modes higher than the system effectively has, so spurious modes are obtained. Furthermore, spurious mode can be obtained at any given order because noise content in the signals or modelling errors.

Therefore, as already stated in Chapter 2 and in the first paragraph of this one, in the identification analysis of real structures is common to overestimate the order of the stochastic model and consequently choose the model that best fit the dynamic behavior of the investigated structure.

As commonly done in practical applications, a graphical tool is used to separate physical modes from noise modes. The most popular tool for differentiating system modes from spurious modes is the stabilization diagram [Peeters (2000)]. A stabilization diagram is simply a plot of increasing model order versus the frequencies identified at each of these orders.

The main motivation behind the use of stabilization diagram is based on the characteristics of the modal parameters that should show up with consistent frequency, damping and mode shape at a various mode orders; whereas spurious modes should show a more erratic behavior at different orders of the stochastic model.

The strategy normally used to extract the modal parameters from a single dataset is generally based on the initial choosing of a sufficient high order for the state-space-model, and consequently to gradually reduce the order of the model. System identification is performed with every model order so this procedure yields a set of modal parameters for each selected order. The modal parameters referred to different model order are then compared according to some present criteria such as:

$$\begin{aligned} \frac{|f_{pi} - f_{qi}|}{f_{pi}} &\leq \varepsilon_f \\ \frac{|\xi_{pi} - \xi_{qi}|}{\xi_{pi}} &\leq \varepsilon_\xi \\ 1 - MAC(\varphi_{pi}; \varphi_{qi}) &\leq \varepsilon_{MAC} \end{aligned} \tag{4.6}$$

where ε_f, ε_ξ and ε_{MAC} are tolerance limits adopted to decide if the mode *i* estimated from the model order *p* is the same mode *j* estimated from the model order *q* (in which *q*=*p*+1, used to compare consecutive model order. The MAC (Modal Assurance Criterion) index shows the degree of correlation between two vectors and it is computed as:

$$MAC(\varphi_1; \varphi_2) = \frac{|\varphi_1^H \, \varphi_2|^2}{[(\varphi_1^H \varphi_1) \cdot (\varphi_2^H \varphi_2)]}$$

where $(\bullet)^{\mathrm{H}}$ means Hermetian operator.

This procedure is repeated for all available set of modal parameters identified at each order in sequential manner. Consequently, only the frequency values of the selected modes are plotted against their corresponding model orders, distinguishing between stable and unstable modes.

Fig. 4.7 shows the stabilization diagram of the simulated academic structure composed of five DOFs. The modal parameters were estimated using the SSI-Cov method and adopting an interval of order from 2 to 60 by steps of two.

In the diagram the separation between spurious modes and physical ones is performed applying the checks on the natural frequencies, modal damping ratios and mode shapes (using MAC index) in consecutive manner as described in **Eq. 4.6**. In particular, stable modes were detected verifying ε_f=0.02, ε_ξ=0.05 and ε_{MAC}=0.02, simultaneously.

It is worth remarking that stabilization diagram is one of the most used post-processing tools for operational modal analysis, specially adopted with SSI procedures. Although it is just a graphical tool in which to report the natural frequencies, of the modes obtained for increasing order of the stochastic state-space model, versus the order itself, the stabilization diagram helps the expert user to define the best order of the model that best fits the dynamic behavior of the investigated system.

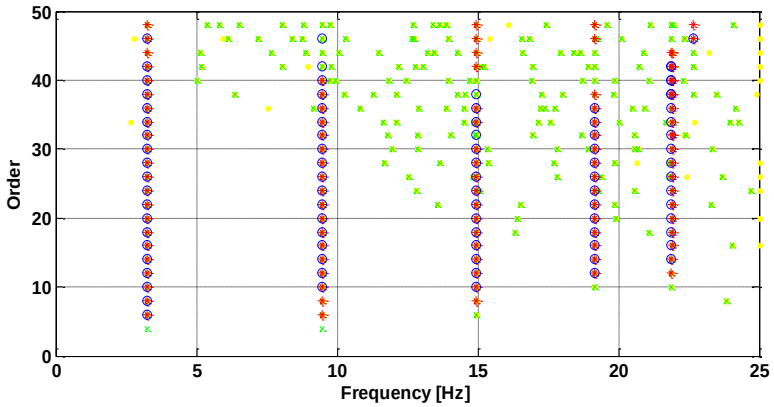

Fig. 4.7. Stabilization diagram. Choosing of the order the best fits the dynamic behavior of the numerical structure

The MPE algorithm presented herein has been developed in order to extract her estimation of the modal parameters in automated way mimicking the choices of an expert user in the identification of the stable alignments that represent the structural modes for increasing model order.

Once again, the MPE procedure used to extract the modal parameters estimates from the output dataset has been developed to simplify the used of the stabilization diagram adopting only one check (see **Eq. 4.5**) on the poles instead of three different checks as reported in **Eq. 4.6** to remove the spurious poles. This means that the automated algorithm requires just one user-defined threshold instead three tolerance limits in the selection of the stable poles, furtherly reducing the user's interaction during the identification process. Moreover, the choice of the best model order is completely removed ant the estimates are automatically extracted applying simple statistical property on the stable alignments that stand out on the stabilization diagram.

4.3.2 Extraction of the modal parameters from the numerical time series

The evaluation of the performance of the presented MPE algorithm was based on the automatic processing of several simulated response time series obtained by applying the white noise excitation at the first level of the structure. Several artificially generated time series of 30 minutes long and sampled at 100 Hz were collected to test the robustness of the algorithm. Thus, the recorded responses were analyzed applying the SSI-Cov method. Hence, some trial runs were executed in order to define the dimension of the correlation matrix (i.e., the time-lag value) and the interval of the model order used to extract the modal estimations from the collected responses.

Fig. 4.8 shows the effects of the different steps on the stabilization diagram. In particular, the diagrams in the left side represent the stabilization diagrams, meanwhile the diagrams in the right side are the frequency vs damping diagrams. Both representations are depicted in order to highlight the cleaning action exerted by each step of the algorithm.

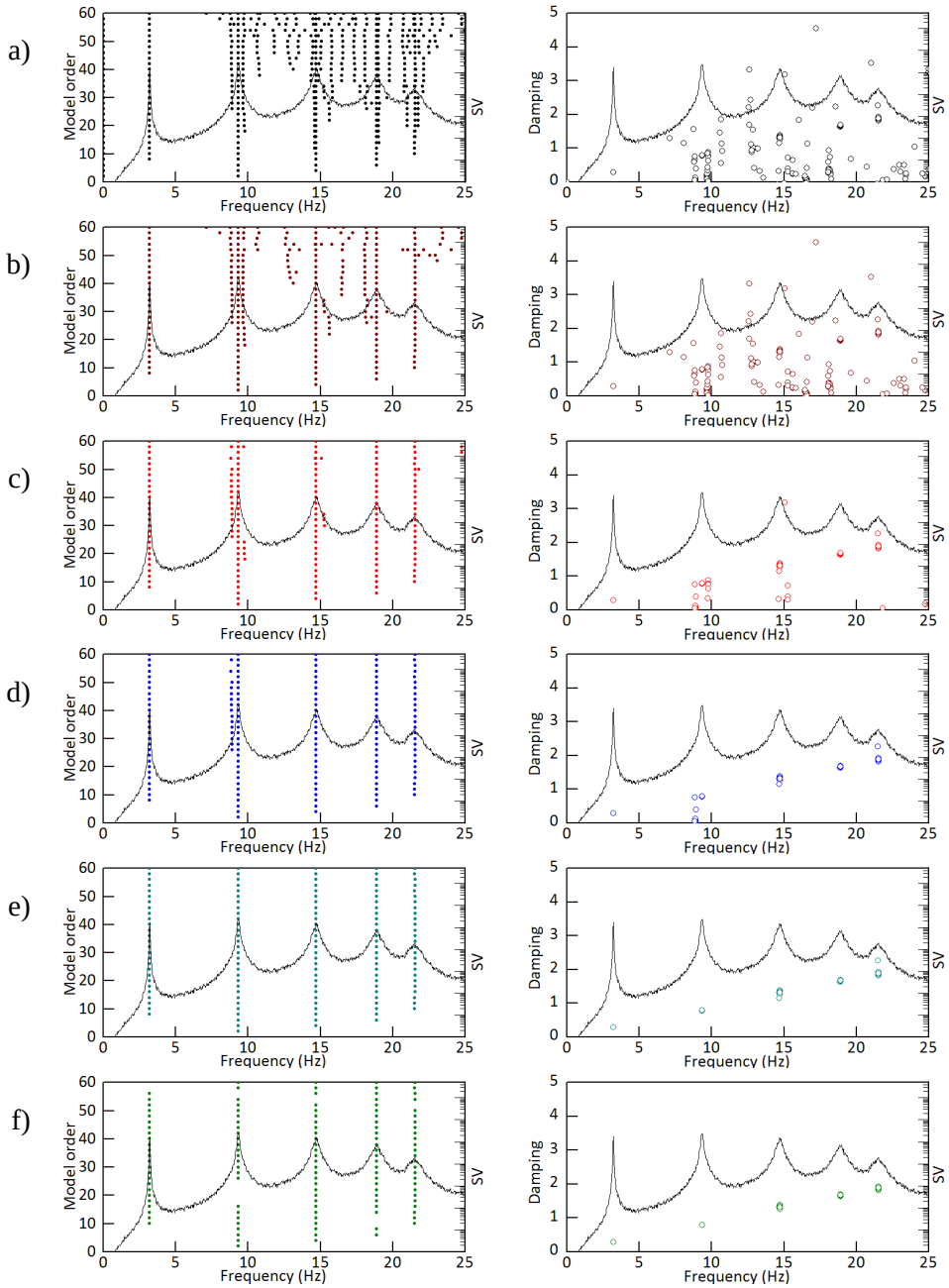

Fig. 4.8. Cleaning actions exerted by each sub-procedure of the developed MPE methodology: a) SSI outputs, b) after modal damping threshold, c) after complexity thresholds, d) stable alignments obtained by clustering process, e) stable alignments after the checking on the clustering results and mode shape sand f) final poles associated to identified structural modes.

In fact, this graphical tool is used to extract the stable alignments composed of stable poles (herein depicted using the natural frequency values) that maintain consistency for increasing model order. In the second diagrams the pair of values (frequency-damping) are mainly used to test the consistency and the accuracy of these estimates during the identification process.

Detailing, **Fig. 4.8**(a) shows all the solutions (in terms of natural frequencies) provided by stochastic models with even orders between 2 and 60. As depicted, the number of SSI outputs grows when the order of the stochastic model increases. Obviously, such solutions contain both modes with physical meaning and numerical modes related to the noise content into the signals. Therefore, the task of the implement algorithm is to mimic the choices that an expert user take on the selection of the stable alignments, where each poles represent a set of modal parameters (i.e., natural frequency, mode shapes and modal damping ratio) associated to a structural mode of the analyzed structure.

In **Fig. 4.8**(b) the results obtained after the removal of higher damped modes are reported, meanwhile **Fig. 4.8**(c) shows the results obtained at the end of the pre-filtering key-step, after the removal of spurious poles with high complexity values on the mode shapes.

Moreover, in the **Fig. 4.8**(d). the resulting stable alignments obtained after the application of the clustering procedure is reported. It is should to be noticed that even in case of numerical example the clustering procedure can provide an incorrect set of modal estimates. This numerical error depends on several factors, such as the definition of the time-lag value, the interval of the model order and also could depends on the incorrect setting of the user-defined thresholds that do not properly filter the numerical modes. Despite these, as already mentioned in the previous Chapter, the creation of the clusters is strictly dependent on the inter-cluster distance value. In fact, the initial tuning of this parameter together with the removal of the shorter clusters do not guarantee that the provided set of estimates is composed of only structural modes. This condition could be more frequent during the analysis of real data in which the collected signals contain

several disturbances due to environmental factors present in the surrounding of the investigate structure. This type of problem required the development of another routine for checking results and removing possible errors produced in the clustering process.

Consecutively, the diagrams in **Fig. 4.8**(e) shows the stable alignments obtained after the execution of the second clustering and the check on the mode shapes. As shown, the numerical mode (with nominal frequency equal to 8.88 Hz) disappears providing the correct set of alignments corresponding to the five modes of the model.

The action exerted by the check on the outliers is shown in **Fig. 4.8**(f). As depicted in the frequency vs damping representation, the removal of the extreme modal damping values within each cluster provides a more accurate estimation of this parameter.

Finally, the estimations of the modal features are extracted by the resulting clusters as follow: mean natural frequency, mean mode shape, median modal damping ratios and geometric mean values for the complexity indices (MPC and MPD, respectively) of the poles inside each group.

Table 4.2 summarizes the most important information and the improvement of the results after the application of the *post-processing* routine that represents the main original aspect of the automated algorithm presented in this Chapter.

Table 4.2. Improvement of the results after the post-accuracy check to improve estimates

Modes	**Before post-processing**				**After post-processing**			
	f	***σ(f)***	***ξ***	***σ(ξ)***	***f***	***σ(f)***	***ξ***	***σ(ξ)***
1	3.197	0.0001	0.280	0.0001	3.197	0.0001	0.280	0.0001
2*	8.883	0.0141	0.062	0.0949	-	-	-	-
2	9.328	0.0011	0.783	0.0049	9.328	0.0010	0.784	0.0025
3	14.706	0.0071	1.319	0.0461	14.707	0.0057	1.324	0.0324
4	18.898	0.0021	1.687	0.0205	18.898	0.0016	1.687	0.0161
5	21.545	0.0117	1.875	0.0831	21.546	0.0071	1.871	0.0345

Two different aspects related to the efficiency of the third block of check have to be pointed out by results reported in the **Table 4.2** the first one is relating to the possible replications of the modes that are removed delivering a consistent set of modal estimates, the second one is referred to the accuracy of all estimates that is generally improved.

In order to provide the consistency of the obtained estimates, the extracted values are compared with the theoretical ones and also with the estimates obtained by a manual choice of the state-space model, as it is summarized in the **Table 4.3**.

Table 4.3. Comparison between the theoretical values together with the manually identified values and the automatically extracted values of the natural frequency

Mode	f_{th} [Hz]	ξ_{th} [%]	$\hat{f}_{10}$ [Hz]	$\hat{f}_{10}$ [Hz]	$\hat{f}_{MPE}$ [Hz]	ξ_{MPE} [%]
1	3.195	0.280	3.195	0.280	3.197	0.280
2	9.327	0.830	9.324	0.960	9.328	0.784
3	14.702	1.310	14.715	1.290	14.707	1.324
4	18.884	1.680	18.907	1.960	18.898	1.687
5	21.536	1.920	21.554	1.780	21.546	1.871

From the inspection of the results reported in the **Table 4.3** it is possible to highlight an excellent correspondence between the theoretical values of the resonant frequencies and the natural frequency estimates obtained by a manual choice of the state-space model and the automatically extracted estimates by applying the developed MPE algorithm.

Furthermore, from the inspection of the damping values it is worth to notice a better correspondence between theoretical values and the estimates provided by the automated algorithm. This means that the choice of the median value calculated among all estimates belong to the same cluster provides a better estimate than one obtained by the manual selection of the stochastic model with lowest order.

To complete the analysis of the MPE (exploited using a simple academic structure), the five mode shapes obtained by the automated identification are reported in **Fig. 4.9**.

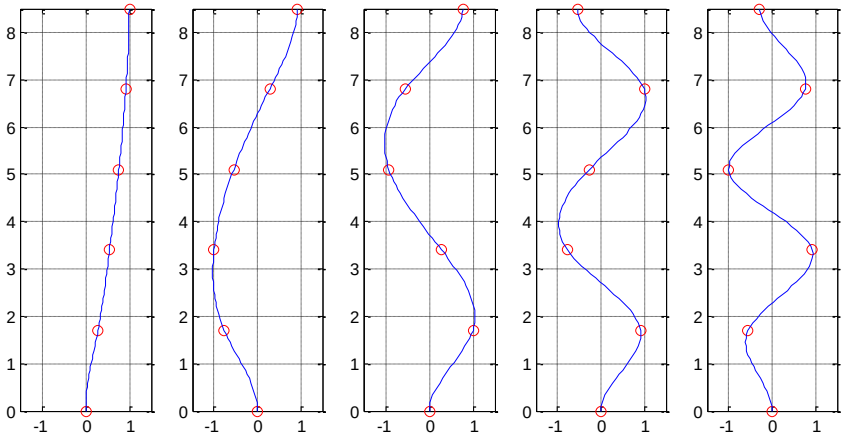

Fig. 4.9. Mode shapes associated to the five identified modes of the structure

From the comparison of the mode shapes provided by the developed algorithm and the theoretical values a very high correspondence is obtained with a MAC value generally higher than 0.99 for all five detected modes.

4.4 Application and validation of the proposed algorithm using real data

The current paragraph is principally focused on the application of the previous developed automatic model identification algorithm, exploring the potentiality of extracting the modal estimates without any user interaction during the identification process. The performance of the proposed method is exemplified on data collected during dynamic tests performed on a complex footbridge and on an ancient bridge both located in the north of Italy.

4.4.1 Application of the algorithm to AVT data collected on a pedestrian footbridge

The first real structure adopted to validate the developed algorithm consists of a steel footbridge placed in the town of Seriate, about 50 km far from [Lai et al. (2017)]. The MPE algorithm is applied to the output response collected during an AVT performed to investigated if the vibration levels of the footbridge exceed the standard comfort limits during in operative conditions. This dynamic test represents an ideal benchmark for an automated procedure of modal parameter estimation because:

- The dynamic characteristics of the footbridge were already extensively investigated using the FDD procedure [Brinker et al. (2001)] and the SSI-Data techniques available in the commercial software ARTeMIS. Hence, reference values of the modal parameters are available for validation purposes.
- The footbridge turns out footbridge [Lai et al. (2017)] to be characterized by a very complex dynamic behavior and a large number of normal modes in the frequency range 0-8 Hz, including closely spaced and weakly-excited modes.

4.4.1.1 Description of the footbridge and the equipment used for the AVT

In more details, the investigated footbridge (**Fig. 4.10** and **Fig. 4.11**) crosses the Serio River and has been built in the "Serio Park" to connect two cycle routes. The suspended deck is 63.90 m long and its width varies between 2.5 m and 5.0 m. The deck consists of timber planks, supported by a grid of steel stringers and floor beams (**Fig. 4.10**b). The floor beams (**Fig. 4.10**b) belong to two classes: (a) the main transverse beams, equally spaced at 3.0 m and characterized by a tapered cross-section and (b) the secondary IPE 120 cross-beams. The stringers include a couple of IPE 330 edge beams and a central girder with a hollow circular section (Ø=298.5 mm). All the longitudinal beams are connected to the main transverse beams through bolted connections capable of restoring the continuity, whereas the connection between the secondary beams and the edge beams allows the secondary beams to rotate around the edge beam axis. The deck is completed by a series of X-braces and by timber planks, 5.0 cm thick and providing the walking surface for the pedestrians.

(a) (b)

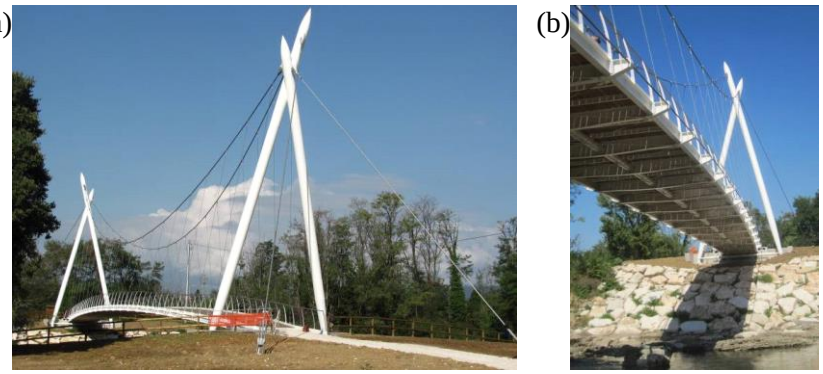

Fig. 4.10. Footbridge crossing the Serio river (Seriate): (a) General view; (b) Underside view of the deck.

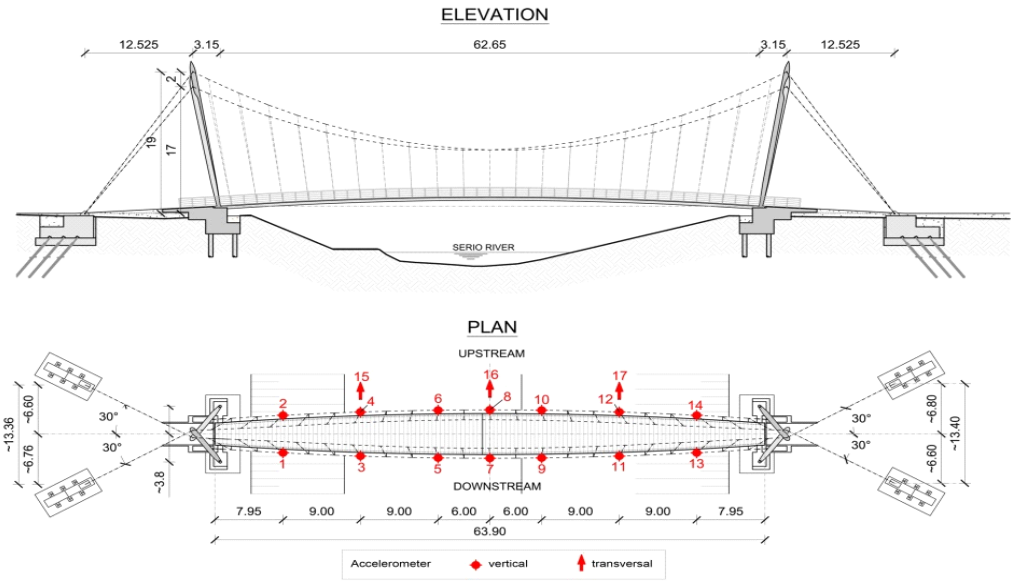

Fig. 4.11. Elevation and plan of the footbridge (dimensions in m). Sensors layout during the field tests.

The suspension system supporting the deck consists of: (a) 4 steel pylons, exhibiting a slight slope with respect to the vertical plane and arranged to constitute two A-shaped portal frames; (b) 2 main suspension cables, of 60 mm diameter, supporting the deck through 42 hangers of 16 mm diameter; (c) 4 backstays, of 60 mm diameter, linking the pylons to the ground. The main suspension cables and the backstays are connected to the top of the pylons as it is shown in **Fig. 4.10**.

As previously pointed out, the dynamic characteristics of the footbridge and its serviceability were extensively investigated right after its completion and before the opening (July 2012). More specifically, ambient vibration tests were firstly performed with the objective of identifying the modal parameters of the bridge; subsequently, walking and running tests were carried out to verify that the human-induced vertical and horizontal accelerations were limited to acceptable values. The response of the footbridge was measured at 17 selected points (**Fig. 4.11**) in a single set-up, using uniaxial WR 731A piezoelectric accelerometers (**Fig. 4.12**). The acceleration responses were recorded with a sampling frequency of 200 Hz, which is fairly larger than that required for the considered footbridge, whose dominant natural frequencies are below 10 Hz. Hence, low pass filtering and decimation were applied to the data before using the identification tools: data were down-sampled to 25 Hz, so to have a Nyquist frequency of 12.5 Hz.

Fig. 4.12. Typical mounting of the accelerometers on site.

4.4.1.2 Application of the automated procedure and validation of the obtained results

Time series of 7200 sec (corresponding to more than 7000 times the fundamental period of the structure) were collected during the ambient vibration tests. The first 3 singular value (SV) lines of the spectral matrix are shown in **Fig. 4.13**: the inspection of the first SV highlights several amplification (i.e. modal) regions and closely spaced peaks of similar amplitude in the two largest SV lines corresponding to the frequency of about 1.9 Hz and 7.4 Hz. Hence, closely spaced modes are likely to occur in those frequency intervals. The clear detection of closely spaced modes (as well as of weakly excited modes) is a typical issue solved by the use of parametric identification methods.

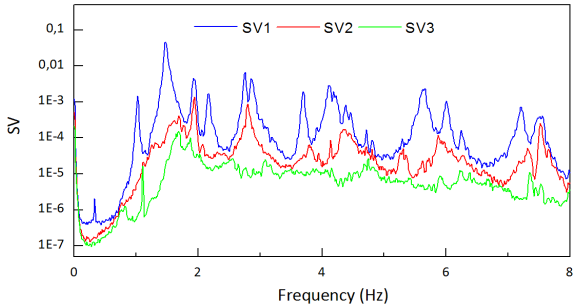

Fig. 4.13. Singular values (FDD) of the spectral matrix of the acceleration measured.

Fig. 4.14 shows the action exerted by each step of the automated algorithm on the stabilization diagrams obtained by the application of the SSI method. Together with the stabilization diagram also the frequency vs. damping diagrams are reported. Specifically, (i) **Fig. 4.14** (a) shows the poles provide by the SSI-Cov method, (ii) **Fig. 4.14** (b) and **Fig. 4.14**(c) show the remaining poles after the check on modal damping ratio and on the mode shape complexity, respectively; (iii) **Fig. 4.14** (d) highlights the cleaning effect exerted by the clustering process and (iv) **Fig. 4.14** (e) show the results obtained after the check on the clustering results; (v) **Fig. 4.14** (f) show the stable alignments after the removing of any possible repetitions of physical modes; finally, (vi) **Fig. 4.14** (g) contains the final alignments corresponding to physical modes after the removal of the outliers.

17 vibration modes of the footbridge were automatically identified in the investigated frequency range. The alignments of stable poles in **Fig. 4.14**(g) generally correspond to well-defined spectral peaks, reported in **Fig. 4.13**. The identified modal parameters of the footbridge (in terms of natural frequencies, damping ratios) and their standard deviations together with the complexity indices associates to the mode shapes are summarized in **Table 4.4**, along with the reference estimates obtained in [Lai et al. (2017)] by using a commercial software. It should be noticed that: (a) there is an excellent correspondence between the reference results and the ones of the present procedure, both in terms of natural frequencies and damping ratios; (b) the standard deviations of damping ratios are much lower than those generally obtained by other OMA techniques.

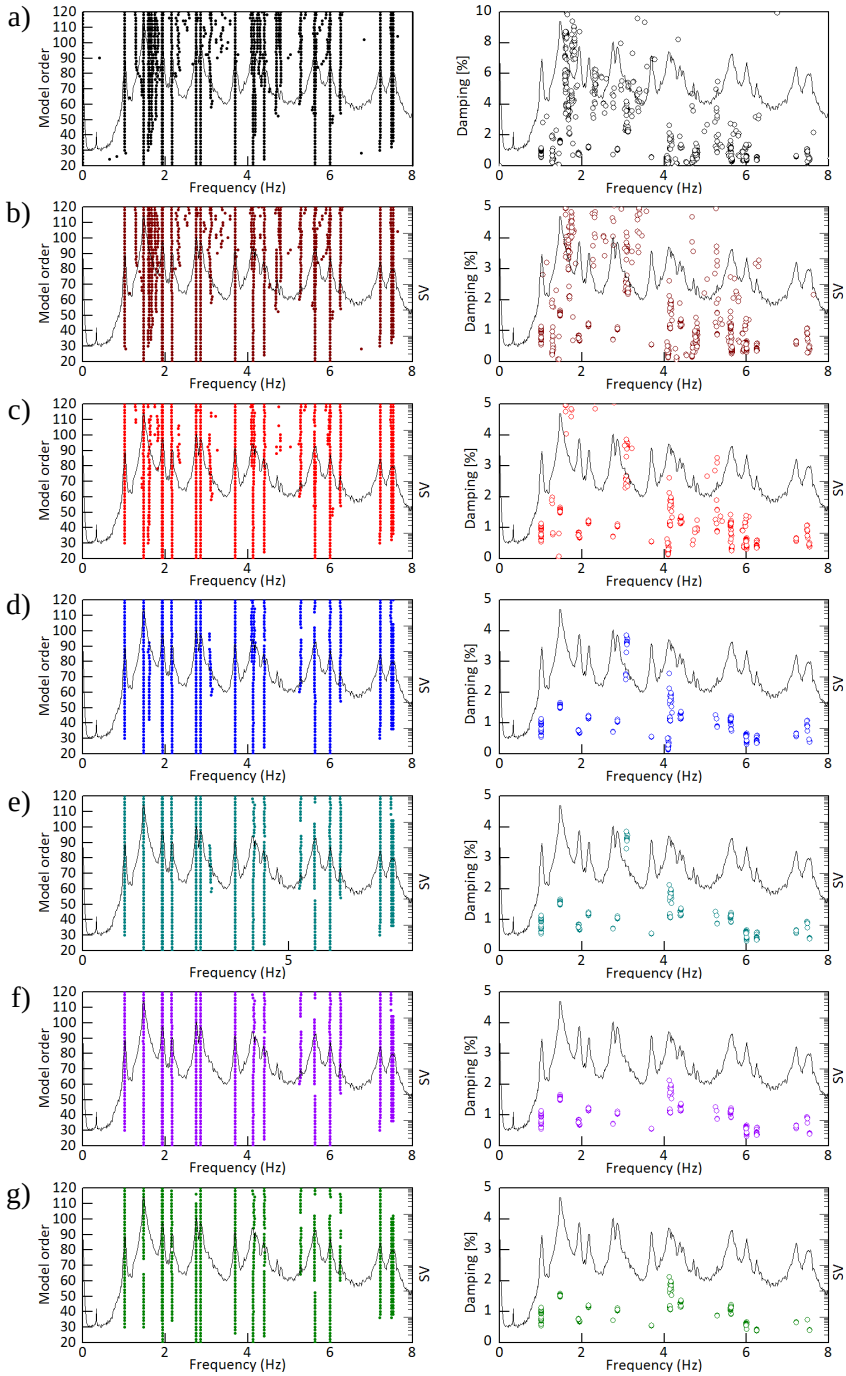

Fig. 4.14. Stabilization diagrams: (a) SSI-Cov outputs; (b) after checking on damping; (c) after checking on mode complexity; (d) after clustering; (e) after new clustering; (f) after checking on mode shapes; (g) after removing the outliers.

It should be noticed that **Fig. 4.14** and **Table 4.4** reveal the capability of the proposed automated algorithm in the identification of three further vibration modes that are not detected in previous analysis.

Two of those modes, with nominal natural frequencies of 5.29 Hz and 6.25 Hz, correspond to weakly excited modes (which are only recognized for higher values of the model order). The third mode, having a frequency of 7.54 Hz, turns out to be very close to another vibration mode (7.49 Hz) of the footbridge. From a deeper inspection of the Fig 4.13, the presence of the two closely-spaced modes around 7.5 Hz are also suggested by the vicinity of the two SV lines in that frequency region.

In **Table 4.4**, a comparison between the dynamic characteristics obtained by a manual analysis of the data (using ARTeMIS) and those ones automatically identified applying the MPE procedure (in the same investigated frequency range) are reported in detail.

Table 4.4. Comparison between modal estimates identified by previous analysis using a commercial software and those ones obtained performing the proposed MPE procedure.

		Reference Values			***Extracted Estimates***					
		FDD	**SSI-Data**		**Automated Procedure - SSI-Cov**					
N°	**Mode**	***f*** **[Hz]**	***f*** **[Hz]**	**ξ [%]**	***f*** **[Hz]**	**σ(*f*) [Hz]**	**ξ [%]**	**σ(ξ) [%]**	**MPC**	**MPD**
1	1B	1.025	1.014	0.75	1.018	0.0012	0.79	0.196	0.999	1.1
2	2B	1.475	1.474	1.58	1.474	0.0002	1.50	0.024	1.000	0.2
3	1T	1.924	1.926	0.53	1.924	0.0008	0.74	0.012	0.996	1.6
4	2T	1.953	1.946	0.66	1.947	0.0001	0.68	0.008	0.900	10.3
5	3B	2.168	2.169	1.2	2.165	0.0012	1.16	0.012	0.999	0.7
6	3T	2.754	2.756	0.74	2.755	0.0001	0.72	0.003	1.000	0.6
7	4B	2.861	2.861	1.32	2.866	0.0004	1.06	0.036	1.000	0.1
8	4T	3.691	3.696	0.61	3.696	0.0001	0.54	0.002	0.999	0.9
9	5B	4.121	4.143	1.69	4.149	0.0130	1.61	0.330	0.996	1.5
10	5T	4.385	4.408	1.11	4.408	0.0046	1.25	0.057	0.998	1.3
11	6T	-	-	-	5.293	0.0015	0.86	0.007	0.989	3.1
12	6B	5.645	5.636	0.94	5.632	0.0063	1.02	0.103	0.998	1.3
13	7T	6.006	6.011	0.75	6.004	0.0033	0.64	0.046	1.000	0.7
14	7B	-	-	-	6.257	0.0038	0.39	0.009	0.838	11.8
15	8B	7.217	7.222	0.73	7.218	0.0004	0.66	0.005	0.978	3.6
16	8T	7.490	7.488	0.78	7.489	0.0001	0.74	0.001	0.997	1.2
17	9B	-	-	-	7.538	0.0003	0.39	0.004	0.928	7.4

In **Fig. 4.15** the modes shapes associated to the 17 identified modes are shown.

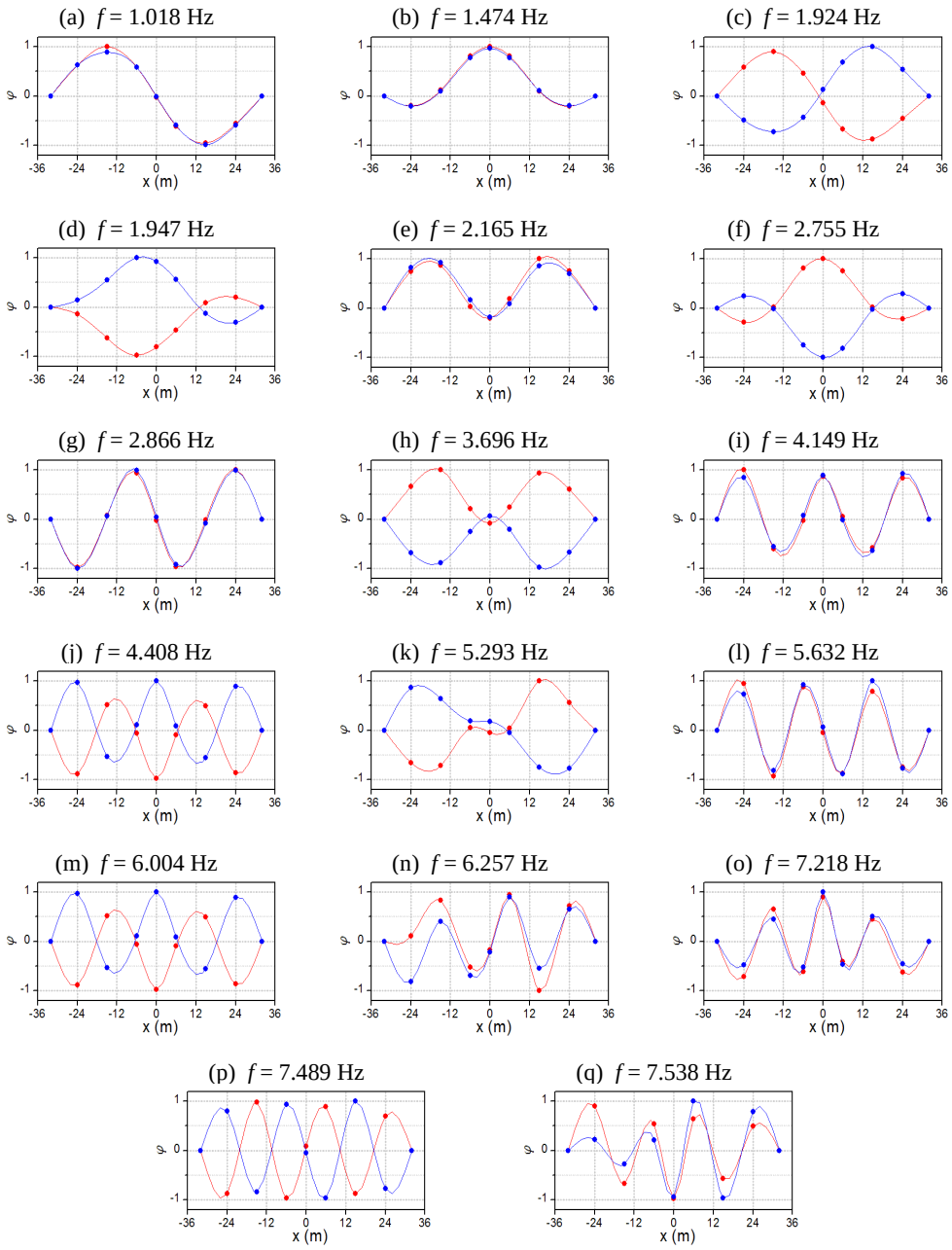

Fig. 4.15. Vibration modes automatically identified by the application of the proposed MPE procedure (red line refers to upstream side of the footbridge, blue line refers to downstream).

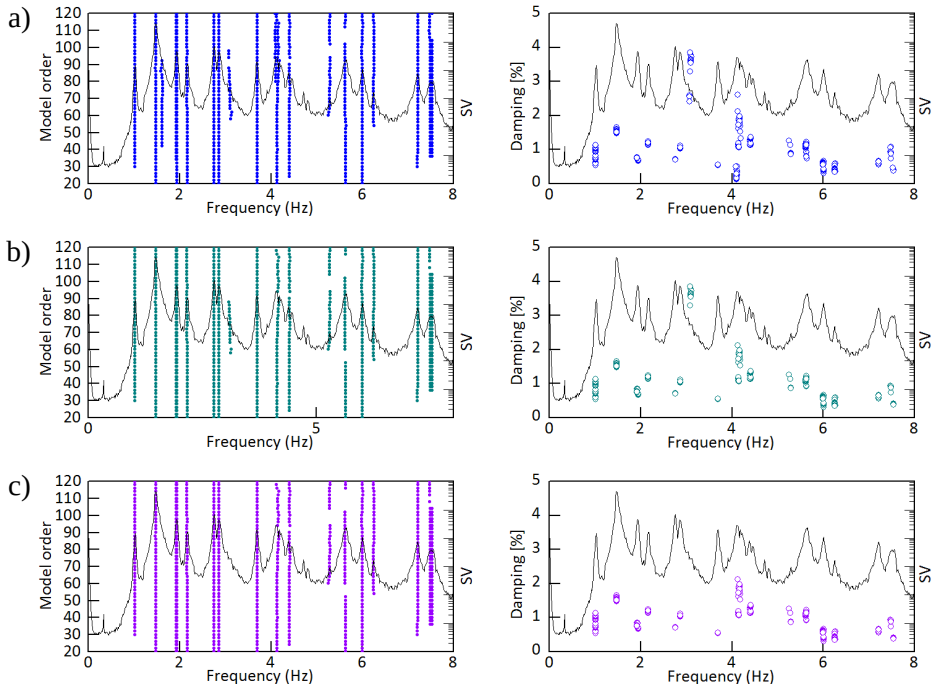

Fig. 4.16. Action exerted by the post-processing on the clustering results. Specifically, the poles obtained by a) clustering procedure; b) new clustering; c) check on the mode shapes, are reported.

Fig. 4.16 highlights the main original aspect related to implemented procedure aimed to provide a more well-founded set of estimates avoiding possible incorrect estimations and/or replications of the structural modes. As highlighted from the consecutive diagrams, any differences compare between the results provided by the cluster procedure shown in **Fig. 4.16**(a) and estimates resulting from first check shown in **Fig. 4.16**(b) and the final alignments depicted in **Fig. 4.16**(c). In fact, some clusters disappeared from the diagram. As already described, the efficiency on the removal of the numerical modes is due to the particular implementation of the *new clustering*, based on the average values and the standard deviations of the estimates obtained in the previous step and the mode shape check, based on the checking of the similarity between the resulting modes. As demonstrated in **Fig. 4.16**(a), possible numerical modes can survive to the clustering procedure delivering a set of modal estimates composed of also spurious modes.

The *new clustering* partially solves the issue; in fact, the sub-procedure removes the cluster associate to a numerical mode with frequency value close to 4 Hz. This is due to the shorter distance threshold that does not permit the allocation of all previous estimates splitting the numerical cluster in two or more subgroups. In this way the numerical mode is removed by the set of structural estimates.

In such case, numerical modes maintain high consistency for increasing model order producing a quite exact replica of the close structural mode. This situation can occur also in case of high value of the time-lag parameter (in case of SSI-Cov method). The *check on the repeated mode shape* recognizes such situation through the construction of MAC matrix in which extra-diagonal components represent the MAC values calculated among all available mode shapes. Hence, if the MAC index exceeds a predetermined threshold, the mode with higher complexity (lower values in term of MPC) is identified as replication and it is removed from the set of structural modes. The outputs of the *check on the mode shape* represent the final set of structural modes automatically provided by the MPE procedure. The last check is performed to remove any outliers of the modal damping ratios that could affect the mean value of this estimate.

From engineering standpoint, some remarks can be drawn:

- The frequency of the fundamental mode is 1.02 Hz and the corresponding mode associated involves anti-symmetrical vertical bending of the deck.
- The footbridge exhibits complex dynamic behavior characteristics (i.e., a large density of vibration modes, two couples of closely spaced modes and five modes in the frequency range 1.9-3.0 Hz), clearly suggesting the occurrence of discomfort issues footbridge [Lai et al. (2017)].
- Almost all modes can be classified as dominant bending (1^{sd}, 2^{nd}, 5^{th}, 7^{th}, 9^{th}, 12^{th} and 15^{th} mode) or dominant torsion (3^{rd}, 6^{th}, 8^{th}, 10^{th}, 11^{th}, 13^{th} and 16^{th} mode).
- There are three modes (4^{th}, 14^{th} and 17^{th} mode) that exhibit coupling between vertical and the transversal components. Furthermore, due to its strong lateral component, it is difficult to plot a clear illustration of the 14^{th} mode.

4.4.2 Application of the algorithm on dynamic tests data of The Olla bridge

The MPE algorithm is used to extract the modal parameters from some dynamic tests performed on a multi-span ancient masonry bridge composed of five arches located nearby to the town of Gaiola in the neighborhood of Cuneo (Northern Italy). This second case study represents another important benchmark for an automated identification procedure because:

- As reported in [Borlenghi et al. (2019)], the dynamic characteristics of the bridge were already investigated using the FDD [Brinker et al. (2001)] technique available in the commercial software ARTeMIS.
- From the analysis performed on several datasets collected during the AVT of the bridge (named as: A, B, C, D, E). The modal parameters were extracted applying the MPE algorithm to dataset B. Five different peaks of the first Singular Value associated to the spectrum matrix of the output responses are clear visible in the investigated interval of frequency equal to 0-12 Hz [Borlenghi et al. (2019)],
- Consequently, the frequency interval of investigation was extended to 20 Hz, allowing the identification of two further vibration modes with considerable complexity degree
- The bridge turns out to be characterized by a complex dynamic behavior also due to the considerable height of the pylons that influences the fundamental modes.
- The reference values of the modal parameters. obtained using the SSI-Data technique implemented in the ARTeMIS code, are available for validation purposes.

4.4.2.1 Description of the bridge and historical background

The Olla bridge (**Fig. 4.17**(a)) is an ancient masonry bridge that crosses the Stura river along the National Road S.S. 21, connecting the French border with the South-West part of Piedmont, throughout the Stura di Demonte Valley. The bridge, built in the 19th century, is approximately 117 m long and consists of five masonry arches, with the arch span being of about 10.0 m (end arches), 20.0 m (intermediate arches) and 25.0 m (central arch). The piers and the abutments are in a good-quality ashlar stone masonry while the arches and the spandrel walls are in brick masonry. As usual, the internal

spandrels and the backfill (i.e., the elements above the arches) are not visible from a direct inspection or geometry survey. Consequently, documentary research and on-site tests are needed to clarify the inner morphology of the structure. In 1857, the route between Cuneo and the French border was declared of national importance and a massive project of renovation and improvement was undertaken. Consequently, between 1865 and 1883 the connection with the French border was completed and starting from 1872 the existing roads was renewed, involving the construction of the Olla bridge.

a)  b) 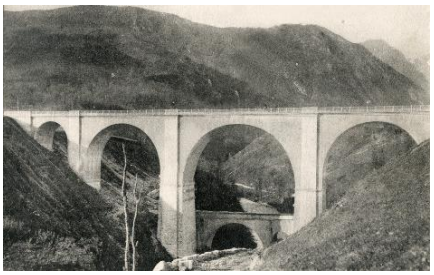

Fig. 4.17. a) View of the investigated masonry bridge from the Stura river; b) Picture of the Olla bridge at the beginning of the 20th century.

The design was assigned to the local chief engineer of the Royal Corp of Genio Civile (Italian public works office), Giovanni Delfino and the bridge was completed in 1887. Starting from 1912, a steam tramway route was created in the Stura valley to connect Cuneo and Borgo San Dalmazio to the small town of Demonte, in the upper part of the valley. The line was crossing the Stura river close to Gaiola, through the Olla bridge (**Fig. 4.17**). The tramway worked until the 2nd World War, when the central arch of the Olla bridge was destroyed by a bomb in July 1944; subsequently, even if the bridge was repaired, but the tramway was completely close in the 1948.

Furthermore, the identification of the construction details of Olla bridge has been particularly difficult, in particular the documentation in the archives of the Genio Civile did not lead to any results. Consequently, the focus of the documentary research moved from the investigated structure itself to the roadway to which the bridge belonged, from the proclamation of National Roads (19th century) to the evolution of the tramway, that for nearly 40 years used the bridge to cross the Stura river.

4.4.2.2 AVTs configuration and primary results using commercial software

As stated, the ancient masonry bridge was subjected to an intense dynamic tests campaign carried out on the 31st of June 2018 including: ambient vibration tests, firstly performed with the objective of identifying the modal parameters of the bridge; subsequently, load tests have been performed to check if the vertical displacements in the center line of each arch were limited to acceptable values.

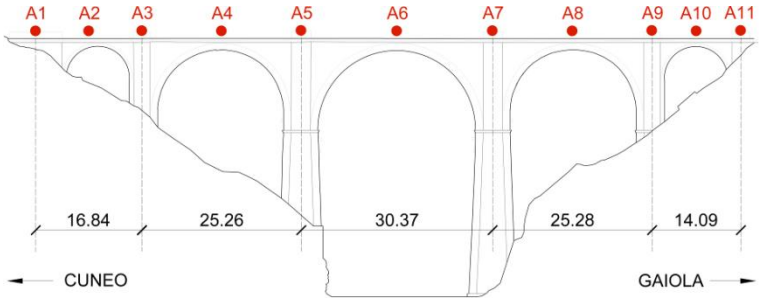

Fig. 4.18. Sensors layout in the dynamic test of 31 July 2018

The lateral responses of the bridge were measured at 11 selected points in a single set-up (**Fig. 4.18**). During the tests, only one lane was open to the traffic and the horizontal response was measured. According with the sensor layout shown in **Fig. 4.18**, 11 cross-sections were instrumented (in correspondence of the center of each arch, pier and abutment) by using 11 high-sensitivity transducers (Uniaxial WR 731A piezoelectric accelerometers, 10 V/g sensitivity and ±0.50 g measuring range) and a multi-channel acquisition system with 4 DAQ modules (NI 9234, 24-bit resolution, 102 dB dynamic range and anti-aliasing filters) to collected the horizontal response.

a) b)

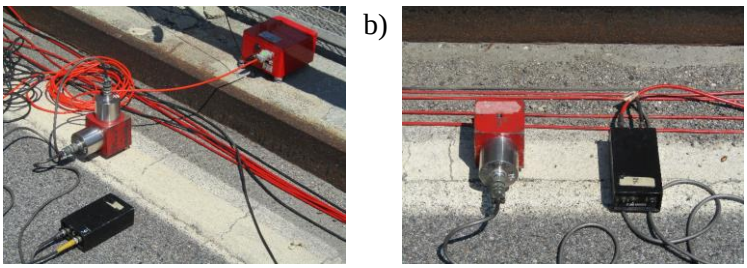

Fig. 4.19. Typical mounting of the accelerometers on site: a) biaxial accelerometer and seismometers, b) horizontal accelerometer.

The responses of the bridge to ambient and operational excitation were acquired using a sampling frequency of 200 Hz and 6 datasets of 2400 s. the sampling frequency is fairly larger than that required for the considered bridge, whose dominant natural frequencies are below 20 Hz. Hence, low pass filtering and decimation were applied to the data before using the identification tools: data were down sampled to 50 Hz, so to have a Nyquist frequency of 25 Hz. Firstly, the modal identification was carried out using the SSI-Data technique available in the commercial software ARTeMIS.

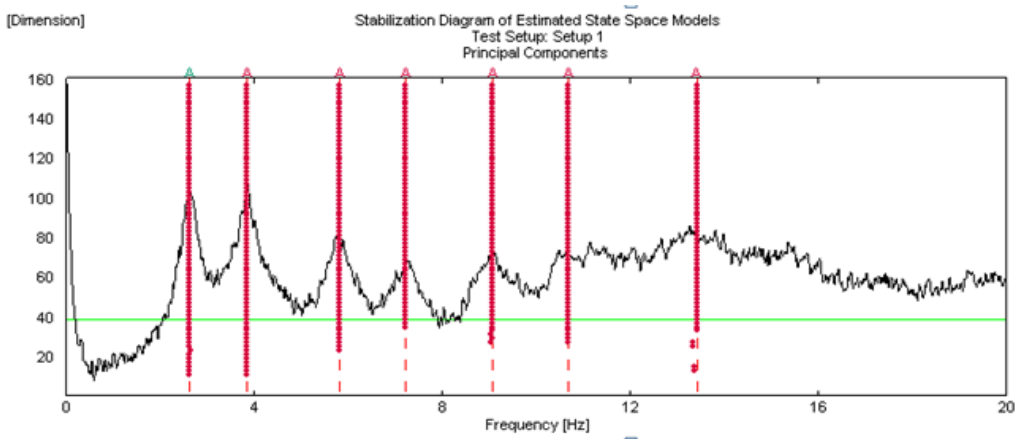

Fig. 4.20. Identification of the resonant frequencies adopting the SSI-Data technique

Fig. 4.20 shows the results of the data processing in terms of first singular value (SV) line obtained by using the non-parametric FDD technique as well as the stable alignments obtained for increasing model order applying the SSI-Data method. As previously stated, in order to investigate the dynamic characteristics of the bridge, several ambient vibration tests (AVTs) were performed on the 31st of July 2018. In this paragraph only the analysis carried out using on a single dataset (dataset D) are reported.

In the frequency range of 0-20 Hz, seven vibration modes have been clearly identified by stable alignments that stand out on the stabilization diagram (see **Fig. 4.20**). The identified (lateral) mode shapes associated to identified structural modes are shown in **Fig. 4.21**. In **Table 4.5** the natural frequencies and the modal damping ratios associated to the structural modes obtained by using the commercial software ARTeMIS are

reported. Moreover, the low value of the standard deviations related to both parameters proving in evidence the good quality of the estimates.

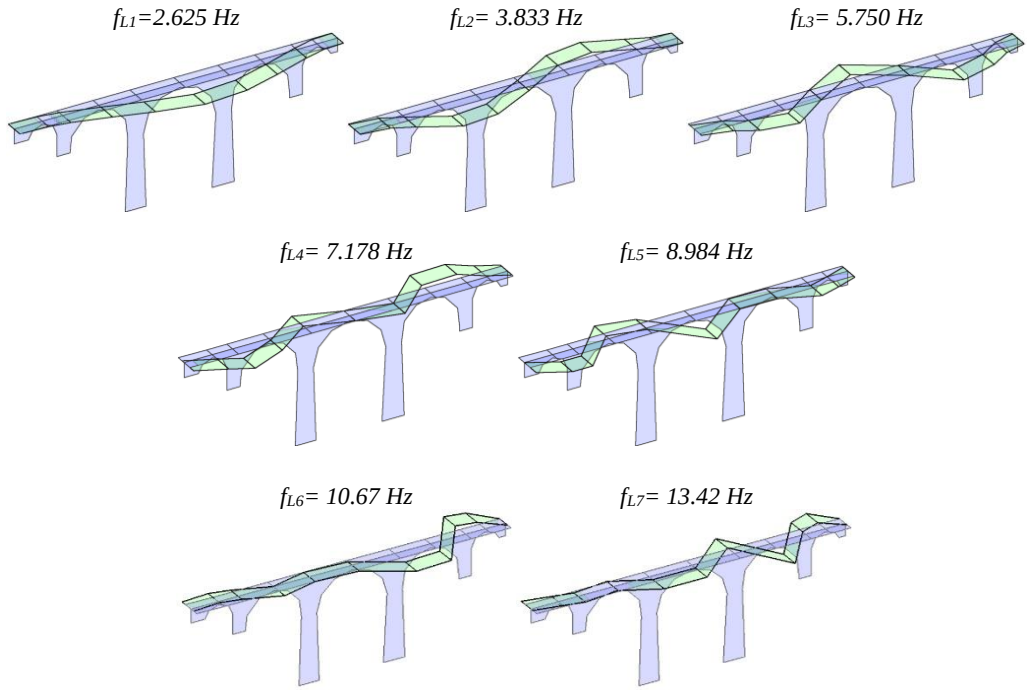

Fig. 4.21. Lateral vibration modes identified using the commercial software ARTeMIS.

Table 4.5. Natural frequencies and damping ratios identified using ARTeMIS software.

n°	***f*** **[Hz]**	**σ(*f*) [Hz]**	**ξ [%]**	**σ(ξ) [%]**
1	2.621	0.0022	1.958	0.1655
2	3.835	0.0018	1.814	0.0388
3	5.802	0.0018	2.728	0.1210
4	7.220	0.0020	3.065	0.0554
5	9.063	0.0049	3.157	0.0772
6	10.67	0.0019	3.514	0.0251
7	13.42	0.0014	3.923	0.0371

Finally, the datasets collected during the AVT were used to validate the MPE algorithm. In the next paragraph the initial tuning of the input parameters and the obtained results are described in detail. For clearness, the MPE algorithm was adopted to extract the estimation of the modal parameters of all 6 collected dataset. Due to the consistency of the results, only the outcomes referred to dataset D are reported.

4.4.2.3 Application of developed algorithm to dynamic tests data

The MPE algorithm was used to extract the modal parameter estimations performing an automatic interpretation of the stabilization diagram in which the SSI outputs are reported for increasing model order. Therefore, after an initial tuning of the input parameters of the SSI-Cov method (i.e., time lag value and interval of model order) the estimation of the modal parameters are obtained following the steps reported below.

After some trial tests, the time-lag value was fix equal to 80 and the model order interval equal to 20-120. Hence, the consecutive steps have been executed setting the threshold values as described in the following:

1. Pre-filtering. Removal of spurious poles applying three threshold criteria on modal damping ratio (i.e., damping limit equal to 5%) and on the complexity degree of the mode shapes (i.e., MPD and MPD equal to 0.7 and 15°, respectively).
2. Clustering. Automated interpretation of a clearer stabilization diagram using the maximum value of the inter-cluster distance equal to 0.02.
3. Post-processing. Removal of possible replications of the structural modes and extreme values (outliers) in order to deliver an accurate set of modal estimates.

It should be noting that the application of the post-processing does not provide significant and reasonable improvements on the estimation of the modal parameters for this case study. This is mainly due to the high quality of the collected data (with high signal/noise ratio value), to the high number of sensors (high redundancy of the response) and to the dynamic characteristics themselves (well-separated modes).

Fig. 4.22 shows the action exerted by each step of the d MPE algorithm on SSI outputs. In more details: (i) **Fig. 4.22(**a) shows all SSI outputs obtained for increasing model order, as well as on the frequency vs. damping; (ii) **Fig. 4.22**(b) shows the remaining poles after the removal of modes with negative damping and highly damped modes; (iii) **Fig. 4.22**(c) shows the action excreted by the complexity thresholds applied to the remain poles; (iv) **Fig. 4.22**(d) highlights the stable alignments obtained by applying the

clustering process; (v) the alignments resulting after the post-processing are reported in **Fig. 4.22**(e), associated to 7 vibration modes of the bridge

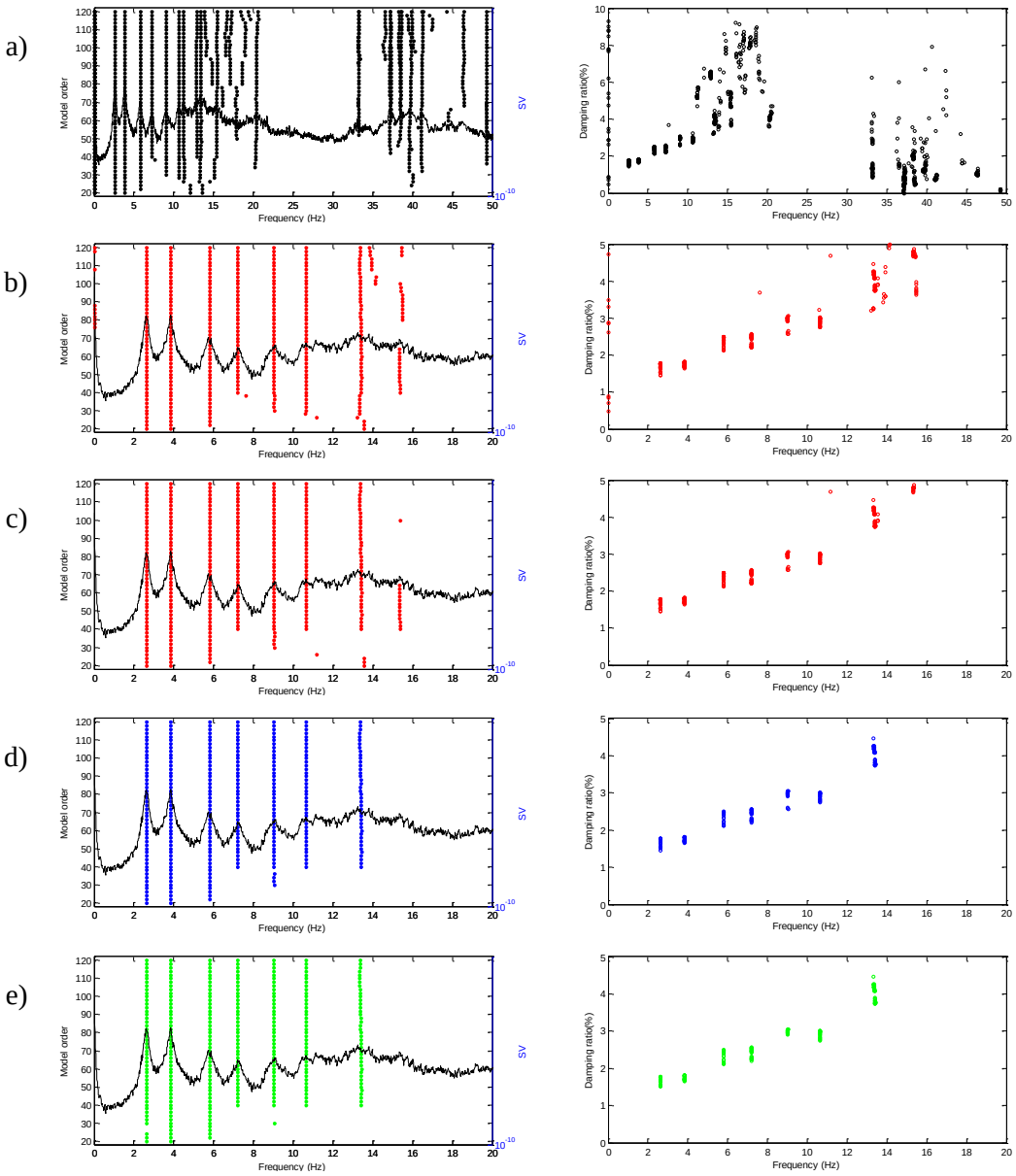

Fig. 4.22. Stabilization diagrams: a) SSI outputs for interval order equal to 20-120; b) poles after removal of high damped modes, c) poles after removal high complexity modes; d) stable alignments after clustering process; e) final clusters after post-processing

Moreover, as depicted in the diagrams, the first five modes can be easily detected also by the local maxima of the first SV line in the correspondence of well-defined spectral peaks. Meanwhile, the last 2 further modes can be identified only in terms of consistency of the modal parameters obtained for increasing model order, since the SV line does not have visible local maxima for higher frequency values. In addition, the last two modes are characterized by a quite high complexity. All dynamic characteristics related to the structural modes of the bridge are summarized in the **Table 4.6**.

In **Table 4.6** are reported the estimates of the natural frequency and the damping ratio together with the corresponding standard deviations associated to each extracted mode are reported. Moreover, in the last columns the MPC and the MPD values associated to each extracted mode shape are also highlighted.

Table 4.6. Comparison between the modal parameters identified by previous analysis carried out with commercial software and those ones automatically obtained by using the proposed procedure.

Modes	**Automated MPE algorith using the SSI-Cov**					
n°	***f*** **[Hz]**	**σ(*f*) [Hz]**	**ξ [Hz]**	**σ(ξ) [Hz]**	**MPC**	**MPD**
1	2.620	0.0002	1.71	0.0853	1.000	0.39
2	3.837	0.0005	1.75	0.0550	0.999	0.85
3	5.796	0.0010	2.41	0.1149	0.998	1.30
4	7.206	0.0056	2.47	0.1325	0.989	2.82
5	9.031	0.0035	2.97	0.0361	0.959	6.99
6	10.637	0.0025	2.94	0.0936	0.847	13.47
7	13.387	0.0034	4.07	0.2101	0.795	11.53

Finally, the configuration of the mode shapes associated to identified modes are shown in **Fig. 4.23**, in which the first three lateral modes of the bridge respect the attendance for this kind of structure. The fundamental mode consists of a symmetrical mode with a maximum lateral displacement of the cross section of the central arch. The second and the third mode are quite regular antisymmetric and symmetric mode, respectively.

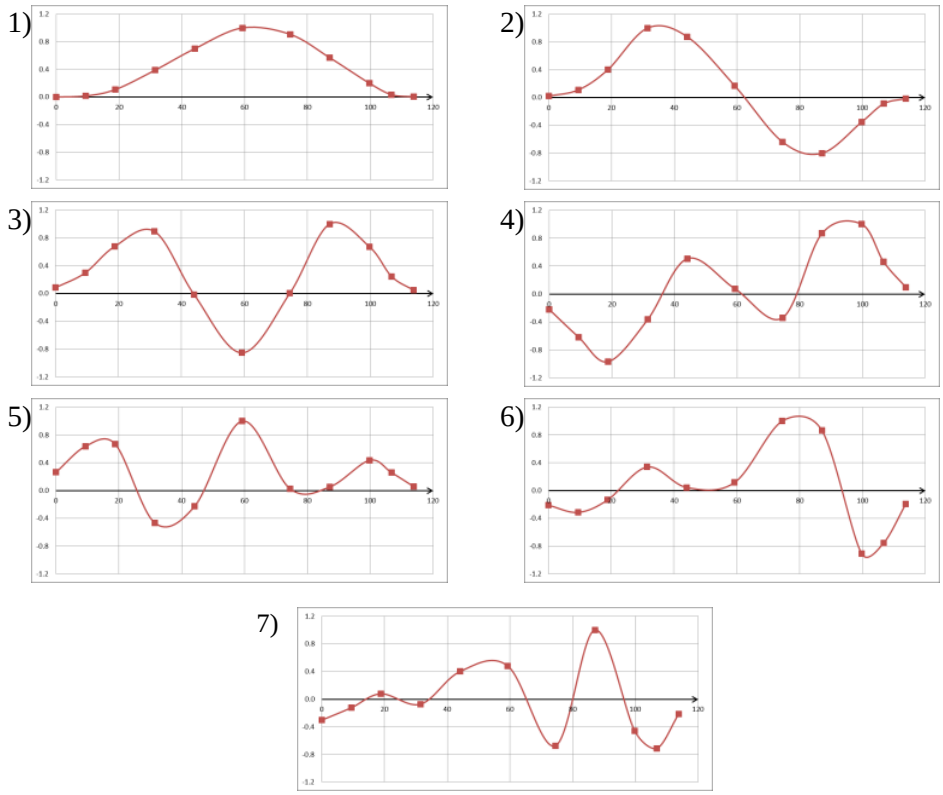

Fig. 4.23. Lateral modes of the bridge automatically identified by applying the MPE procedure

From the comparison of the results obtained by commercial software (**Table 4.5**) with those ones obtained by the application of the MPE algorithm (**Table 4.6**) a very good correspondence can be highlighted. Furthermore, the excellent match between the estimates of mode shapes provided by ARTeMIS (see **Fig. 4.21**) and those ones automatically identified (see **Fig. 4.23**) by proven the robustness of the implemented MPE algorithm

It should be noticed that: a) a good correspondence between the obtained results and those already published in literature [Borlenghi et al. (2019)] also provides a further validation of the algorithm presented in this Chapter, b) the standard deviation of the natural frequency estimates provided by MPE algorithm are lower than those provided by commercial software; c) further information can be obtained by the complexity indices

(i.e., MPC and MPD) regard the complexity degree of the identified modes, and d) the modes with higher frequency are characterized by a high complexity.

Concluding, from engineering standpoint, some remarks can be drawn:

- The natural frequency of the fundamental mode is 2.62 Hz and the corresponding mode associated involves symmetrical lateral bending of the deck with a bending of the central pylons and a maximum displacement of the central arch of the bridge.
- As expected, the first 7 deformation modes present quite regular shapes. In particular, the first four lateral modes are characterized by symmetrical and anti-symmetrical geometric shapes, typically for this kind of structure.
- The last two identified modes (over 10 Hz) have more irregular shapes with high complexity of the mode shape components.

4.5 Conclusions

An analysis algorithm capable of extracting modal parameters from single dataset collected during AVT or within a continuous dynamic monitoring purpose has been developed and presented in this Chapter.

The algorithm is devoted to analyze the collected data adopting SSI techniques (i.e., SSI-Data or SSI-Cov method, developed in time-domain) that involve the use of correlation functions among the time structural responses or the projection of the time series recorded during the dynamic test. The MPE algorithm is exploited only using the SSI-Cov method. It is worth noting that its performance is guaranteed also using other techniques involving the construction and the interpretation of stabilization diagrams.

The development of this algorithm is based on the consequently application of three key-steps, oriented to remove most of spurious poles before to perform the clustering process. This approach permits a more accurate and faster execution of the clustering process. Moreover, the post-processing step removes or limits the dependence of the modal

parameter estimations by the user-defined parameter (i.e., the inter-cluster distance threshold) used in the clustering process.

Each key-step of the MPE algorithm was deeply described in this Chapter in order to clearly provide the main improvements developed for the automation of the identification process. Consequently, the performance of the developed algorithm was demonstrated by extraction of the modal parameters from the artificially acceleration time series generated using a simple numerical system composed of five DOFs.

Subsequently, the algorithm was used to extract the modal features of two different case studies analyzing the output responses recorded during dynamic tests. The former was a lively footbridge located in the neighborhood of Milan characterized by a very complex behavior and by a high number of vibration modes. The latter was an ancient masonry bridge built in the norther of Italy (Piedmont) and composed of several archer subjected to the ageing effect of the environmental factors.

The analysis carried out on data collected on the footbridge have been compared with those ones previously obtained using the commercial software. The robustness of the procedure is also pointed in evidence by the estimation of ill-excited modes with higher complexity degree that they were not identified in the previously analysis [Lai et al. (2015)].

The MPE algorithm was also validated by the analysis of the structural responses collected during the AVTs carried out on The Olla bridge. The modal estimates obtained with the MPE algorithm were confirmed by those ones identified with the SSI parametric method available in ARTeMIS in which seven fundamental modes of the bridge have been detected by stable alignments that stand out on the stabilization diagram.

Despite the high number of sensors used to carried out the AVTs of the two case studies described in this Chapter, the implemented MPE procedure is capable to provide a reasonable set of modal estimates also in case of simple dynamic system composed of a reduced array of sensors. As reported in [Marrongelli et al. (2019a), Marrongelli and

Gentile (2019)] the present algorithm was used for the identification of the modal parameters of ancient towers in which the structural response is recorded by just a few accelerometers installed on the upper part of the constructions.

Concluding, the applications of the MPE algorithm presented in this Chapter demonstrate the good performance of the developed strategy based on three consecutive key-steps: on the pre-filtering, applied to remove certain spurious poles, on the clustering approach, applied to group poles belong to the same structural mode and on the post-processing, carried out to provide more accurate estimates with low uncertainty values.

Chapter 5

AUTOMATED MODAL IDENTIFICATION ALGORITHM USING TRI-DIMENSIONAL STABILIZATION DIAGRAMS

Contents

5.1 Introduction

As reported in previous Chapter, the development of efficient vibration-based Structural Health Monitoring (SHM) methodologies capable to timely detecting the onset of anomalies and possible damage in structures is still a challenging task, especially for large infrastructures, complex constructions and historic buildings.

SHM based on OMA approach always requires an initial phase to calibrate the input parameters to perform the analysis and extract a reasonable set of modal parameters. As already mentioned, many approaches have been proposed in literature for the automation of OMA process, but the development of tools that can automatically perform a fully automated identification is still a crucial step.

Within this context, this Chapter focuses on the development of a fully automated OMA procedure, which involves the construction and the automated interpretation of tri-dimensional stabilization diagrams, avoiding the initial tuning of the input parameters that characterize the SSI techniques. In particular, the present implementation is aimed at provide a further improvement in the automation of the identification process avoiding: a) the selection of the model order used to characterize the state-space model and b) the initial tuning and then the choice of the time-lag parameter or the row-blocks value used to define the Toeplitz matrix in the SSI-Cov or the Hankel matrix in the SSI-Data, respectively. As it will be demonstrated in this Chapter, this initial tuning is replaced by selecting an appropriate interval of the parameter avoiding any human interaction.

Therefore, a fully automated identification algorithm was developed for OMA-based SHM strategy that involves the use of tri-dimensional stabilization diagram. The developed algorithm is firstly exploited using a simple numerical structure and subsequently, its performance is tested adopting data collected by continuous dynamic monitoring system installed on two important infrastructures: the *Infante D. Henrique* bridge [Magalhães et al. (2008)], located in Portugal, and the *San Michele* bridge [Gentile and Saisi (2011), Gentile and Saisi (2015)], located in Italy. The good results obtained reveal the robustness of the proposed methodology.

5.2 Proposed algorithm of automated MPE

As previously pointed out OMA-based SHM requires the automation of OMA, thus the of efficient tools apt to avoid the human interaction and mimic the user's choice is still a challenge task [Reynders et al (2012)]. These reasons have led to the development of further complex approaches based on more sophisticated algorithms that partially solve such limitations, such as the parametric methods based on the fitting of a numerical models based on experimental data. As well known, the application of a parametric method requires the definition of initial input parameters that need to be tuned in the initial phase, to obtain a good performance of the algorithm and provide satisfactory results, as deeply described in [Magalhães (2010)].

Although the developed strategy described in this Chapter can be adopted with any identification technique that involves the construction of stabilization diagrams. Despite this, in this Chapter the performance of the proposed algorithm is exemplified focusing its application on the outputs provided by the application of the SSI-Cov method and on the construction of the correlation matrix. It is worth remarking that the algorithm proposed herein can be also coupled with the SSI-Data identification technique based on the construction of projection matrix.

As described in Chapter 2, the SSI-Cov method is a robust identification technique generally chosen because of its stability and convergence. The extraction of the modal features is performed using the collected output response signals through a sophisticated sequence of commands aimed at identifying the state matrix A, which contains all the dynamic properties of the system, and the output matrix C. These matrices are obtained through a series of operations that begin with the construction of the correlation matrix of the measured responses. Then, the resulting data is consecutively organized in a Toeplitz matrix, which it is decomposed by the Singular Value Decomposition (SVD) procedure, then the so-called observability matrix is extracted from such factorization. Adopting some properties concerning the stochastic linear systems and through the resolution of a least-square equation (using the Moore-Penrose pseudo-inverse procedure) the

observability matrix is used to define the matrices A and C [Van Overschee and De Moor (1996)] associated to a state-space model and then to extract the modal parameters.

But it is worth mentioning that the selection of the state-space model requires *a-priori* definition of the time-lag value and the order of the stochastic model used to characterize the dynamics of the structure under analysis. In case of real structure, it is not possible to fix *a-priori* these parameters; thus, an initial "tuning" becomes mandatory to find the best pair of them that characterize the dynamic behavior of the investigated system.

Initially, as described in Chapter 2, the extraction of the modal parameters was performed identifying a stochastic model that best fit the behavior of the system. In common practice, the model is defined exploring a wide interval of both input parameters (i.e. model order of the stochastic model and time-lag parameter of the covariance function), choosing that pair which provides better solutions and reasonable modal estimates. This task is executed manually, requiring a strong interaction of an expert user during the analysis of the data.

Nowadays, in the context of automatic processing, the most appropriate way to partially overcome the strong user interaction during the analysis of the collect signals is to perform some essential tests selecting different time-lag values and overestimating the model order (as described in Chapter 4). Thus, the modal estimates are extracted by those stable alignments that stand up on the stabilization diagram at the end of the analysis process.

Furthermore, in the context of continuous dynamic monitoring process, once the input parameters (i.e. time-lag and min/max model order) have been selected, they are normally used in conservative way for the entire monitoring process. This strategy is based on the fact that the dynamic behavior of the investigated structure does not change over time. This hypothesis is not always confirmed because there is no certainty that a selected time-lag parameter provides the most accurate solution during the whole monitoring process.

This aspect is very important to ensure a correct identification of the dynamic features over time [Zabel et al. (2016)]. For this reason, to provide a solution to this uncertainty, in the present proposed methodology the modal features are obtained exploring a wide interval of both input parameters characterizing the results with a high redundancy of the SSI outputs and involving the construction of tri-dimensional stabilization diagrams.

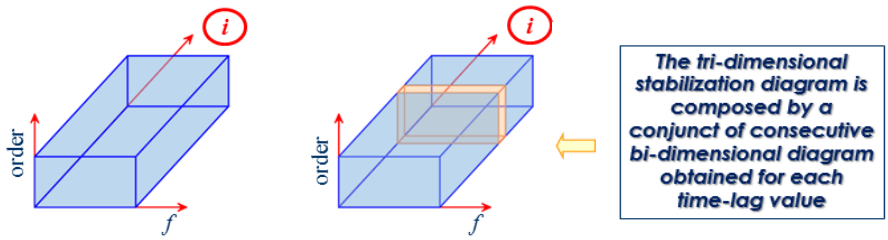

Fig. 5.1. Construction of tri-dimensional stabilization diagram

The main objective of the procedure described herein is to perform an automated estimation of the modal parameters, avoiding the initial tuning of the input parameters of the parametric method. To reach this task, increasing time-lag value and increasing model order were chosen in a conservative way to construct a tri-dimensional stabilization diagram as depicted in the **Fig. 5.1**. Hence, the automated procedure, composed by four different steps aimed at mimicking the choice of an expert user during the identification process, has been developed as follows:

1. Application of SSI-Cov method (or other parametric method with similar outputs) for increasing values of the input parameters selecting a wide range of the model order and time-lag value (or number of block-row data in case of SSI-Data method) and construction of the 3D stabilization diagram.
2. Removal of spurious poles applying three single mode validation criteria at the obtained poles based on modal damping ratio value and on the complexity degree of the mode shapes estimate associated to each pole.
3. Interpretation of the clearer 3D stabilization diagram through an innovative clustering procedure generalized to complex modes.
4. Removal of possible replications of the structural modes and extreme values in order to deliver a more accurate set of modal estimates.

Once the SSI method is performed for increasing time-lags and increasing model orders, and the outputs have been reported on a tri-dimensional stabilization diagram, the consecutive step consists of a series of checks aimed at detecting and removing spurious that do not have physical meaning (typically noise modes). The procedure used to extract the modal parameters of the tri-dimensional diagram is conceptually very similar to the MPE already described in Chapter 4. In fact, a sequence of consecutive checks is conceivability applied in order to perform a primary classification between spurious and physical poles using a pre-selected damping ratio threshold. So, estimates exhibiting negative damping and highly damped modes (i.e. modes with damping ratio larger than 10%) are conceivably associated to the noise content and removed.

Further single-mode validation criteria were adopted to detect noise modes using the MPC and the MPD index. Both indices are based on the quantification of the complexity degree of the mode shapes. As known, when the structural system is proportionally damped, the mode shapes are real and the components lie on a straight line in the complex plane, this means that the covariance between the imaginary and real part of each component can be used as a measure of the complexity degree, through the MPC index; in addition, the distance between the best straight line associated to the mean component of mode shape and every single (weighted) component can also be used as single-criterion check, with the MPD index, as shown in [Reynders et al. (2012)].

Once most of spurious poles are removed from the diagram, the third step of the proposed algorithm is the clustering procedure. This procedure is inspired by the contribution firstly proposed by [Magalhães et al. (2009)] and modified in the recent work by [Cabboi at al. (2017)], but in the present implementation the clustering procedure presents a further improvement that solves some issues related to complex components associated to obtained mode estimates.

A similar strategy was implemented to extract the modal parameters from a multi-setup ambient vibration test carried out on a non-reinforced arch bridge located in the north of Portugal obtaining satisfactory results [Marrongelli et al. (2017)].

5.2.1 MAC vs. MACX

In order to generalize the clustering procedure to all possible cases and to extend the approach to modes with relevant complex components, the limitation related to the MAC index was removed adopting the MACX criterion described in [Vacher et al. (2010)].

It is worth remarking the basic assumptions regarding the dynamic properties of linear systems; in fact, if the conditions of linear and time invariant systems are verified (as described in Chapter 2), the mechanical models used to represent the dynamic behavior of an investigate structure are based on the fundamental equations of the dynamic in which the system is expressed by **Eq. 2.1**. If the matrices M, K and D are positive definite and symmetric and they are diagonalizable in the same basis, the eigenvectors of the system in **Eq. 2.1** are identical to those ones of the associated undamped system (D=0). In addition, if the damping matrix D are composed by relatively small components, then the poles of the system λ_k are complex and stable.

Under this assumption, each pair of conjugated poles (λ_k and $\bar{\lambda}_k$) share the common eigenvector ψ_k and this vector is *real-valued.* This means that the eigenvector is a complex vector, so ψ_k coincides with its conjugated form $\bar{\psi}_k$. The associated mode is defined by the pair of poles (λ_k and $\bar{\lambda}_k$) and the mode ψ_k is defined to be *real*.

On the contrary, when the above hypothesis is not complied with, each mode is complex. Hence, each mode of the system is characterized by a pair of conjugated poles (λ_k and $\bar{\lambda}_k$) and the relative pair of conjugated eigenvectors (ψ_k and $\bar{\psi}_k$) [Vacher et al. (2010)]. So, which one of the two vectors should be considered to compute the MAC index? The Modal Assurance Criterion (MAC) is a measure of the degree of linearity between two vectors. Thus, defining the vectors μ_1 and μ_2, the MAC can be defined as:

$$\mathrm{MACX}(\mu_1;\mu_2) = \left(\frac{|\mu_1^* \cdot \mu_2|}{\|\mu_1\|\,\|\mu_2\|}\right)^2 = \cos^2(\mu_1;\mu_2) \tag{5.1}$$

in which $(\cdot)^*$ means *conjugate-transpose* of a complex vector. So, the product $\mu_1^* \cdot \mu_2$ is called *Hermitian inner product* between two vectors.

This definition can be interpreted geometrically since the MAC index depends on the angle between two vectors. Although this criterion can be applied to both real-valued and complex-valued vectors because it is insensitive to the modulus and the phase of the vectors, it is sensitive to the phase scatter between vector components. In other word, the MAC index is a well-suited to the analysis of mono-phase vectors but, on the contrary, it is sensitive to the conjugate operations of complex vectors with scattered phases.

The solutions of a dynamic system (**Eq. 2.1**) described through a stochastic state-space model (**Eq. 2.72**) are defined by taking into account the sign of the imaginary part of the poles λ_1 and λ_2. Hence, the MAC index is calculated selecting the two vectors which are associated with the poles λ_1 and λ_2 with *imaginary parts of the same sign.*

As described in [Vacher et al. (2010)], a complex eigenvector is computed up to a multiplicative complex factor. In this way the phase of an eigenvector or (in the same way) of a mode shape is given up an angle β. Considering to perform the normalization of the mode shapes of this arbitrary phase by searching the value of $\tilde{\beta}$ instead β, making the complex vector "*as real as possible*". Remarking, the angle $\tilde{\beta}$ is not the phase corresponding to the component of the mode shape with larger real part.

Defining $\hat{\beta}_1$ and $\hat{\beta}_2$ as the angles that solve the optimization problem reported below:

$$\left(\hat{\beta}_1;\hat{\beta}_2\right) = \arg\max_{\beta_1,\beta_2}\left|\mathrm{v}_1^{\mathrm{T}}(\beta_1)\cdot \mathrm{v}_2(\beta_2)\right| \tag{5.2}$$

In which $v_1(\beta_1)$=Re($\mu_1 \cdot e^{-i\beta_1}$) and $v_2(\beta_2)$=Re($\mu_2 \cdot e^{-i\beta_2}$). From this expression, it is possible to derive the first expression of the MACX criterion, that is valid for any type of vectors (i.e., complex vectors):

$$\mathrm{MACX}(\mu_1;\mu_2) = \left(\frac{\left|\hat{\mu}_{\mathrm{r}1}^{\mathrm{T}}\cdot\hat{\mu}_{\mathrm{r}2}\right|}{\|\hat{\mu}_{\mathrm{r}1}\|\,\|\hat{\mu}_{\mathrm{r}2}\|}\cdot\frac{\|\hat{\mu}_{\mathrm{r}1}\|}{\|\tilde{\mu}_{\mathrm{r}1}\|}\cdot\frac{\|\hat{\mu}_{\mathrm{r}2}\|}{\|\tilde{\mu}_{\mathrm{r}2}\|}\right)^2 \tag{5.3}$$

In which the value of the vectors $\hat{\mu}_{r1}$ and $\hat{\mu}_{r2}$ are described in [Vacher et al. (2010)]. From the Eq. 5.3, it is possible derive a simpler expression that can be directly computed from the original vectors μ_1 and μ_2 considered for the MAC index, as follows:

$$\mathrm{MACX}(\mu_1;\mu_2)=\frac{\left(\left|\mu_1^{\mathrm{H}}\cdot\mu_2\right|+\left|\mu_1^{\mathrm{T}}\cdot\mu_2\right|\right)^2}{\left(\mu_1^{\mathrm{H}}\cdot\mu_1+\left|\mu_1^{\mathrm{H}}\cdot\mu_1\right|\right)\left(\mu_2^{\mathrm{H}}\cdot\mu_2+\left|\mu_2^{\mathrm{H}}\cdot\mu_2\right|\right)} \tag{5.4}$$

It is worth remarking that this formulation is quite similar to the classical MAC since it is only needed to perform the following substitution in the expression of the MAC index:

$$\left|\mu_1^{\mathrm{H}}\cdot\mu_2\right|=\frac{1}{2}\left(\left|\mu_1^{\mathrm{H}}\cdot\mu_2\right|+\left|\mu_1^{\mathrm{T}}\cdot\mu_2\right|\right) \tag{5.5}$$

Furthermore, by the results provided in [Vacher et al. (2010)], it can be notice that the MACX criterion generally gives greater values than MAC criterion, in fact from the comparison of the analysis carried out on aeroelastic models, the correlation expressed by the application of the MACX is much more effective of the MAC index.

Taking into account the information reported in the well-known paper [Vacher et al. (2010)] as well as the criticism about the use of MAC index described in [Allemang (2003)] this approach was adopted for the implementation of a new clustering algorithm. The new clustering algorithm has been developed in order to take into account the possible issues related to the complex components of the mode shapes associated to the poles in the stabilization diagram but also of the complexity values of the mode shapes associated to the reference modes used in the clustering process itself.

For clearness, the MACX criterion is used in the matric of the new clustering approach accordingly to the previously normalization and the roto-translation of the mode shapes components used in the Hermitian product. Moreover, the use of the MACX criterion in the clustering process should deserve a deep investigation regarding the use of the reference mode and its generation obtained by a mere averaging process of the mode shapes into the cluster even if the mode shapes are not exactly mono-phase. In practical situation, the mode shapes of a physical system are not exactly mono-phase vectors even if the above hypothesis about structural modelling are supposed fulfilled.

This analysis is very important because the MAC criterion is not quite appropriate to process complex vectors. The extension of the MAC index (i.e., MACX index) is

constructed from a physical interpretation of the modal contribution derived by several measurements of a dynamic system

Using this metric, the clustering process has been developed with the objective of grouping all poles that share same characteristics in terms of modal parameters (i.e., natural frequency and mode shape) also in case of high complexity of the mode shapes components. The new metric implemented in the clustering approach is defined as:

$$\mathrm{d_{i,ref}} = \frac{|\mathrm{f_{i,ref}} - \mathrm{f_{i,j}}|}{\mathrm{f_{i,ref}}} + 1 - \mathrm{MACX}\left(\varphi_{\mathrm{i,ref}}; \varphi_{\mathrm{i,j}}\right) \tag{5.6}$$

where $d_{i,ref}$ represents the inter-cluster distance, obtained by the distance between each candidate pole and the reference pole of the cluster, $f_{i,ref}$ and $\phi_{i,ref}$ represent the mean frequency and mean mode shape of the reference pole updated for increasing model order, whereas $f_{i,j}$ and $\phi_{i,j}$ are the same modal parameters corresponding to *j-th* "current pole". The procedure is repeated in order to scan all available poles and it is stopped only when all poles are grouped into the clusters. As demonstrated in several works present in literature [Magalhães et al. (2009), Reynders et al. (2012), Ubertini et al. (2013)] the noise modes do not have consistency in terms of modal parameters and they are spread inside many small clusters, then all those clusters with dimensions less of one third of the tallest cluster are considered as numerical modes and then deleted. In current application, this condition could be really restricted, therefore in a conservative perspective this value has been halved, reducing this limit to *n/6*, where *n* is the number of elements belongs to the biggest cluster.

The last step of the proposed methodology is aimed at improving the accuracy of the final modes estimations and it is already extensively described in the previous paragraph. Remembering, the first check consists of an agglomerative clustering approach based on an application of a *k-mean* cluster algorithm in which the centroids of the clusters are known, and they have been already defined by the mean frequencies and mean mode shapes provided by the previous cluster procedure. This operation is performed in order to recovering any possible estimates lost during the initial association phase and

removing others that fall inside the defined threshold due to continuous updating of the reference cluster pole. The second check is aimed at removing any possible replication of the physical modes in the stabilization diagram. This check tends to avoid this possibility recognizing possible replication and deleting that one with higher complexity component. In the last the main improvement of this sub-procedure. This check is aimed at reducing the scatter that could affect the estimates. The removal of the outliers is performed by applying simple rules based on the so-called *box-plot* tool, as reported in a practical application described in [Marrongelli et al. (2017)]. In case of 3D diagram this check was carried out on both distributions of natural frequencies and damping ratios, separately.

Finally, the delivered outputs obtained by the application of developed methodology are: the mean natural frequency, the mean mode shape and the median modal damping ratio belonging to each detected cluster and their statistical properties provided by the standard deviation of the distributions associated to the aforementioned estimates. Besides this, the developed OMA procedure provides also the main complexity values (in term of MPC and MPD values) associated to the resulting modes. It is worth mentioning that these two indices are not obtained by a simple calculation from the resulting mode shapes (that should deserve some issues in the definition of the mean mode shapes) but they are defined by the distribution of the values associated to each estimate (i.e., pole) inside the final representative clusters.

5.2.2 Application of the algorithm on a simple numerical structure

The proposed algorithm was validated checking the modes of vibrating of a simple numerical structure composed by 5 DOFs (all the geometrical and mechanical characteristics of the structure are described in Chapter 4, **Fig. 4.6**). Several 30 min long datasets of acceleration time series were simulated to test the proposed identification algorithm. Each dataset is composed by five acceleration series related to each floor of the numerical structure. The extraction of the modal estimates was performed applying the SSI-Cov technique to the time series collected setting the frequency sample at 50 Hz.

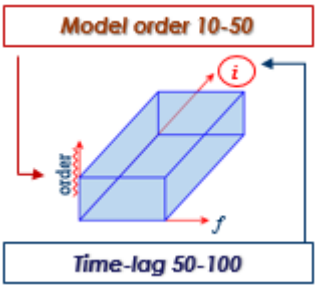

Fig. 5.2. Input parameters used for the modal identification of the numerical structure

For the testing, the interval of the time-lag parameter was defined from 50 to 100, meanwhile the model's order was set in a conservative way between 10 and 50 (**Fig. 5.2**).

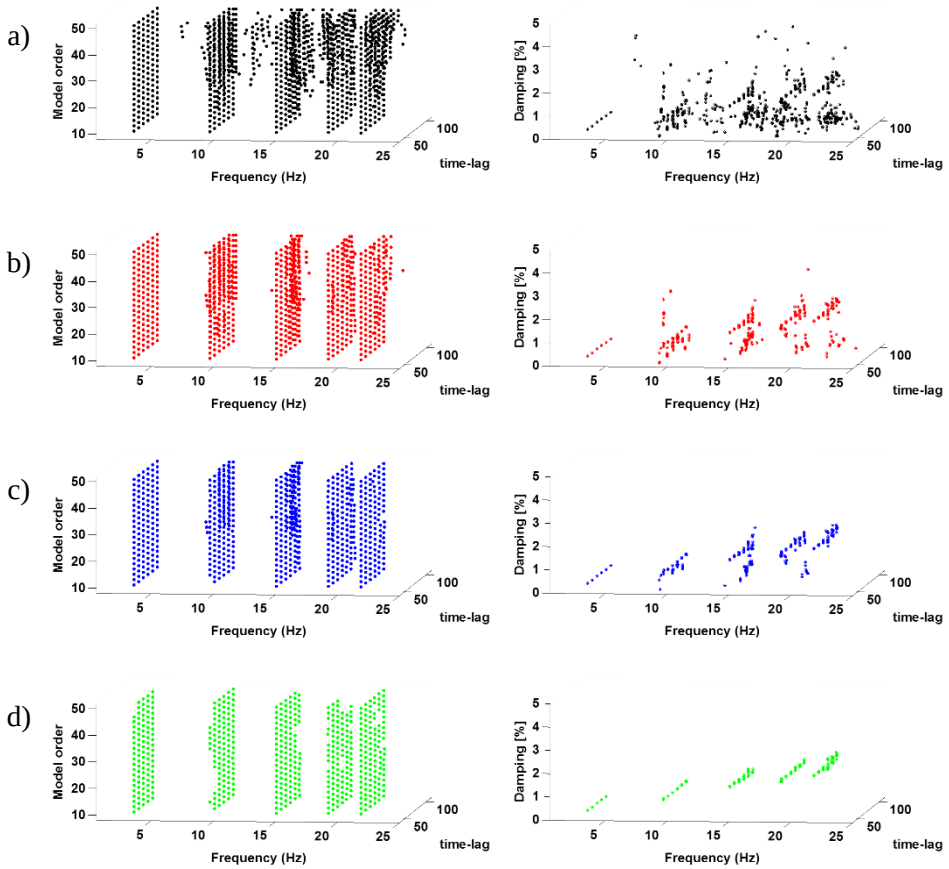

Fig. 5.3. Tri-dimensional stabilization diagram: (a) SSI-Cov outputs; (b) after pre-filtering check; (c) after clustering; (d) after post-processing check.

Fig. 5.3 shows the consecutive 3D stabilization diagrams and the corresponding frequency vs damping diagrams obtained after the cleaning action exerted by the main *key-steps* of the proposed 3D-MPE algorithm. In details: **Fig. 5.3**(a) shows all output poles obtained by SSI-Cov method, **Fig. 5.3**(b) shows the remain poles after the checks on modal damping ratio and on the complexity of the mode shape, **Fig. 5.3**(c) highlights the performance of the clustering process and finally **Fig. 5.3**(d) contains the stable planes composed by only stable poles after the application of the post-processing tool.

The good accuracy of the proposed identification algorithm is confirmed by the results of both sets of estimates (i.e., natural frequency and modal damping ratio) with a general improvement of the standard deviations associated to both estimates. Furthermore, the two complex indices confirm that all identified modes are real, as expected.

Table 5.1. Modal parameters, standard deviations and complexity indices obtained

Modes	f **[Hz]**	$\sigma(f)$ **[Hz]**	ξ **[%]**	$\sigma(\xi)$ **[%]**	**MPC**	**MPD**
1	3.197	0.00003	0.280	0.0002	1.000	0.12
2	9.329	0.00095	0.781	0.0037	0.999	0.23
3	14.705	0.00371	1.325	0.0125	0.992	0.45
4	18.892	0.00216	1.653	0.0239	0.997	0.26
5	21.553	0.00513	1.721	0.0298	0.998	0.71

The developed 3D-MPE algorithm has been used to extract the modal parameters of two important infrastructures in Europe: the *Infante D. Henrique* bridge located in Porto and the *San Michele* bridge located in the neighborhood of Milan. Therefore, the implemented algorithm has been also used to perform the continuous monitoring of two infrastructures obtaining good quality and lower uncertainty of the results [Marrongelli et al. (2018c)].

5.3 Application to data collected on *Infante D. Henrique bridge*

The first real structure herein considered to demonstrate the robust performance of the developed methodology is the Infante D. Henrique Bridge. It crosses the Duoro River and connects the city of Porto to Gaia.

5.3.1 Description of the bridge

The Infante D. Henrique bridge [Magalhães et al. (2008), [Magalhães (2010)] is composed of two mutually interacting fundamental elements: a very rigid pre-stressed concrete box beam supported by a reinforced concrete arch with a span of 280m that rises 25m from abutments and crown. After its construction, a dynamic monitoring system was installed in the bridge. This is essentially composed by 12 force balance accelerometers and 2 digitizers. Due to its symmetry, the mode shapes are approximately symmetric, therefore it was decided to instrument just one-half of the bridge. So, the accelerometers were distributed along four sections between mid-span and the abutment at Porto bank with three sensors for each section: one to measure the lateral acceleration and other for vertical acceleration at downstream and upstream sides.

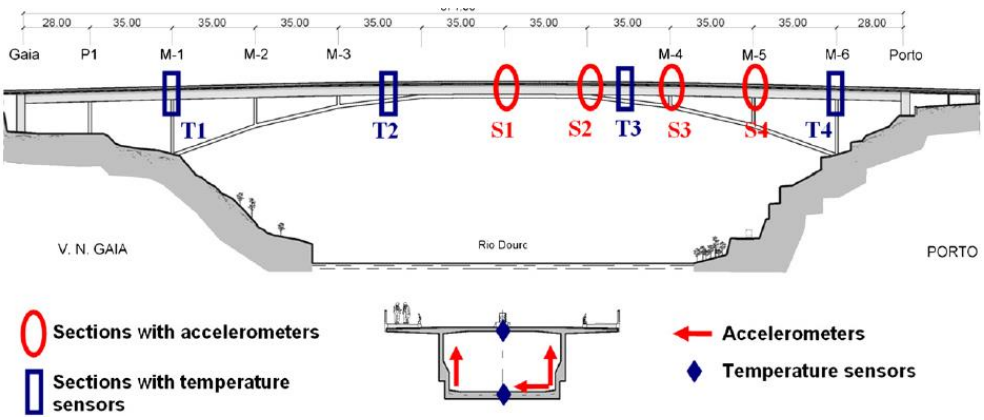

Fig. 5.4. Scheme of the monitoring system and the temperature sensors installed on the Infante Dom Henrique bridge [Magalhães et al. (2008)]

5.3.2 Application of the automated procedure to a single collected dataset

The developed 3D-MPE procedure has been used to perform the automatic identification of the modal parameters adopting a wide range of time-lag value to fit the operational responses of the bridge. In the current application the minimum value of time-lag was set equal to 10, with an increasing step of 10 units until reach the maximum value of 100. Meanwhile the model order interval was set in conservative way between 20 and 100, as reported in the previous works [Magalhães et al. (2008), Magalhães (2010)].

As mentioned before, the methodology is based on the construction and on the automatic interpretation of a 3D stabilization diagram composed by all outputs obtained by each run of the parametric method. This means that SSI-Cov method was performed for increasing model order and time-lag, providing a huge quantity of estimates composed by physical and spurious poles that need to be separated (see **Fig. 5.5**(a)). Thus, when the first step of the developed procedure is achieved, the removal of spurious poles was performed adopting three selected criteria based on application of three different thresholds. Such values were not very restrictive because the bridge may have complex modes, but they were fixed ensuring the elimination of noise modes with very high complexity and damping: 5% for damping, and 0.75 and 20° for MPC and MPD respectively. As already stated in several works, the clustering procedure could also be performed by avoiding the removal of spurious poles, because the consistency of noise modes dramatically changes for different model orders and they should not affect the correct classification. This second option is strongly discouraged in the present application, because the non-elimination of spurious poles from the diagram and the consequently classification into shorter clusters make the clustering process very time-consuming without proving any improvements at the resulting estimates. Therefore, the removal of certain spurious poles is always recommended. In **Fig. 5.5**(b) the effect of the pre-filtering on the spurious poles in the analysis of a recorded dataset of Infante D. Henrique bridge is shown.

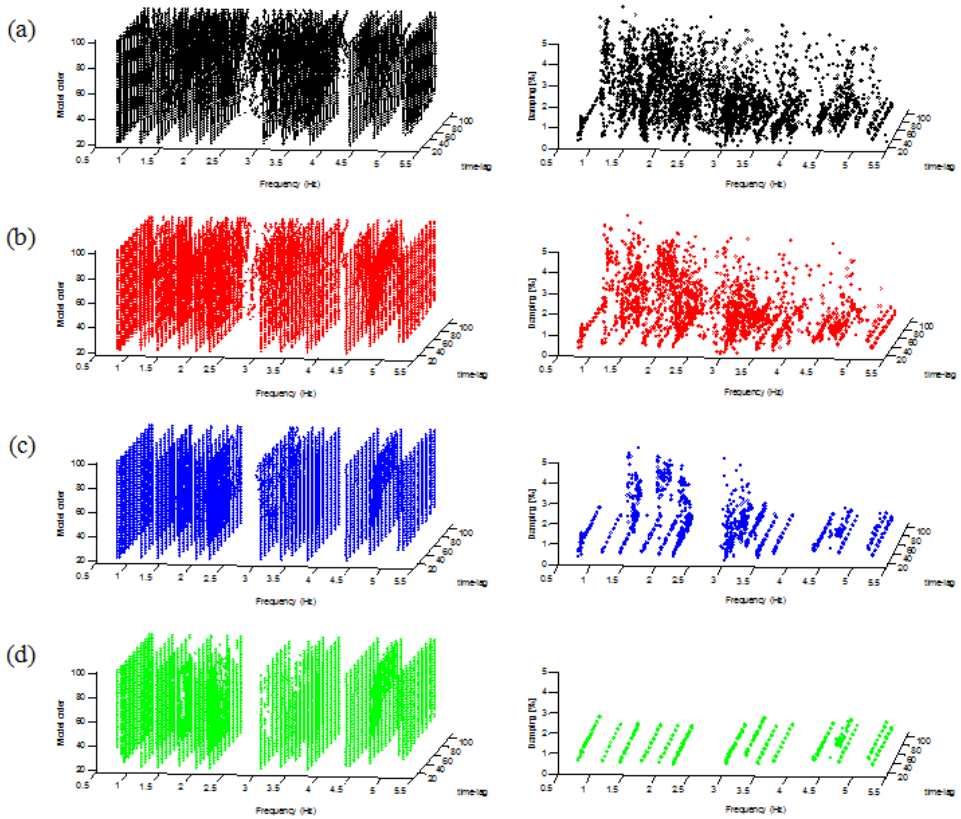

Fig. 5.5. Stabilization diagram: (a) obtained SSI-Cov outputs; (b) after checking on damping and modal complexity; (c) after clustering process; (d) after post processing check.

Subsequently, the clustering procedure proposed herein consists of the application of the formula described in **Eq. 5.6** to all remaining poles belong to the diagram. Its application is based on the similarity between possible candidate mode and the reference one (which is constantly updated when one estimates is linked into the cluster). The success of the clustering procedure is mostly depended on a selection of a distance threshold value that allows for the correct grouping of poles that share the same characteristics in terms of modal parameters. This threshold was set equal to 0.03. Hence, the distance between the reference pole (defined in terms of mean frequency and mean mode shape of all poles grouped into the cluster) and candidate pole have to be shorter than such prefixed distance.

The metric in **Eq. 5.6** is used to scan all available poles until all estimates have been grouped. Moreover, in this procedure the single-linkage is used, this ensures that only one estimate can be introduced into the cluster for every model order and every time-lag value. In other words, two different estimates obtained with the same model order cannot be included in the same cluster. An application of the developed clustering algorithm is shown in **Fig. 5.5**(c). To conclude the validation, the final "stable planes" obtained after the application of the post-processing sub-procedure are shown in **Fig. 5.5**(d).

It is worth mentioning that extending of the investigated frequency interval to 5.5 Hz, with regard to previously published results, four further modes of the bridge with a more complex behavior have been identified. To compete the first test of the developed procedure using real data, the automatically identified modal parameters of the bridge (in term of natural frequencies, modal damping ratio and standard deviations of these estimates) together with the complexity indices associated to the identified modes, are summarized in **Table 5.2**. Meanwhile, the mode shapes associated to the structural modes are shown in **Fig. 5.6** and **Fig. 5.7**.

Table 5.2. Modal parameters: natural frequency, modal damping ratio, standard deviations and complexity indices of the structural modes obtained applying the 3D-MPE to a single dataset.

n°	Mode	f [Hz]	$\sigma(f)$ [Hz]	ξ [%]	$\sigma(\xi)$ [%]	MPC	MPD
1	L1	0.777	0.0001	0.47	0.0007	0.994	2.75
2	V1	0.823	0.0004	0.87	0.0079	1.000	0.72
3	V2	1.145	0.0001	0.48	0.0056	1.000	0.56
4	V3	1.414	0.0003	0.42	0.0134	1.000	0.42
5	L2	1.751	0.0001	0.44	0.0103	0.989	3.64
6	V4	2.013	0.0003	0.42	0.0164	1.000	0.37
7	T1	2.228	0.0015	0.42	0.0229	1.000	0.45
8	V5	3.035	0.0024	0.51	0.0571	1.000	0.51
9	T2	3.340	0.0016	0.86	0.0145	0.997	1.60
10	V6	3.519	0.0002	0.44	0.0115	0.996	2.36
11	T3	3.766	0.0005	0.53	0.0088	0.990	2.36
12	V7	4.379	0.0029	0.65	0.0626	0.999	1.57
13	V8	4.659	0.0061	0.70	0.1737	0.857	15.99
14	T4	4.752	0.0004	0.53	0.0042	0.992	2.15
15	T5	5.207	0.0002	0.72	0.0034	0.975	4.01
16	V9	5.273	0.0002	0.39	0.0025	0.999	0.94

From the main results reported tin the **Table 5.2** it should be noticed that: a) an excellent correspondence between the obtained results and those already published in literature, in terms of natural frequency and also modal damping ratio is shown, b) the standard deviation of the natural frequency estimates and also of the damping ratios are lower than those obtained with other OMA techniques, c) extending the investigated frequency range to 5.5 Hz, the proposed automatic algorithm detects four further modes not identified in the previous works. The mode shapes associated to the 16 identified mode are reported in **Fig. 5.6** and **Fig. 5.7**, using different colors to highlight the lateral and the vertical components; in particular with the green color is reported the component on the lateral mode of the bridge. Alternatively, with red and blue colors are reported the components in the vertical direction associated to the upstream and downstream side of the bridge, respectively.

It is should remarked that the dynamic system installed on the Infante D. Henrique bridge is composed by 12 accelerometers disposed in 4 instrumented cross-sections of the structure in order to measure the vibrations corresponding to an half part of the bridge (specifically the side toward indirection of the city of Porto). Therefore, the identified mode shapes depicted in both **Fig. 5.6** and **Fig. 5.7** are referred to half part of the bridge.

It is worth noting that different colors have been used to describe the different behavior of the identified mode shapes. Hence, the components of the lateral modes were depicted with green line; meanwhile, for vertical components were used the red line for the upstream side and the blue line for the downstream line of the bridge, respectively. In this way, the diagram reported in **Fig. 5.6**(1), describes the mode shape of the first symmetrical fundamental lateral mode of the bridge, pointed out by the zero-values of the vertical components (red and blue lines). Meanwhile, the diagram in **Fig. 5.6**(2), the shows the first fundamental anti-symmetrical bending mode of the bridge, demonstrated by the fact that the lateral components are zero (green line) and the vertical components of the sensors located in both sides of the bridge (red and blue line) move in-phase.

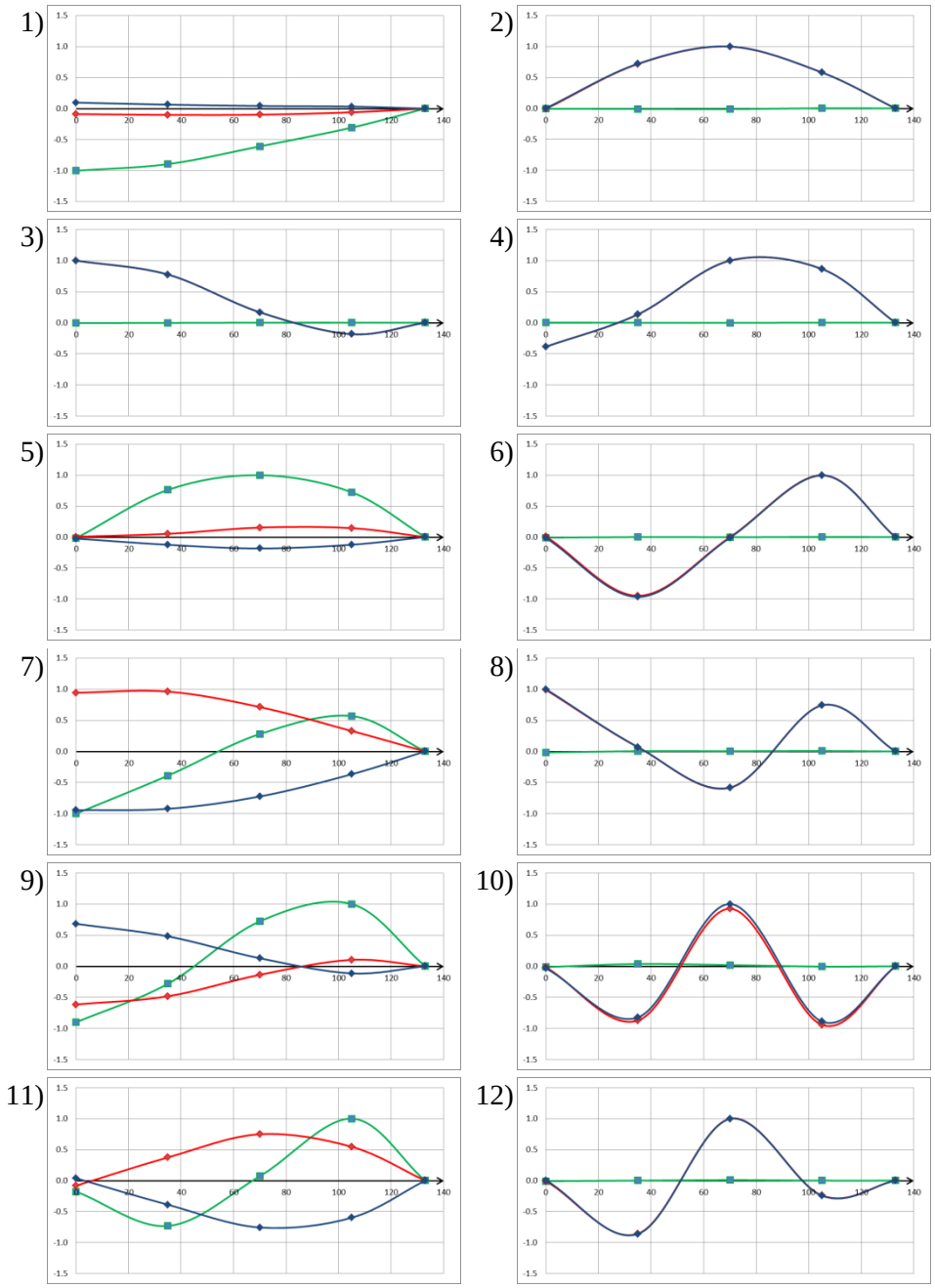

Fig. 5.6. First 12 vibration modes automatically identified by the proposed methodology (green line, blue line and red line are referred to lateral, vertical upstream and vertical downstream components, respectively). See **Fig. 5.4** for location of the sensors.

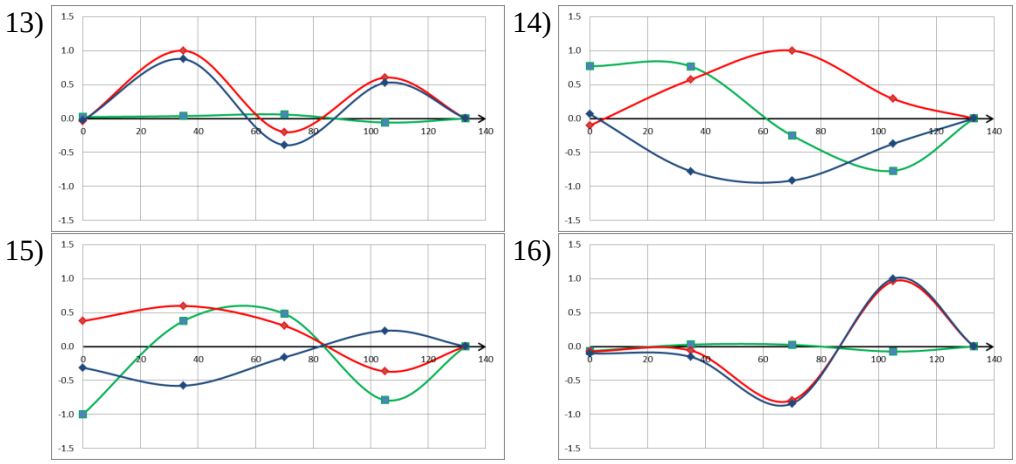

Fig. 5.7. Four further modes of the bridge detected extending the interval of investigated frequency to 5.5. Hz. See **Fig. 5.4** for location of the sensors.

In **Fig. 5.7** are reported the identified mode shapes associated to stable alignments detected extending the investigation of the frequency interval to 5.5 Hz. From engineering standpoint, some remarks can be drawn:

- The frequency of the fundamental lateral mode is 0.777 Hz and the corresponding mode involves a symmetrical lateral bending of the deck.
- The first vertical mode of the bridge was detected with natural frequency equal to 0.823 Hz and the corresponding mode associated involves anti-symmetrical vertical bending of the deck.
- The bridge exhibits a complex dynamic behavior characterized by a large density of vibration modes in a reduced frequency range, closely spaced modes and one complex mode with nominal frequency equal to 4.66 Hz [Marrongelli et al. (2018d)].
- Two purely lateral modes of the bridge have been detected (1^{st} and 5^{th} mode).
- Almost all identified modes can be classified as dominant bending (2^{nd}, 3^{rd}, 4^{th}, 6^{th}, 8^{th}, 10^{th}, 12^{th}, 13^{th} and 16^{th} mode) or dominant torsion (7^{th}, 9^{th}, 11^{th}, 14^{th} and 15^{th} mode).
- Four further identified modes were extracted extending the interval of investigated frequency to 5.5 Hz (see **Fig. 5.7**) that are not identified by previous analysis.
- Furthermore, a structural mode with high complexity component was detected with nominal frequency equal to 4.66 Hz (13^{th} identified bending mode).

5.3.3 *Application of the proposed algorithm to a continuous monitoring period*

The MPE algorithm described herein has been coupled with a simple modal tracking procedure to automatically process data continuously collected by the monitoring system installed on Infante D. Henrique Bridge. As shown in the previous paragraph, the investigated frequency interval was extended to 5.5 Hz and four further structural modes were identified in addition to the 12 modes reported in previous publications. Thus, the new set of 16 identified modes was used as reference parameters for the tracking process. In the context of continuous dynamic monitoring, the most representative features (normally natural frequencies) are plotted over the time in order to study their evolution and detect any possible anomalies in the "normal" behavior of the structure. To reach this task, every set of modal estimates, obtained by the analysis of each dataset, is linked to the reference baseline list through a comparison performed among modal estimates.

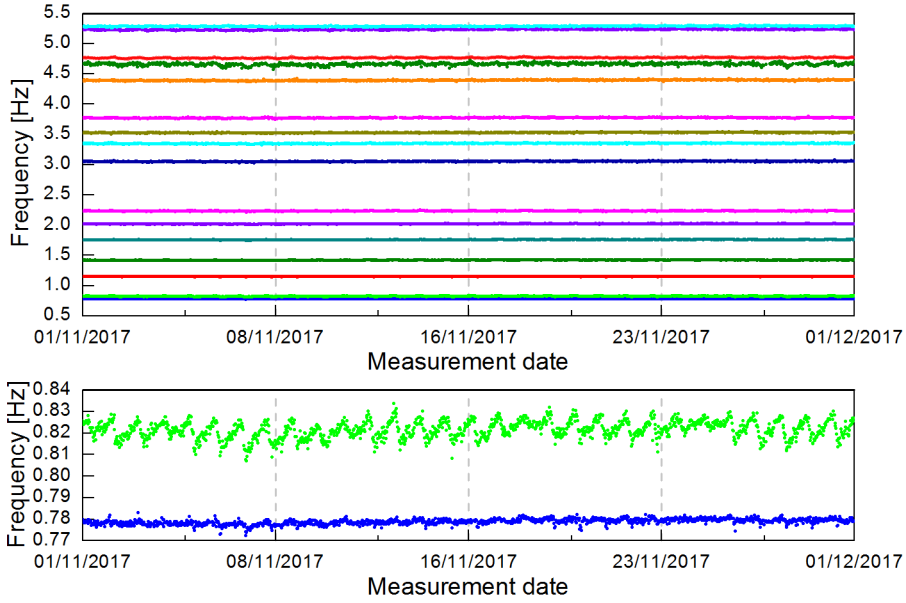

Fig. 5.8. Evolution of the natural frequencies of the modes automatically identified during the period from 01/11/2017 to 30/11/2017. Overview of the natural frequencies and zoom of the lower frequencies of the bridge

There are several approaches to perform a correct tracking process [Magalhães et al. (2009), Reynders et al. (2012), Cabboi et al. (2017)], the most successful procedures are usually based on the use of a fix baseline (associated to pre-defined structural modes) or based on adaptive baseline (continuously updated after the analysis of each dataset). In this example, a fixed reference list associated to the modes extracted from the dataset collected on the 1st of November 2017 was used. Then, continuous monitoring process was achieved comparing each new set with the 16 selected modes, and their evolution are shown in **Fig. 5.8**. Moreover, the zoom of the two identified modes with lower frequency value highlights the robust performance of the developed methodology, capable to correctly identified closely spaced modes also subjected to the effects of the environmental and operational conditions (i.e. temperature variation and traffic loads).

Table 5.3. Main results obtained by the continuous dynamic monitoring of the bridge

Mode	SR	f_{mean}[Hz]	σ(f) [Hz]	ξ_{median}[%]	σ(ξ) [%]	MAC_{mean}	MAC_{min}	MPC_{mean}	MPD_{mean}
L1	100.00	0.78	0.001	0.43	0.104	1.00	0.94	1.00	1.51
V1	100.00	0.82	0.004	1.16	0.389	1.00	0.98	1.00	1.31
V2	100.00	1.15	0.002	0.45	0.086	1.00	1.00	1.00	0.30
V3	100.00	1.42	0.002	0.45	0.106	1.00	0.99	1.00	0.41
L2	100.00	1.75	0.003	0.47	0.096	0.99	0.92	0.99	3.09
V4	100.00	2.02	0.003	0.49	0.146	1.00	0.98	1.00	0.90
T1	100.00	2.23	0.004	0.47	0.141	1.00	0.98	1.00	0.50
V5	100.00	3.05	0.006	0.48	0.132	1.00	0.98	1.00	0.63
T2	99.86	3.34	0.006	0.50	0.110	0.99	0.94	0.99	2.22
V6	99.79	3.52	0.005	0.41	0.100	0.99	0.92	0.99	3.12
T3	96.46	3.77	0.006	0.47	0.107	0.98	0.84	0.96	3.20
V7	99.93	4.39	0.008	0.57	0.145	1.00	0.98	1.00	2.10
V8	83.61	4.66	0.020	1.18	0.311	0.91	0.73	0.93	8.31
T4	99.44	4.76	0.009	0.63	0.115	0.99	0.90	0.99	2.50
T5	96.32	5.23	0.008	0.55	0.094	0.98	0.85	0.97	3.09
V9	97.22	5.28	0.006	0.46	0.070	0.98	0.87	0.97	5.18

Table 5.3 summarizes the most relevant results obtained by the application of the developed 3D-MPE algorithm to data collected in one month of monitoring of the bridge. Specifically, in the first column the type of the investigated modes is reported. In the second column the success rate associated to each mode is quantified; as shown 10 modes were identified in all recorded datasets (success rate of 100%), just one mode was

identified with a lower success rate (equal 83%); meanwhile, the success rate of other 5 modes were identified with a rate higher than 96%. Columns 3-6 present the mean values with the standard deviations of the natural frequencies, and the median values with standard deviation of the modal damping ratios associated to each identified mode, respectively. In the columns 7-8, the mean and the minimum value of the MAC index obtained during the monitoring are reported. Finally, in the columns 9-10 the mean values of the two complex indices, MPC and MPD, are also reported.

The last two columns provide relevant information about the behavior of the investigated modes; in fact, as reported in **Table 5.3**, all identified modes are strictly real except for the 8th vertical bending mode, in which the complex component is not negligible. Such information is confirmed by both complex indices but also by the graphical representation of the mode shapes depicted in **Fig. 5.7**(13), the maximum and minimum value of the modal displacement associated to each component in upstream and downstream side of the bridge are not reached at the same instant but they maintain a mutual delay, typically of complex modes.

5.4 Application to real data collected on *San Michele bridge*

In order to demonstrate the robustness of the MPE proposed herein, the current approach has been exemplified also using data continuously collected on an important Italian Cultural Heritage structure: the San Michele Bridge [Busatta (2012); Gentile and Saisi (2011), Gentile and Saisi (2015)].

5.4.1 Description of the bridge and historical background

San Michele Bridge is one of the most important Italian Cultural Heritage monuments of the 19th century. It was built in 1889 and it consists of an iron arch that supports a box girder to links the small town of Paderno to Carlusco d'Adda in the north of Italy (about

50 km far from the city of Milan). It is characterized by the main parabolic iron arch with span of 150m long that rises 37.5m. The upper girder is 266 m long and it is supported by nine equally spaced bearing, Due to the difficulty of performing a regular maintenance, the state of preservation of the bridge is quite poor and several structural components are significantly damaged by corrosion. Moreover, the increase in traffic in the last decades is gradually worsening the maintenance of its security status; for these reasons, it was decided to carry out several ambient vibration tests in order to understand the dynamic behavior of the bridge and to plan some damage mitigation strategies to preserve the historic bridge [Gentile and Saisi (2011); Busatta (2012)]. Furthermore, test results highlighted some issues in the behavior of the bridge that need to be deeper analyzed. For these reasons, a permanent dynamic monitoring system was installed for SHM purposes.

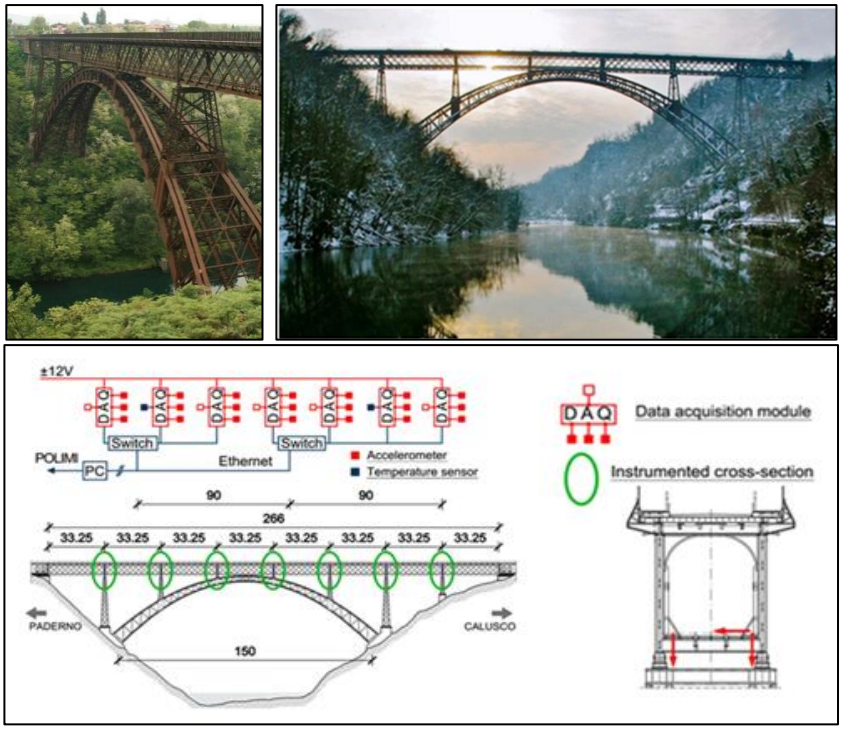

Fig. 5.9. Layout of the monitoring system and views of the San Michele iron arch bridge (1889).

5.4.2 Extraction of the modal parameters estimates of the historical bridge

The proposed methodology was initially applied to several single dataset collected during the first day of the selected monitoring period, in order to extract the best set of modal estimates that it will be used as reference list for continuous dynamic monitoring process. The vertical and horizontal acceleration time series recorder during the monitoring process were processed separately. In this paragraph, only the results related to the analysis of the horizontal output response of the bridge are reported. It is worth mentioning that collected data were initially pre-processed to remove parts of the signals that do not comply with the basic assumptions of OMA applications (e.g. [Gentile and Saisi 2015]) and then filtered and re-sampling to 20 Hz.

Table 5.4. Modal parameters, standard deviations and complexity indices of the identified modes

n°	f [Hz]	σ(f) [Hz]	ξ [%]	σ(ξ) [%]	MPC	MPD
1	0.991	0.0001	0.33	0.0137	0.999	0.83
2	1.345	0.0001	0.56	0.0269	0.997	1.59
3	1.646	0.0002	0.60	0.0132	0.992	2.03
4	2.014	0.0004	0.55	0.0076	0.983	3.60
5	2.160	0.0004	0.78	0.0101	0.980	3.75
6	2.508	0.0002	0.75	0.0021	0.895	8.70
7	2.802	0.0002	0.89	0.0208	0.972	4.92
8	3.122	0.0006	0.53	0.0051	0.895	11.26
9	3.530	0.0013	1.12	0.0231	0.974	5.17
10	3.800	0.0006	0.63	0.0122	0.919	8.21
11	4.020	0.0117	0.42	0.3688	0.846	10.77
12	4.078	0.0029	0.25	0.0321	0.898	10.96
13	4.126	0.0014	0.35	0.0069	0.981	4.55
14	4.383	0.0004	0.41	0.0056	0.909	6.74
15	4.789	0.0007	0.40	0.0130	0.933	8.53

As reported in [Busatta (2012), Gentile and Saisi (2015), Cabboi et al. (2017)] 15 lateral modes of the bridge were expected. The proposed algorithm was used to extract the evolution of these features during a winter period, setting the initial parametric inputs as follows: time-lag interval from 20 to 100 (increasing value equal to 10) and model's order interval as 30-150 (step equal to 2). **Table 5.4** shows the results automatically obtained by structural responses collected during the 19th of February 2012 at 9 a.m., where 15 different modes have been detected. A graphical representation of the identified modes of the bridge is provided by **Fig. 5.10**.

Moreover, the polar plot representation highlights the remarkable complexity associated to several investigated modes. As described in [Cabboi et al. (2017)], the complexity of the mode shapes could depend on various factors (i.e. linkage, synchronization problem, high noise ratio) and non-linear behavior of the structure (generally related to non-proportional damping or hysteretic factors). Therefore, the choice of the thresholds adopted to remove most of spurious poles is still related to the expected characteristics of investigated structure and some trial tests are required to define them. In this application, the thresholds used to remove spurious poles from the tri-dimensional stabilization diagram were set equal to 0.4 and 25° for MPC and MPD, respectively. So, all estimates obtained by SSI-Cov method with complexity values lower than aforementioned limits were considered as noise modes and removed.

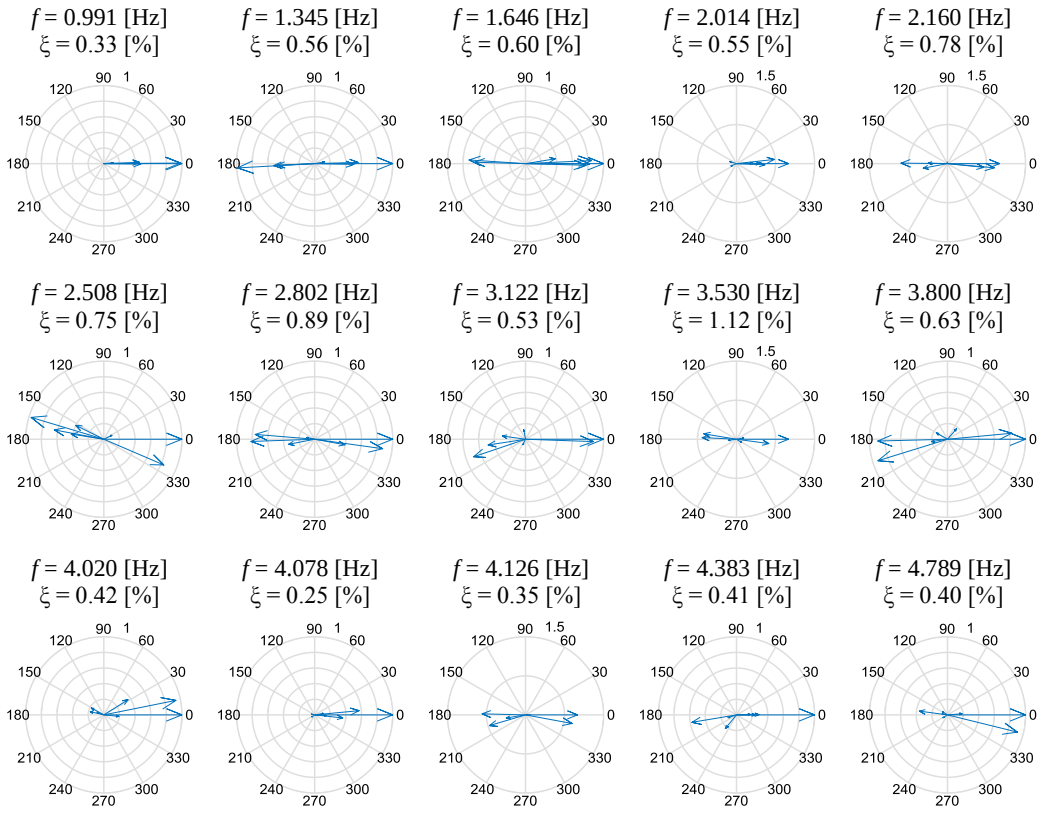

Fig. 5.10. Reference parameters of the 15 modes: natural frequency, modal damping ratio and mode shapes represented in a polar plot

5.4.3 *Application of the proposed algorithm to a short period of monitoring*

Once the baseline list has been defined, the identification algorithm was applied to one-month of monitoring data collected on San Michele Bridge in order to track the natural frequencies evolution and to find any possible anomalies in the normal behaviour of the bridge. Despite modal tracking is a well-known problem for permanent monitoring purposes, its application is not always straightforward. The tracking process proposed herein exploits the similarity measurements already presented in [Cabboi et al. (2013); Gentile and Saisi (2015)], involving the frequency variation and the MAC index (necessary to separate the close spaced modes). Instead the short period of monitoring, the linking process was performed using static rejection thresholds applied to frequency variation and MAC index separately, such thresholds were fixed to 0,20 Hz and 30%, respectively. The results of the automated identification of the natural frequencies of the bridge, are shown in **Fig. 5.11**.

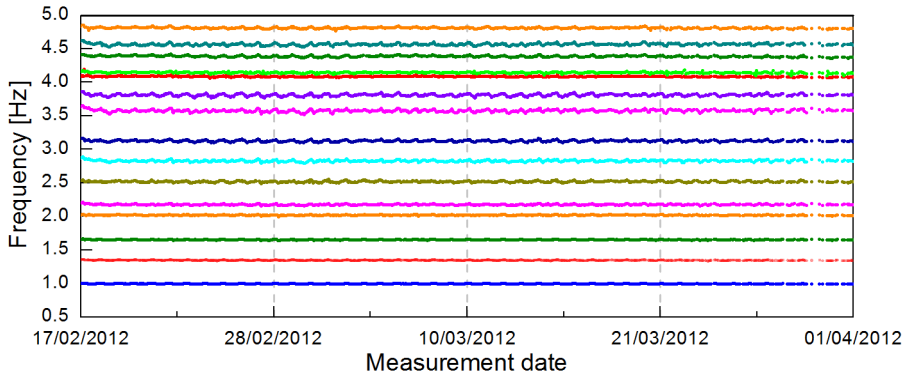

Fig. 5.11. Evolution of the natural frequencies of the lateral modes of the bridge identified during the period from 17/02/2012 to31/03/2012

In order to highlight the environmental and operational effects on the natural frequency estimates, a zoom of the frequencies evolutions within the investigated period associated to modes with lower frequencies are reported in the **Fig. 5.12**. The daily fluctuations of the natural frequencies are clearly shown in the graphical representations highlighting the strong dependence between the extracted natural frequency estimates and environmental factors (i.e. temperature fluctuations).

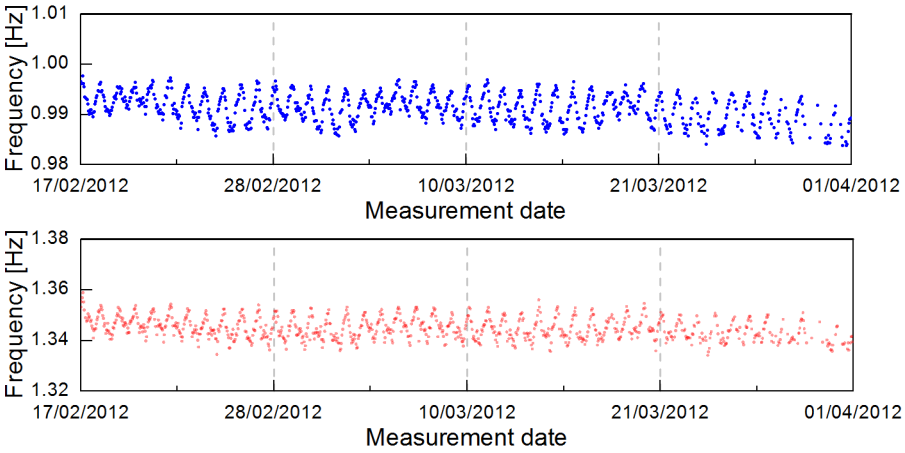

Fig. 5.12. Zoom of the natural frequency evolution associated to the first lateral mode (blue dots) and to the second lateral mode (red dots) of the *San Michele* bridge

Moreover, main statistical information of the modal identification of the 15 detected identified modes of the bridge are reported in **Table 5.5**. As shown, also in this case the robust performance of the proposed methodology is confirmed by the high success rate (higher than 96%) for all structural modes.

Table 5.5. Results of the continuous monitoring of San Michele Bridge

n°	SR	f [Hz]	σ(f) [Hz]	ξ [%]	σ(ξ) [%]	MPD	MPD
1	100.00	0.995	0.0095	0.257	0.0875	0.999	1.05
2	100.00	1.356	0.0251	0.497	0.1885	0.990	2.24
3	100.00	1.662	0.0327	0.538	0.2088	0.973	3.73
4	100.00	2.032	0.0409	0.509	0.2009	0.926	4.56
5	99.80	2.201	0.0650	0.634	0.1958	0.905	6.82
6	97.43	2.545	0.0737	0.731	0.2019	0.894	8.49
7	99.93	2.865	0.0883	0.644	0.2143	0.869	7.90
8	99.86	3.161	0.1003	0.526	0.2060	0.855	11.80
9	100.00	3.623	0.1092	0.695	0.2861	0.929	5.51
10	100.00	3.841	0.0898	0.553	0.1692	0.916	8.31
11	100.00	4.105	0.0654	0.375	0.2215	0.838	9.72
12	99.93	4.154	0.0331	0.277	0.1473	0.780	12.93
13	96.75	4.405	0.0501	0.350	0.0857	0.909	12.48
14	99.59	4.580	0.0566	0.486	0.1280	0.933	15.57
15	92.79	4.812	0.0264	0.350	0.1378	0.999	6.77

In more details, in the second column of the **Table 5.5** the success rate (SR) values referred to each investigated mode is reported. Columns 3-4 present the mean values and standard deviations of the identified natural frequencies. The standard deviations highlight the low scatter of the obtained estimates during the tracking process, as well as same trend is seen for the damping ratios (columns 5 and 6). Finally, in the columns 7-8 are shown the mean values, MPC and MPD associated to all modes during the one-month monitoring period. It is worth mentioning the relative high values associated to the complexity indices, demonstrating the high complex component related to almost all structural modes.

5.5 Conclusions

In this Chapter a recently developed methodology for automated modal parameter estimation based on the construction and interpretation of tri-dimensional stabilization diagrams is presented. The performance of the developed algorithm is exploited extracting the modal parameters of a simple numerical stricture composed by 5-DOFs. Later, it was used to identify the modal parameters of two large infrastructures: the Infante Dom Henrique bridge (Portugal) and the San Michele bridge (Italy). Consequently, the robustness of the developed modal identification algorithm was demonstrated in the context of continuous monitoring applications, analyzing short periods of monitoring data collected on the bridges.

The goal of the proposed methodology is based on two different aspects apt to provide a more generalized automated procedure for the identification problems. The first aspect is related to the human interaction in a very primary stage of the identification process. In detail, the new methodology provides a further effort in the automation of the identification process avoiding the user choice in the definition of the input parameter of SSI-Cov method (i.e. time-lag) used to construct the correlation matrix. The second aspect is related to a further generalization of the developed procedure to complex cases through a new clustering approach based on the use of MACX index.

From the analysis of data collected on the two cases studies, the performance of the developed 3D-MPE algorithm was proven by the high success rate in the identification of their structural modes. In the former case, 16 structural modes were identified with a success rate generally higher than 97%. Moreover, the obtained results also show the ability of the implemented algorithm in the identification of closely spaced modes, as it shown by the first lateral mode and the first vertical mode with frequencies of 0.78 Hz and 0.82 Hz, respectively. The monitoring results also show very coherent mode shapes, that maintain high consistency during the entire investigated period with MAC values generally higher than 0.98.

In the second application, 15 lateral modes of the bridge were successfully identified and tracked. The good performance of the algorithm allows the high success rate in the tracking of the bridge modes. Moreover, the high complexity of some mode shapes highlights the effects of the improvement implemented in the clustering process; in fact, the generalization of the clustering procedure to complex modes through the use of the MACX index allows an efficient generation of representative clusters and, consequently, a better performance of the tracking process.

From the resulting outputs concerning the analysis of both bridges, the evolution over time of the modal parameters (mainly natural frequencies) confirms the influence of the environmental factors as well as the operational loads on the dynamic behavior of both bridges.

Concluding, the application of the proposed 3D-MPE algorithm could be of great interest in the context of continuous dynamic monitoring of real scale structures. A deeper analysis of the uncertainty related to obtained estimations (i.e., analysis of the evolution in time of the standard deviations) will be very useful to understand and quantify the robustness and the flexibility of the implemented methodology of delivering coherent sets of structural modes.

Again, it should remark that the evolution of the natural frequencies in the referred monitoring periods are obtained completely avoiding the initial tuning of the input

parameters (i.e. time-lag and model order) of the SSI-Cov parametric methods just using a wide range of both parameters. This result demonstrates the great improvement in the automation of the identification process.

Chapter 6

DEVELOPMENT OF A NOVEL STRATEGY OF MODAL TRACKING

Contents

6.1 Introduction

Within the context of OMA-based SHM, the tracking process deserves a special attention because it directly provides the input for the statistical tools adopted to detect any novelty or abnormal changes in the dynamic behavior of the investigated system. The efficiency of the Modal Tracking (MT) process is evident for SHM purposes because the good performance of this tool allows for the full automation of the monitoring process and, consequently, a relevant reduction of human interaction during the continuous assessment of structures. The importance of an effective design of the tracking procedure is crucial in order to handle correctly large amounts of collected information regarding the continuous dynamic monitoring of large infrastructures, generally characterized by widespread monitoring systems, as well as for ancient constructions, in which the monitoring systems (composed by a reduced array of sensors) are generally subjected to limited conditions that do not make the monitoring process easy and straightforward.

In the last decades, the SHM strategy based on the vibration monitoring and operational modal analysis has received increased attention and many monitoring systems have been implemented in structures and infrastructures, all over the world. Well-known examples of permanently monitored structures in different countries include: the *Akashi Kaikyo Bridge* in Japan [Katsuchi et al. (1998)], the *Tsing Ma Bridge* in Hong Kong [Wong (2004)], the Seohae Bridge in Korea [Koh et al. (2004)], the *Infante Dom Henrique Bridge* in Portugal [Magalhães et al. (2008)], the *Tamar Bridge* in UK [Cross et al. (2013)] and the *Oresund Bridge* in Denmark [Peeters et al. (2009)]. Other applications concern important infrastructures [Ni et al. (2009), Ni et al. (2011)], slender footbridges [Caetano et al. (2010)] and Cultural Heritage constructions in Italy, such as the *Gabbia Tower* in Mantua [Saisi et al. (2015); Gentile et al. (2016)] and *San Pietro Bell-Tower* in Perugia [Ubertini et al. (2016); Ubertini et al. (2018)].

The growing scientific and practical interest in dynamic monitoring and OMA-based SHM has many motivations, such as: (a) the possibility of obtaining information on the health condition of the structure in quasi-real time, (b) the easy extraction of the complex

behavior of new constructions as well as ageing structures, (c) the monitoring of the most meaningful features in order to highlight the occurrence of any damage or anomalies in the structures. Thus, over the years, the increasingly large number of permanently monitored structures has driven an increase in the demand for automation of the analysis process devoted to the identification of modal parameters and the tracking of their time evolution.

Despite this, only a few strategies have been developed in literature to manage the MT phase using parametric identification methods [Magalhães et al. (2009), Cabboi et al. (2017), Zonno et.al. (2018)] or also devoted to the use of methods based on non-parametric techniques as developed in [Rainieri and Fabbrocino (2009)].

One of the most popular approaches adopted to perform the tracking of the structural modes is based on checking the similarity of the modal parameters in terms of natural frequency and mode shape (through the MAC index). The aim of such strategy is to follow the time evolution of the investigated modes through: a) exploiting the consistency of the modal parameters over time, b) adopting a reference baseline set of modes and c) calibrating rejected thresholds to account for variations associated to the thermal effects or dynamic loads.

In common practice, the reference modes are generally defined through previous ambient vibration tests but also by performing a one day monitoring to better characterize the dynamic behavior of the investigated structure. Therefore, these reference modes represent the initial state of the monitoring project and they are generally known as MT parameters. It is worth mentioning that the number of modes in the reference list plays a crucial role during the monitoring process because it defines the number of available slots for the tracked modes. Hence, their definition is very important in the beginning of the monitoring process and it is not always straightforward.

Moreover, threshold values – defined as *rejection thresholds* – are adopted to guarantee a correct linking between reference modes and each candidate mode bounding the tracking zone associated to each reference mode in which the subsequent estimate is checked.

Nevertheless, the choice of the rejection thresholds is very important as well for a correct tracking because their definition is strictly related to both daily and seasonally evolutions of the modal features (more frequently natural frequencies), which are completely unknown in the beginning of the monitoring process. Normally, an initial tuning of these values is performed in the initial stage of the process, taking into account the fluctuation of the modal parameters in the first days of monitoring and making some assumptions on their future evolutions in the summer/winter period. Clearly, the use of pre-defined or fixed threshold values to discriminate between different modes does not guarantee the correct tracking of the features because of the environmental and operational effects. In other words, a manual updating of such bound conditions to mainly cover the seasonally variations are often required along the monitoring process, implying periodical user intervention that does not allow for the full automation of the process.

A good solution to this issue was proposed in [Cabboi et al. (2017)], in which the tracking is based on the automatic definition of *self-adaptive rejection thresholds*. This strategy is oriented towards automatically establishing the values of the rejection thresholds scanning all distances, in terms of natural frequencies and MAC values, between reference modes belonging to the baseline reference list and all modes estimates previously tracked. This solution solves one of the main problems of the tracking process related to daily and seasonal temperature variations, making the procedure completely automated. Nevertheless, even the use of adaptive thresholds might lead to drawbacks when dealing with very simple monitoring systems, because the availability of a limited number of sensors does not always provide a good discrimination between different mode shapes, even more evidently in case of closely–spaced modes with similar mode shapes. Moreover, the design of the adaptive rejection thresholds described in [Cabboi et al. (2017)] is not suitable to cover the effects induced by extreme and unexpected environmental conditions that could suddenly change the dynamic response of the structure and then the modal parameters. Hence, in order to provide a more robust strategy for MT purposes, the presented tool introduces some aspects aiming at ensuring the complete automation of the process and solving the aforementioned issues.

Finally, to give continuity to the work developed in the previous Chapters, the performance of the MT algorithm was exploited adopting both automated modal identification algorithms described in Chapter 4 and Chapter 5. In particular, the automated OMA procedures (i.e., MPE and 3D-MPE) were applied to data collected during the continuous dynamic monitoring of two different Italian Cultural Heritage structures: *The Gabbia* masonry tower and the *San Michele* arch bridge.

6.2 Automated algorithm for Modal Tracking

As already stated in the introduction to this Chapter, the MT procedure herein described has been developed to perform the automated tracking of modal parameters in the context of a continuous dynamic monitoring process. This procedure can be coupled with any parametric and non-parametric technique that provides the estimation of both natural frequencies and mode shapes during the identification analysis, such as: the SSI-Cov [Peeters and De Roeck (1999)] and the SSI-Data method [Van Overschee and De Moore (1996)] developed in the time domain, as well as the p-LSCF method [Peeters et al. (2004)] in the frequency domain, and the FDD method [Brincker et al. (2001)] based on the decomposition of the spectral matrix.

The main aspects characterizing the MT procedure proposed herein are the following: a) exploiting the consistency of the modal parameters over time, b) adopting a short training period to make the process fully automated; c) using *adaptive reference values* together with *self-adaptive rejection thresholds* aimed at covering the induced modal parameters variations due to thermal effects d) allowing for the correct tracking of the structural modes using a dynamic reference baseline list, that is continuously updated after the analysis of each dataset.

First of all, it should be highlighted that the modal tracking procedure herein presented is rooted in the use of a dynamic reference list of modes, composed by a set of natural frequencies and a set of mode shapes associated to the selected reference modes. In this

way, the tracking of the selected modes is performed using the Euclidean distance in terms of natural frequency and MAC index, between each reference mode and the current identified modes obtained after the analysis of each collected dataset.

The use of dynamic references instead of fixed reference modes seems to be very promising because this strategy is based on the assumption that the variation of the modal parameters between two consecutive datasets is very low, so this condition makes the tracking of two consecutive mode estimates easier. Unfortunately, this strategy could fail in case of closely-spaced modes with similar mode shapes or in case of outliers with similar characteristics to the reference ones. In these cases, if the tracking of one mode "jumps" to a similar close mode or to a sequence of outliers it could cause the failure of the process. Then, a manual intervention is needed to restore the correct reference values. To overcome this problem, threshold values have been introduced. Therefore, the linking between the current reference mode and the "new" estimate is successfully performed when the two conditions (thresholds) applied on the natural frequency variation and MAC index variation, are both satisfied.

Subsequently, in order to avoid the manual tuning of the reference list in different periods of the year, an "adaptive strategy" is adopted. Thus, in order to cover the variation of the reference parameters (principally natural frequencies) due to periodic (seasonally) environmental variations, the pre-selected thresholds become adaptive after a brief period of monitoring allowing for the full automation of the MT process.

For this reason, the proposed algorithm combines two different strategies to overcome the aforementioned issues and to allow for the correct tracking of structural modes even in case of closely-spaced modes with similar mode shapes. These strategies are:

a) the use of a dynamic reference baseline list of modes, which is continuously updated after the analysis of each new dataset;
b) the creation of self-adaptive thresholds, which are fully adaptive after a brief training and which limit the tracking zone associated to each reference mode allowing for the correct performance of the process.

Fig. 6.1 shows a schematic representation of the developed MT strategy. As shown, the procedure works based on two different stages: *during the training period* (grey slots) and *after the training period* (blues slots). Unlike other tracking approaches, in the present algorithm the length of the training period plays an important role because it is chosen to achieve a consistent population of estimates that is used to define the adaptive thresholds. In fact, once the defined number of estimates is reached, the threshold values are automatically calculated allowing for the full automation of this process.

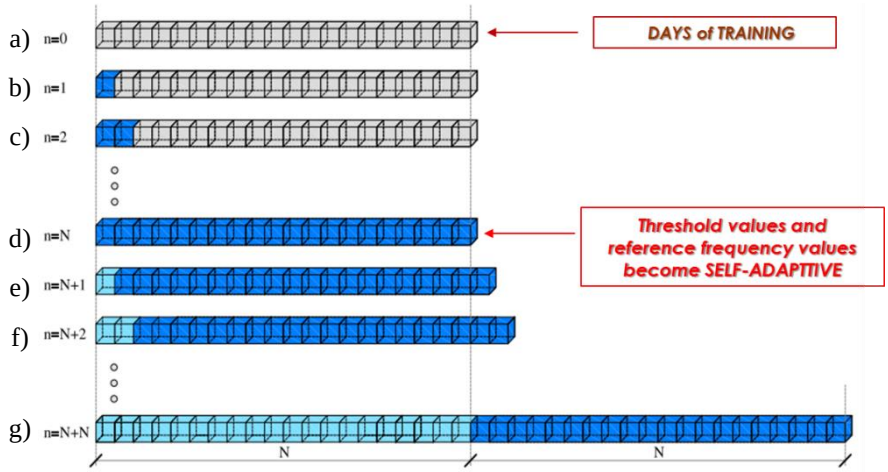

Fig. 6.1. Scheme of the new Modal Tracking strategy – Training period (grey cubes) and Tracking window used for the definition of adaptable thresholds (blue cubes)

The length of the training period is determined by a parameter (i.e., *N*) which should be defined taking into account some basic aspects related to: a) the type of monitored structure, b) to the characteristics and the design of the dynamic system (e.g., type, number and configuration of sensors) and c) the quality of the collected data (i.e., noise/signal ratio).

More in detail, during the training period, the modal tracking of the identified modes is allowed by two sets of pre-selected thresholds associated to both estimates of natural frequency and mode shape of each selected mode. These values are selected taking into account the fluctuations of the modal parameters during the first hours of monitoring.

Moreover, considering the assumed short period of initial training, the setting of these thresholds should be done without imposing restrictive conditions. From common practice, by adopting conservative set of thresholds equal to d_{MAX}^{f}=0.20 Hz for the natural frequencies variations and equal to d_{MAX}^{MAC}=0.20 for mode shapes variations (i.e., MAC=0.80), the tracking should be performed successfully.

Fig. 6.1 exemplifies and explains the automated MT algorithm presented in this section, in which each step of the algorithm refers to a single selected structural mode. In **Fig. 6.1**(a), the "training period" is illustrated with grey cubes: this interval is defined to store a consistent number of modal estimates apt to ensure a proper~~ly~~ definition of both self-adaptive thresholds. **Fig. 6.1**(b) shows the first association of the structural modes performed after the analysis of the first collect dataset. The linking between the current mode and the reference mode is performed when two positive checks (in terms of distance rejections that might be smaller than threshold values) are obtained. In fact, the current pole is associated to the reference estimate if the distances in terms of natural frequency and MAC variation are both lower than pre-defined limits. Subsequently, **Fig. 6.1**(c) illustrates how the tracking window (see blue cubes) grows after performing correct associations. This process goes on until the last available slot is filled completing the training period, as shown in **Fig. 6.1**(d).

Once the training period has expired and the number of minimum estimates (i.e., n=N) is reached, simple statistical tools are applied to the stored estimates. Thus, the *static* thresholds previously defined become *adaptive*. The definition of the adaptive thresholds is described in the follow equations:

$$d_{i-ref}^{f} = \sqrt{std\left(d_{i-ref,j}^{f}\right)} = \sqrt{std\left(\sum_{j=1}^{N}\left|f_{i-ref} - f_{j}\right|\right)}$$
$$d_{i-ref}^{MAC} = \sqrt{std\left(d_{i-ref,j}^{MAC}\right)} = \sqrt{std\left(\sum_{j=1}^{N} MAC\left(\boldsymbol{\varphi}_{i-ref};\, \boldsymbol{\varphi}_{j}\right)\right)} \quad (6.1)$$

where $std(d^{f}_{i-ref,j})$ and $std(d^{MAC}_{i-ref,j})$ are the standard deviations associated to the calculated distances – computed in terms of natural frequency and MAC, respectively – between the *j-th* estimates (*j=1… N*) related to *i-th* reference monitored mode.

In order to make the procedure more sensitive to the modal parameter variations, when all available slots have been filled, the number of estimates (defined by *N*) used to define the adaptive thresholds is maintained in a conservative way for the subsequent analysis. This means that after the analysis of each new dataset ($n=N+j$ with $j>0$) the tracking window (depicted in **Fig. 6.1**(e-f) with blue cubes) slides by one position, incorporating the last identified estimate and removing the first allocated one. This strategy makes it possible to obtain consistent tolerance values based on the same quantity of estimates. Finally, **Fig. 6.1** (g) shows how the *tracking window* moves during the monitoring process, making the thresholds updating effective. It is further noted that the computational cost of the thresholds updating is drastically reduced, also due to the very compact quantity of allocated memory continuously used in the definition of the distance thresholds.

Despite this improvement, the performance of this MT algorithm could fail in case of anomalous variations in the "normal" behavior of the monitored parameters, caused by extreme variations of environmental factors. For these reasons, in order to guarantee an accurate tracking of the structural modes also during such unexpected and extreme variations, a further improvement has been implemented.

Thus, when the training period has expired (**Fig. 6.1**(d)), along with the static thresholds, the reference frequencies (defined in the static baseline list) become adaptive as well. This operation is performed averaging all frequency estimates stored in the blue slots of the tracking window. This improvement is well exemplified in **Fig. 6.2**.

As depicted in **Fig. 6.2**, the red dash line is used to indicate the frequency reference value and its evolution during the tracking process. During the training phase, the reference frequency remains constant and equal to the initial value. **Fig. 6.2**(a) reports the

definition of self-adaptive thresholds without performing the upgrade of the frequency reference. As shown, in case of anomalous variation, the threshold values can grow exponentially and might lead to an overlap between different tracking zones. This condition might affect the tracking process causing loss of estimates, or possible incorrect associations among different modes, or its complete failure. Therefore, to overcome these issues the reference values of frequency have been made adaptive as well. As shown in **Fig. 6.2**(b), this improvement helps avoid the enlargement of the distance rejections providing a more accurate tracking of the investigated modal features.

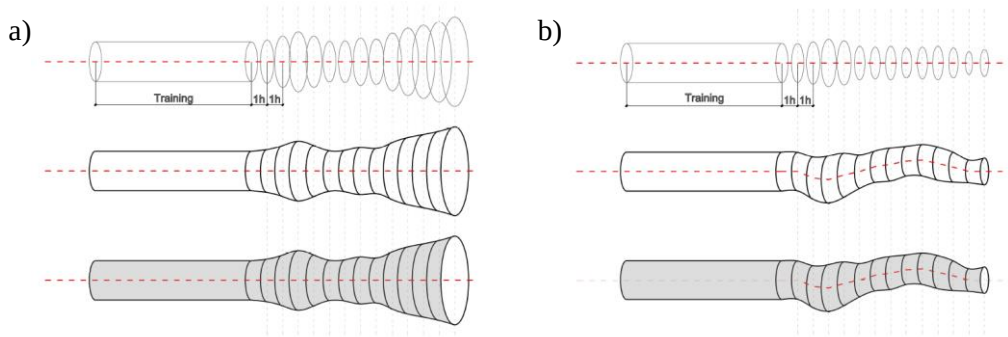

Fig. 6.2. Application of the new proposed MT strategy: (a) without adaptive frequency reference; (b) using the adaptive frequency values

Following this strategy, the definition of adaptive thresholds and adaptive reference frequencies makes it possible for the MT algorithm to comply with several important aspects: 1) guaranteeing an accurate tracking due to the flexibility and adaptability of the rejected thresholds obtained from a very limited number of estimates, 2) limiting the enlargement of the thresholds and the overlap of the tracking zones that could lead to incorrect associations of modes, 3) providing an accurate evolution of the structural modes even in case of anomalous structural changes due to environmental and operational conditions, and 4) conceivably reducing the number of outliers during the tracking.

As will be shown in this Chapter, the MT procedure is tuned out to be promising for several SHM applications for large infrastructures, with diffused monitoring systems

composed by high number of sensors, or also for Cultural Heritage buildings, in which the continuous monitoring is generally performed using a reduced number of sensors.

In order to better understand the performance of the developed MT procedure, the main tasks executed during the analysis of each dataset are resumed below. It should be noted that the inputs provided for the MT algorithm are composed by a double array of reference parameters –a set of natural frequencies and a set of mode shapes – and two vectors of tolerance values – one vector associated to the frequency variations and one vector associated to the MAC variations. In the beginning of the process the first task performed by the MT algorithm consists of a duplication of the reference values and the tolerance values associated to each structural mode. Specifically, the first reference set of parameters and tolerances are defined *static baseline reference list* and *static thresholds*. Accordingly, the second set of reference and tolerances are defined as *dynamic baseline reference list* and *pre-selected* or *fixed thresholds*, as reported in the scheme below.

From this point on, in order to make it easier for the reader to understand each step carried out by the algorithm, some simplification has been introduced: the s*tatic baseline reference list* and the *dynamic baseline reference list* are re-named as *static list* and *dynamic list*, respectively.

Static list		*Static thresholds*	
Reference frequencies	*Reference modes*	*Frequency thresholds*	*MAC thresholds*
$\begin{bmatrix} f_{1,s} \\ f_{2,s} \\ f_{3,s} \end{bmatrix}$	$\begin{bmatrix} \varphi_{1,s} \\ \varphi_{2,s} \\ \varphi_{3,s} \end{bmatrix}$	$\begin{bmatrix} \Delta f_{1,s} \\ \Delta f_{2,s} \\ \Delta f_{3,s} \end{bmatrix}$	$\begin{bmatrix} \Delta d_{MAC1,s} \\ \Delta d_{MAC2,s} \\ \Delta d_{MAC3,s} \end{bmatrix}$

Dynamic list		*Fixed thresholds*	
Reference frequencies	*Reference modes*	*Frequency thresholds*	*MAC thresholds*
$\begin{bmatrix} f_{1,d} \\ f_{2,d} \\ f_{3,d} \end{bmatrix}$	$\begin{bmatrix} \varphi_{1,d} \\ \varphi_{2,d} \\ \varphi_{3,d} \end{bmatrix}$	$\begin{bmatrix} \Delta f_{1,d} \\ \Delta f_{2,d} \\ \Delta f_{3,d} \end{bmatrix}$	$\begin{bmatrix} \Delta d_{MAC1,d} \\ \Delta d_{MAC2,d} \\ \Delta d_{MAC3,d} \end{bmatrix}$

Furthermore, it is worth remarking that the whole process is composed by two consecutive stages defined as: *during the training period* and *after the training period*. Moreover, in the initial step, (i.e., *n=0*) the *static list* and the *dynamic list* coincide, as well as the *static thresholds* and the *fixed thresholds*. The stages are described as follows:

1. *During the training period*. The monitoring process begins with the analysis of the first collected dataset. After the first run of the MPE algorithm, an array of mode

estimates (defined by both sets of natural frequencies and mode shapes) is delivered to the MT algorithm. Subsequently the following steps are performed:

1.1. For $n=1$, each current pole belong to the set of extracted estimates is kept on only if two different checks are satisfied. The Euclidean distances, in terms of frequency and MAC, between the two sets of reference modes (for the *static list* and the *dynamic list*, respectively) and the current mode estimate are computed. The first check is satisfied when the distances between the reference mode in the *static list* and the current pole is lower than the corresponding *static thresholds*, for both parameters (natural frequency and mode shape). In the same way, the second check is also performed between the mode in the *dynamic list* and the same current pole. If the distances are smaller of the *fixed thresholds* then also the second condition is achieved and the current pole is retained (i.e., linked to the reference one in the *dynamic list*).

1.2. It could be possible that various poles with similar estimates, like vibration modes characterized by closely-spaced frequencies and a low discriminant between mode shapes, could satisfy both conditions previously described and can be retained as possible candidates. When this condition occurs, only the pole with the shortest distance between the mode shape of the mode in the *dynamic list* and the mode shape of the current pole is selected. This is the most important aspect related to the proposed algorithm because it solves the issue related to those modes with closely-spaced frequencies and similar mode shapes.

1.3. The procedure described in the points 1.1 and 1.2 is repeated for reference modes in order to track all structural modes.

1.4. Hence, once all estimates provided by the MPE algorithm have been scanned and the reference modes successfully tracked, the modal parameters in the *dynamic list* are replaced by the last identified ones. Meanwhile, the *static list* and the *fixed thresholds* do not change.

1.5. For $1<n\leq N$ the tasks in the points 1.1, 1.2, 1.3 and 1.4 are repeated in a consecutive manner in order to reach the last available dataset (the *N-th* set of outputs) defined in the training period.

In order for the reader to better understand the performance of the MT procedure during the training period, it should be noted that the modes in the dynamic list are continuously updated and each mode is tracked to the closest mode with similar mode shape. This choice assumes that the variation of the mode shapes between two consecutive records might not change significantly as could occur for the natural frequencies.

Moreover, during the training period, the tracking is totally entrusted to the checking performed on the *dynamic list* through the *fixed thresholds*, because the boundary conditions defined by the *static thresholds* have the same value as the *fixed thresholds* and also both checks are quite similar.

2. *After the training period*. When the training period has expired and the *N-th* dataset has been analyzed, the *static list* and the *static thresholds* change, and their values are defined automatically by applying simple statistical tools (as defined in **Eq. 6.1**) to the stored modal estimates.
   2.1. For *n=N+1*, the modes present in the *static list* are subjected to a "shifting" consisting on a separation between the set of natural frequencies and the set of mode shapes. The first one becomes adaptive (*adaptive list*) and the second one remains as a fixed reference list of modes (*static list*).
   2.2. For *n=N+1*, the thresholds associated to the *static list* become adaptive, through using the statistical properties of the natural frequency values and mode shapes configuration: Following the **Eq. 6.1** the *static thresholds* are now defined as *adaptive thresholds*.
   2.3. The tracking procedure does not change and continues being based on a double checking of the Euclidean distance, in terms of both natural frequency and MAC value, between the two sets of reference modes (for the *adaptive/static list* and the *dynamic list*) and the current possible structural mode. The first condition is satisfied if the Euclidean distances between the possible mode and the reference mode, defined by the *adaptive frequency* and the *static mode shape*, are shorter than the *adaptive thresholds* for both natural frequency and mode shape. Meanwhile, the second check continues to be performed in terms of the

Euclidean distance between the same candidate pole and the mode in the *dynamic list*. It should be remarked that this check is almost always confirmed because the "weight" of the first check performed by *adaptive thresholds* is dominant due to more restrictive conditions imposed by adaptive values. This second check continues to have an important role in the MT process because it ensures the tracking of the mode with the lowest variation (in terms of frequency and mode shapes) compared to the last identified one, avoiding the comparison of outliers.

2.4. When all candidates have been scanned and assigned, the tracking window slides by one position incorporating the last set of tracked modes and removing the oldest one (see **Fig. 6.1**).

The points 2.1, 2.2, 2.3 and 2.4 are repeated in continuous way allowing the continuous monitoring of the structure.

Again, the strategy behind the developed algorithm deserves to be emphasized. In fact, as described, after the training period, the frequency values in the static list become adaptive, too, loosing, in this way, the information relating to their initial values. Notwithstanding this, the information can be easily recovered. Meanwhile, the baseline set of mode shapes does not change during the monitoring process describing the initial state of the structure which is supposed to be undamaged. This choice makes it possible to provide the evolution of the structural modes in terms of MAC indexes and then to develop an alternative OMA-based SHM strategy based on mode shape variation (e. g., [Marrongelli et al. (2019b)]) that could be very promising for the SHM of structures with widespread monitoring systems.

Finally, as will be shown in the next paragraph, the presented MT algorithm was used to monitor the dynamic features of two different case studies.

In the first case study (the *Gabbia Tower*) the evolution of the modal parameters is obtained by adopting a "period of training" of four days as reported in [Marrongelli et al. (2019a)]. As will be shown in the next paragraph, this strategy allowed for the automatic tracking of a local mode of the tower, which is characterized by a high fluctuation of the

natural frequency. Moreover, the automated monitoring was performed without any further adjustment to the reference values and thresholds along the monitoring period. Subsequently, in the second case study (the *San Michele Bridge*) the adaptability of this strategy allows for the correct automation of the tracking process adopting just two days of training. As demonstrated during monitoring, the good performance of the MT tool means that no estimates are lost during extreme thermal conditions (see [Marrongelli et al. (2019b)]).

6.3 Validation using data collected on the *Gabbia Tower*

The acceleration time series collected by a simple monitoring system installed on the upper part of the tower were processed using the SSI-Cov method based on the correlation matrices of the measured structural responses. The provided SSI-Cov outputs were used to extract the modal parameter estimates of the tower using the MPE algorithm (described in Chapter 4), that involves the construction of bi-dimensional stabilization diagrams, and MT algorithm described in the previous paragraph.

Principally, this case study was used to test the performance of the implemented OMA tool (composed by both MPE and MT) and the accuracy of the provided results in the context of a permanent dynamic monitoring process.

Afterwards, the validation of the methodology was performed through a comparison between the results obtained automatically and those previously extracted by the manual inspection of the resonant frequencies obtained using the commercial software ARTeMIS (see [Marrongelli et al. (2019a)]).

Finally, the good match between the automatically obtained results and the manually extracted estimates demonstrates the robustness of the developed methodology capable of providing accurate sets of modal estimates and performing the automated modal tracking of the tower without any further user interactions.

6.3.1 Description of the tower

The *Gabbia Tower* [Saisi et al. (2015), Gentile et al. (2016), Guidobaldi (2016)] with its 54.0 m in height, is the tallest tower in Mantua. The tower was erected in 1227 and it was part of the defensive system of the Bonacolsi family (i.e., Lords governing Mantua during the 13th century). The structure is built in solid brick masonry and the load bearing walls are about 2.4 m thick at the base, except in the upper levels, where the wall thickness decreases to about 0.7 m and where a two-level lodge is hosted. As shown in **Fig. 6.3**, the tower is nowadays part of an important palace, whose load-bearing walls seem to be not effectively connected to the tower, whereas various vaults and floors of the palace are directly supported by the tower.

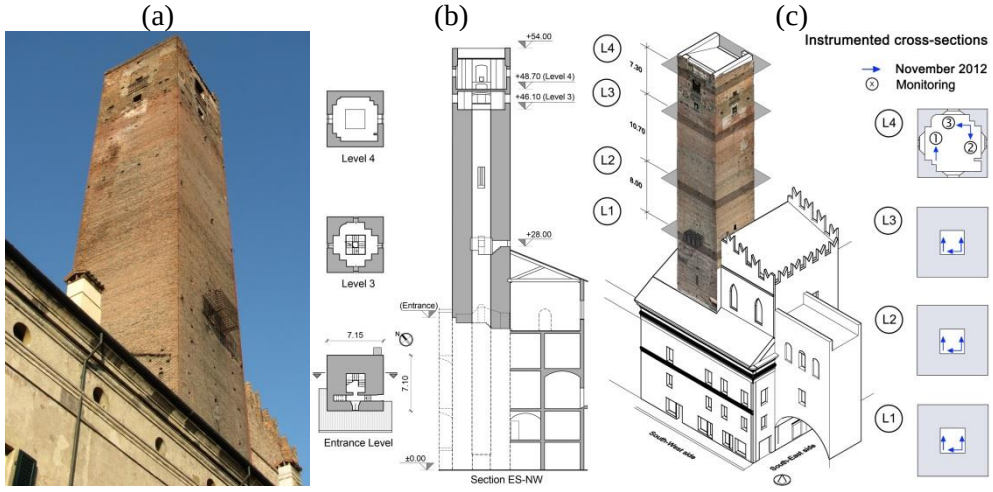

Fig. 6.3. (a) View of the *Gabbia Tower* in Mantua, Italy; (b) Sections of the tower (dimensions in m); (c) Instrumented cross-sections and layout of the accelerometers during the preliminary tests (November 2012) and the continuous dynamic monitoring.

While the main part of the building, below about 46.0 m above ground level, did not exhibit any evident structural damage (with the materials being only affected by superficial decay), the upper part of the tower turned out to be in a poor state of preservation [Gentile et al. (2012)].

After the seismic sequence event that mainly affected the Garfagnana region (Tuscany) in June-May 2012 [Luzi et al. (2013)], the tower was subjected to an intense on-site inspection using a movable platform and deeper visual inspection [Saisi and Gentile (2015)] that highlighted the poor state of preservation of the upper part of the tower, exhibiting extensive masonry decay characterized by evident discontinuities mainly due to structural changes that had occurred over time. Meanwhile, no evident damages were observed in the main part of the building, up to about 46 m above ground level.

6.3.2 Dynamic characteristics of the tower previously investigated

In order to extract the principal modes of vibration of the tower two series of ambient vibration test were in the 2012 [Saisi and Gentile (2015)]. The first test was carried out between 31/07/2012 and 02/08/2012 and it was aimed at evaluating: a) the dynamic characteristics of the tower, b) possible effect induced by the poor state of preservation of the upper region of the tower on the global behavior, and c) the possible effect of the temperature on natural frequencies. Meanwhile, the second test was carried out on 27/11/2012 with the objectives of evaluating: a) the possible effect of the added wooden roof on the dynamic characteristics of the tower and b) the modal parameters estimates to use for the consequently dynamic monitoring process.

The AVT performed in the second campaign was preparatory to the continuous dynamic monitoring of the tower. The modal identification was performed considering time windows of 3600 sec and applying the SSI-Data [Peeters and De Roeck (1999)] available in the commercial software ARTeMIS.

The identified dynamic characteristics of the tower [Gentile et al. (2016), Guidobaldi (2016)] are summarized in **Fig. 6.4**. The results allowing for the installation of only three accelerometers in the upper available level (see **Fig. 6.3**(c)) were considered enough for the identification of structural modes that are normally excited at the low amplitude of ambient vibration detected in the structure. In addition, one local mode was identified at

9.89 Hz (**Fig. 6.4**) and involved torsion of the upper part of the tower. The presence of a local mode provided further evidence of the structural effect of the change in the masonry quality and morphology (including un-toothed opening infillings and discontinuities) observed in the upper part of the tower during the visual inspection.

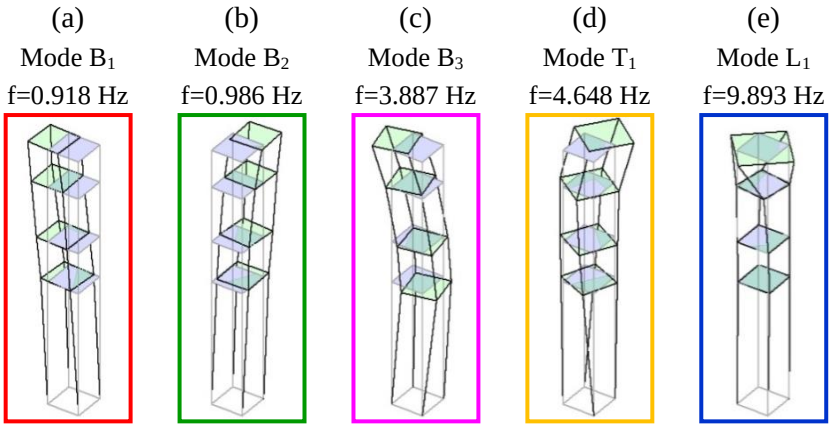

Fig. 6.4. Five vibration modes were identified in the preliminary ambient vibration tests: (a-b-c) bending modes, d) torsion mode and e) local mode involving the upper part of the structure.

As shown in **Fig. 6.4**, five principal modes of vibration were identified in the frequency range 0-10 Hz, in which:

1. Two closely-spaced modes were identified around 1 Hz with dominant bending behavior in two orthogonal planes of the tower,
2. A third mode with a high bending component (second order) was identified with a frequency value equal to 3.88 Hz,
3. A fourth mode characterized by a torsional component was detected at 4.65 Hz,
4. A local mode that involves a torsional contribution of the upper part of the tower was extracted with the frequency value of 9.89 Hz.

Finally, the five structural modes were used as reference for the continuous dynamic monitoring of the tower. The process started on 17 December 2012. The main results and the analysis of the whole period of monitoring of the tower are described in detail in [Guidobaldi (2016)] as well as in the recent publishing [Gentile et al. (2016)] in which

the correlations between investigated natural frequencies and measured environmental factors are also highlighted.

6.3.3 Identification of the reference modes of the tower

In this paragraph the main results obtained by the application of the proposed OMA methodology, composed by the MPE algorithm (Chapter 4) that involves 2D stabilization diagrams together with the proposed MT algorithm, to data collected during seven months of continuous monitoring of the masonry tower (from 17/12/2012 to 15/07/2013) are summarized [Marrongelli et al. (2019a)]. During this period more then 4600 1-hour long datasets where continuously collected by the monitoring system. Each dataset was recorded with a sampling frequency of 200 Hz and subjected to a pre-processing before to be analyzed. In particular, the collected datasets were low-pass filtered – using a classic 7^{th} order Butterworth filter with cut-off frequency of 20 Hz – and decimated 5 time reducing the sampling frequency from 200 Hz to a lower value of 40 Hz.

The SSI-Cov method was adopted to process the collected acceleration time series through the construction of the correlation matrices of the measured responses. For the application of the MPE using SSI-Cov technique three input parameters need to be defined: the number of reference outputs, the maximum order of the stochastic model and the time-lag. Since the monitoring system was composed by only three sensors, all recorded channels were used as references. On the contrary, both maximum order of the stochastic model and the time-lag were selected after some preliminary tests.

It was concluded that good quality of the stabilization diagram was achieved adopting a time-lag value equal to 80 (80/20 =4 seconds → 4 x 0.918 =3.67 times the fundamental period of the tower) and setting the maximum values of the model order equal to 100.

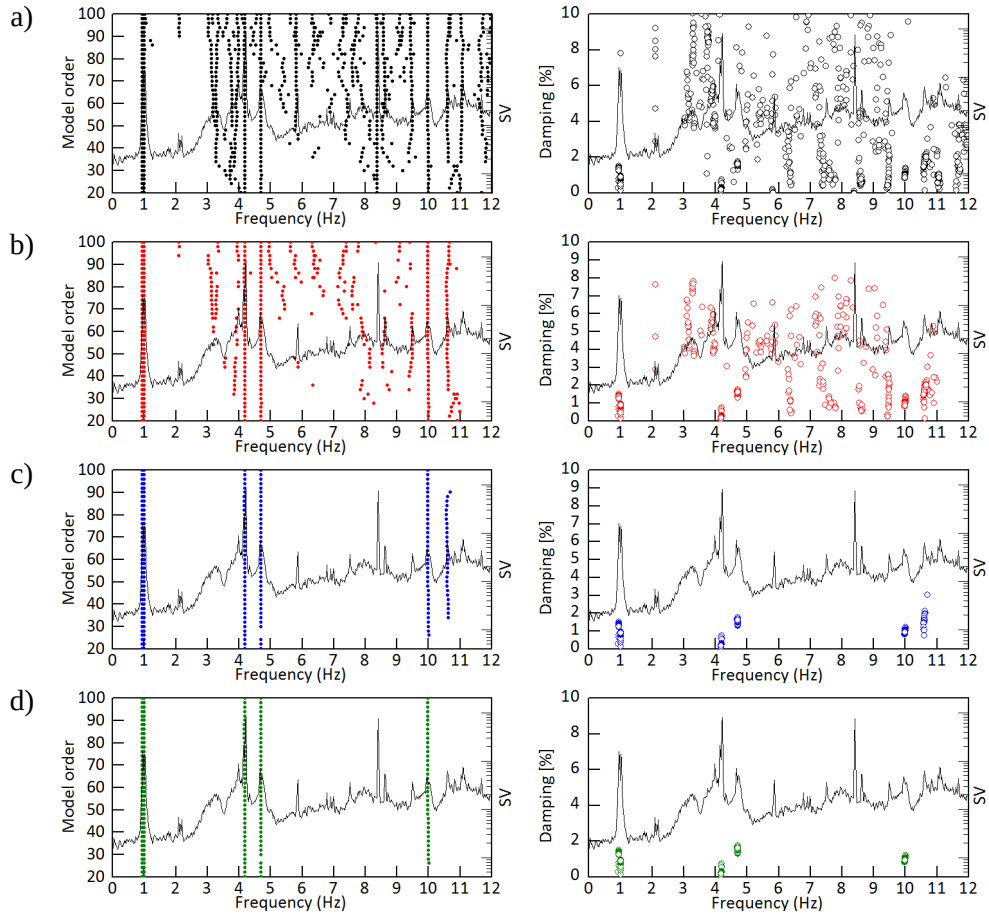

Fig. 6.5. Stabilization diagrams: (a) obtained SSI-Cov outputs; (b) after pre-filtering check; (c) after clustering procedure; (d) after the post-processing to improve accuracy (final results) [Marrongelli and Gentile (2019a)].

Fig. 6.5 summarizes the results of the application of the newly developed MPE procedure to one single dataset recorded on 17/12/2012. In detail, the diagrams in **Fig. 6.5** show the typical cleaning action exerted by the different steps of the MPE procedure on the stabilization diagrams. More in detail: (a) **Fig. 6.5**(a) shows the SSI outputs obtained for increasing model order; (b) **Fig. 6.5**(b) shows the results obtained after the pre-filtering step; (c) **Fig. 6.5**(c) shows the stable alignments obtained by the clustering process and (d) **Fig. 6.5**(d) contains the final alignments of stable poles corresponding to physical modes performed after the removal of a replicating mode provided in the previous step.

All plots in **Fig. 6.5** also show the first Singular Value (SV) line of the spectral matrix, which is the mode indication function used in the FDD method [Brincker et al. (2011)] to highlight the resonant frequencies of the tower.

In particular, the quality of the diagrams has been obtained by applying the SSI-Cov technique to the response time signals recorded by the monitoring system installed on the upper part of the tower. The identification process was performed firstly by defining the time-lag, equal to 80, and the interval of model order, equal to 20-100. The SSI outputs provided for increasing model order are shown in **Fig. 6.5**(a).

Subsequently, the spurious modes were removed from the stabilization diagram applying single validation criteria on each pole. In this way, highly damped modes and highly complex modes were removed setting the damping threshold equal to 5% and the two complex thresholds equal to MPC_{lim}=0.6 and MPD_{lim}=15°, respectively (see **Fig. 6.5**(b)). Hence, the clustering process was performed adopting an inter-cluster distance threshold equal to d_{lim}=0.025 to the remain poles providing six stable alignments stand out on the stabilization diagram (see **Fig. 6.5**(c)).

It is worth noting that due to the reduced number of sensors of the monitoring system possible aliasing could affect the provided estimations. Therefore, the threshold used to check the similarity between mode shapes was set as: MAC_{lim}=0.99. Finally, the checking performed on the outliers removes the extreme values providing a more accurate estimation of the modal parameters associated to the stable alignments in stabilization diagram (see **Fig. 6.5**(d)). Finally, the resulting estimates were selected as reference parameters and they were used in the tracking process.

The graphical results shown in **Fig. 6.5** highlight the robust performance provided by the MPE procedure, with all modes of the tower (**Fig. 6.4**) being clearly detected, notwithstanding the low level of measured acceleration (which is testified by the large number of spurious poles in **Fig. 6.5** as well as by the inspection of the first SV line) and the limited number of available sensors.

6.3.4 Continuous dynamic monitoring of the tower

The developed tools (i.e., MPE and MT) were used to perform the continuous dynamic monitoring of the *Gabbia* masonry tower. The output responses collected during a monitoring period of over six months, from 12/12/2012 to 30/06/2013, were analyzed in order to extract the evolution in time of the modal parameters. Afterward, the automated process was performed using a very short training period of only four days. This means that after four days of continuous processing, in which at least 96 estimates for each reference parameters were stored, the continuous monitoring was fully automated.

Fig. 6.6 and **Fig. 6.7** report the evolution in time of the natural frequencies and the variation of the mode shapes (using the MAC index) related to the five structural modes provided by the monitoring of the tower. Specifically, the diagrams report both periods previously defined as: "during training" and "after training". The dark vertical line drawn in all diagrams indicates the end of the short training period, in which the rejection thresholds associated to all natural frequencies and MAC values were set as: $d_{i,max}^{f}$=0.30 Hz and $d_{i,max}^{MAC}$=0.30, respectively. After this period, the rejection thresholds become adaptive. At the same time, also the reference frequencies become adaptive. This further improvement allows for an easy tracking of possible modes also subjected to significant variations (see **Fig. 6.6**(e)).

The monitoring process was performed using the SSI-Cov method, conservatively maintaining the values of the input parameters previously described for the modal parameter estimation.

In order to better clarify the MT procedure, **Fig. 6.6** reports the evolution of the identified frequencies with the associated adaptive thresholds for all structural modes. It is worth highlighting that after a short period of training, the continuous updating of the adaptive thresholds enables the fully automated tracking without any user interventions and conceivably prevents the comparison of outliers. Similarly, the threshold associated to the MAC values is updated as well, during the tracking phase. The variation of the MAC index and its threshold associated to each monitored mode are shown in **Fig. 6.7**.

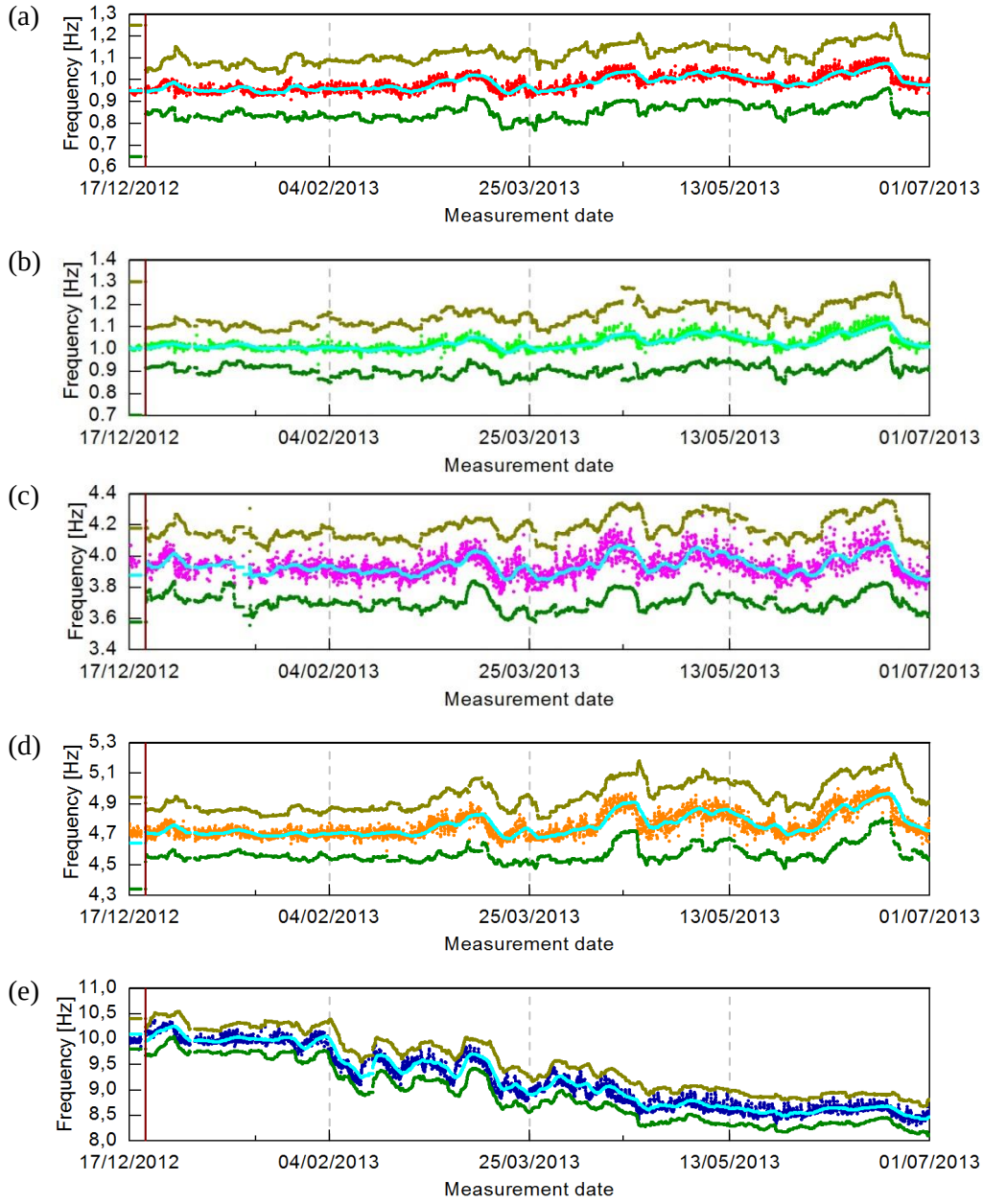

Fig. 6.6. Time evolution (from 17/12/2012 to 30/06/2013) of the identified natural frequency and the corresponding adaptive thresholds: (a) First bending mode; (b) Second bending mode; (c) II order bending mode (d) Torsion mode; (e) Local mode.

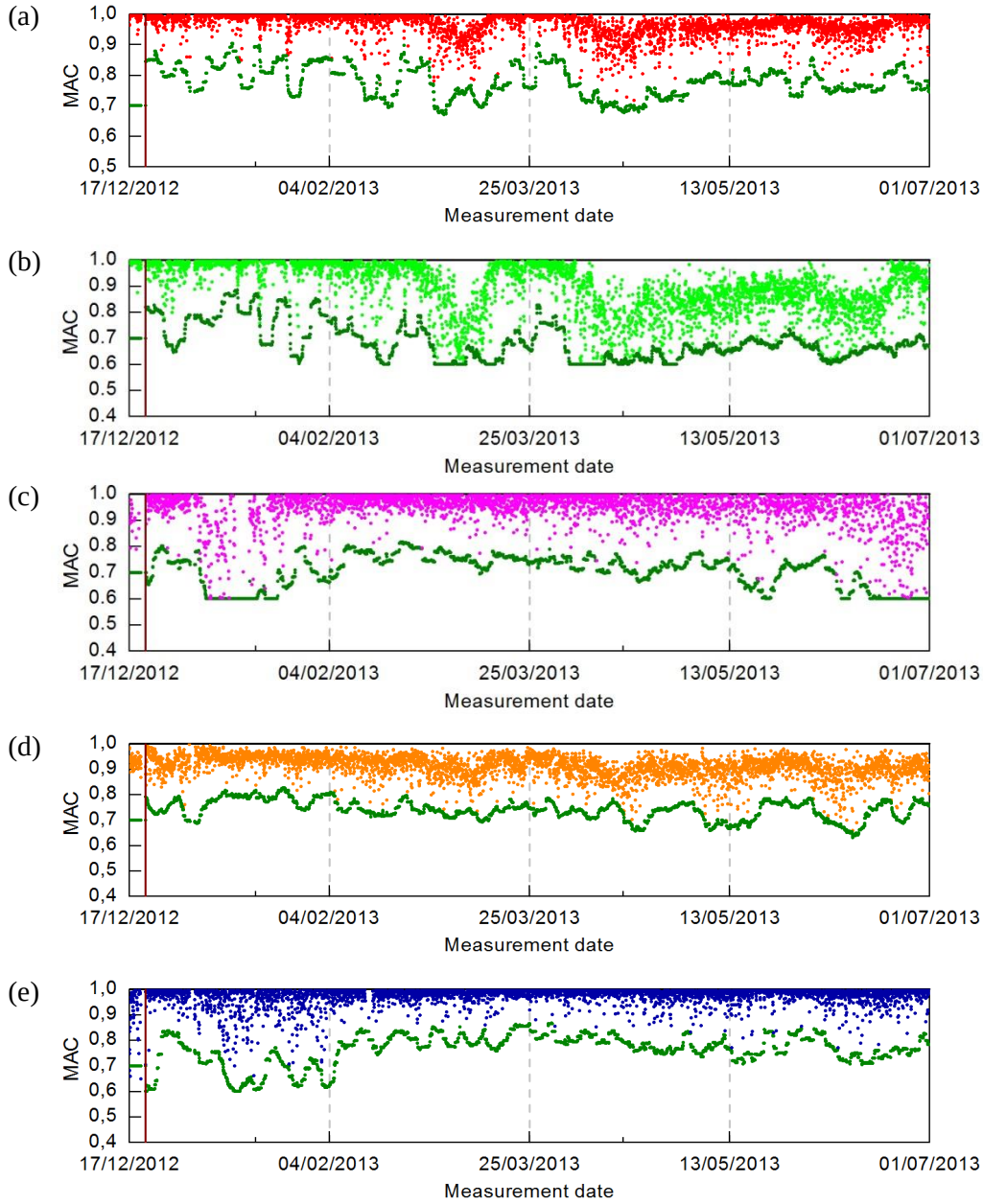

Fig. 6.7. Time evolution (from 17/12/2012 to 30/06/2013) of the MAC value and the corresponding adaptive threshold: (a) First bending mode; (b) Second bending mode; (c) Third bending mode (II order) (d) Torsion mode; (e) Local mode.

6.3.5 Comparison between manually identified results and automatically provided outputs

In order to demonstrate the reliability of the developed tools in real applications, the automatically extracted results obtained by the analysis of seven months of data continuously collected on the *Gabbia Tower* were compared with those obtained by a manual interpretation of the stabilization diagram provided by the SSI-Data method implemented in the commercial software ARTeMIS .

The investigated monitoring period spans from 12/12/2012 to 30/06/2013 and includes 4651 1-hour datasets, each composed of three collected acceleration time series.

Fig. 6.8 shows the variations of the modal frequencies, obtained by the manual investigation (**Fig. 6.8**(a)) and by the automated approach (**Fig. 6.8**(b)), respectively. A comparison between the diagrams highlights a clear similarity between manually and automatically obtained results. Moreover, the time evolution of the local mode (blue line) confirms the robustness of the implemented MT algorithm able to provide the evolution of the modal parameters also when they exhibit a significant change over time.

In conclusion, the main results are reported in **Table 6.1**. In particular, the first column identifies each vibration mode. In the the second and third column the success rate associated to manually and automatically extracted frequency is quantified, respectively. In the last column, the percentage of commonly identified values – within a frequency tolerance lower than 0.02 Hz – is reported, highlighting the goodness of the obtained results for the first two bending modes, the torsion mode and the local activation mode.

Concluding this paragraph, it is worth to highlight a vertical line (violet color) in both graphics of **Fig. 6.8**. This line puts in evidence the occurrence of a far-field seismic event that took place on 21/07/2013 and changed the dynamic behavior of the structure [Gentile et al. (2016)]. This condition was pointed out through an instantaneous frequency shift in all investigated natural frequencies [Gentile et al. (2016)].

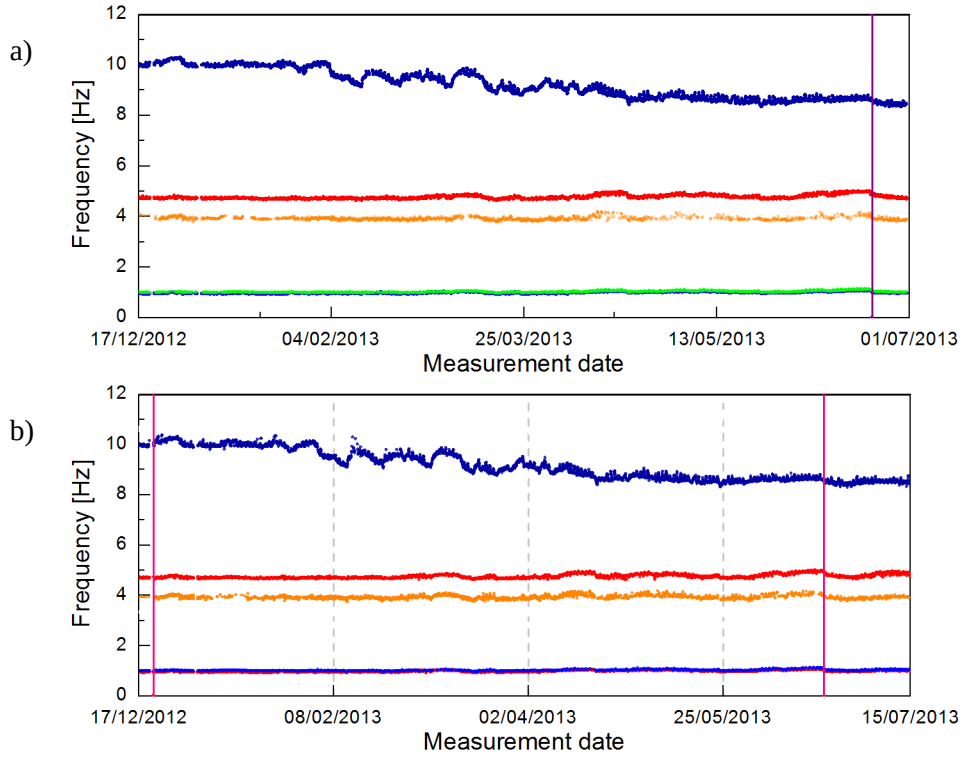

Fig. 6.8. Time evolution of the identified natural frequencies: (a) Manual results from 17/12/2012 to 30/06/2013; (b) Automatically identified results from 17/12/2012 to 15/07/2013

Table 6.1. Comparison between manually and automatically identified natural frequencies.

Mode Type	Manual identification rate [%]	Automated identification rate [%]	Correspondences with Δf<0.02 Hz [%]
1st bending	80.97	95.16	95.43
2nd bending	80.56	88.11	94.22
3rd bending	31.25	69.98	47.21
Torsion	76.53	93.18	91.06
Local	78.89	91.96	92.19

This phenomenon can not be appreciated by the global scale used to represent the frequency evolutions reported in **Fig. 6.8**, so a clearer representation of the first two frequencies was reported in **Fig. 6.9**. From the inspection of the diagrams in **Fig. 6.9** the daily fluctuation of the natural frequencies induced by temperature variations together

with the frequency shifts occurred during the seismic event are clearly identified [Saisi et al. (2015), Saisi and Gentile (2015)]. Moreover, an excellent match between the manual and automatically results is highlighted in the diagrams depicted in **Fig. 6.9**.

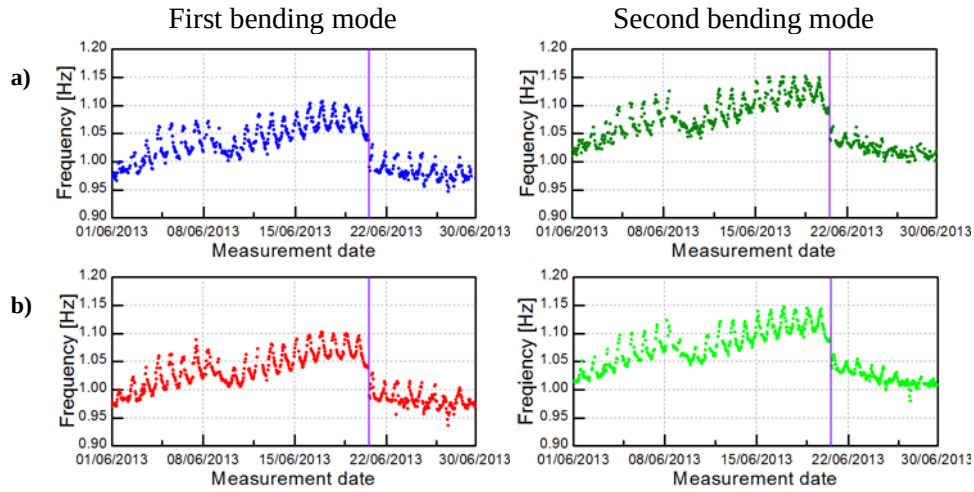

Fig. 6.9. Zoom of the first and second natural frequency obtained during the monitoring period from 01/06/2013 to 30/06/2013; a) Manually detected modes (blue and olive colors, respectively); b) Automatically provided modes (red and green color, respectively)

6.4 Application to data collected on the *San Michele Bridge*

6.4.1 Brief introduction of the case study: San Michele Bridge

The developed MT algorithm was used to extract the evolution in time of the modal parameters estimates obtained by the continuous analysis of the data collected on an important ancient Italian bridge: the *San Michele Bridge* [Busatta (2012), Gentile and Saisi (2015)]. As already described in the previous Chapter, this ancient bridge is one of the most important Italian Cultural Heritage monuments of the 19th century. It was built in 1889 and it consists of an iron arch that supports a box girder, linking two small towns in the neighborhood of Milan.

For the main characteristics and the relevant issues related to the poor state of conservation of the bridge, the reader is remanded to Chapter 5, in which a review of the main results obtained in the previous analysis campaign is reported in detail.

Fig. 6.10. View of the *San Michele Arch Bridge*

It should be remarked that the modal parameters estimations of the bridge were extracted using the SSI-Cov identification technique and applying the MPE procedure that involves the construction and the automatic interpretation of tri-dimensional stabilization diagrams described in Chapter 5.

Once again, since the acceleration time series of the lateral and the vertical components were collected separately, in this application only the horizontal accelerations were processed. Moreover, as will be demonstrated in the next paragraphs, a particular period of monitoring, in which the bridge was subjected to extreme environmental conditions, has been selected demonstrating the full adaptability of the developed methodology in the identification of the modal parameters even in case of high variation in the "normal" behavior of the structure.

6.4.2 Definition of the reference modes for the continuous monitoring of the bridge

As reported in previous works [Gentile and Saisi (2015), Cabboi et al. (2013)] 15 lateral modes of the bridge were expected. The input parameters of the algorithm proposed herein were set as follows: all 7 available channels were considered as references, the time-lag interval was set from 20 to 100 (increasing value equal to 10) and the model order interval equal to 40-140 (adopting a step value equal to 2). Moreover, the interval investigation frequency was maintained between 0 and 5 Hz as highlighted in **Fig. 6.11**.

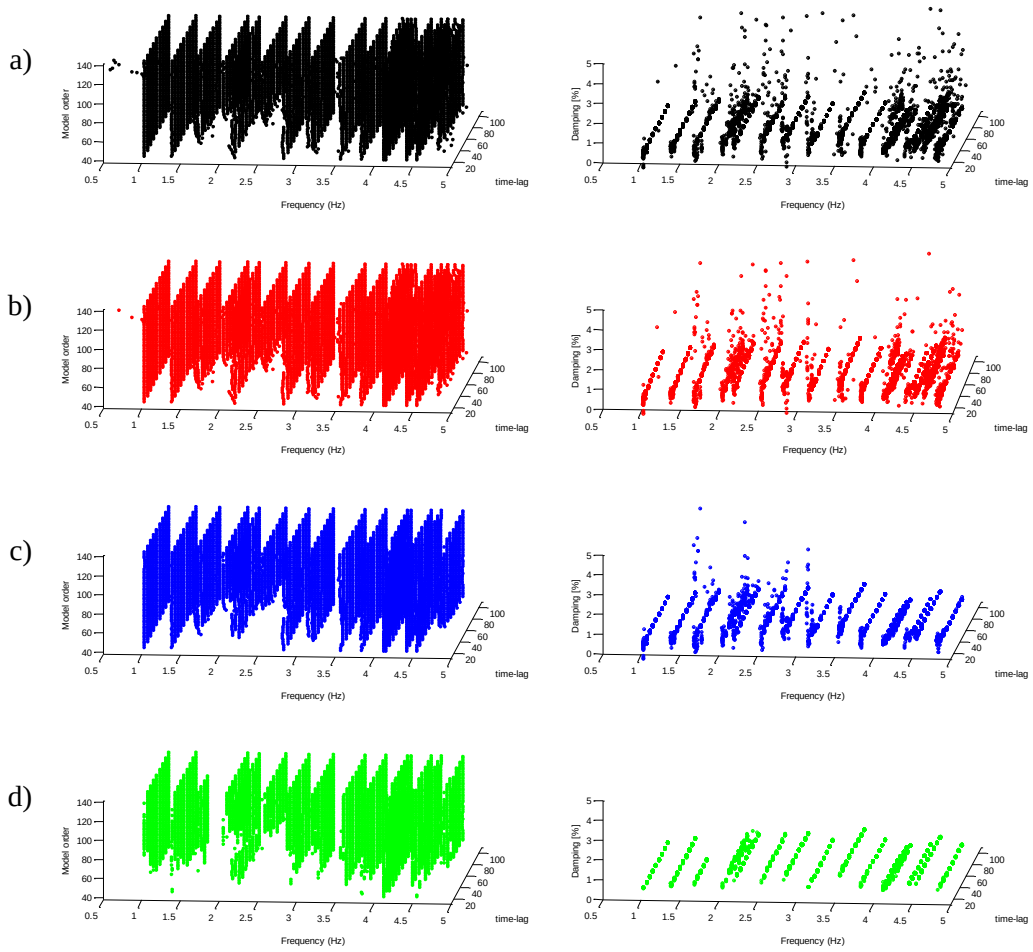

Fig. 6.11. Stabilization diagram and frequency vs damping representation of the reference modes obtained by the application of the 3D-MPE algorithm: (a) SSI outputs, (b) estimates after pre-filtering, (c) resulting clusters and (d) final outputs.

According to the previous analysis reported in Chapter 5, in which the complexity component of the structural modes is highlighted, the chosen user-defined parameters adopted to remove most of the spurious poles in the tri-dimensional stabilization diagram and perform the clustering process were set in a conservative way maintaining the values already defined. Therefore, the thresholds were set equal to 0.4 and 25° for MPC and MPD respectively and adopting an inter-cluster distance tolerance limit equal to 0.025.

Adopting the aforementioned criteria, some trial tests were carried out in order to find the reference baseline list needed to perform the automated monitoring of the bridge. However, the most representative set of structural modes was extracted by the report recorded on *19/01/2012* at *4 p.m*. The resulting clusters that stand out in the stabilization diagram, after the application of the 3D-MPE algorithm, are depicted in **Fig. 6.11** together with the corresponding frequency vs damping diagrams.

In **Fig. 6.12** the graphical representations of the 15 lateral modes of the bridge automatically extracted applying the 3D-MPE algorithm is shown in detail.

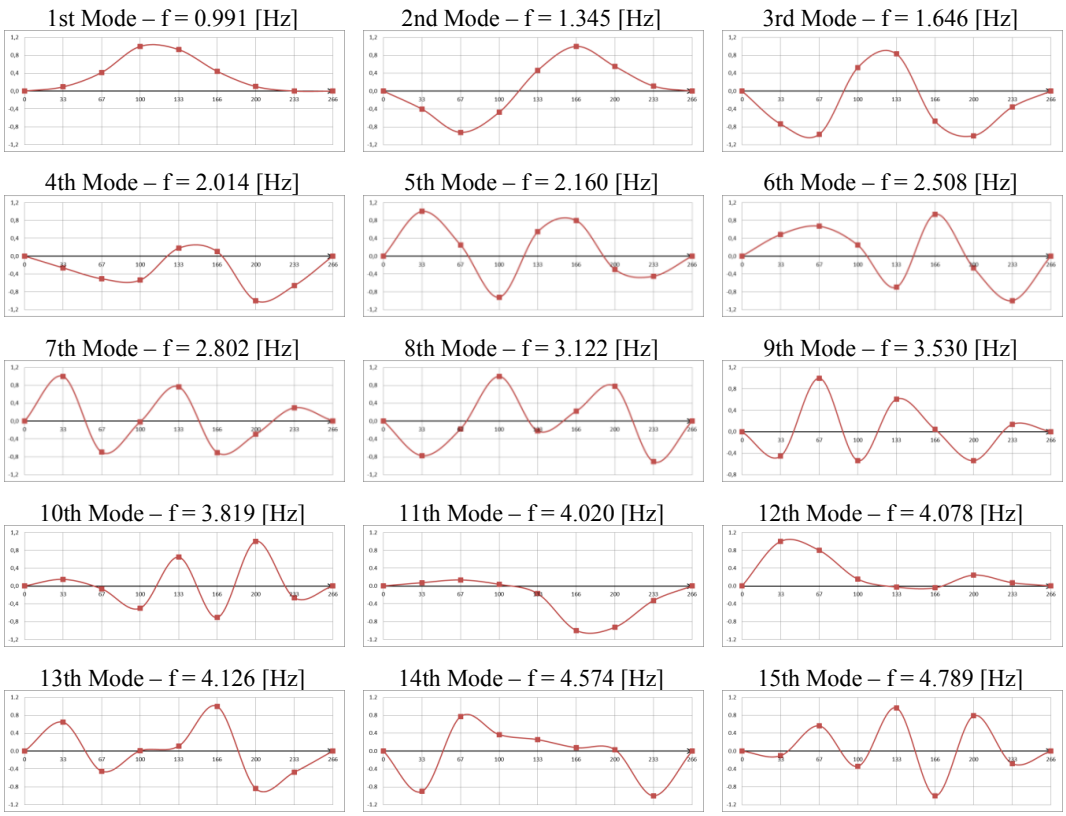

Fig. 6.12. Vibration modes automatically identified by the proposed methodology.

Table 6.2 summarizes the main results in terms of natural frequency, modal damping ratio and complexity values automatically obtained by the application of the 3D-MPE algorithm to the output responses collected on the 19th of January 2012.

Table 6.2. Modal parameters, standard deviations and complexity values of obtained modes

n°	f [Hz]	σ(f) [Hz]	ξ [%]	σ(ξ) [%]	MPC	MPD
1	0.991	0.0001	0.33	0.0137	0.999	0.83
2	1.345	0.0001	0.56	0.0269	0.997	1.59
3	1.646	0.0002	0.60	0.0132	0.992	2.03
4	2.014	0.0004	0.55	0.0076	0.983	3.60
5	2.160	0.0004	0.78	0.0101	0.980	3.75
6	2.508	0.0002	0.75	0.0021	0.895	8.70
7	2.802	0.0002	0.89	0.0208	0.972	4.92
8	3.122	0.0006	0.53	0.0051	0.895	11.26
9	3.530	0.0013	1.12	0.0231	0.974	5.17
10	3.819	0.0006	0.63	0.0122	0.919	8.21
11	4.020	0.0117	0.42	0.3688	0.846	10.77
12	4.078	0.0029	0.25	0.0321	0.898	10.96
13	4.126	0.0014	0.35	0.0069	0.981	4.55
14	4.574	0.0004	0.41	0.0056	0.909	6.74
15	4.789	0.0007	0.40	0.0130	0.933	8.53

Moreover, using the polar plot representation, the complexity degree associated to the identified structural modes is highlighted. As described in [Cabboi (2013)], the high complexity of the mode shapes could depend on various factors (i.e. linkage, high noise ratio, synchronization problem) and non-linear behavior of the structure (generally related to non-proportional damping or hysteretic factors). For this case study, the previous assumptions can be justified by the poor state of maintenance of the structure subjected to high corrosion of the iron components.

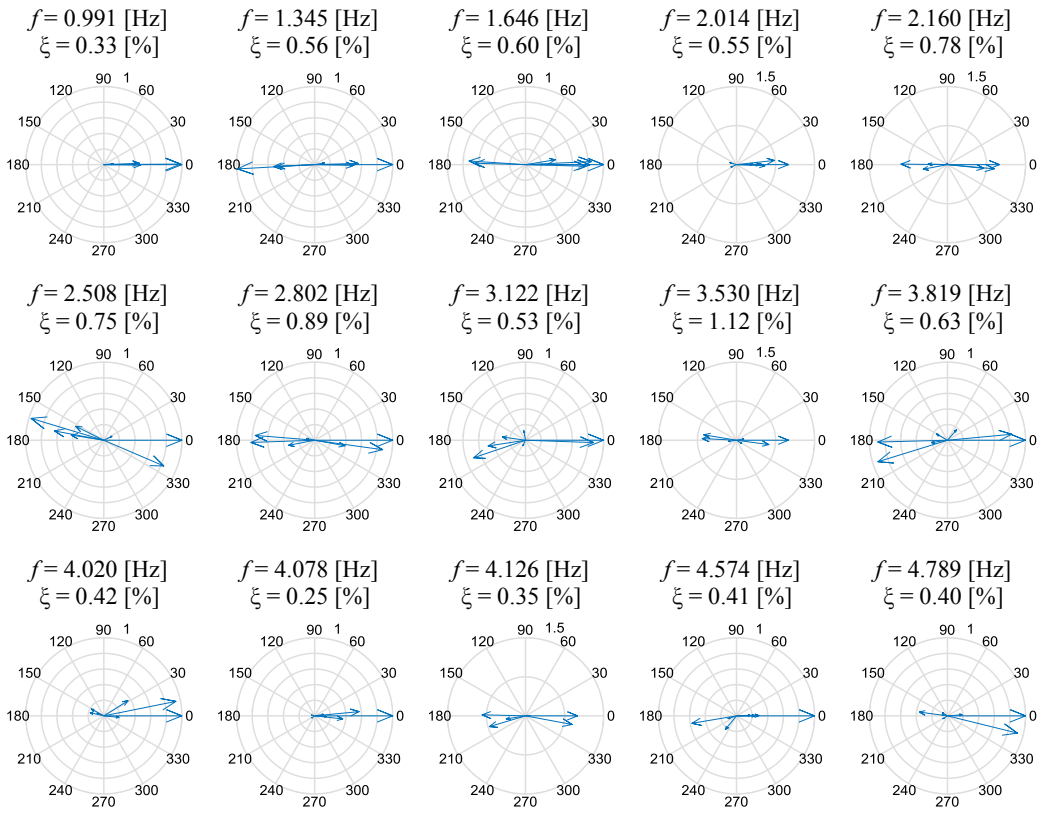

Fig. 6.13. Reference parameters of the first 15 modes: natural frequency, modal damping ratio and mode shapes represented in a polar plot

6.4.3 Tracking of the natural frequencies and mode shape variations of the bridge

As already pointed out, the input parameters provided to the automated MT algorithm consist of a baseline list of reference modes with the corresponding fixed thresholds. The modes shapes and the natural frequencies reported in **Fig. 6.13** represent the reference modes adopted for the tracking.

The results presented in this paragraph refer to the interval of monitoring from 19/01/2012 to 31/03/2012, in which the bridge was subjected to an intense snowfall that strongly characterized the dynamic response of the bridge. In fact, in the winter period

(February 2012) extreme thermal conditions changed the "normal" behavior of the structure. The modal parameters changed dramatically and they only gradually recovered their previous values after a period of two weeks, when the extreme conditions disappeared.

The collected data were analyzed automatically, using the identification tools developed during this work. In particular, the initial thresholds were defined taking in to account the daily fluctuations of the modal parameters (i.e. natural frequencies and mode shapes) and they were set as follows: $d_{i,max}^{f}$=0.20 Hz and $d_{i,max}^{MAC}$=0.10, respectively. Meanwhile, due to the high number of reference sensors and the good quality of the recorded signals, the length of the training period was set equal to only 2 days. Hence, the reference modes together with the rejection thresholds became self-adaptive after only 48 hours, guaranteeing the full automation of the process and avoiding any further user interactions (see **Fig. 6.15**).

The results of the automated identification based on the application of the developed OMA algorithms (3D-MPE and MT) are shown in **Fig. 6.14**. Both diagrams show the thermal effects of the extremely low temperatures on the natural frequencies (see **Fig. 6.14**(a)) and on the mode shapes (see **Fig. 6.14**(b)) (through MAC value) of all investigated lateral modes.

Furthermore, the inspection of the diagrams reveals a very good performance of the MT algorithm. In fact, all expected modes were identified exhibiting a fairly good success rate even in anomalous conditions and high variations of both modal parameters (i.e., natural frequency and mode shape) without relevant loos of identification.

The diagrams point out the strong dependence of the modal parameters on temperature variations. As can be observed, the thermal effect is clearly visible on all extracted natural frequencies. On the contrary, the impact of the freezing temperature seems not to affect the mode shapes with lower frequencies; meanwhile, such effect is clearly visible on the mode shapes of higher structural modes.

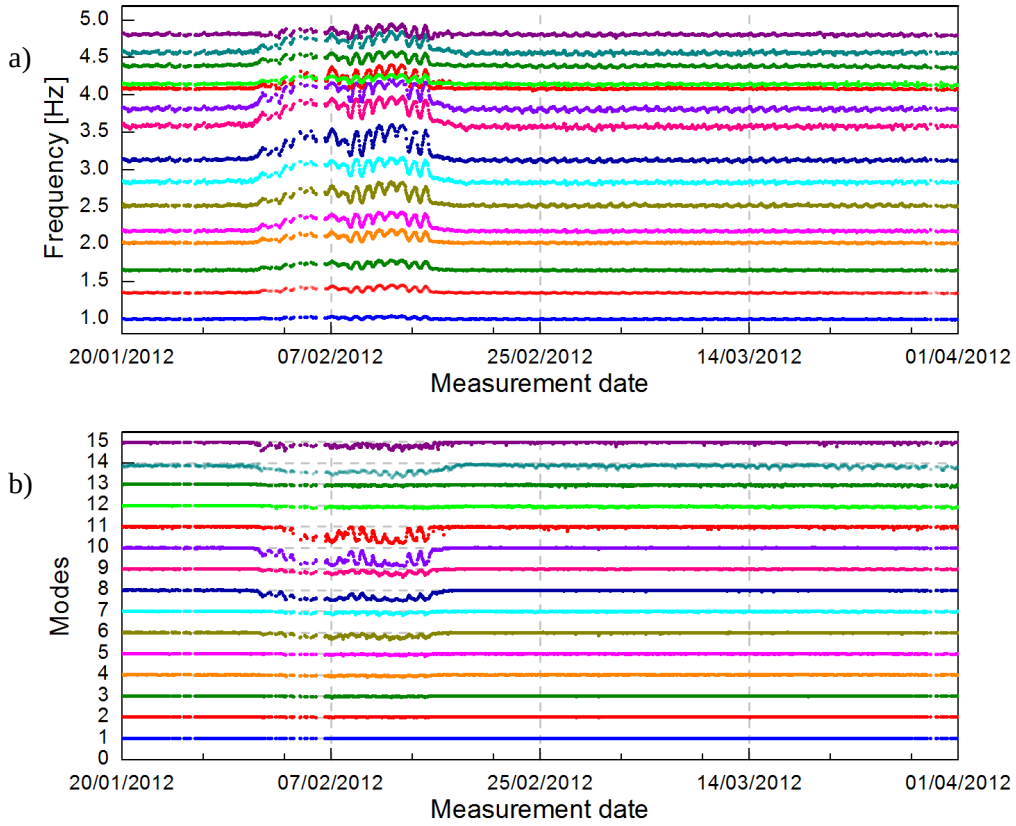

Fig. 6.14. Tracking results of the modes automatically identified during the period from 20/02/2012 to 31/03/2012; (a) Evolution of the natural frequencies; (b) Evolution of the MAC index associated to each investigated mode.

Clearer illustrations of trends of the modal features together with the associated adaptive thresholds are reported in **Fig. 6.15**. Specifically, the plots are referred to the 4th, 7th, and 9th identified mode of the bridge. From the outcomes obtained at the end of the freezing period, it is possible to point out the cyclic evolution of the natural frequencies, strongly driven by daily temperature fluctuations.

On the contrary, the tracking of the MAC values reveals a non-relevant dependence of mode shapes estimates on daily temperature variations and this seems to demonstrate that mode shapes are less sensitive to environmental effects. Despite this result, during the *ice-period* the mode shapes variations are clearly highlighted.

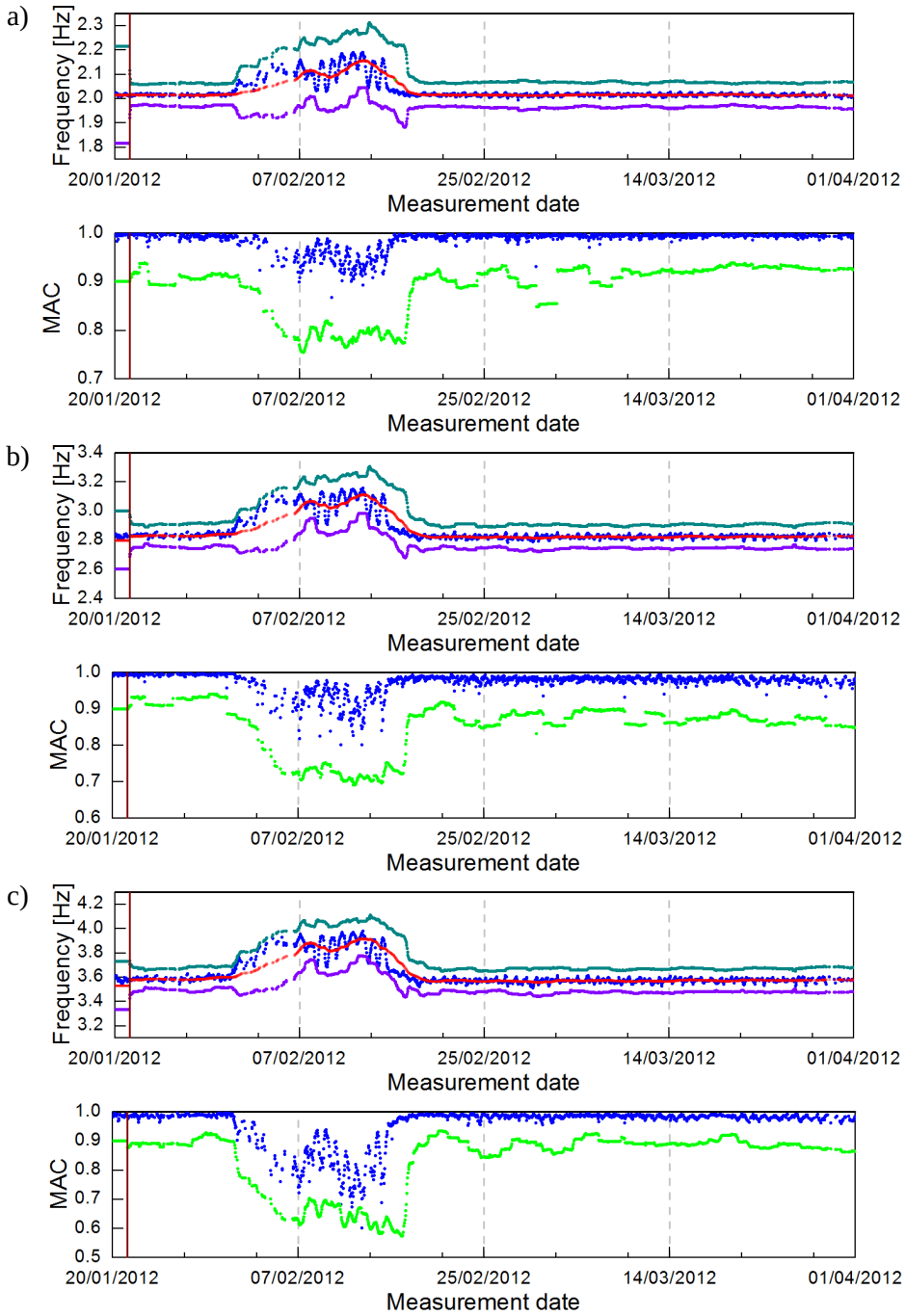

Fig. 6.15. Evolution of the natural frequency and the MAC index in the monitoring period from 20/01/2012 to 31/03/2012 associated to: (a) 4th, (b) 7th and (c) 9th modes.

6.5 Conclusions

In the present Chapter a new strategy for MT is described and exploited in detail. The innovative approach introduced by the developed procedure is characterized by the simple design of the thresholds, calculated using only a limited array of previous estimates. This approach has proved to be effective allowing for the automated monitoring of the investigated structure with less computational effort with respect to other existing approaches.

Moreover, the array of data defined as *tracking window*, used to continuously update the dynamic thresholds and the reference frequencies, ensures a greater adaptability of these parameters during the tracking process. It is worth highlighting the capability of the procedure to cover the effects induced by extreme environmental conditions or anomalous structural behavior, avoiding the failure of the process.

As demonstrated in the first application, the MT procedure does not fail in the continuous identification of the structural modes (more specifically of the local mode) even in case of anomalous variations of the dynamic features. In this case, the choice of a short training period (only 4 days) seems to be effective for the correct tracking. Meanwhile, in the second case study, the procedure delivers an accurate evolution of the modal parameters also in case of strong changes caused by thermal effects, needing two days of training.

Furthermore, the validation of the whole algorithm was carried out through a comparison between the results obtained by the automated algorithm and those independently obtained by a manual interpretation of a large number of stabilization diagrams using ARTeMIS. A very good match among automatically and manually extracted values is provided, demonstrating the robustness of the developed method.

Chapter 7

DAMAGE DETECTION STRATEGY BASED ON PATTERN RECOGNITION MODELS

Contents

7.1 Introduction

Support Vector Machines (SVMs) are popular techniques for forming decision boundaries that separate data into different classes. Interesting papers and excellent books present in literature describe these techniques and their application in different research fields. Comprehensive reading of the main concept related to SVMs can be obtained from [Schölkopf et al. (2000), Tax and Duin (1999)], whereas for a deeper analysis the excellent book [Bishop (2006)] is suggested. These techniques belong to that class of methods used for classification problems called domain-based novelty detection that requires the definition of a boundary margin based on training data. Typically, they are not sensitive to specific sampling or density of the target class because they describe the target using a boundary, or a domain, and not through the class density. This means that the boundary, or better to say the novelty boundary, is not detected by all datapoints of the input data, but it is obtained through the location of those data that lie closest of the boundary itself (normally detected in a transformed space), called support vectors. Hence, the distribution of the datapoints that are not support vectors are not included in the identification of the decision boundary, as demonstrated in [Tax and Duin (1999), Hu et al. (2003)].

Originally, the SVM models were developed because ideally suited for binary pattern recognition and used to perform the classification of data linearly separable. Hence, through adopting support vectors these techniques can separate and classify the input data constructing and maximizing the separating margin between two classes.

Since the introduction of the original idea, described in the next Section, several improvements have been implemented to make the algorithm more robust and efficient, such as: (a) the Robust Support Vector Machines (RSVMs) algorithm, developed to address the overfitting problem caused by the noise in the training dataset [Hu et al. (2003)] or (b) the strategy developed by [Schölkopf et al. (2000)] in which the novelty boundary condition is defined through a kernel function obtained transforming the input

data from the original space into a "feature space". Another approach, the Support Vector Data Description (SVDD) method, proposed by [Tax and Duin (1999)], defines the novelty boundary adopting hyperspheres with minimum volume the cover all (or almost all) the "normal" class.

Moreover, some extension of the SVDD approach have recently been proposed [Wu and Ye (2009)] to improve the margin boundary using small spheres and large margin or using some slack variable and set of hyperspheres with different centers and radii [Le et al (2011)]. In the last decades, large amount of works presents in the literature has been produced on the use of SVM methods for classification and novelty detection problems, some of them are shown below in order to provide a more accurate view of these applications in very different fields [Manevitz and Yousef (2002), Sotiris et al. (2006), Li (2008), Li et al. (2011)].

Over the years, different algorithm based on SVM have been implemented and improved aimed at solving most disparate classification problems in several research fields. This trend has also interested the Civil Engineering field, addressing special attention to application regarding damage assessment. Hence, during the past years, several methods of novelty procedure for SHM purposes have been proposed in literature. In general, most of these methods consist of evaluating some indexes or indicators that allow for detecting any possible anomalies and damages on the structure, possible locations and even the extension of the damaged regions [Yan et al. (2007)], determining if in the structure is present an abnormal behavior associating a probability of "true detection" (probability of detect the damage in the structure when it is affectively present in the mechanical system).

On other hand, in SHM approaches for civil engineering structures the first step consists of detecting the occurrence of anomalies in the normal structural behavior, and subsequently localize such anomalies in the structure. For this purpose, several studies have been performed using statistical tests and pattern recognition approaches based on comparison of data extracted by healthy and damaged conditions [Zhang (2007), Iwasaky

et al. (2004)]. These approaches are efficient and useful when the structural response can be obtained with high level of confidence. Moreover, these methods proved to be effective when relatively small sets of data are used for the training and testing phase, however large number of features and input data lead to hard time consuming [Chun et al. (2005)].

A strategy to detect possible anomalies was described in [Guo (2006)]. From the results obtained by the application of this methodology was demonstrated how the loss of information can lead to an incorrect classification providing false alarms for damage detection. Many other techniques have been developed to detect several damage scenarios using modal parameters estimations, an excellent work is described in [Trendafilova and Heyleno (2003)] where an unsupervised learning classification algorithm was developed and used to detect several structural damage states through the natural frequencies extracted by vibration responses of a cantilever bean.

7.2 SHM procedures using pattern recognition models: background

As previously pointed out, SVM algorithms are aimed at separating two different classes using a discrimination function which is automatically computed during the classification process of the training datasets. Within the context of SHM and damage detection of civil engineering structures [Sohn et al. (2002)], two classes of data are assumed over time, corresponding to undamaged and damaged condition.

Although, SVM algorithms are normally used for two-class classification problems, extension to multi-classes classification can be done but this aspect will not be treated in this Dissertation, because the SHM procedure proposed herein is developed following a binary condition: absence or presence of damage, and no other states are allowed.

Hence, in order to simplify the discussion about the pattern recognition algorithms proposed herein an important clarification has to be done: the novelty detection strategy developed in this work was implemented in order to distinguish between and classify series of data belonging to two different classes. Therefore, for each run of the algorithm, if the classification fails it means that data are not separable, then they belong to the same class. Otherwise they are separable.

In SHM applications if the classification does not provide a clear separation of the data means that the structural damage is not identified. On the contrary, the successful detection of two classes implies that an instantaneous damage or a structural anomaly occurred in the monitored system.

The SVMs are generally based on a geometric approach, consisting of the construction of an optimal separating surface – a hyper-plane – which divides the data population in two groups with different statistical characteristics. The hyper-plane is equidistant from the two classes defining a margin zone between them. Similarly to Neural Network classification, the input data are supposed to belong to different classes and the outputs consist of the target binary vectors (labels) corresponding to each class. In case of linear separable data, the SVM algorithm searches the optimal solution to classify the data by maximizing the distance between the hyper-plane and the extreme values of the two classes, so called Support Vector (**Fig. 7.1**).

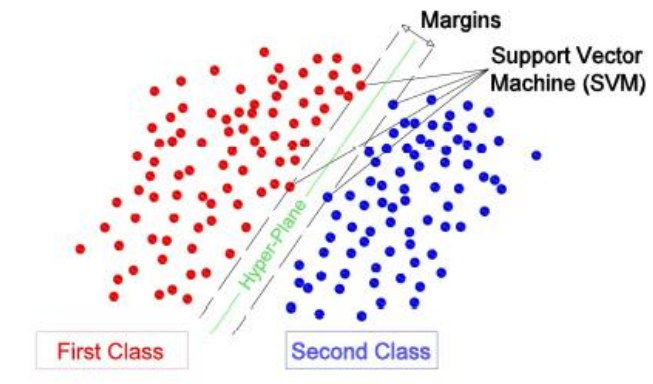

Fig. 7.1. Scheme of two separated classes through hyper-plane and support vector

7.2.1 Support Vector Machine: maximum margin classifiers

This paragraph begins with the construction of the separating surface between two simple classes of data composed by few data points that consists on the basic steps of more sophisticated pattern recognition models. Hence, the simplest representation of linear discriminant function of a vector of data x is obtained as follows:

$$y(x) = w^T x + w_0 \tag{7.1}$$

where w is called weight vector, and w_0 is a bias (not be confused with bias in statistical sense). Defining with *D* the dimensional space of the input data, the correspond decision boundary is defined by the relation $y(x) = 0$ which corresponds to a *(D-1)*-dimensional hyperplane within *D*-dimensional input space. So, an input vector x is assigned to class C_1 if $y(x) \geq 0$ and class C_2 otherwise. Considering two points $x_A$and x_B both of which lie on the decision surface, because it is $y(x_A) = y(x_B) = 0$ the vector w that is orthogonal to every vector lying within the decision surface if given by the equation: $w^T(x_A - x_B) = 0$. Then, the vector w determines also the orientation of the decision surface. Similarly, if x is a point of the decision surface, then $y(x) = 0$, the normal distance from the origin to the decision surface is given by:

$$\frac{w^T x}{\|w\|} = -\frac{w_0}{\|w\|} \tag{7.2}$$

where the bias parameter determines the location of the decision surface. Moreover, the value of y(x) gives a signed measure of the perpendicular distance r of the point x from the decision surface. Considering an arbitrary point x and let $x_\perp$be its orthogonal projection onto decision surface, the equation of x is given by:

$$x = x_\perp + r\frac{w}{\|w\|} \tag{7.3}$$

Therefore, multiplying both sides of this results for $\boldsymbol{w}^T$ and adding w_0, using **Eq. 7.1** it is possible to obtain:

$$r = \frac{y(x)}{\|w\|} \tag{7.4}$$

A geometrical illustration of a linear discriminant function is shown in **Fig. 7.2**. The decision surface, shown using the red line, it is perpendicular to w and its displacement from the origin is controlled by the w_0. It is also designed the orthogonal distance from a general point x from the decision surface is given by $y(x)/\|w\|$.

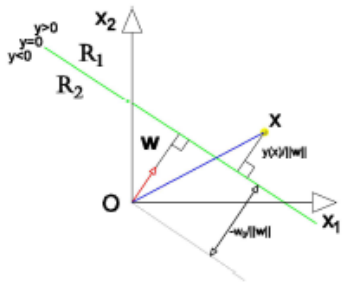

Fig. 7.2. Construction of a simple decision surface between the origin and a generic point

SVM began popular some year ago for solving problem in classification and regression and novelty detection; an important property of support vector machines is related to the definition of the model parameters obtained through solving a convex optimization problem, in which any local solution corresponds to a global optimum. To highlight this property the two-class classification problem is defined using a linear model as follows:

$$y(x) = w^T\Phi(x) + b \tag{7.5}$$

where $\Phi(x)$ denotes a fixed future-space transformation and b the bias parameter. The dual representation is described in terms of kernel function, in which the training datasets comprises N input vectors $x_1 \ldots x_N$ with corresponding target values $t_1 \ldots t_N$ where $t_n = [-1,1]$, and the new data points x are classified according to the sigh of $y(x)$.

Assuming that the training point are linearly separable in a feature space, there is at least one choice of the parameters w and b that allows the function represented in the form expressed in **Eq. 7.5** satisfies the conditions: $y(x_n) > 0$ for points having $t_n = +1$ and $y(x_n) < 0$ for points having $t_n = -1$, that's means $t_n y(x_n) > 0$ for all training data.

Follow this way, there are many solutions to perform an exact separation of the classes and it depend on initial values chosen of w and b as well as on the order in which the data points are presented. Normally, the aim is to try to find the solution that give the smallest generalization error.

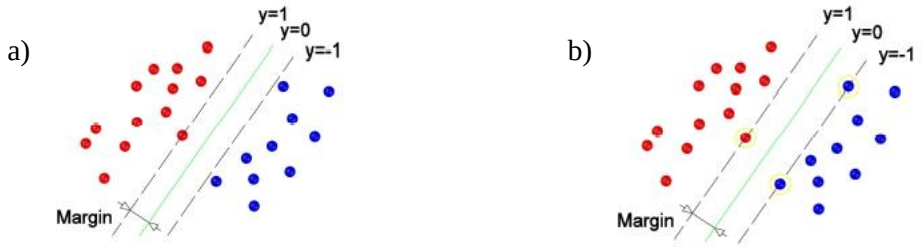

Fig. 7.3. Margin between two classes of data: a) general solution, b) maximization of the margin

The support vector machine approach tends to solve this problem thought the use of the concept of the margin, which is defined by the smallest distance between the decision boundary and any sample points. As demonstrate in **Fig. 7.3**, the SVM technique the decision boundary is chosen to be the one in such margin is maximized (see **Fig. 7.3**b).

The perpendicular distance of a point x from a hyperplane defined by $y(x) = 0$ where $y(x)$ takes form from **Eq. 7.5** is given by $|y(x)|/\|w\|$. The optimal surface is calculated taking into account all the solution in which all data points are correctly classified, in other words, the optimal surface is detected when $t_n y(x_n) > 0$ for all n. Therefore, the distance of a point x_n to the decision surface is given by:

$$\frac{t_n y(x_n)}{\|w\|} = -\frac{t_n y\left(w^T \Phi(x_n) + b\right)}{\|w\|} \tag{7.6}$$

The maximum margin solution is found optimizing the parameters ***w*** and b that minimize the distance of the closest point x_n from the data set, as follows:

$$\max_{w,b}\left\{\frac{1}{\|w\|}\min_n\left[t_n y\left(w^T \Phi(x_n) + b\right)\right]\right\} \tag{7.7}$$

The direct solution of this problem would be very complex; thus, it is converted into an equivalent problem that is much easier to solve. The simplification is performed to re-scaling w → kw and b → kb, the decision surface is given by unchanged formula:

$$t_n y\left(w^T \Phi(x_n) + b\right) = 1 \tag{7.8}$$

obtained scaling the formula expressed in **Eq. 7.6** by the values $t_n y(x_n)/\|w\|$. So, if all data points are close to the surface and satisfied the following constraints:

$$t_n y\left(w^T \Phi(x_n) + b\right) \geq 1 \qquad n = 1 \dots N \tag{7.9}$$

then, **Eq. 7.9** is the canonical representation of the decision surface (i.e. hyperplane) [Bishop (2006)]. and the optimization problem re-written in this form simply requires the maximization of the $\|w\|^{-1}$to be solved, which is equivalent to minimizing $\|w\|^2$. Therefore, the next equation is used to solve quadratic programming problem trying to minimize a quadratic function subjected to a set of linear inequality constraints:

$$\min_{w,b} \frac{1}{2}\|w\|^2 \tag{7.10}$$

Furthermore, to solve the constrained optimization problem, the Lagrange multipliers are introduced (i.e. $\alpha_n \geq 0$). Follow this way, for each constraint in **Eq. 7.9** the Lagrangian function must be solved:

$$L(w, b, \alpha) = \frac{1}{2}\|w\|^2 - \sum_{n=1}^{N} \alpha_n \cdot [t_n y\left(w^T \Phi(x_n) + b\right) - 1] \tag{7.11}$$

where $\alpha = (\alpha_1, \alpha_2, \dots, \alpha_n)$ where each multiplier corresponds to each constraint. In order to solve the problem defined in **Eq. 7.11** the derivatives of $L(w, b, \alpha)$ with respect to w and b are set equal to zero, obtaining the conditions expressed in the following equations:

$$w = \sum_{n=1}^{N} \alpha_n t_n \Phi(x_n) \tag{7.12}$$

$$0 = \sum_{n=1}^{N} \alpha_n t_n \tag{7.13}$$

Finally, removing w and b from $L(w, b, \alpha)$ using the conditions in **Eqs. 7.14** and **7.13**, the dual representation of the maximum margin problem is given by:

$$\tilde{L}(\alpha) = \sum_{n=1}^{N} \alpha_n - \frac{1}{2} \sum_{n=1}^{N} \sum_{m=1}^{M} \alpha_n \alpha_m t_n t_m k(x_n, x_m) \tag{7.14}$$

in which $\tilde{L}(w, b, \alpha)$ subjected to the following constrains has to be minimized:

$$\alpha_n \geq 0 \quad n = 1, \dots, N \tag{7.15}$$

$$\sum_{n=1}^{N} \alpha_n t_n = 0 \tag{7.16}$$

In **Eq. 7.14** it is also defined as kernel formulation [Bishop (2006)] of the dual problem, in which the kernel function is defined by $k(x, x') = \Phi(x)^T \Phi(x')$. Until this point the SVM model has been introduced under the hypothesis that training data points were linearly separable in the feature space $\Phi(x)$ and the resulting support vector machine provides the exact classification of the training data of the original input space x. The problem is defined as a quadratic programming problem in which a quadratic function needs to be optimized subjected to α_n constraints. The kernel formulation also makes clear the role of the constraints that ensuring the kernel function be positive definite, which means that Lagrangian function is bounded below.

Concluding, the new points can be evaluated through the sign of y(x) defined in **Eq. 7.5** Such equation can be re-written expressing the value of the parameters $\{\alpha_n\}$ and substituting w (**Eq. 7.12**) in the kernel function, giving the following formula:

$$y(x) = \sum_{n=1}^{N} \alpha_n t_n \Phi(x, x_n) + b \tag{7.17}$$

Moreover, several kernel function can be used to define the optimal separation surface and maximizing the margin between the two separable classes as: linear function, polynomial function (with different order), kriging function, radial basic function, Sigmoid function, etc. After some initial tests, best results in the classification of the data were obtained adopting Gaussian Radial Basis (GRB) function. Accordingly, the GRB function was adopted as kernel function of the SVM model to construct the hyper-plane surface for all further applications developed in this Dissertation.

7.2.2 Overlapping class distribution: generalization using soft margin

In practice, the problem of the minimum of $\tilde{L}(\alpha)$ (**Eq. 7.14**) subjected to the constraints described in **Eq. 7.15** and **Eq**. **7.16** is ill-conditioned because the class-distributions are not always well-separated, and they may overlap, so the separating surface which correspond at an exact separation of the training data can lead to a poor generalization. Accordingly, the mathematical approach used to construct the separating surface is modified and improved in order to permit to any data-points be on the "wrong side" of the margin boundary.

The strategic approach is developed to provide a penalty value to each misclassification and such penalty increases with the distance of the boundary surface. More specifically, a slack variable, $\xi_n \geq 0$ with $n = 1 \ldots N$, was introduces for each training data point. For the data points that are inside or on the correct side of the margin boundary these variable values are equal to zero, meanwhile such values are equal to $\xi_n = |t_n - y(x_n)|$ for other points. For those points that are on the decision boundary conditions $y(x_n) = 0$ they have $\xi_n = 1$, on the contrary, points with $\xi_n > 1$ are misclassified. A simple graphical description is given by **Fig. 7.4**, where some points belong to a specific class are misclassified fallen in the opposite side defined by the decision surface: $y(x) = 0$.

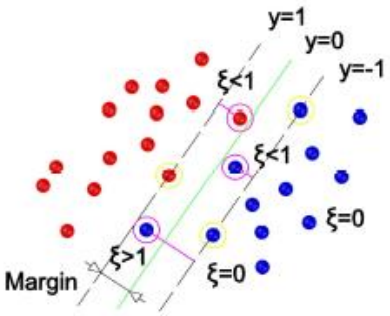

Fig. 7.4. Misclassified points that fallen outside decision boundary (red line)

The classification constraints described in **Eq. 7.9** are replaced with:

$$t_n y(x_n) \geq 1 - \xi_n \qquad n = 1 \ldots N \tag{7.18}$$

in which the slack variables are constrained to satisfy $\xi_n \geq 0$. Detailing, those data points that have $\xi_n = 0$ are positioned on the margin or in the right side of the margin. Data points which $0 < \xi_n \leq 1$ lie inside the margin, in the correct side of the decision boundary. Meanwhile, those points which $\xi_n > 1$ are positioned on the wrong side of the decision boundary and they are misclassified. These new defined constraints avoid the construction of the hard margin constraint that can lead to an incorrect generalization of the data training allowing the creation of a soft margin that permits the misclassification of some points. It is worth noting that while stack variables permit the partial overlapping between the class distributions, this operation is still sensitive to the outliers because the penalty for misclassification increase with increasing distances of the points with respect to decision boundary, so it increases linearly with ξ.

Introducing the soft margin, the goal of this framework consists of minimizing the margin softly penalizing those points that fall outside the decision boundary. As stated, the formula that needs to be minimize is expressed in the following:

$$C = \sum_{n=1}^{N} \xi_n + \frac{1}{2}\|w\|^2 \tag{7.19}$$

where the parameter $C > 0$ controls the trade off between the slack variable penalty and the margin.

Hence, the minimization described in **Eq. 7.19** is subjected to new constraints (**Eq. 7.18**) which together with the assumptions of $\xi_n \geq 0$ lead to Lagrangian equation as:

$$L(w, b, \xi, \alpha, \mu) = \frac{1}{2}\|w\|^2 + C\sum_{n=1}^{N}\xi_n - \sum_{n=1}^{N}\alpha_n \cdot [t_n y(x_n) - \sum_{n=1}^{N}\mu_n\xi_n] \qquad (7.20)$$

where $\{\alpha_n \geq 0\}$ and $\{\mu_n \geq 0\}$ are Lagrangian multipliers that respect very restrained boundary conditions (see [Bishop (2006)]). Therefore, constructing the margin and optimizing with respect the w, b and $\{\xi_n\}$ as follows:

$$\frac{\partial L}{\partial w} = 0; \quad w = \sum_{n=1}^{N}\alpha_n t_n \Phi(x_n) = 0 \qquad (7.21)$$

$$\frac{\partial L}{\partial b} = 0; \quad \sum_{n=1}^{N}\alpha_n t_n = 0 \qquad (7.22)$$

$$\frac{\partial L}{\partial \xi_n} = 0; \quad \alpha_n = C - \mu_n = 0 \qquad (7.23)$$

Using the derivatives **Eq. 7.21**, **Eq. 7.22** and **Eq. 7.23** and eliminating w, b and $\{\xi_n\}$ from the Lagrangian equation, the result does not change respect to that one obtained for the separable data:

$$\tilde{L}(\alpha) = \sum_{n=1}^{N}\alpha_n - \frac{1}{2}\sum_{n=1}^{N}\sum_{m=1}^{M}\alpha_n\alpha_m t_n t_m k(x_n, x_m) \qquad (7.24)$$

The expression described in **Eq. 7.24** is identical to the one obtained for separable case - in which the data are well-separable in two difference classes without misclassifications (**Eq. 7.14)** except for the constraints that are somewhat different:

$$0 \leq \alpha_n \leq C \qquad (7.25)$$

$$\sum_{n=1}^{N}\alpha_n t_n = 0 \qquad (7.26)$$

Looking at last constraints, it is worth noting that $\alpha_n \geq 0$ because Lagrangian multipliers, as well as also $\mu_n \geq 0$, that implies $\alpha_n \leq C$. So, minimizing **Eq. 7.24** the constrains in **Eqs. 7.25** and **7.26** are obtained for $n = 1 \ldots N$. Furthermore, the **Eq. 7.25** is named *box constrains*.

Concluding, the Lagrangian equation form described in **Eq. 7.24** subjected to the constraints (**Eqs. 7.25** and **7.26**) and obtained minimizing **Eq. 7.20** with respect the w, b and $\{\xi_n\}$, represents a quadratic programming problem. Once again, it is worth to be remarkable that if the equation **Eq. 7.21** is substituted into **Eq. 7.5** the prediction of the new data points can be performed using **Eq.** 7.17**.** This can be easily expressed adopting an easy explanation: a subset of data-points that have $\alpha_n = 0$ do not contribute to the predictive modes describe in **Eq. 7.17.**, meanwhile the remain ones constitute the support vectors and they have $\alpha_n > 0$, hence they must satisfy the follow equation:

$$0 \leq \alpha_n \leq C \tag{7.27}$$

At this point, $\alpha_n < C$ if implies $\mu_n > 0$ that requires $\xi_n = 0$, so the points lie on the margin. Otherwise, if $\alpha_n = C$ the points fall inside the margin, and they are correctly classified if $\xi_n \leq 1$ or misclassify if $\xi_n > 1$. Finally, to determine the best value of b of **Eq. 7.5** all those points called support vectors in which $0 < \alpha_n < C$ and have $\xi_n = 0$ so that $t_n y(x_n) = 1$ will satisfy the following formula:

$$t_n \left(\sum_{m \in S} \alpha_m t_m k(x_n, x_m) + b \right) = 1 \tag{7.28}$$

and the numerical solution can be obtained by averaging:

$$b = \frac{1}{N_{\mathbb{M}}} \sum_{n \in \mathbb{M}} \left(t_n - \sum_{m \in S} \alpha_m t_m k(x_n, x_m) \right) \tag{7.29}$$

where $\mathbb{M}$ denotes the set of indices of data points having $0 < \alpha_n < C$.

7.2.3 Cross validation SVMs: k-fold technique

The cross-validation technique is frequently used to evaluate the capability of the SVM model to generalize the characteristics of the input data [Kohavi (1995)]. Moreover, this technique is largely employed in several problems with the objective of modeling prediction.

Frequently, the efficiency of the SVM models are defined through a single straightforward test divided into two consecutive phases: the training phase, in which a selected trance of input data is employed for the training of the algorithm (normally 75% of data are used for this first phase), and the test phase, in which the trained model is used to classify the remain 25% of data.

As already mentioned, this technique is commonly used for different problem studies where the prediction of some characteristics belong to data-population plays an important role in the classification problem. In fact, its use is aiming at minimizing the prediction error (generally associated to a specific set of data) performing several tests on the same data-population and at extracting the prediction error from the average value obtained by several examinations of the input data. In the reference [Kohavi (1995)] also emphasizes the choice of 10 folds to obtain an optimal minimization of the incorrect predictions.

Fig. 7.5 shows a graphical representation of the cross-validation technique adopting ten different folds. The picture clearly describes the methodology associated to this technique as described in the following: 1) Execution of a partition of inputs into several subgroups, 2) selection of first available fold for the test phase, 3) performance of the training process of the model using the other remained folds end 4) execution of the classification test using the resulted model obtained by training phase. Normally, the final goal of this approach is to provide an average value of the predictor errors and to demonstrate if the model has a good accuracy level or not.

Fig. 7.5. Application of k-folds technique to provided dataset

Thus, the performance of the model developed in this work is obtained by a stratified cross-evaluation approach of the k-fold technique choosing 10 different folds, as shown in **Fig. 7.5**. This technique is conceivability used to analyze set of data and providing the most appropriate prediction that is representative of the entire population.

This task can be resumed in the following bullet points:

1- Partition of the entire input dataset into several sub-groups as indicated by k number,
2- Selection and hold apart the first sub-group from other folds (red color group in the first column of **Fig. 7.5**),
3- Training of the SVM model using the remaining (k-1) subgroups of data (grey color),
4- Testing of the SVM model on the first sub-group previously hold,
5- Extraction of the prediction error associated to the test process,
6- Repetition of the steps 1-5 for several times equal to k, in order to execute the test covering the entire input data introduced into the procedure.
7- Provide an average value obtained by the *k* tests performed.

As already stated, the estimation of the best representative SVM models is based on the execution of two phases aimed at characterizing the population of data with defining a representative separating surface and consequently performing a proper classification. Generally, for the first phase 75% of the input data (randomly selected) are used for the training process; consequently, the remaining 25% of the inputs is used to perform the testing phase and extract the prediction value.

On the contrary, using the *k-fold* technique the classification of the data is performed scanning all input data and providing an estimate of the prediction referred to the whole set of input data. To exemplify, using the cross-validation technique with *k=5*, the prediction error is estimated with 5 different results producing a more representative and homogeneous average value with respect to the input set.

In the work developed herein, several tests were performed in order to obtain an optimal pair of values (i.e. length of the input data and k-fold number). The analyses were generally performed using a variable number of input estimates together with k-fold values equal to 4, 8 and 10. As it is shown in the next Section, better results are obtained setting the number of folds equal to 10.

7.3 Developing damage detection algorithm based on OMA parameters and SVM models

The identification of structural damage in Civil Engineering structures using dynamic measurements has led to the development of several techniques in the last decades. Methods based on strain energy deviation, on curvature mode shapes and on flexibility matrix analysis, among others they were the most mentioned and used in the first years of research for SHM purposes. On the other hand, methodologies based on OMA procedure are relatively young. They have received important attention during recent decades principally due to their easy execution even in operational conditions. In the last years many methods have been developed based on the OMA approach oriented to damage detection. Most of them are based on the modal analysis, specifically on the natural frequencies. Although these techniques are mostly efficient to identify structural alterations in numerical models, they have difficulties in practical applications with experimental data. Follow this trend, a novelty damage detection approach based on the application of computational intelligence and pattern recognition models on modal parameters estimates has been developed and it will be presented in this Section.

The novelty approach proposed herein is developed to automatically detect structural changes in the "normal behavior" of the structures using the evolution of the modal parameters provided by the continuous monitoring process. In fact, the modal features, such as: the estimates of the natural frequencies or the variations of the mode shapes (using MAC, MPC and MPD indices) are used as input values of the implemented algorithm.

This new methodology is composed by the mathematical approach (described in the § 7.2.1) and the cross-validation technique (explained in the § 7.2.2), which are implemented to provide a best classification of the input data reducing the contribution of possible misclassification.

As a matter of fact, the core of the implemented strategies consists of application of SVM model in order to perform a classification of data in two different classes associated to damaged and undamaged scenario. This strategy is inspired by the so-called *true damage approach* [Santos et al. (2013)] that consists of the construction of an SVM model, thorough the definition of a separating margin of a specific representative system condition and, consequently, to use this margin to find any other possible scenario in which the data distribution has same (or quite similar) statistical characteristics.

Hence, the algorithm is forced to recognize two pre-imposed classes by assigning binary labels to the input data, 50% of the labels as *true* and the other 50% *false*. This means that in case of correct classification all data-points belong to undamaged scenario should be associated to the *true* label, meanwhile all data-points belong to damage scenario should be associated to the *false* labels.

Unlike what is generally done, in the damage detection algorithm proposed herein the SVM model is not developed to estimate a prediction of the experimental data, on the contrary, the model is defined and used to recognize a specific structural condition given by the occurrence of the two different scenarios. This condition is recognized only when a clear change (or discontinuity) occurs in the trend of the data.

As a matter of fact, when the damage occurs the trend of the modal parameters might permanently change, allowing the separation of the data into two classes. Otherwise, if the algorithm fails to differentiate between both classes it means that all data-points belong to the same class and no damage is detected.

Two different strategies have been implemented to perform the novelty approach. A simple scheme of the first strategy, named as Consecutive Segment Analysis (CSA) is reported in **Fig. 7.6**. The algorithm works with two consecutive *data-segments* to investigate possible anomalies in evolutions of the adopted sensitive damage features.

Fig. 7.6. Scheme of the first damage detection strategy (CSA, Consecutive Segments Analysis)

The estimations used as sensitive features are reported in the picture with black circles. As shown, both data-segments move together following the identification of the modal parameters. Alternatively, in **Fig. 7.7** is reported a simple scheme of the second strategy developed for the damage detection algorithm. This strategy has been implemented using a fix reference group of data and another group that moves accordingly to the continuous monitoring of the structure. The algorithm tries to find possible anomalies checking the statistical variations between the data provided by the two input-segments. For this reason, the second strategy is also named as Separate Segment Analysis (SSA).

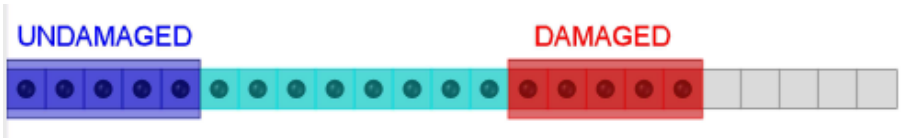

Fig. 7.7. Scheme of the second damage detection strategy (SSA, Separate Segments Analysis)

The main objective of both novelty strategies is to automatically recognize and discriminate two different states: a) non-damaged and b) damaged state, associating a probability value to the correct classification obtained after each run of the procedure.

The aim of this purpose is to prove the occurrence of a structural damage through the accuracy of the model reached in the classification problem. In fact, the SVM model performs a separation of the data only when the damage is present in the input data.

Furthermore, in order to remove any misunderstanding, it is worth remarking that the SVM accuracy can reach the maximum value (i.e. 100%) only if the 50% of data-points is associated to undamaged condition and the other 50% is associated to damage one and it can be possible only if the damage is located in the middle of the input data. As it will be described in the next Section, this information it is very relevant because it defines the maximum length of the data-segments and the usefulness of this algorithm to provide an alarm in almost real time in case of unquestionable anomaly.

It is worth highlighting that the novelty analysis is performed directly on the estimates "corrupted" by environmental and operational factors, because such effects are not filtered out before the application of the damage detection algorithm.

This means that the SHM purpose can be performed contextually with the automated identification and the continuous monitoring of the modal features avoiding any further manual interaction during the monitoring process.

In this way, the most important aspect related to this approach is given by the capability of the algorithm to provide information about the healthy state of the structure overcoming of the long period of monitoring (*training period*) devoted to investigating and removal of the effects due to environmental conditions. Therefore, this alternative OMA-based SHM approach permits to reduce a high quantity of monitoring costs also improving the efficiency of the SHM purpose.

The efficiency of the proposed strategies is firstly exploited through numerical data provided by a simulated continuous monitoring of the simple structure composed by 5 DOFs. Subsequently, the validation of the novelty approach will be performed using experimental data collected during the continuous dynamic monitoring of the *Gabbia* tower [Gentile and Saisi (2015); Gentile et al. (2016)].

Application to numerical data

The procedure based on the pattern recognition model is exemplified adopting a simple MDOF system: a shear type structure composed by five masses (floors) excited by a Gaussian white noise applied to the first level of the structure. The structure model has been used for validation of the proposed technique and it consists of a system composed of five DOFs deformable as a two-dimensional shear-type multi-story frames as presented in **Fig. 7.8**. The geometrical and mechanical properties of the numerical model have already been presented in Chapter 4. Therefore, five simulated numerical acceleration time series were recorded (one for each floor) and used in order to validate the novelty procedure. Furthermore, two different damage scenarios have been simulated to test the robustness of the developed strategies detecting possible structural anomalies.

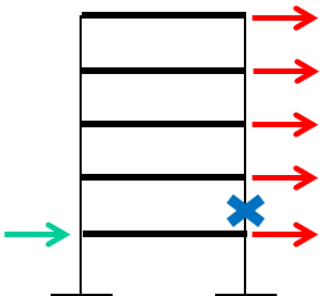

Fig. 7.8. Scheme of the numerical structure composed by 5 DOF. Location of the damage

The model herein presented was used to generate a set of acceleration time response signals associated to five DOFs. The main characteristics are reported in the following:

1. Simulation of more than 30 days (1000 hours) with sampling frequency set at 50 Hz,
2. Length of each dataset equal to 3600 s (90000-time steps = 30 minutes).
3. Excitation was introduced at first level of the structure by means of a stochastic process described by a zero mean Gaussian distribution ($f(t) \rightarrow N(0,1)$).
4. Operational effects were simulated by using a uniform random variability of 5 % for masses and 2 % for damping ratios of the corresponding nominal values.
5. Structural stiffness was considered as a function of the temperature in order to simulate environmental effects on the structural model. Therefore, the temperature variations measured on January 2018 by *Osservatorio di Brera* (weather station located in the center of Milan) were used to simulate the environmental effect on the modal parameters.

6. After 150 hours of the simulated monitoring a structural damage was mimicked with a stiffness reduction of 2% at the second level, as shown in **Fig. 7.8**.

Under these conditions, numerical acceleration time series have been generated and used to simulate the output structural responses of a numerical structure subjected to environmental effects. Hence, the estimation of the modal parameters (i.e. natural frequencies, mode shapes and modal damping ratios) and the complex indices (i.e., MPC and MPD) have been extracted from the data applying the automated MPE algorithm described in Chapter 4. The modal parameters modes extracted by the first generate dataset (**Fig. 7.9**) were used as reference modes for the tracking process.

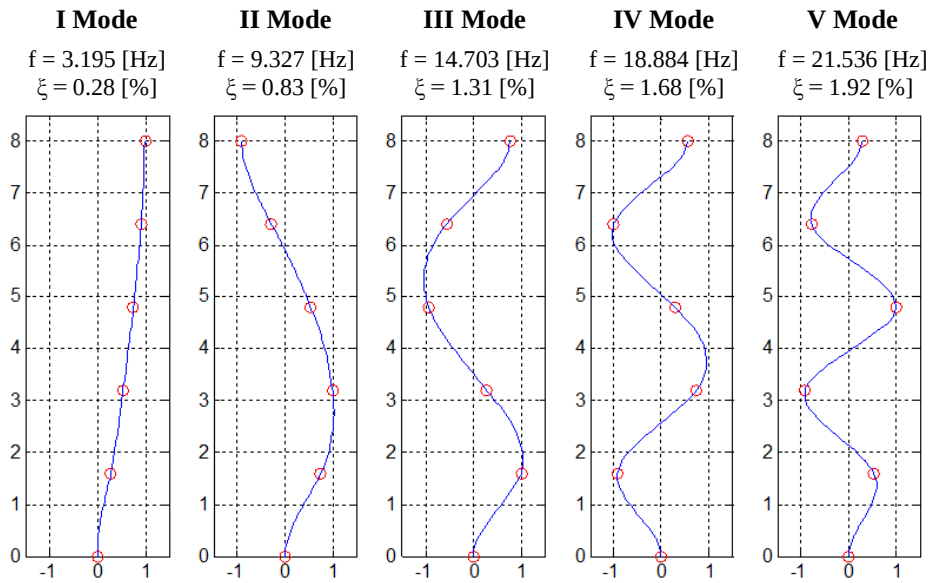

Fig. 7.9. Five identified modes of vibrating of the structure. Natural frequencies and mode shapes representation used as reference baseline list for the monitoring process

In **Fig. 7.10** the simulated frequencies evolutions of the simple academic 5-DOFs system subjected to environmental factors are reported.

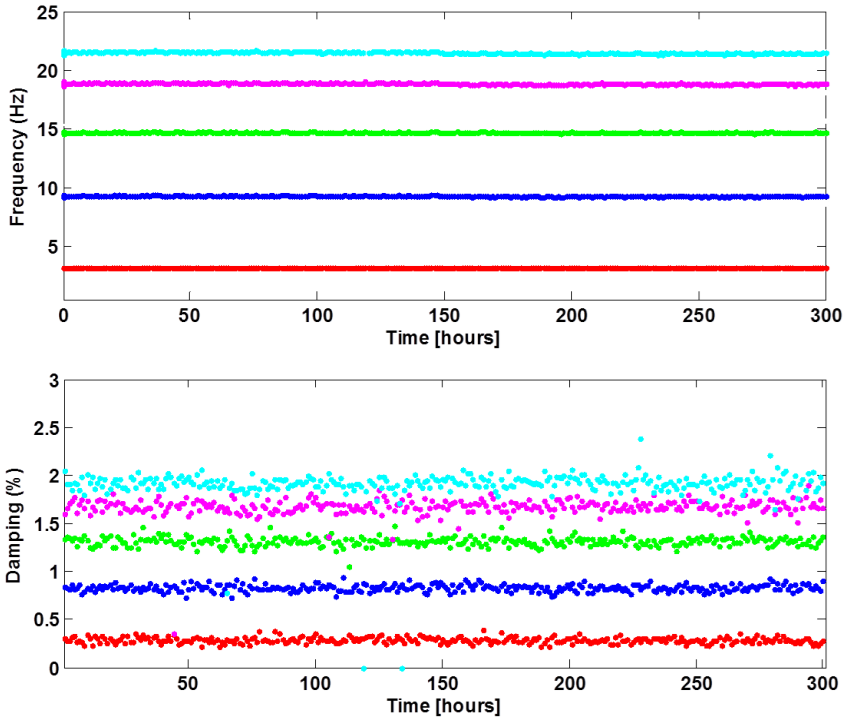

Fig. 7.10. Tracking of the natural frequencies and modal damping ratios of the five identified modes

Subsequently to the tracking process, the SHM procedure proposed herein was tested. Both developed strategies have been adopted to identify the simulated damage during the monitoring process discriminating between undamaged and damaged conditions. The exploiting of the proposed damage detection algorithm was carried out using the natural frequency estimates because they are more sensitive features to structural.

Furthermore, the data provided to the algorithm where continuously partitioned into *10* different groups using the *k-fold* function (see § 7.2.2) and performing *k* different tests, as exemplified in **Fig. 7.5**. The application of the *k-fold* technique permits to improve the accuracy of the results in the classification, reducing the contribution provided by possible outliers that are present in the data-sequences. Then, the classification rate is extracted averaging the *k* values of accuracy associated to each performed test.

7.3.1 First strategy based on "consecutive segments analysis"

In this Section the first strategy of the developed SHM procedure based on pattern recognition model – defined as CSA strategy – is described in detail. This approach consists of the use of two consecutive segments of input data (i.e., natural frequency estimates) directly selected from the evolution in time such parameters This means that after each run of the OMA procedure and the extraction of the modal features from the recorded output responses, the novelty procedure can be applied in automatic way without any further handling of the data resulting from the tracking process.

The length of the segment is very important for the performance of the novelty analysis because it defines the exact number of data population that have to be provided to the algorithm to solve the classification problem. Such segment is continually updated performing a "shifting" of the input-data after the analysis of each recorded dataset. Exemplifying, this task is obtained removing the modal estimates associated to the oldest identified mode and englobing the new ones provided after each run of the OMA procedure. **Fig. 7.11** exemplifies the CSA strategy and describes how the input data are provided to the novelty detection algorithm, also highlighting the time-step between the classification process respect with the tracking process.

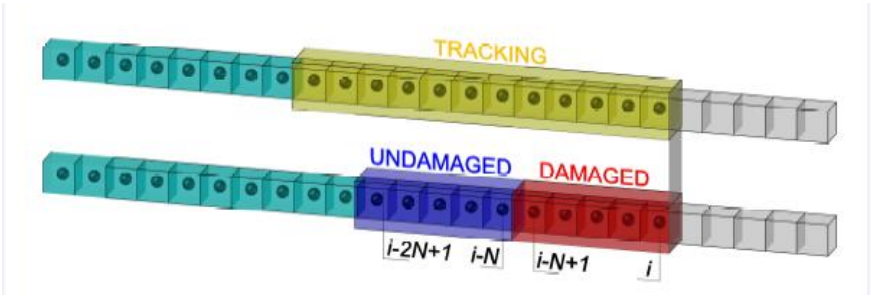

Fig. 7.11. Step delay between the continuous dynamic monitoring process and the damage detection approach performed by CSA strategy

As explained above, after a small period required to calibrate the SVM model, the novelty analysis can be "hooked" at monitoring process (**Fig. 7.11**) in order to perform

the continuous damage assessment contextually with the extraction of the modal parameters estimates with just a short period of delay (i.e. one hour).

In more details, the *CSA strategy* of the novelty detection procedure is based on a *consecutives segments* that they are used to describe to different scenarios. It means that the inputs on the SVM model are composed by two consecutive equal long segments of data. Since the natural frequencies are the most sensitive features in the context of SHM purpose the input data are composed by a sequence of natural frequency estimates referred to a selected set of vibration modes, as exemplified in **Fig. 7.11**. The association between the data-points and labels of the two reference classes is performed in very simple way after the definition of the length of the reference segments (i.e. *N*). So, each single label is connected to each estimate in order to assign the first segment of data to the first class that corresponds to the *undamaged condition*, and, otherwise, the second data-segment to the second class that is referred to the *damaged condition* of the structure (**Fig. 7.11**).

The CSA strategy of the novelty detection algorithm can be detailed as follows. Defining with the parameter *i-th* a generic dataset of output responses collected by the monitoring system and with *N* the length of each segment-scenario, the first input value associated to the first position of the *Class I* corresponds to the frequency estimate extracted from the *[(i-2N)+1]-th* collected dataset previously analyzed. Meanwhile, the value located in the last position of the *Class I* is extracted by the *[(i-2N)+N]-th* dataset (blue cubes in **Fig. 7.11**). Thus, the first value in the *Class II* corresponds to the estimates extracted by *[(i-2N)+N+1]-th* dataset and the last value in the *Class II* is the estimate extracted by *i-th* dataset (red cubes in **Fig. 7.11**). Therefore, the last estimate in the *Class I* and the first value in the *Class II* belong to two consecutive recorded, this is the meaning of the *consecutive segment scenario*, as depicted also in the **Fig. 7.12**..

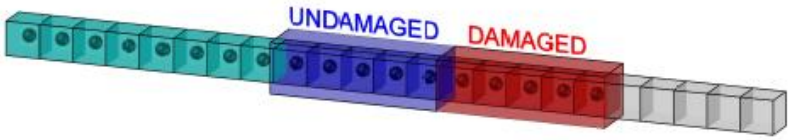

Fig. 7.12. Example of the first strategy of novelty detection (CSA strategy). Association between Class I and Class II to undamaged and damage condition, respectively.

To clarify this selection of the input data of the model, in the **Fig. 7.13** are represented three consecutive time instants of the SHM process. As already explained, defining with N the number of estimates associated to each class and considering the generic time instant i in which the *i-th* dataset is already analyzed; then, the inputs associated to the *Class I* of the SVM model corresponds to those estimates into the interval segment equal to [(i-2N)+1; i-N]. Indeed, the input values associated to the *Class II* correspond to the follow segment [(i-N)+1; i]. In additions, for the consecutive time instant $i + 1$, the segments of data shift one position and the relative intervals are given by [(i-2N)+2; (i-N)+1] for the *Class I* and [(i-N)+2; i+1] for the *Class II*, respectively, and so on. Hence, the data selecting has been implemented in order to guarantee the same number of inputs to the SVM model associating N values to the *Class I* and N values to the *Class II*.

Fig. 7.13. Example of the first strategy (CSA strategy) in 3 consecutive application steps

One of the objectives of this Chapter is to simulate a continuous dynamic process of a simple MDOF structure in which different damage scenarios have been introduced and to

test the performance of the developed novelty strategy. Accordingly, the statistical value is used in order to provide the accuracy of the SVM model on the classification of *1-fold* sequence of data after the training of the model using *(n-1)-folds* and repeating this process in order to cover all available data-points.

Then, the procedure is applied in order to perform an optimal classification of the data in which a probability value is associated to the performed classification and it can reach the maximum value equal to 100% only if a structural damage occurred. In more detail, the probability associated to the occurred damage can reach 100% only if the data-points (selected estimates) are correctly classified into two groups and when the anomaly is located exactly in the middle of the two classes of input.

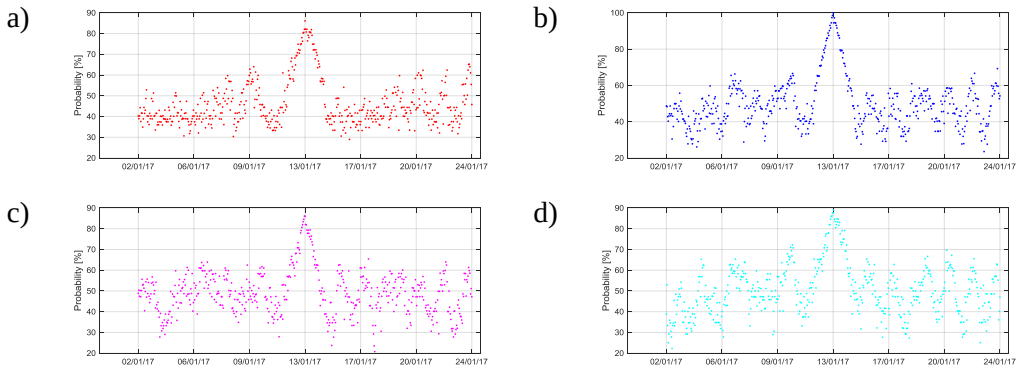

Fig. 7.14. Application of the CSA strategy. Probability of occurred damage obtaining by analyzing each natural frequency separately. Probability values associated to the a) first, b) second, c) forth and d) fifth natural frequency evolution, respectively

In **Fig. 7.14** are shown the main results obtained applying the developed novelty procedure (CSA strategy) to the frequency estimates extracting by simulated numerical acceleration time series created accordingly with the characteristics of the 5-DOFs system described in Chapter 4. It is worth noting that the modal estimates were obtained coupling the MPE algorithm (described in Chapter 4) and the MT procedure (described in Chapter 6) to the simulated accelerations. Moreover, in order to test the sensitivity of the algorithm to structural anomaly, a damage was simulated after 150 hours with a reduction of the stiffness value (2% of the nominal value).

The diagrams in **Fig. 7.14** show the probability values provided by the application of the novelty detection algorithm to the frequencies evolutions of the 5-DOFS system (see **Fig. 7.10**). As shown, a clear bell shape can be noted exactly in correspondence of the occurred damage. It is worth noting that to a slightly reduction of stiffness corresponds a slightly shift of the nominal values of natural frequencies that cannot be easily detected. This strategy is able to recognizes this variation and to performs a correct association of the estimates belong to the undamaged and damaged conditions.

Finally, inspecting the resulting diagrams, the bell-shaped described by the probability value are highlighted. Moreover, the peaks exactly appear in correspondence of the frequency shift when the damage occurred. This result is very important because it shows how the anomaly (i.e., reduction of localized stiffness) can be detected in all almost investigated frequencies. Therefore, a combination of all probability associated to the monitored modes can be used as damage feature for SHM purpose based on pattern recognition model.

7.3.2 Second strategy based on "separate segments analysis"

In this Section the first strategy of the developed SHM procedure based on pattern recognition model – defined as CSA strategy – is described in detail. This second strategy consists of the use of two separate segments of input data in which the first segment does not evolve over time and it is used as a *fixed reference state*, meanwhile the second segment changes over time together with the monitoring process. To clarify this aspect, it is worth to notice that modal parameters in the reference state are referred to undamaged condition, meanwhile the estimates belong to the second segment are continuously updated after each run of analysis and they are referred to a *moving state* that follows the monitoring process and exploring possible changes in the structural response. **Fig. 7.15** exemplifies the SSA strategy and describes how the input data are provided to the algorithm. It can be noticed as the moving state (associated to damage condition) is continuously updated with new estimates provided by the tracking process.

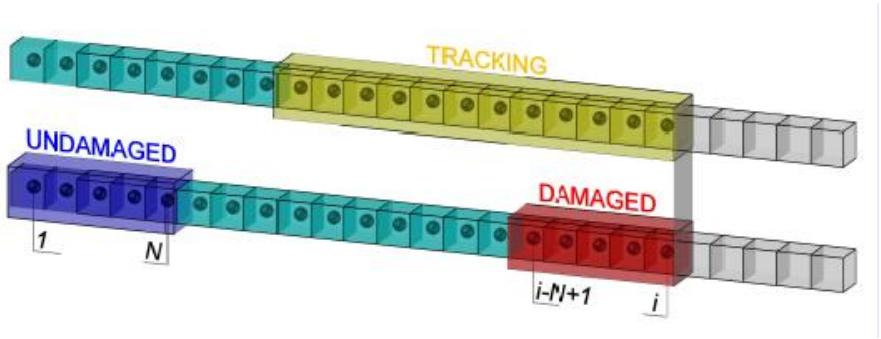

Fig. 7.15. Step delay between the continuous dynamic monitoring process and the damage detection approach performed by SSA strategy

For the second developed strategy, the input of the model is organized into two separate segments (or classes) with same length and composed by series of extracted modal parameter. As shown in **Fig. 7.16**,, the undamaged scenario is associated to the *Class I* meanwhile the damaged one to *Class II*. Thus, under the hypothesis, the structure should does not suffer/have any damage during the initial reference scenario (i.e. fixed reference state) at the beginning of the monitoring process, in order to characterize the undamaged condition in the fixed segment. On the contrary, the second segment represents the *damage scenario* and it is used to find any anomalies over the time. Once the N parameter is defined, the values inside the *Class I* correspond to the frequency estimates extracted in the initial phase, from the analyses of the 1^{st} to *N-th* dataset. Meanwhile, for a generic dataset defined by *i*, the first element in the *Class II* corresponds to the estimates extracted by *[i-N+1]-th* dataset and the last value is the estimate extracted by *i-th* dataset. A graphical representation about this approach is shown in the **Fig. 7.16**.

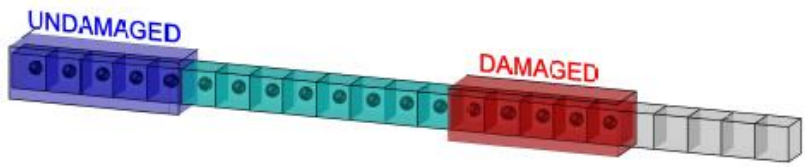

Fig. 7.16. Example of the second strategy of novelty detection (SSA strategy). Association between Class I and Class II to undamaged and damaged condition, respectively.

In order to clarify this strategy, three consecutive time instants of this SHM purpose are represented in **Fig. 7.17**. As shown, the undamaged condition is always fixed, while the damage condition moves following the continuous monitoring process. Again, also in this strategy the input data are selected in order to guarantee the same number of inputs to the $Class\ I$ and to the $Class\ II$.

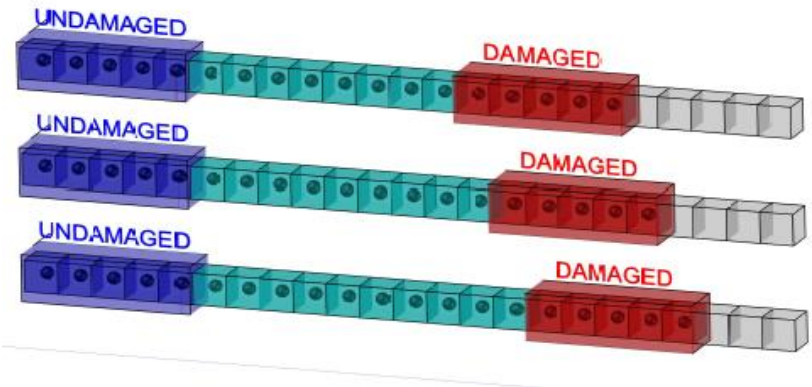

Fig. 7.17. Example of the second strategy (SSA strategy) in 3 consecutive application steps

As expected, the same acceleration time series already adopted to exploiting the CSA strategy has been used to test the efficiency of this SSA implementation. As done for the first approach a simulated damage was introduced after 150 hours of the monitoring process. The sensitivity of the SVM model included in the SSA strategy has been tested in order to recognize such variation.

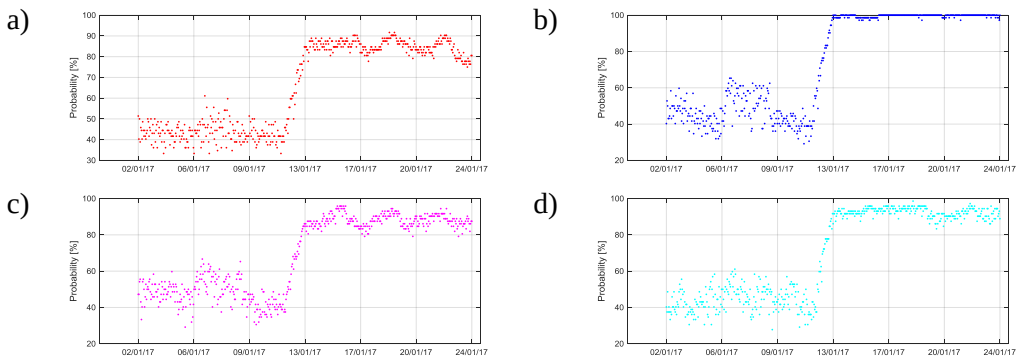

Fig. 7.18. Damage prediction provided by the classification of each series of identified frequency using the SSA strategy. Results obtained providing as input of the SVM model: a) first, b) second, c) forth and d) fifth natural frequency evolution, respectively

An excellent classification has been achieved and the main results obtained for each natural frequency evolution are shown in **Fig. 7.18**. It can be noticed the expected trend of the SVM probability associated to the identification of the damage through the application of the SSA approach. In all four cases the performance of the algorithm is quite excellent. The discrimination of the two scenarios (i.e. undamaged and damage state) is quite perfect and the probability of the occurrence of the structural damage rises more than 90% in most cases. It is worth mentioning that the main idea behind the implementation of this second novelty detection approach (i.e., SSA strategy) is quite different from the first one (i.e., CSA strategy), but it is basically orientated to provide the same information about occurred damages in the structure during the in-service conditions. The main difference between both strategies is provided by a different key to reading the results: in the first, the probability associated to the damage describes a visible bell-shape with a gradual increase in the probability associated with the damage followed by a subsequent decreasing, with a maximum in correspondence of the occurred variation. On the contrary, in the implementation the second strategy, the probability remains constantly high after the anomaly (**Fig. 7.18**). This means that the statistical properties between the two segments of data are changed (caused by the damage) and such differences are maintained over time.

Concluding, if the first approach provides a clear information about the occurrence of the damage in the structure, the second approach should provide information about the duration of such damage over time. These aspects will be deeply clarified and highlighted in the final conclusions of this Chapter.

Due on the fact that the first strategy is able to provide an accurate information about the occurrence of consecutive damages without any further user's interaction during the continuous assessment, the approach has been used to identify the structural damage occurred on a real structure. Experimental data collected by the simple monitoring system installed on the *Gabbia* tower have been used for the application of the proposed strategy confirming the damage occurred on the tower during a far-field earthquake.

7.4 Validation and application using experimental data

Being the natural frequencies of vibration effective and convenient damage sensitive features for vibration-based SHM application, the proposed CSA strategy was used to detect possible anomalies in the "normal" behavior of an ancient construction, using two different combination of input data: the first, using only identified natural frequency estimates, and the second, adding to obtained frequency estimates also the collected temperature values.

The combination of natural frequencies with the recorded temperatures was firstly introduced to avoid and manage the occurrence of false positives during the execution of the novelty detection algorithm. In fact, introducing also the temperature values the SVM model characterizes the conjunct of data taking into account the relation between identified frequencies and average recorded temperatures, so false positives strictly dependent on the temperature variation should be avoided.

7.4.1 Continuous dynamic monitoring results of the Gabbia Tower

In this Chapter the main results obtained by the application of the developed novelty procedure to experimental data collected on an important Italian ancient construction are reported. The aim is to demonstrate the robustness of the novelty detection procedure on detecting the structural damage using the evolution in time of the natural frequencies obtained by the continuous dynamic monitoring of the *Gabbia* tower, located in Mantua, Italy. As reported in Chapter 6, this masonry tower was built in the XIII century and it represents an important Cultural Heritage building for the city of Mantua. After a seismic event occurred in the 2012, the tower was subjected to an intensive study aimed at identifying its vulnerability, checking its state of conservation an at achieving the structural behavior as demonstrate by previous analysis [Saisi and Gentile (2015), Saisi et al. (2015)].

Subsequently, a second campaign of dynamic tests was carried out to deeply understand the state of preservation of the tower and to extract a reasonable set of modal parameters that it will be adopted as reference values for the continuous dynamic monitoring of the tower. As reported in [Saisi and Gentile (2015), Saisi et al. (2015)], five principal modes were clearly extracted in the frequency range between 1 and 10 Hz.

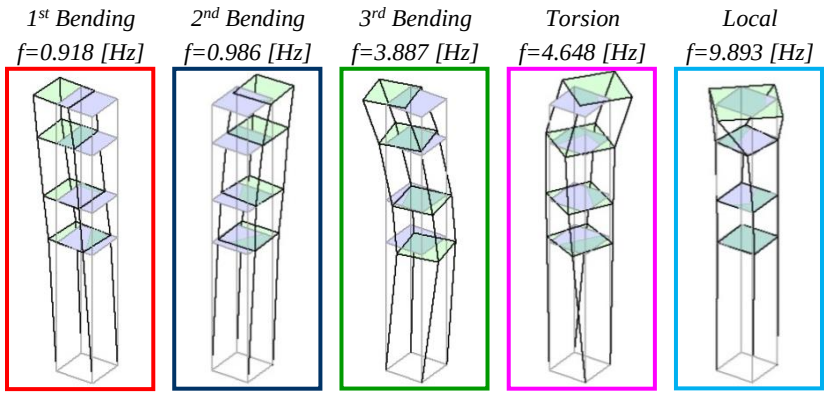

Fig. 7.19. Modal parameters estimate used as reference values for the monitoring process

In **Fig. 7.19**, the principal modes of vibrating identified in the second campaign and used as reference modes for the subsequent continuous permanent monitoring were reported. As shown, different colors have been associated to the identified modes aimed at clearly understanding and reading of the graphical results obtained by monitoring process.

The 21st of June 2013 the monitored tower was subjected to a far-field seismic event, that produced a damage in the structure, already confirmed by several studies carried out in the period after this event [Gentile et al. (2016)]. As already mentioned in Chapter 5, the permanent monitoring of the *Gabbia* tower started on December 2012, and the earthquake occurred the 21st of June 2013, for this reason only a reduce period of monitoring was used to define and validate the new novelty approach. Thus, the monitoring period selected as interval time reference using to test the procedure was from the 1st June 2013 until the 15th of July 2013.

It is worth mentioning that the modal parameters used to validate the novelty procedure were extracted from acceleration time series collected by monitoring system installed on

the tower. The evolution in time of the natural frequencies were obtained applying the implemented Modal Parameter Estimation (MPE) algorithm together with the Modal Tracking (MT) procedure already presented in Chapters 3 and 5, respectively.

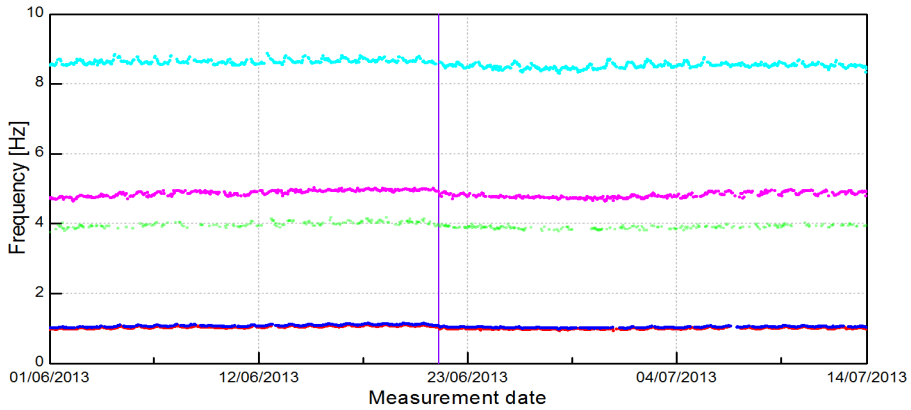

Fig. 7.20. Evolution in time of natural frequencies obtained from 01/06/2013 to 14/07/2013

In **Fig. 7.20** the evolution of the natural frequencies of the five reference modes identified during the second campaign [Saisi et al. (2015)] is shown. The vertical line depicted on the diagram highlights the seismic event occurred on the 21st of June 2013.

7.4.2 Validation of the algorithm using the frequency estimates of the Gabbia Tower

As shown in the previous Chapter, the good performance of the developed OMA tool (e.g. MPE and MT procedures) was demonstrated by the high values of the identification success rate (SR) of each structural mode of the tower. Afterward, a shorter monitoring period of 44 days (from the 1st of June to 14th of July 2013 (1056 hours)) was used to validate the novelty procedure; in particular during this period the first natural frequency was identified in 975 times (SR equal to 92,42%), the second natural frequency appears in 915 times (SR equal to 86,81%), the third frequency in 374 times (SR equal to 36,53%), fourth and fifth frequency appear in 882 times and 921 times (SR equal to 83,68% and 87,38%).

According with the results obtained by tracking process (**Fig. 7.20**), only the frequency values with higher SR were used as input for the SHM application, specifically were used the frequency evolution of the first and second bending mode, the torsional mode and the mode associated to the local mode of the upper part of the tower.

Due to the lack of detail of the diagram shown in **Fig. 7.20**, the evolution of each natural frequency obtained in the reference period is individually reported in the following figure using a properly scale-factor.

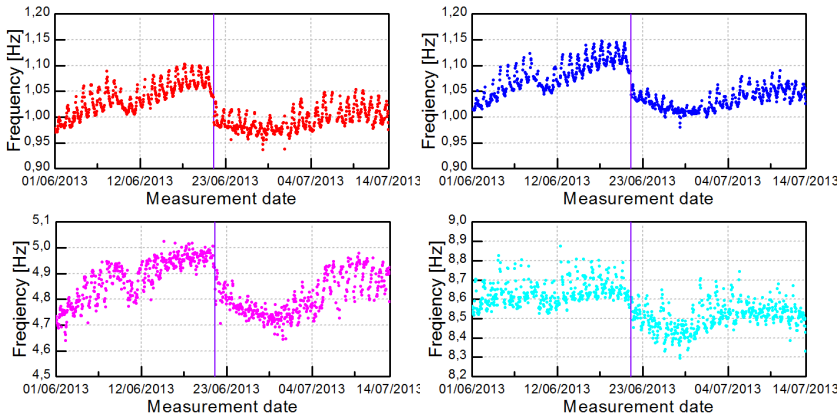

Fig. 7.21. Extraction of the selected natural frequency evolution of the first two bending modes, the torsion model and the local mode obtained from 01/06/2013 to 14/07/2013

From the inspection of the diagrams depicted in **Fig. 7.21** the frequency shift represents a common aspect for all investigated modes (more evident in the first and in the second bending mode). Therefore, as highlighted, the seismic event caused a permanent change (i.e. structural damage) in all frequencies' trends. Moreover, it is worth remarking that frequency "gap" is not re-absorbed by the structure describing a global change of the dynamic and mechanical behavior of the tower.

As already mentioned in this Thesis, at 21st of June 2013 the tower was subjected to a seismic event which led to a structural damage in the tower. This scenario is principally highlighted by a slightly decrease of the natural frequencies associated to the principal modes [Gentile et al. (2016)].

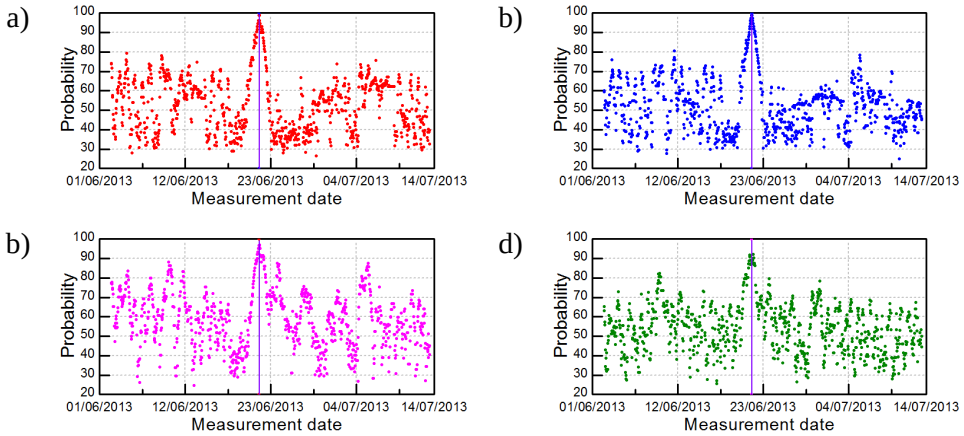

Fig. 7.22. Damage predictions observed by classification of the frequency estimates of the: a) first bending mode; b) second bending mode; c) torsional mode and d) local mode of the tower

The occurrence of damage was demonstrated using a selected interval of data in which the SVM model is forced to recognize two difference scenarios, associating the 50% of input data to undamaged state and 50% to damage state (48 hours long for each scenario), as shown **Fig. 7.22**. As expected, SVM is sensitive enough to classify the two conditions recognizing the anomaly that appears in all fundamental modes. In fact, when the damage occurs, the accuracy of the SVM model clearly increases.

When the probability reaches 100% means that all data were right associated to undamaged and damage scenario and this condition can be possible only if damage is located exactly in the middle of the input interval of data (i.e., in CSA strategy). The results obtained by the application of this strategy to the natural frequencies evolution of the tower are shown in **Fig. 7.22**. The accuracy of the classification performed by the SVM model is an indicator of anomaly behavior and the high value of its peak means that a damage occurred. This condition is clearly highlighted by the first two frequency evolutions in the present case study.

As declared in the beginning of this paragraph, in order to have a deeper view on structural behavior and also to investigate any possible effects of ambient conditions (i.e. temperature) on modal parameters, a second implementation of the CSA strategy has

been developed introducing temperature values measured during the monitoring process [Marrongelli et al. (2018b)].

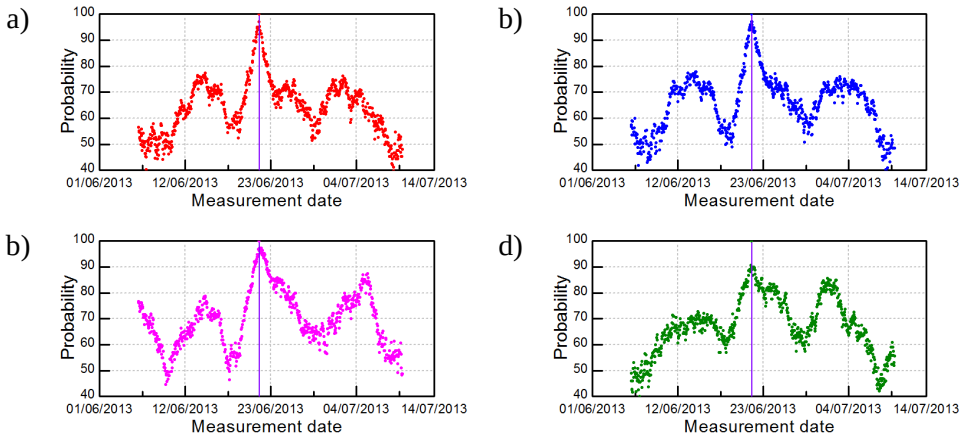

Fig. 7.23. Damage predictions observed by classification of the frequency estimates of the: a) first bending mode; b) second bending mode; c) torsional mode and d) local mode of the tower

Basically, the analysis was performed in the same way of the previous implementation, adding to the sequences of frequency estimates also the average temperature collected for each hour of monitoring data. As shown in **Fig. 7.23**, in all four analysis the model provides a very high probability of occurred damage when the earthquake occurred. It is worth mentioning that high variability of temperature makes more difficult the right classification of the structural condition, for this reason it was necessary to use a larger segments of input data (240 total hours, 120 for each state). This means that possible damage can be fully detected only after 5 days from its occurrence making this implementation less effective of those ones in which only the same estimates are used as inputs data.

Finally, in order to make more legible the obtained results, the accuracy values provided by the SVM model for each natural frequency were put together in order to use the average values as damage sensitive indicator. The mean value has been calculated for both implementations and the graphical results are shown in **Fig. 7.24**.

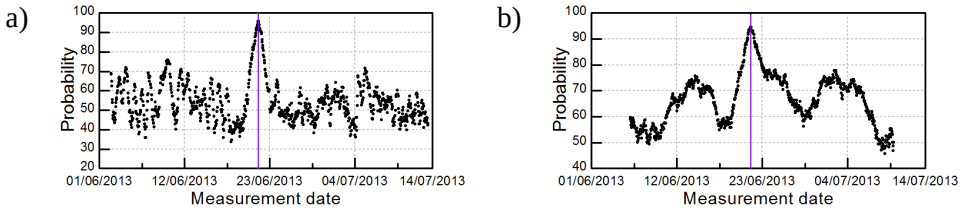

Fig. 7.24. Average probability value (CSA strategy) associated to occurred damage: a) first implementation, b) second implementation with temperature measurements

The graphical results highlight the possibility of using the average values as damage sensitive feature in the implemented damage detection strategy. Although a good performance has also been obtained using the average temperature measurements, the implementation that works only with frequency estimates provides a faster identification of damages in the structure. Furthermore this outcome provides a further advantage relative to the cost of the monitoring system in which the temperature sensors could be avoided toward installing a compact monitoring system composed only by transducers, This result makes evident the straightforward possibility of using this strategy for the continuous assessment of historical buildings even with permanent system composed by limited array of sensors. Finally, in the next Chapter the estimations obtained by seven months of continuous dynamic monitoring of the *Gabbia* tower will be used to exploit and validate the implemented novelty strategy.

7.4.3 Application of the novelty damage detection algorithm to monitoring data

Due to the fact that the unsupervised approach seems to work better if the classification does not involve also the temperature values [e.g., Marrongelli et al (2018b)], only the frequency estimates obtained during the whole monitoring period of the tower were used to set the SVM model and to demonstrate the robust performance of the implemented strategy.

As mentioned in Chapter 6, the permanent monitoring of the tower was performed for over two years starting on 17th of December 2012 [Gentile et al. (2016)]. During the

monitoring period the tower was subjected to a far-field earthquake that produced a structural change in its dynamic behavior. Therefore, the experimental data collected during seven months of monitoring were used to validate the implemented CSA strategy and to automatically detect the structural damage occurred during the seismic event.

In Chapter 6 the automatically identified natural frequencies evolutions (from 17/12/2012 to 15/07/2013) are reported in detail. Hence, the SVM models, defined in the previous Section, were adopted to analyze and classify such estimates extracted by the continuous monitoring application. Moreover, from the results obtained in the previous paragraph, the structural anomaly e is much more evident in the first frequencies instead those ones associated to torsion and local mode. So, only the evolution of the frequencies associated to the first and second bending modes have been used to test the developed damage detection algorithm.

The SVM models defined by the following parameters: k-folds=10, σ=1.5 and C=10, have been used. In additions, the length of the data segments provided to the model were set equal to 96 elements (48 elements for each undamaged and damaged condition).

Fig. 7.25 shows the application of the CSA strategy to seven months of monitoring. As shown, the probability value associated to the occurred damage fluctuates around its average value of 50%. This means that no information can be extracted by these results, because the SVM model can not distinguish between the undamaged and damage state, this means that the data are mixed. Moreover, this condition implies that no damage state exists in the input data. Hence, the absence of structural anomaly is clear confirmed, and the integrity of the structure is not compromised.

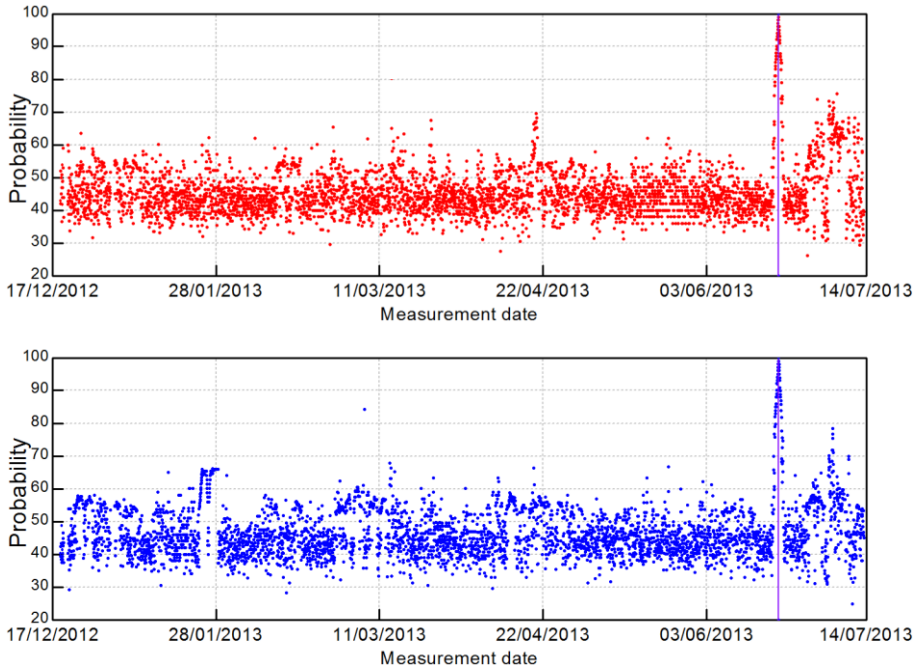

Fig. 7.25. Application of the novelty algorithm to continuous monitoring data: natural frequency estimates related to the first and second bending mode (from 17/12/2012 to 14/07/2013)

From the inspections of the two diagram some considerations can be pointed out:

1) The structural change due to the damaged occurred in the tower was fully identified by the algorithm providing a clear peak in the probability associated to the occurred damage.
2) No further anomalies were detected in the previous period of monitoring.
3) No spurious peaks of the damage probability appear during the monitoring phase, demonstrating the robustness of the implemented methodology.
4) The effects of the environmental factors on the natural frequency estimates (i.e. temperature fluctuation) do not affect the analysis and the detection of the damage.
5) The continuous assessment was carried out using a length of each input segment equal to 48 elements. This parameter permits the automated identification of the occurred damage in the structure after only 48 hours from its occurrence.

The obtained results confirm the information pointed out by previous analysis carried out using different damage detection approaches as already reported in other works [Gentile and Saisi (2015), Gentile et al. (2016), Guidobaldi (2016)]. The absence of false positive in the diagrams in **Fig. 7.25** also confirms the robustness of the newly developed damage detection algorithm and its reliability on SHM applications.

Afterward, in order to test the sensitivity of the SVM model in the automatic detection of structural anomalies, some artificial damages were simulated along the monitoring period of the tower. In particular, two frequency shifts were used in the evolution of the first two natural frequencies adding a drop of frequency in the winter period and at the end of the spring period in order to test the robustness of the algorithm in two different environmental conditions (with different daily temperature and humidity fluctuations).

Moreover, the amplitude of the frequency shifts was defined by taking into account the real frequency drop caused by the far-field earthquake that occurred on the 21st of June 2013. In particular, the shifts were set in order to provide a similar frequency drop to the one that had occurred during the seismic event (equal to 5% of the mean value of the frequency associated to the first and second mode, respectively). The evolution of the corrupted frequency estimates used to demonstrate the efficiency of the strategy presented herein is reported in **Fig. 7.26**.

The graphical results obtained by the analysis of the whole set of monitoring data are provided in **Fig. 7.27**. From the inspection of both diagrams in **Fig 7.27** the capability of the SVM model regarding the identification of structural anomalies by using frequency estimates as damage sensitive features has been demonstrated. In particular, the algorithm performs a correct classification of the data identifying structural damage in the winter period as well as in the spring period in which the structure is subjected to high thermal variations and different environmental conditions.

a)

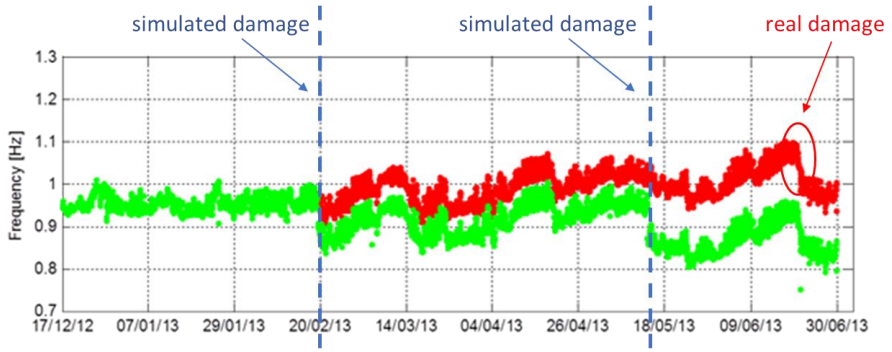

b)

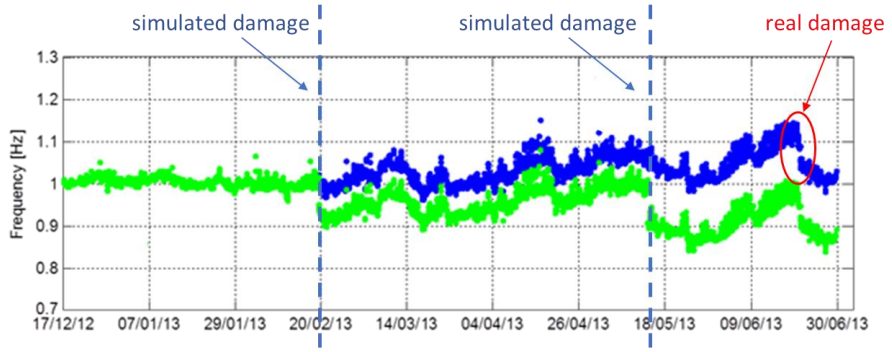

Fig. 7.26. Frequencies evolutions imposing a frequency shift: a) 1st frequency: real trend with red dots, corrupted values with green dots, b) 2nd frequency: real trend with blue dots, corrupted value with green dots.

As shown, the probability values of the occurred damage obtained by analyzing the "corrupted trends" of the fundamental frequencies of the tower are reported in **Fig. 7.27**. The first and the second peak in both diagrams indicate the correct identification of the simulated damages in the structures.

These results point to an important outcome related to the novelty detection strategy presented in this Dissertation. In fact, it is possible to define *a-priori* the accuracy of the model according to the input parameters and the population of input data provided to the model in order to define the boundary decision surface. As previously described in this Chapter, the pattern recognition model defines a soft margin obtained by penalizing some data-points (i.e. frequency estimates) that could fall outside the decision boundary; there values are treated as outliers (see § 7.2.2).

Following this strategy, it is possible to define a soft margin in which to find the optimal separation surface that could be recursively used to classify the input-data within continuous assessment purposes.

a)

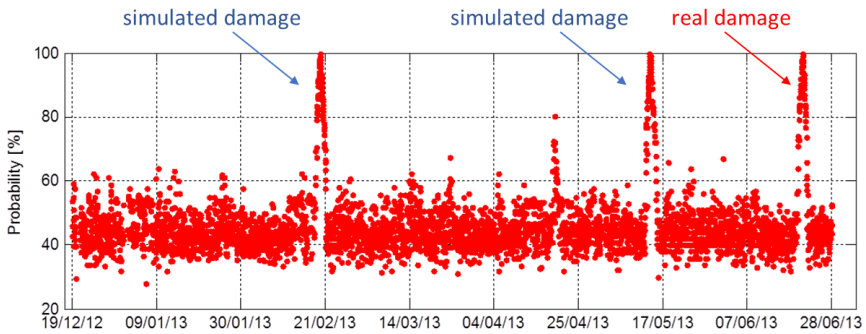

b)

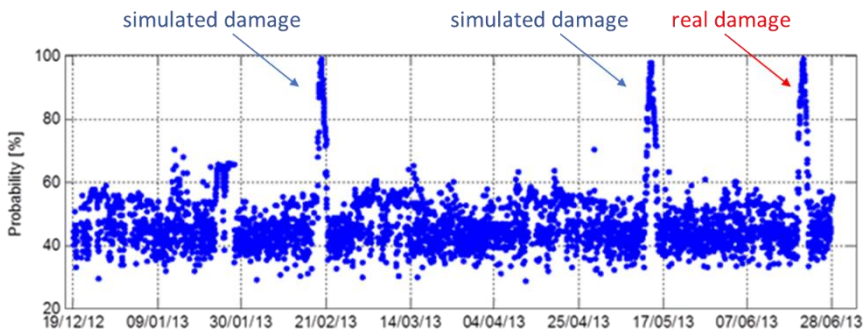

Fig. 7.27. Probability values obtained applying the SCA strategy to the monitoring data of the two fundamental frequencies of the tower. Probability of occurred damage associated to a) 1st natural frequency and b) 2nd natural frequency.

Finally, the identification of the anomalies artificially created in the fundamental frequencies of the tower further proves the efficiency of the developed algorithm regarding the damage detection approach and its capability to automatically identify structural anomalies without any human interventions on the data.

7.5 Conclusions

This Chapter focuses on the development of an alternative OMA-based SHM approach based on the application of pattern recognition models on the modal parameters automatically identify by recently developed OMA algorithms.

A brief review of the classification algorithms based on SVM models is given in the beginning of this Chapter, highlighting the main improvements obtained in different field of application over the years. Hence, the mathematical implementation of the classical SVM technique used for binary pattern classification problems is described in detail.

Subsequently, this Chapter focuses on the implementation of the damage detection purpose based on OMA parameters and SVM models. The novelty approach was developed in two different strategies: the Continuous Segment Analysis (CSA), which involves the use of two consecutive segments of data associated to two different structural conditions, and the Separate Segments Analysis (SSA), which uses a fixed segment of input data to characterize the reference scenario and a moving segment associated to the damaged condition. Both strategies are aimed at recognizing two different classes of data associated at two structural conditions constructing an optimal surface and maximizing a separation margin.

Both strategies (CSA and SSA) proposed herein were exploited using numerical data generated using a simple 5-DOFs system already used to describe the algorithms presented in the previous Chapters. Consequently, in order to validate the proposed methodologies, experimental data collected by permanent monitoring system installed on the *Gabbia* masonry tower were used. As described in previous papers [Saisi and Gentile (2015), Saisi et al. (2015)], after the seismic event occurred on May 2012, the tower was subjected to an extensive research program performed to assess its state of preservation and the structural condition. Then, a simple monitoring system aimed at monitoring the dynamic property and helping the preservation of the historic tower was installed.

Seven months of continuously collected data were firstly analyzed using the developed OMA procedures to extract the evolution in time of the modal parameters. Thus, the novelty CSA strategy has been applied to confirm the permanent damage occurred during the earthquake of 21/06/2013. Two different implementations of the CSA were applied to the extracted natural frequencies of the tower (i.e. using only frequency estimates or using pairs of frequency and temperature values). From the results obtained by both approaches a clear permanent change of the structural condition occurred during the earthquake has been highlighted.

Concluding, the applications described in this Chapter reveal the capability of the damage detection approach in the context of SHM purposes making this approach very promising for the automated continuous assessment also for structures with monitoring systems composed by a limited array of sensors. In this way, the information obtained by continuous monitoring might be used by artificial intelligence models to generate a properly alarm in case of structural damage after a very short time of delay.

Furthermore, it is worth mentioning the damage detection approach proposed herein can be used with several type of input data. In particular, the first strategy (i.e., CSA strategy) is particularly indicated to be used with natural frequency estimates because the environmental effects. Meanwhile, the second strategy (i.e., SSA strategy) can be used with the evolution in time of other parameters/indices related to the mode shapes variations, such as MAC index or MPC and MPD indices. Thus, the second strategy is particularly suitable for SHM purposes of structures with widespread monitoring systems.

Chapter 8

CONTINUOUS DYNAMIC MONITORING OF A HISTORIC STRUCTURE: THE SAN GOTTARDO BELL-TOWER

Contents

8.1 Introduction

The increased uptake of the OMA-based SHM strategy in the last decades makes this approach very effective for the continuous assessment of several types of constructions for the purposes of damage detection, as described in many works present in the literature as [Magalhães et al. (2012), Gentile et al. (2016), Comanducci et al. (2016)]. The recent improvement of the OMA-field has driven the development of powerful tools aimed at performing the automated identification and tracking of the dynamic features associated with the structural modes. In this way, the automation of the process became a mandatory requirement for performing an efficient long-term monitoring, which is a fundamental step for any damage detection applications.

As is well known, the modal parameters estimates are affected by environmental conditions (typically temperature and wind) that need to be removed or at least reduced in order to detect possible anomalies in the structural behavior which could be masked by such effects. In the classical approach, these effects (principally on the natural frequencies) are removed using techniques typically based on multivariate statistical methods, such as multiple regression models or Principal Component Analysis (PCA), in order to define a "normal condition" of the structure and subsequently apply any novelty detection approaches [Worthen et al. (2002), Yan et al. (2005), Magalhães et al. (2012), Mosavi et al. (2012), Dakermann et al. (2014), Comanducci et al. (2015)]. In this way, small structural changes should be conceivably detected; otherwise, the healthy state of the structure is confirmed if no significant deviation of the data from the normal condition is observed.

Conversely, recent developments are driving the possibility to perform a continuous assessment of the structural condition using the modal parameters estimates without filtering out the external effects (see e.g. [Marrongelli et al. (2018c)]). The applications of these strategies have been demonstrated quite effectively also by using a reduced number of sensors, making these strategies very promising in the context of preserving Cultural Heritage (CH) constructions.

This Chapter focuses on the application of the developed SHM methodology on the monitoring data of a real structure: the *San Gottardo Bell-Tower*. The tower, dating back to the 12th century, is located in the center of Milan and its octagonal shape gives it a unique architectural appeal in the skyline of the historical center of the city. The data continuously recorded by a simple monitoring system installed on the top of the tower have been processed using the automated OMA algorithms, described in Chapters 4 and 6, to perform the continuous monitoring. Moreover, the dynamic characteristics of the tower were assessed by means of an ad-hoc AVT performed to confirm the set of structural modes previously identified during the permanent monitoring. Subsequently, the novelty damage detection approach (described in Chapter 7) is used to automatically detect possible anomalies in the normal behavior of the tower.

It is worth mentioning that the developed SHM strategy presented herein is particularly suitable for the automated assessment of ancient constructions, performed by inspecting the evolution in time of the frequency estimates. To reach this challenging task, the proposed methodology combines the performance of three algorithms developed in this Dissertation and aimed at: 1) extracting the set of modal parameters estimates from the analysis of each single collected dataset, 2) ensuring the correct tracking of the most meaningful features over time, and 3) highlighting possible damages and anomalies occurred in the structure, analyzing the evolution of the modal frequencies under environmental conditions. It is also worth highlighting that this last task is performed by applying the CSA damage detection strategy to the sequence of OMA estimates without removing the effects of the environmental factors. From the obtained results, a promising approach toward a more widespread and systematic implementation of vibration-based SHM strategy for CH preservation will be demonstrated.

This Chapter begins with the presentation of the case study, including the historical background, together with a brief description of the installed monitoring system. Then, the dynamic characteristic of the ancient tower, obtained by applying the developed OMA algorithms (i.e. 2D-MPE and MT), are presented in detail. Thus, the main results obtained during two years of permanent monitoring are shown in detail highlighting the evolution

in time of the natural frequencies associated to eight identified modes. The correlation of the natural frequencies with the main environmental variables is also described, pointing out the non-linear correlations between external factors and modal features.

Furthermore, the structural integrity of the tower is demonstrated by the application of the developed SHM strategy to a wide period of monitoring (10 months from 01/01/2018 to 30/09/2018) pointing out the absence of structural anomalies and damage.

Finally, the robustness of the novelty approach has been demonstrated by simulating structural damages in the dynamic behavior of the tower through slight frequency shifts. As shown, the algorithm correctly identifies the small changes in the frequency evolutions that have been simulated in different time-periods (i.e., winter and summer period). Then, a sensitivity analysis has been performed in order to understand the potentiality of the developed strategy, obtaining very satisfactory results.

8.2 Description of the *San Gottardo in Corte Bell-Tower*

8.2.1 Description of the tower

The church of *San Gottardo in Corte* (Milan, Italy), situated in the near vicinity of the Milan Cathedral, was completed in 1336. Originally, it was a chapel attached to the residence of the Duke of Milan. The building was initially dedicated to the Virgin, to whom the Milanese were very devoted at the time of the construction, and subsequently to San Gottardo. The church included a slender bell-tower (**Fig. 8.1**(a)) and the architect responsible for the tower was Francesco Pegorari, as testified by a stone at the base of the building.

Even if a comprehensive geometric survey of the structure is not yet available, two different construction phases of the tower can be noted; they consist of a stone masonry square basement of 12.0 m, an octagonal portion in solid brick masonry up to the height of 41.0 m and a high cusp. The internal portion of the tower is shown in **Fig. 8.2**.

a) b)

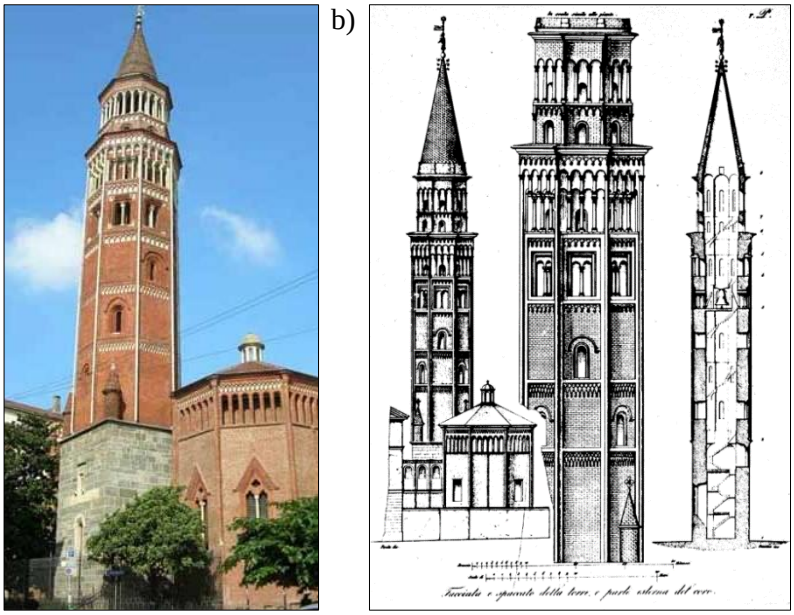

Fig. 8.1. Bell-tower of the church of San Gottardo in Corte, Milan: (a) view of the bell-tower and the San Gottardo in Corte Church and (b) ancient drawings of the building.

Since the tower exhibits only one wooden floor, at about 32.0 m, corresponding to the level of the bell chamber, the monitoring system was installed at that level. As shown in **Fig. 8.2**, the architecture of the circular staircase makes it very difficult to access the tower and consequently to perform a dynamic test though instrumenting different levels of the tower.

Fig. 8.2. Bell-tower of the church of San Gottardo in Corte: internal view of the bell-tower, the circular wooden staircase and the only wooden floor of the building.

This issue is the main reason why it was not possible to carry out a vibration test before the beginning of the monitoring process, and why that test was performed later. Meanwhile, the tower has been permanently instrumented since November 2016.

8.2.2 Installed monitoring system

The monitoring system installed in the *San Gottardo Tower* includes two bi-axial seismometers (electro-dynamic velocity transducers), one 24-bit digitizer (6 channels, ΣΔ A/D converter, 8 Gb Ram on board for data storage) and one UMTS modem for data transfer.

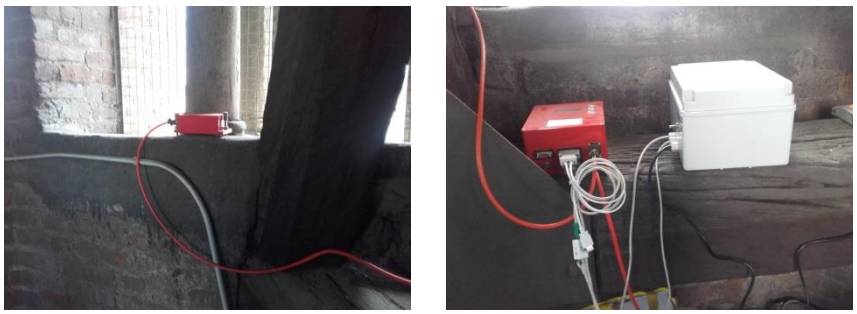

Fig. 8.3. Measurement devices installed in the *San Gottardo Bell-Tower*.

The automated modal identification was performed using time windows of 3600s (corresponding to more than 3500 times the fundamental period of the tower), in order to comply with the widely agreed recommendation of using an appropriate duration of the acquired time window to obtain accurate estimates from output-only data [Cantieni (2005)]. The sampling frequency was 100 Hz, which is much higher than the frequency required for the investigated structure, as the significative frequency content of signals is below 12 Hz. Hence, low pass filtering and decimation were applied to the data before the use of the identification tools. In more detail, after low-pass filtering the data through a 7th order Butterworth filter with cut-off frequency of 12.5 Hz, the velocity time series were down-sampled from 100 Hz to 25 Hz.

8.3 Definition of the reference baseline list of modes for continuous dynamic monitoring

Due to the difficulty of carrying out a dynamic test through covering several levels of the tower, it was firstly decided to install the monitoring system in the one wooden floor of the tower in order to record a few days of output response with the purpose of identifying the modal parameters, especially the resonant frequencies, associated to the structural modes.

It is worth to remark that the dynamic monitoring system of the historical tower has been in continuous operation since the 26th of October 2016 and its dynamic response has been continuously collected using a sampling frequency of 100 Hz. Every hour, the signals are collected in a new dataset that is initially stored in the backup memory of the system and subsequently sent to *Politecnico di Milano* in order to be analyzed. Hence, the recorded data are firstly pre-processed (including the elimination of the offset, filtering and re-sampling at 12.5 Hz) and consequently analyzed adopting the SSI-Cov technique to identify the modal parameters.

The identification algorithms described in Chapter 4 and 6 and the damage detection algorithm described in Chapter 7 are then explored using the data collected on the *San Gottardo* masonry tower.

Firstly, the MPE algorithm operating on 2D stabilization diagrams was adopted for the identification of the dynamic characteristics of the tower. The input parameters of the algorithm were tuned using the data collected during the first days of monitoring. In particular, the analysis of the first days of monitoring data was performed to define and justify the selection of the modal parameters (i.e. natural frequencies and mode shapes) adopted as reference values for the tracking process. Therefore, the continuous monitoring of the *San Gottardo* masonry tower effectively starts from the 1st of November 2016.

As already stated, the SSI-Cov method was adopted as identification method. Special attention should be given to the selection of the user-defined parameters associated to this

technique (i.e. the time-lag value and the maximum order of the stochastic model) and those adopted to perform the 2D-MPE algorithm (i.e., the threshold values). As previously described, this identification method is based on the construction of the correlation matrix of the measured signals and on the solution of the state-space model performed for increasing model order. Hence, two parameters define the correlation matrix: the reference channels and the maximum time-lag value. After some preliminary tests, stabilization diagrams with good quality were obtained adopting correlation functions with 90 points (90/12.5 = 7.2 seconds →7.2 x 1.04 = 7.48 times of fundamental frequency). Meanwhile, due to the reduced number of installed sensors, all channels were used as reference and, after some tests, the maximum order of the state-space model was fixed at 120. This last value ensures the comparison of a sufficient number of stable poles in the diagram, in which to detect the stable alignments associated to the structural modes.

The modal parameters resulting from the analysis carried out in the beginning of the monitoring phase are shown in **Fig. 8.4**. Due to the fact that only two points of the only transversal cross-section of the tower are permanently instrumented by biaxial sensors, the assumption of "stiff diaphragm" has been adopted in **Fig. 8.4** (indeed, 3 modal deflections were used to draw the deformed shape and the 4th one was used to verify that the main assumption was basically satisfied). The inspection of **Fig. 8.4** reveals that the first two couples of modes involve bending in two orthogonal N-S and E-W planes of the octagonal cross-section, whereas modes 5-6 seem to involve coupling between bending and torsion. The last couple of identified modes involves bending in two orthogonal planes, which are different from N-S and E-W.

From the analysis carried out on a single recorded dataset, eight structural modes were clearly detected. Hence, from these results the main natural frequencies and the mean mode shapes, which define the rigid displacements of the one walk-on accessible floor (see **Fig. 8.4**), were used as baseline reference list for the continuous monitoring process.

The main values and the statistical properties of the extracted structural mode are depicted in **Fig. 8.4** reported in **A representation** of the mode shapes associate to the identified

modes is shown in **Fig. 8.5.** The polar plot provides further information about the complexity degree associated to each extracted mode shape underlining both the real and imaginary part of the components. As shown, the imaginary parts are negligible, so the mode shapes are real.

Table 8.1.

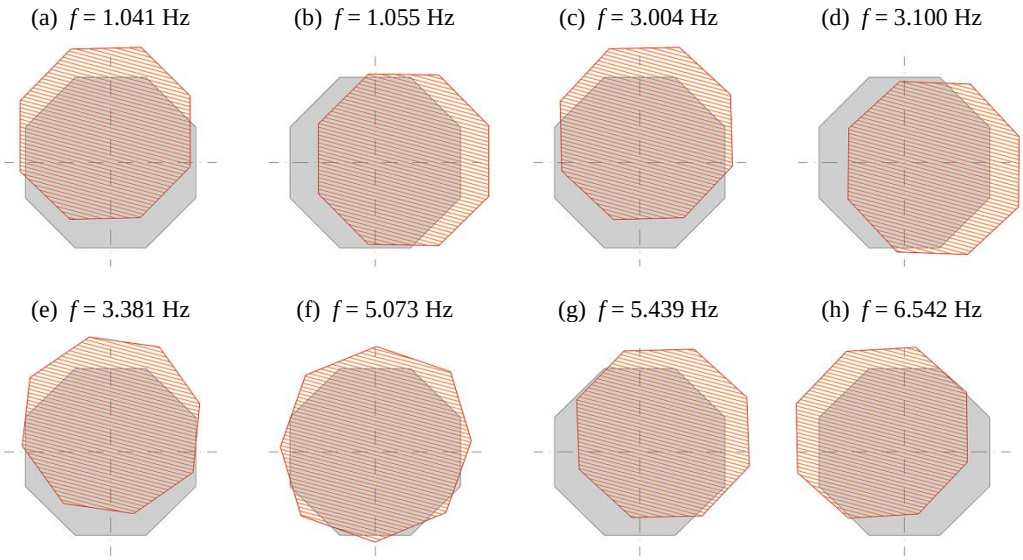

Fig. 8.4. Automatically identified vibration modes (N-S: vertical axis) of the San Gottardo Bell-Tower. Natural frequency and displacement of the wooden floor in the assumption of "stiff diaphragm" associated to: (a) Mode 1; (b) Mode 2; (c) Mode 3; (d) Mode 4; (e) Mode 5; (f) Mode 6; (g) Mode 7 and (f) Mode 8.

A representation of the mode shapes associate to the identified modes is shown in **Fig. 8.5**. The polar plot provides further information about the complexity degree associated to each extracted mode shape underlining both the real and imaginary part of the components. As shown, the imaginary parts are negligible, so the mode shapes are real.

Table 8.1. Statistics of the identified reference modes applying the MPE algorithm to structural response recorded on 26/10/2016.

Modes	***f* [Hz]**	**σ(*f*) [Hz]**	**ξ [%]**	**σ(ξ) [%]**	**MPC**	**MPD**
1	1.041	0.0001	0.43	0.0013	1.00	2.36
2	1.055	0.0001	0.41	0.0035	0.97	5.46

3	3.004	0.0002	0.97	0.0099	1.00	1.04
4	3.100	0.0014	0.89	0.0575	1.00	1.34
5	3.381	0.0006	0.71	0.0095	1.00	1.71
6	5.073	0.0026	1.00	0.0179	1.00	1.00
7	5.436	0.0162	3.02	0.5119	0.95	6.14
8	6.542	0.0285	2.72	0.3265	0.99	2.50

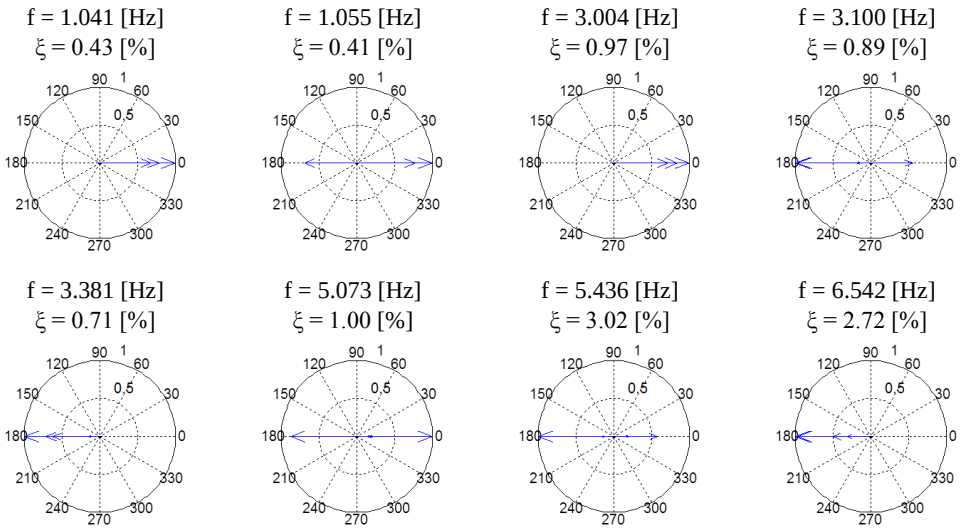

Fig. 8.5. Reference modal parameters of the SSI-Cov method. Natural frequencies, modal damping ratios and mode shapes represented in polar plot, for all identified modes.

8.4 Ambient Vibration Test and principal vibration modes

On the 21st of March 2017 the AVT was carried out to extract the modal parameters of the tower and, more specifically, the mode shapes associated to the natural frequency estimates obtained during the first months of the monitoring process. The dynamic test was performed using 8 high-sensitivity accelerometers (see **Fig. 8.6**(b)). The layout of the installed sensors is reported in **Fig. 8.6**(a).

The database collected during the AVT of the tower was processed using two different identification algorithms implemented during the development of the present work. Firstly, the classical FFD was used in order to have a quick estimation of the most relevant modes through the local peaks of the first Singular Value (SV) which is the mode indication function adopted in the FDD method extracted by the spectra matrix. Subsequently, the parametric SSI-Cov technique was also applied.

a) b)

Fig. 8.6. Ambient vibration tests performed on 21/03/2017: a) layout of the sensors used for the AVT; b) biaxial accelerometers positioned in the four available levels of the tower.

The results provided by the application of both methods have been presented in [Marrongelli et al. (2018a)], highlighting the correspondences between the peak values of the first SV and the stable alignments that stand out in the stabilization diagram.

In **Fig. 8.7**, the typical stabilization diagram obtained by applying the SSI-Cov method is reported. As shown, the diagram contains all mode estimates (spurious and physical ones) provided by models with even orders between 20 and 120. As is visible, models with higher order overestimate the solutions of the dynamic problem modelling also the noise content into the signals. This condition implies the comparison of spurious poles that do not have physical meaning characterized by high or negative damping and/or by high complex modal components of mode shapes. Therefore, the developed MPE [(Marrongelli et al. (2018b); Marrongelli et al. (2019a)] algorithm is applied in order to remove all spurious

poles and to obtain only the stable alignments composed by certain physical poles that maintain consistency in terms of modal parameters for increasing model order.

The user-defined thresholds adopted to perform the MPE algorithm and deliver a clearer stabilization diagram were set as follows: damping threshold equal to 5%, complexity thresholds associated to MPC and MPD index equal to 0.8 and 15°, respectively. Meanwhile the inter-cluster distance threshold used to construct the representative clusters of the structural modes was defined in a conservative way equal to 0.025. These tolerance values allow for a clear appearance of eight vertical alignments representative of the eight structural modes of the tower.

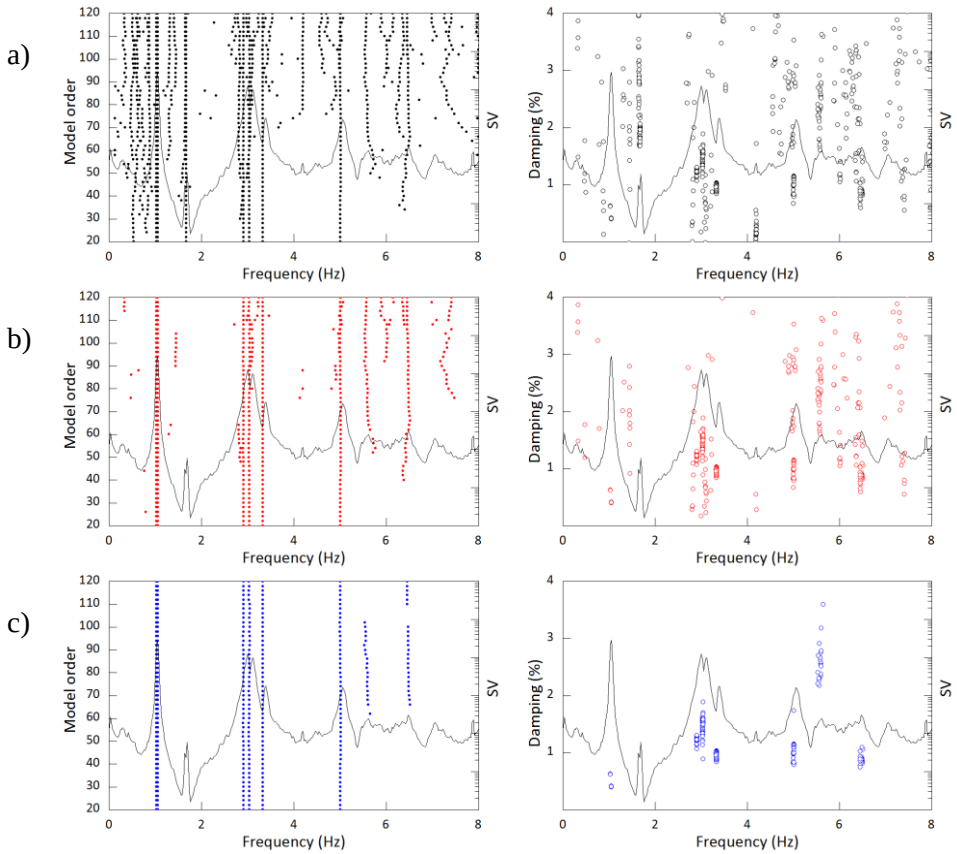

d)

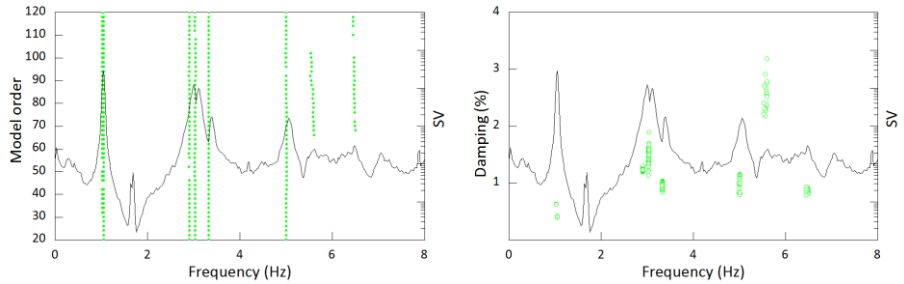

Fig. 8.7. Stabilization diagrams (San Gottardo Bell-Tower): (a) resulting from SSI-Cov; (b) after the pre-filtering; (c) after the clustering; (d) after the post-processing to improve the estimate accuracy (final results).

Fig. 8.7 refers to one 1-hour dataset recorded by the installed monitoring system on 21/03/2017. It shows the typical cleaning action exerted by the various steps of the proposed MPE procedure on the stabilization diagrams. In particular: 1) **Fig. 8.7**(a) shows the results initially obtained applying the SSI-Cov method for increasing model order; 2) **Fig. 8.7**(b) shows the performance of the pre-filtering step on the SSI outputs (i.e., after the check on damping and mode shape complexity); 3) **Fig. 8.7**(c) illustrates the effect of the clustering process on the remaining poles; and 4) **Fig. 8.7**(d) contains the final alignments of stable poles corresponding to physical modes of the structure. As mentioned before, it is worth noting that the first SV line of the spectral matrix is depicted in all plots of **Fig. 8.7**, highlighting the correspondence between the local SV's peaks and the stand out alignments of stable poles.

(a)	(b)	(c)	(d)	(e)	(f)	(g)	(h)	(i)
Sensors layout	f = 1.040 Hz	f = 1.058 Hz	f = 3.004 Hz	f = 3.110 Hz	f = 3.373 Hz	f = 5.066 Hz	f = 5.569 Hz	f = 6.495 Hz

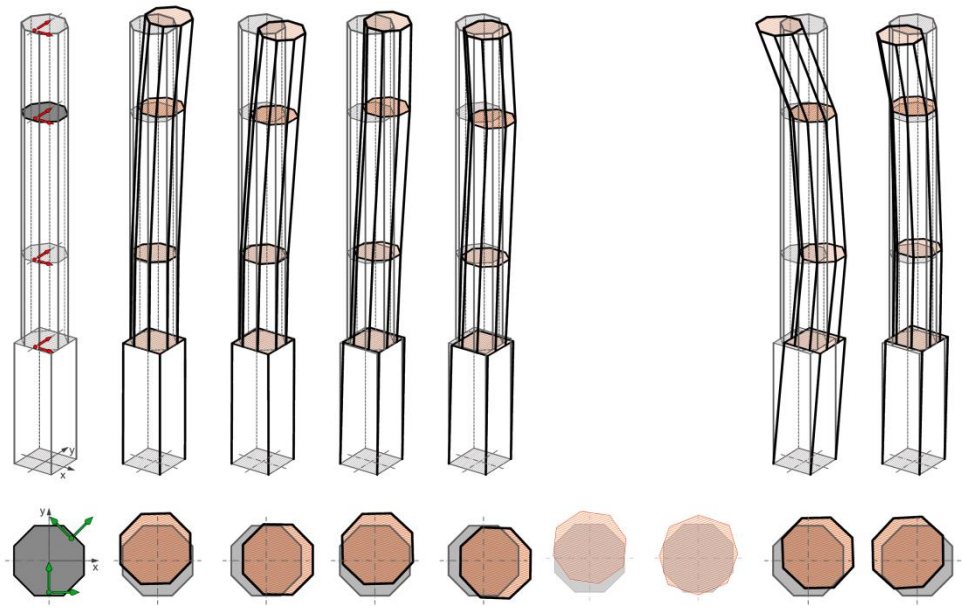

Fig. 8.8. San Gottardo Bell-Tower: (a) Sensors layout in the test of 21/03/2017 (red arrows) and in the permanent monitoring (green arrows); (b)-(i) Automatically identified modes (Y-axis: N-S direction).

Furthermore, the inspection of **Fig. 8.7** highlights that: (a) within the investigated frequency range (0-8 Hz), the alignments of the stable poles in the stabilization diagram provide a clear indication of 8 tower modes and 6 of those alignments of stable poles correspond to well defined local maxima in the first SV line of the FDD procedure; (b) the last two modes, although weakly excited, are clearly identified as the model order increases and (c) as it is common for historic towers [Gentile et al. (2016); Ubertini et al. (2017); Cabboi et al. (2017); Ubertini et al. (2018); Azzara et al. (2018)], the resonant frequencies of the two lower modes are closely spaced.

The diagrams reported in **Fig. 8.7** refer to the analysis of a single record collected by the monitoring system, meanwhile the results reported in **Fig. 8.8**. refer to the modes obtained by the dynamic test performed at the same time using 8 high-sensitivity accelerometers. The inspection of the representation reported in **Fig. 8.8**. allows for the following comments: (a) the first couple of modes (**Fig. 8.8**(b-c)) involve bending in two orthogonal

N-S and E-W planes of the octagonal cantilever, without significant participation of the square basement; (b) the higher couples of bending modes (**Fig. 8.8**(d-e) and **Fig. 8.8**(h-i)) occur in orthogonal planes, which are different from N-S and E-W, and do involve an appreciable motion of the basement; (c) modes 5 and 6 (**Fig. 8.8**(f-g)) involve coupling between bending and torsion. The complete representation of those mode shapes cannot be uniquely defined using the adopted sensor layout, even introducing the assumption of "stiff diaphragm", and is not shown in **Fig. 8.8**.

8.5 Continuous dynamic monitoring of the historic bell-tower

The modal parameters described in **Fig. 8.5** were used as reference values for the continuous monitoring of the *San Gottardo Bell-Tower*. As reported in Chapter 5, the tracking of the modal parameters is performed by the MT algorithm that directly works on the evolution of the natural frequency estimates and on the variation of the mode shapes over time. Then, the developed OMA methodology composed by the 2D-MPE algorithm and the MT tool was used to investigate the evolution of the structural modes of the tower in the context of a continuous monitoring purpose.

Once the baseline reference list of modal parameters was defined, the continuous monitoring was performed maintaining the same pre-selected tolerance values previously defined for the identification analysis and setting the threshold values for the tracking process, as follows: d_{i-ref}^{f} = 0.02 Hz and d_{i-ref}^{MAC}=0.90.

It is worth mentioning that, conversely to the indication reported in [Marrongelli at al. (2018a)] the “training period” of the tracking procedure can be greatly reduced to 5 days instead of the 15 days declared in [Marrongelli at al. (2018a)], improving the speed of process automation, using a reduced number of estimates that seems to be sufficient for the definition of the adaptive thresholds without reducing the efficiency of the implemented strategy.

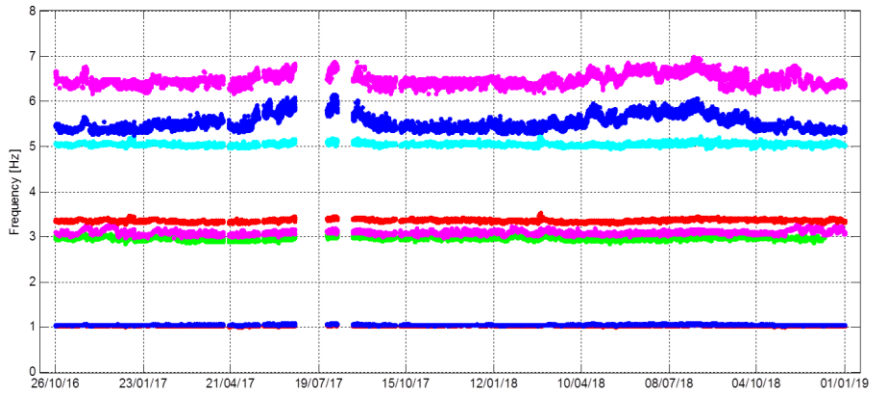

Fig. 8.9. Time evolution of the identified natural frequencies from 01/11/2016 to 31/12/2018

According to the previous analysis, the time-lag parameter was maintained in conservative manner equal to 90 and the data was fitted using stochastic subspace models of the order *n*, varying between 20 and 120. The MT procedure was finalized to track the evolution in time of the natural frequency estimates belonging to the 8 structural modes. The main results of more than two years of continuous dynamic monitoring, specifically from the 1st of November 2016 to the 31st of December 2018 are summarized in **Fig. 8.9**.

The main statistical values associated to the evolution of the natural frequencies obtained during more than two years of monitoring are summarized in **Table 8.2**, in which the mean value (f_{ave}), the standard deviation (σ_f) and the extreme values (f_{min}, f_{max}) of each modal frequency are reported.

Table 8.2. Statistics of the natural frequency estimates automatically identified in the monitoring period from 01/11/2016 to 31/12/2018.

Modes	f_{ave} [Hz]	$\sigma(f)$ [Hz]	f_{min} [Hz]	f_{max} [Hz]
1	1.039	0.008	1.015	1.078
2	1.055	0.009	1.034	1.097
3	2.976	0.036	2.871	3.079
4	3.090	0.047	2.982	3.291
5	3.371	0.028	3.294	3.483
6	5.059	0.032	4.961	5.226
7	5.510	0.155	5.252	6.182
8	6.450	0.117	6.177	6.779

It should be noticed in **Table 8.2** that the standard deviations: (a) are very low (0.008-0.009 Hz) for the lower 2 modes; (b) range between 0.028 Hz and 0.047 Hz for the subsequent 4 modes and (c) became larger than 0.1 Hz for the higher modes.

8.6 Correlation between natural frequency estimates and environmental factors

As stated, it should be noted that the monitoring system installed on the *San Gottardo Tower* does not include any sensors for measuring the environmental parameters since temperature and humidity data were available from the neighboring weather station *Osservatorio di Brera*. Thus, the temperature, the humidity and the speed of wind were collected and used to investigate the main correlations between these factors and the extracted modal features, in particular on the natural frequency estimates.

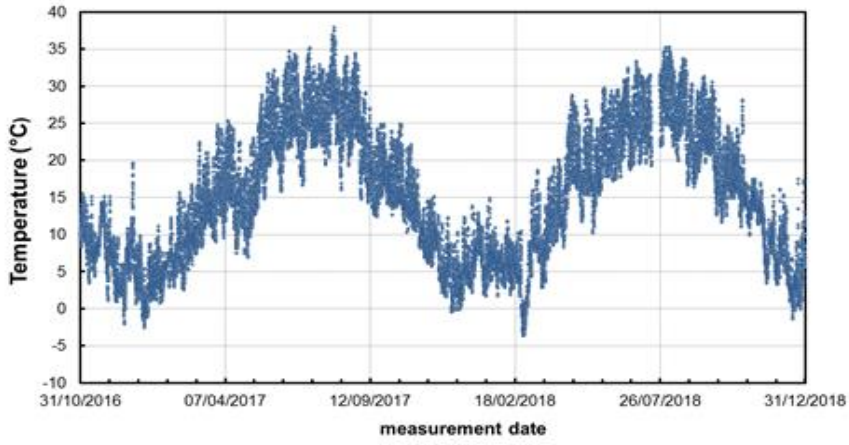

Fig. 8.10. Time evolution of the outdoor temperature measured from 01/11/2016 to 31/12/2018

Fig. 8.10 presents the evolution of the air temperature during a period of about 26 months, from 01/11/2016 to 31/12/2018, and shows a temperature range between –2°C and +38°C, with significant daily variations in sunny days.

The inspection of the evolution in time of the temperature (**Fig. 8.10**) and the modal frequencies (**Fig. 8.9**) clearly suggests that the frequency generally increases with increased temperature in the hot season [Gentile et al. (2016), Ubertini et al. (2017), Cabboi et al. (2017), Ubertini et al. (2018), Azzara et al. (2018)]. On the other hand, the correlation between resonant frequencies and temperature (**Fig. 8.11**) reveals a more complex and non-linear dependence on temperature.

Fig. 8.11 shows the correlations between the natural frequencies identified during the first year of monitoring (from 01/11/2016 to 31/12/2017) and hourly average temperatures recorded during the same period along with the best-fit lines. As reported, the correlations highlight that each best-fit line tends to be non-linear for almost all identified frequency trends. In fact, it is possible to notice a double behavior of the identified frequencies in relation to the measured temperature values. This trend is confirmed also by the results obtained during the second year of monitoring, as reported in **Fig. 8.12**.

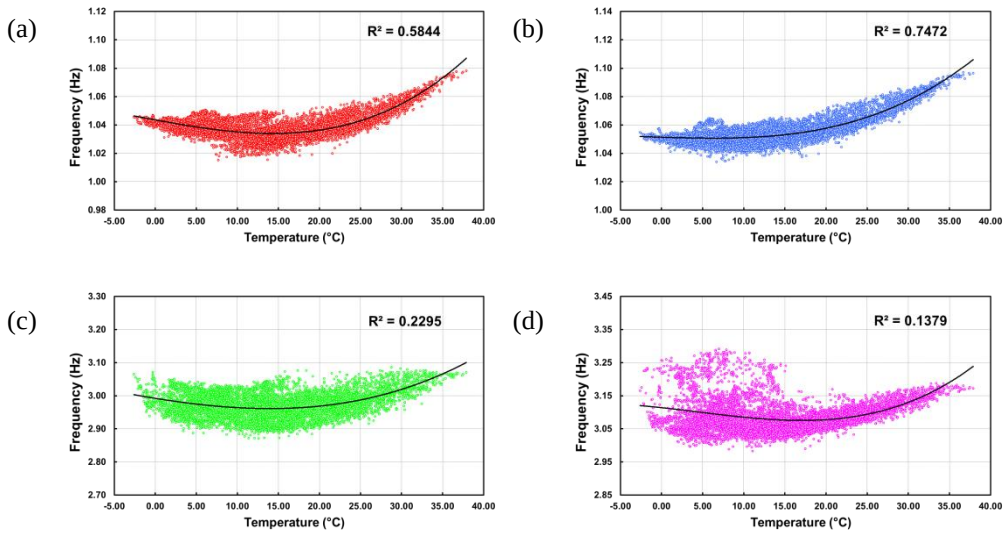

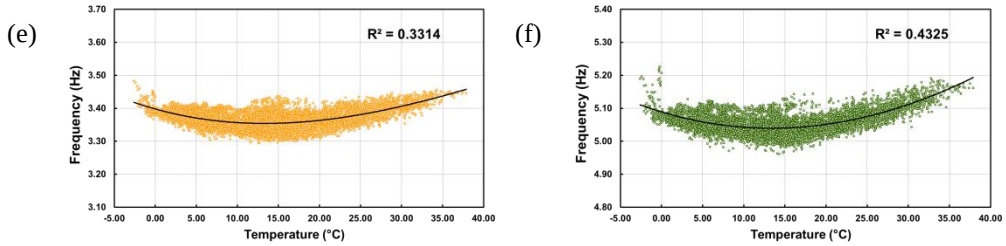

Fig. 8.11. Correlation between automatically identified frequencies during the 1st year of monitoring (from 01/11/2016 to 31/12/2017) and measured temperature: (a) Mode 1; (b) Mode 2; (c) Mode 3; (d) Mode 4; (e) Mode 5; (f) Mode 6.

From the inspection of the diagrams in **Fig. 8.12** the non-linear correlations between the temperature measurements and extracted natural frequency estimates are highlighted. The best-fit line is non-linear for all six identified frequency trends. More in detail, the non-linear frequency-temperature correlation (**Fig. 8.11** and **Fig. 8.12**) turns out to be characterized by the increase of modal frequencies with increased temperature, when $T \geq 15$°C (in agreement with a trend that has been commonly observed on masonry towers [Gentile et al. (2016), Ubertini et al. (2017), Cabboi et al. (2017), Azzara et al. (2018)]), but also by the increasing of natural frequencies with decreased temperature, when $T \leq 10$°C.

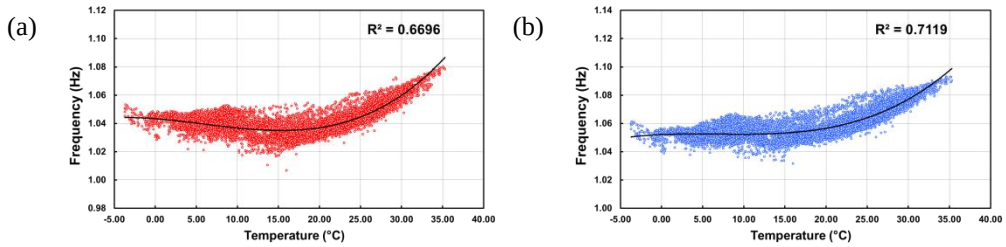

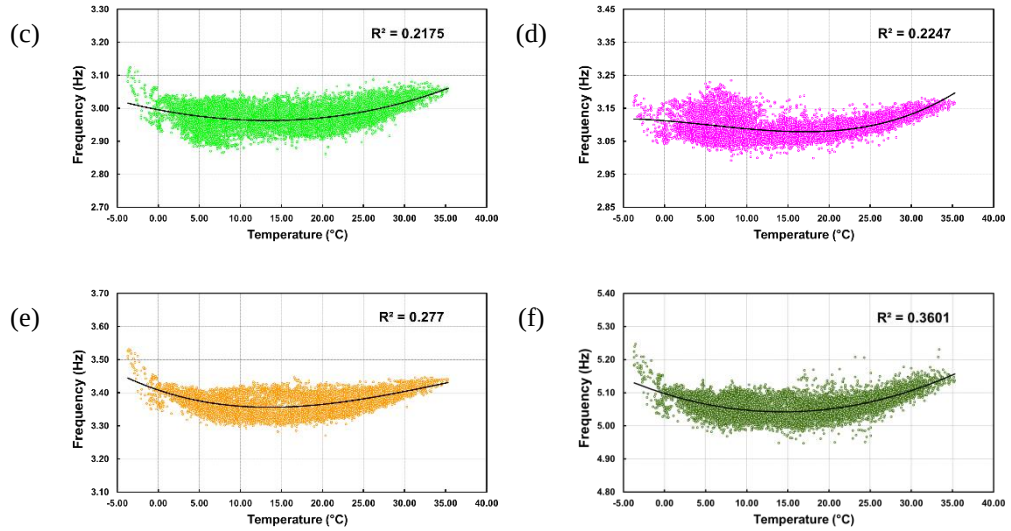

Fig. 8.12. Correlation between automatically identified frequencies during the 2nd year of monitoring (from 01/01/2018 to 01/01/2019) and measured temperature: (a) Mode 1; (b) Mode 2; (c) Mode 3; (d) Mode 4; (e) Mode 5; (f) Mode 6.

As shown in the diagrams, in the first temperature range between negative values and 10°C, an unusual behavior of the correlation is pointed out. In fact, the frequency value slightly decreases with increased temperature. Afterward, this trend tends to become more stable in the temperature range between 10°C and 15°C, describing a local minimum of the frequency-temperature correlation common for the first six natural frequencies. Subsequently, the frequency values clearly increase with increasing temperature (T>15°C), as usual.

This behavior might depend on two distinct factors: (a) the thermal effect induced by temperature variations produces a thermal expansion of the materials and (b) the circular wooden staircase anchored to the tower that might provide a sort of circling effect on the slender part of the tower.

A possible motivation of the observed behavior (for T>15°C) can be explained though: (a) with the increase in temperature, the induced circling effect of the wooden staircase

becomes less dominant (due to thermal expansion), (b) the closure of the small discontinuities, micro-cracks and superficial cracks in the masonry, induced by the thermal expansion of the materials, provides a temporary increase of global stiffness in the tower. This behavior is clearly described by the ascending branch of the best-fit line, in which the frequencies increase with increased temperature, as it is described in some papers present in the literature, as well as [Cantieni (2014), Saisi et al. (2015)].

On the contrary, when the temperature decreases, the effect of the thermal expansion becomes less evident and this behavior tends to lose its effect. Furthermore, in the interval (10°C-15°C), in which the frequency values are almost constant, there is an inversion trend of the frequencies that tend to increase with decreased temperature.

This second behavior becomes more evident for T<10°C and it might depend on induced effects of the circular wooden staircase present inside the tower (due to low temperature). More in detail, the different mechanical characteristic of the solid bricks and the staircase produce two opposite effects on the identified dynamic response to the gradual loss in stiffness due to the opening of the superficial cracks, the staircase might induce an opposite behavior due to a circling effect on the slim-upper part of the tower, giving more rigidity.

Thus, in the interval temperature between 10°C and 15°C, the gradual loss of the effect due to the circular wooden staircase is balanced by the increasing of stiffness provided by the closure of micro-fractures and cracks. This effect describes a local minimum for all best-fit lines associated to the frequency-temperature correlations.

Same analyses were carried out using the measurements of the humidity recorded by the weather station *Osservatorio di Brera* on over 2 years of monitoring.

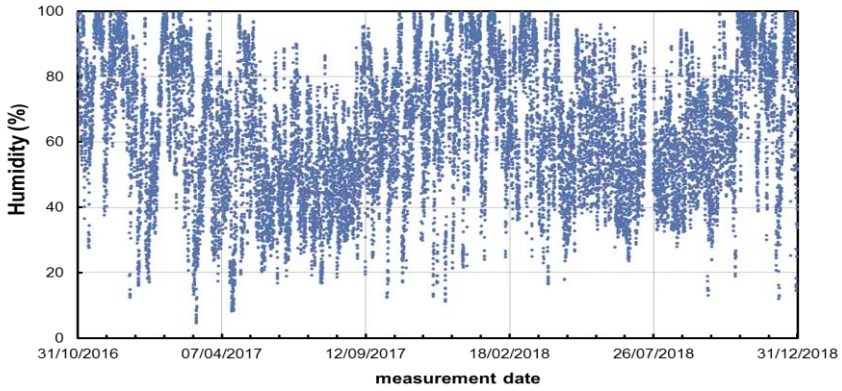

Fig. 8.13. Time evolution of the outdoor humidity measured from 01/11/2016 to 31/12/2018

In **Fig. 8.14**, the correlations between the resonant frequencies of the tower and the humidity measurements collected during the two years of monitoring period are reported. From the inspection of the diagrams there is not a clear correlation between the sets of modal parameters and the humidity values. In fact, there is not a recognizable dependence between the humidity variation and the estimations of the natural frequency associated to modes 1-6.

The lack of direct measurements of the external factors on the structure (i.e. temperature and humidity) and the uncertainty related to the variations induced on natural frequencies by these factors do not allow for a proper application of regressive techniques and methods to efficiently remove such effects. In fact, this lack of direct measurements does not allow for a correct definition of empirical laws of correlation between the resonant frequencies and the environmental factors that act on them. Generally, this condition could be a relevant issue for the continuous assessment of those constructions based on the natural frequencies features, because the uncertainty of these correlations does not allow a ful understanding of the dynamic behavior of the structure that could be masked by induced effects.

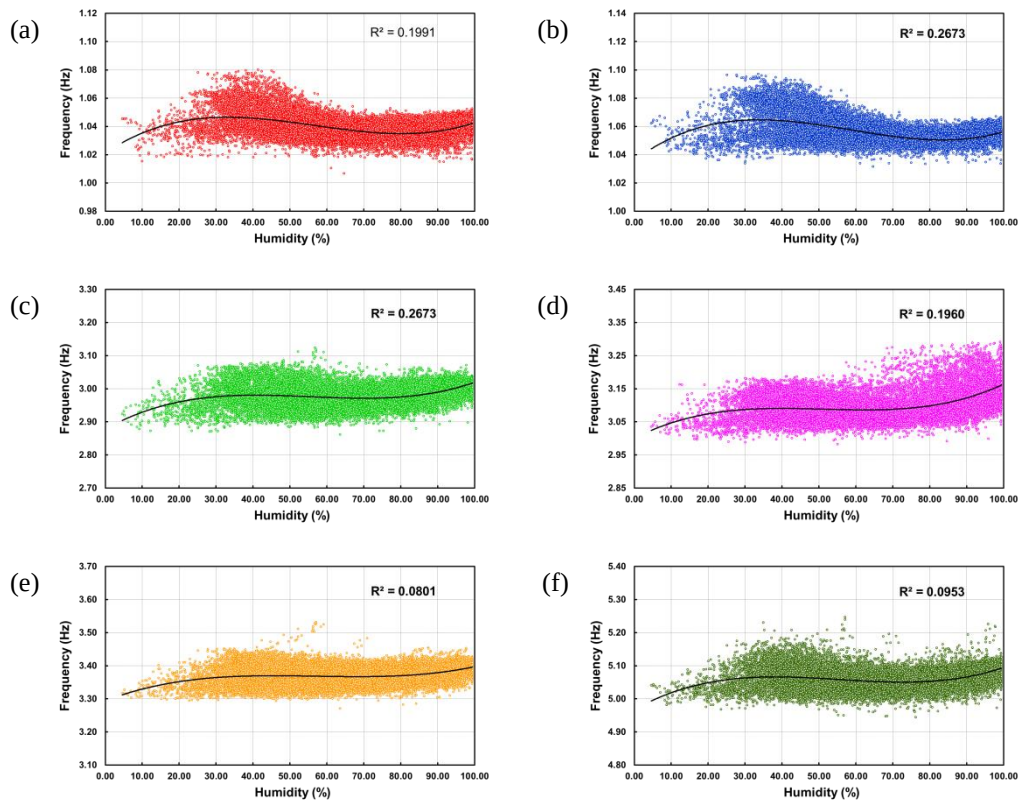

Fig. 8.14. Correlation between automatically identified frequencies and recorded humidity data: (a) Mode 1; (b) Mode 2; (c) Mode 3; (d) Mode 4; (e) Mode 5; (f) Mode 6.

An efficient approach generally adopted to remove the environmental effects on the natural frequency estimates without getting direct measures of environmental parameters consists of the application of the Principal Component Analysis (PCA) in order to reduce the dimension of the investigation problem, by substituting the group of correlated dependent variables (i.e., the eight resonant frequencies) with a smaller group composed by a reduced number of independent variables (i.e., principal components). For the correct application of the PCA method it is necessary to have a linear correlation degree among the structural features in order to perform the diagonalization of the correlation matrix and to extract the PCs that explain the major proportion of the variance of the original variables. The analysis carried out on the extracted natural frequencies points out a strong linearity, obtained

between the first and the second resonant frequencies, while at the same time, fewer correlations are obtained between the first frequencies and the others. Moreover, the frequencies evolution associated to the modes 7 and 8 seem to be uncorrelated with the first ones. This primary analysis gives rise to doubts about the correct application of the PCA analysis to the present case study.

Due to these considerations, the continuous assessment of the *San Gottardo Bell-Tower* was performed adopting and applying the damage detection strategy implemented during the development of this Dissertation. Thus, in the following, the performance of the SHM strategy applied to continuous monitoring data is shown. Furthermore, in order to test the robustness of the developed procedure in the detection of structural anomalies, some damages were simulated through small frequency shifts in the evolution of the identified natural frequencies.

8.7 Application of the damage detection algorithm to monitoring data

The damage detection strategy described in Chapter 7 was adopted to perform the continuous assessment of the healthy state of the masonry bell-tower. This analysis was carried out applying the CSA (Consecutive Segments Analysis) strategy to an entire set of continuous monitoring results (in terms of natural frequencies evolutions) in which the process does not suffer any arrest and stops. The continuity of the results provided by the developed OMA algorithm (i.e., 2D-MPE and MT algorithms), together with the high success rate of the identified structural modes, should guarantee the correct performance of the novelty detection algorithm and avoid incorrect classifications that could appear in case of a persistent loss of estimates.

As already stated in Chapter 7, the damage detection algorithm (in both CSA and SSA implementations) works with a series of input data selected in order to define two different

classes (i.e., Class I and Class II) that refer to two different structural conditions (i.e., undamaged and damaged) of the structure within the continuous monitoring process.

Once again, it is worth underlining the fact that the procedure does not require a long training period to define the parameters of the SVM model used for damage detection purposes. For the present case study, two weeks of monitoring data, in which the structural modes were identified with a high success rate, have been enough to define the initial parameters of the model and carry out the investigation for structural anomalies in the monitoring results. In **Fig. 8.15** the reference period of monitoring selected to perform the continuous assessment of the tower is reported. For the practical application, only the natural frequency estimates associated to the first six structural modes (with lower frequencies) were selected and used as input values. This choice is due to the success rates associated to the identified modes, which are close to 99%.

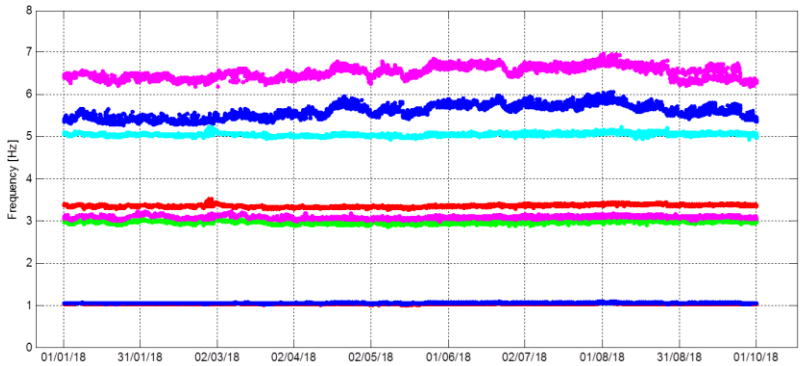

Fig. 8.15. Reference period of monitoring selected to perform the continuous assessment of the tower. The implemented CSA strategy was applied to the period from 01/01/2018 to 30/09/2018

As reported for the previous application (the *Gabbia* tower described in Chapter 7), after some initial tests the length of the data segments used as input of the SVM model was defined equal to 48 elements. This value indicates that the algorithm works with a population of modal estimates equal to 96 elements (in which 48 elements are flagged as undamaged and other 48 elements are flagged with damaged labels). Moreover, this value seems to produce the best results in the investigation for small frequency drops.

It is worth noting that by selecting this length for both data segments (undamaged and damaged), the occurrence of any damages is fully provided after 48 runs of the algorithm. This means that, when the damage occurs in the structure, it should be automatically and precisely identified after only 48 days. Furthermore, it should also be highlighted that: if the continuous monitoring is performed by collecting the response of the structure with 30-minutes long datasets, a damage with the same amplitude might effectively be detected with a delay of only 24 hours from its occurrence.

The main results in the continuous assessment of the *San Gottardo Bell-Tower* in the reference period, from the 1st of January 2018 to the 30th of September 2018 using the CSA strategy are reported in **Fig. 8.16**.

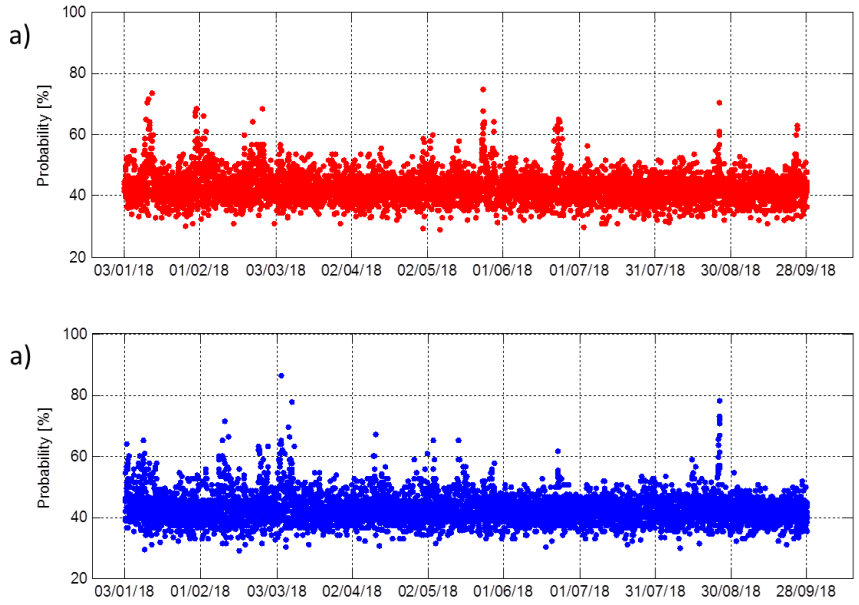

Fig. 8.16. Examples of probability values obtained by the application of the damage detection algorithm (CSA strategy) to the monitored features from 01/01/2018 to 30/09/2018 adopting; a) first frequency and b) second frequency estimates

From the inspections of the diagrams in **Fig. 8.16** the absence of any peaks of the probability value is highlighted. As stated in Chapter 7, this condition is obtained when the

algorithm fails in the classification of input data. In other words, the algorithm is not able to separate the population of data into two classes, thus performing a misclassification of the inputs. This continuous misclassification proves two important facts: 1) the data are not separable and 2) the input data belong to the same class of data (class with same statistical properties). However, if the initial condition of the investigated structure is supposed to be undamaged, the graphical results presented in **Fig. 8.16** suggest that the undamaged state is changeless over time and that no damage occurred during this period.

The results provided by the application of the novelty damage detection strategy suggest that the structural integrity of the masonry tower is maintained over the investigated monitoring period.

8.8 Simulation and identification of structural damages on the *San Gottardo Bell-Tower*

In order to demonstrate the efficiency of the proposed novelty algorithm, a structural damage was simulated through a frequency shift. As shown in the previous paragraph, the ancient construction did not suffer any anomalies during the reference investigated period from 01/01/2018 to 30/09/2018. Despite this result, some trial tests were carried out to verify the sensitivity of the models to simulated damages. The following diagrams report the results obtained applying a common frequency shift, with a nominal value of 0.05 Hz, to the evolution of the first six natural frequencies (applied on 15/02/2018). As it will be described in **Table 8.3**, the probability of the occurred damage associated to six natural frequencies is reported in the following. In particular, the application of the CSA algorithm to the first and the second natural frequency evolution is reported in **Fig. 8.17**. Meanwhile, the results related to the higher frequencies are reported in **Fig. 8.18**.

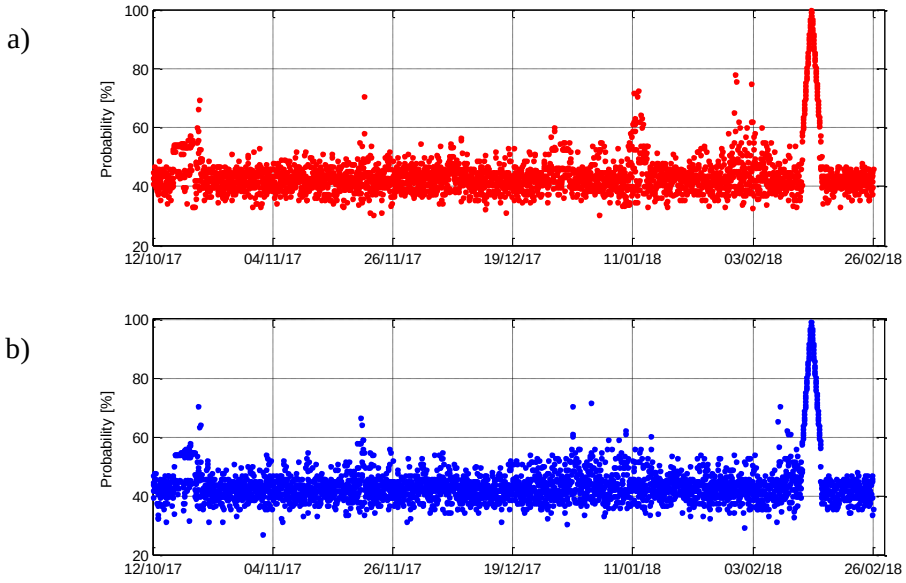

Fig. 8.17. Probability value associated to the occurred damage obtained applying a frequency shift to the a) firs and b) second frequency evolutions

As demonstrate by the graphical results illustrated in **Fig. 8.17**, the simulated damaged is clearly detected by the SVM model, which provides one clear peak in terms of occurred probability, which reaches 100%. This means that the algorithm performs a perfect classification, allocating 50% of the data to the undamaged condition and another 50% to the damaged condition. On the contrary, from the inspection of the diagrams reported in **Fig. 8.18**, some spurious peaks appear in the damage probability associated to the analysis of higher frequencies. These spurious peaks are mainly due to a loss of estimates, which leads to an incorrect classification that does not depend on structural conditions.

In fact, from a deeper investigation of the results obtained, it can be highlighted that the spurious peaks occurred when the mode was not identified in various consecutive datasets during the continuous monitoring process. This loss could provide a shift among the provided estimates, which the algorithm recognizes as a drop in frequency and then as a damage. This condition is clearly evident when the loss of information is not isolated, but it persists for some consecutive hours at least. This situation is not a relevant issue because spurious peaks (not related to changing of structural conditions) should not appear

simultaneously in all frequencies, and they can be removed averaging the values of probability obtained by each individual frequency, as shown in **Fig. 8.19**

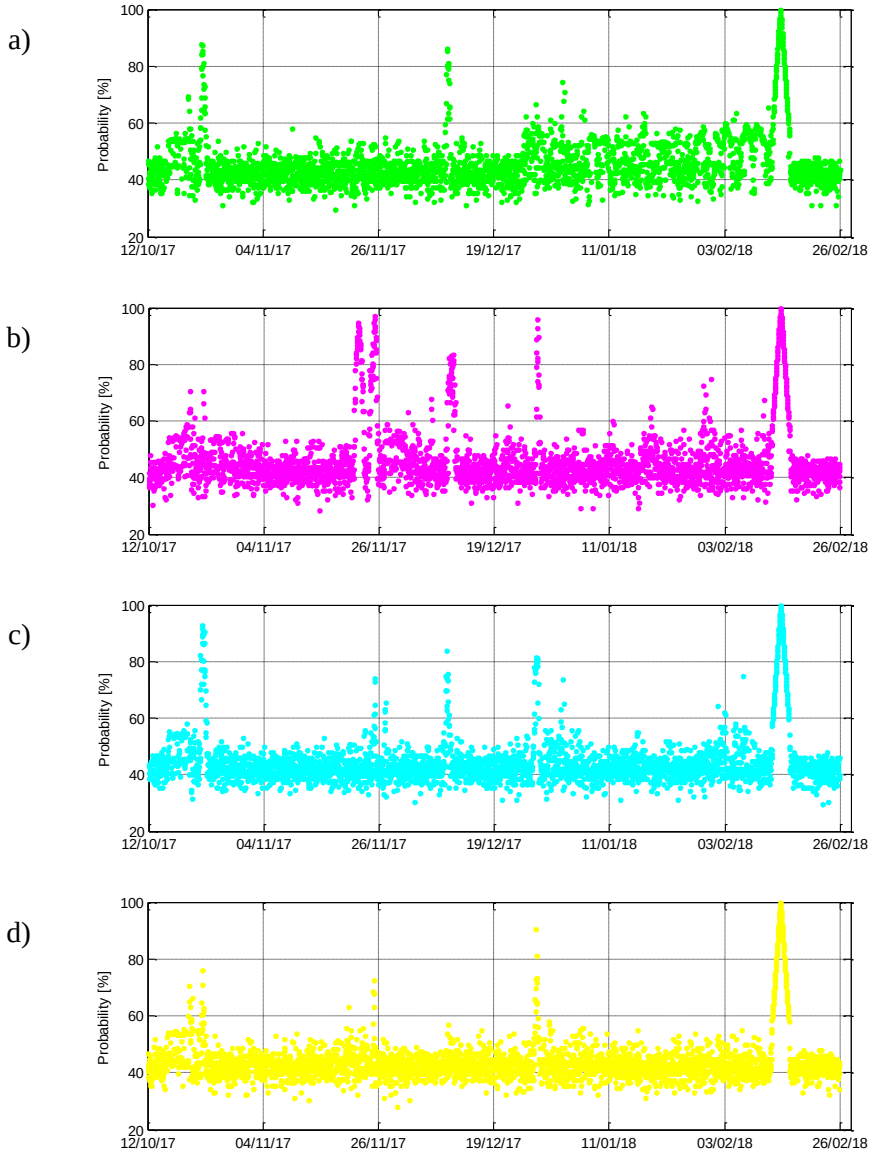

Fig. 8.18. Probability value associated to the occurred damage obtained applying a frequency shift to the a) 3rd, b) 4th, c) 5th and d) 6th frequency evolutions, simultaneously

As depicted, averaging the values obtained independently by each singular application, the spurious peaks associated to false positive are almost removed. On the contrary, the peak associated to the occurred damage remains clearly visible on the diagram.

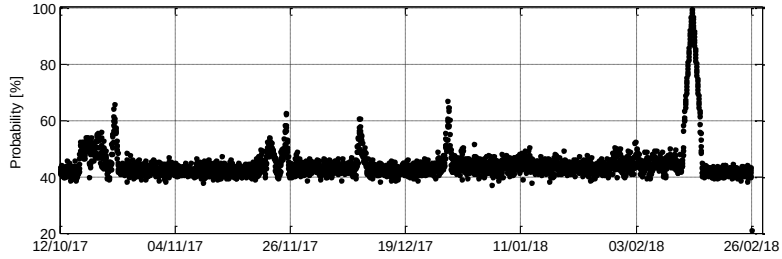

Fig. 8.19. Damage indicator obtained averaging the probability of occurred damage obtained analyzing the first six natural frequencies of the tower

Subsequently, a deeper investigation was performed to test the efficiency and the sensitivity of the developed algorithm in the identification of small simulated damages. Therefore, several shifts with increasing amplitude were introduced in the evolutions of the resonant frequencies as summarized in **Table 8.3**.

Table 8.3. Nominal frequency shifts applied on the monitored frequencies (CSA strategy)

Mode	**Δ*f* 0.05 Hz**	**Δ*f* 0.04 Hz**	**Δ*f* 0.03 Hz**	**Δ*f* 0.02 Hz**	**Δ*f* 0.015 Hz**	**Δ*f* 0.01 Hz**	**Δ*f* 0.005 Hz**
1	yes	yes	yes	yes	yes	yes/no	no
2	yes	yes	yes	yes	yes	yes/no	no
3	yes	yes	yes/no	no	no	no	no
4	yes	yes	yes/no	no	no	no	no
5	yes	yes	no	no	no	no	no
6	yes	yes	no	no	no	no	no

As reported in **Table 8.3**, the pattern recognition model is able to recognize anomalies with very small entity, if the latter is applied to the trend of lower frequencies. On the contrary, the same model is less effective in the analysis of higher frequencies. As is obvious, this result depends on the statistical properties of the frequency distribution belonging to each feature provided to the SVM model. In other words, when the data distribution is compact (with low standard deviation), the detection of small frequency variations is easier. Otherwise, high scatter does not allow for the correct classification of the data. It is worth

noting that the damage detection approach presented herein can detect structural anomalies with a nominal value less than 1% of the mean frequency value associated to each investigated mode. This outcome is a very good result for this alternative SHM strategy.

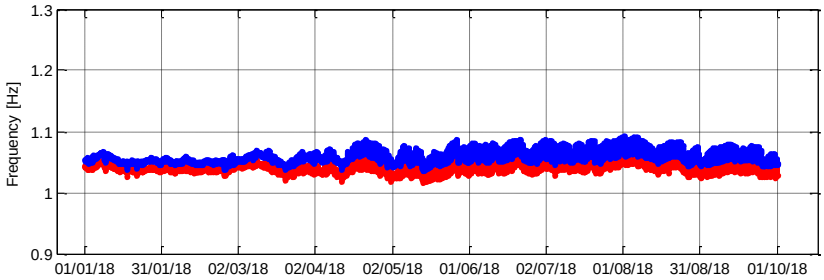

Fig. 8.20. Representation of the first two natural frequencies trends in the reference monitoring period of eight months (from 01/01/2018 to 31/09/2018) using a different scale

Thus, considering the previous results, only the first two frequencies were used as damage sensitive features for in the further applications.

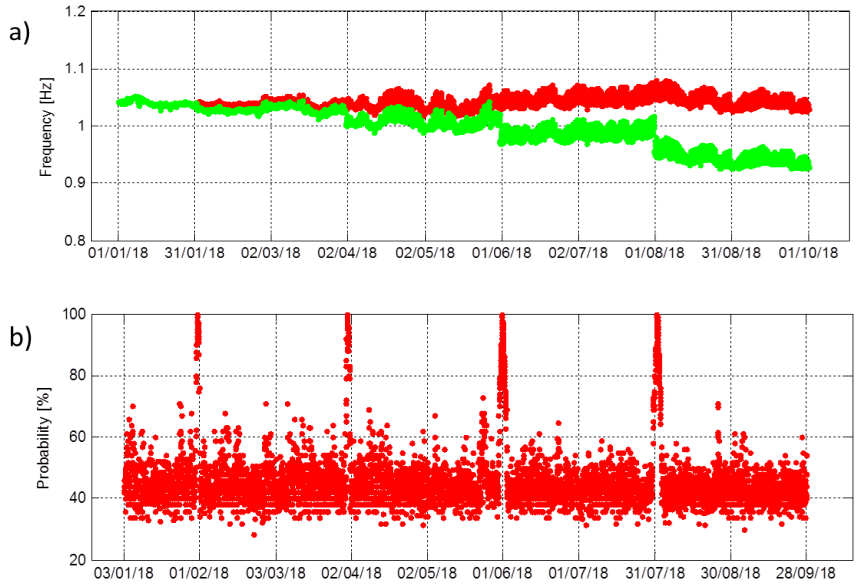

Fig. 8.21. Application of the CSA strategy to modal features: a) evolution of the first frequency estimates (red dots) and "corrupted estimates" (green dots); b) damage indicator obtained from the analysis of the corrupted values

In **Fig. 8.20**, a zoom of the first and the second frequency evolution in the reference monitoring period adopted for the sensitivity test is depicted. Meanwhile, **Fig. 8.21** and **Fig. 8.22** show the obtained estimates and the corrupted evolutions of the first and second frequency respectively, after the application of four different frequency shifts. The input parameters of the SVM model used by CSA algorithm are: N=96 (48 elements for each undamaged and damaged condition), k-folds=10, σ=0.3 and C=3, respectively.

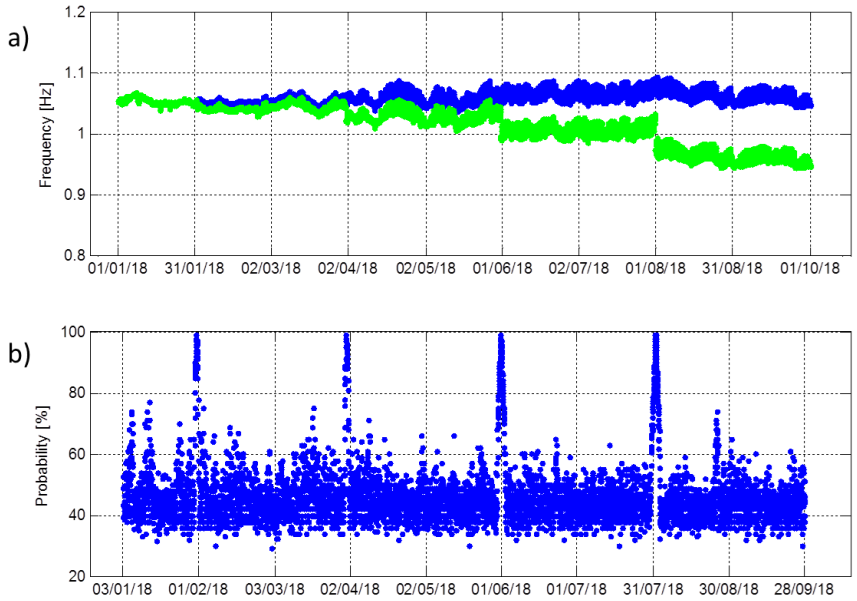

Fig. 8.22. Application of the CSA strategy to modal features: a) evolution of the second frequency estimates (blue dots) and "corrupted estimates" (green dots); b) damage indicator obtained from the analysis of the corrupted values

As reported in **Fig. 8.21** and **Fig. 8.22**, four different damages were simulated during the reference monitoring period of eight months (from 01/01/2018 to 31/09/2018). The damages were simulated with an increasing frequency shift. The first one was simulated during the winter period (1st of February 2018) with a minimum shift of 0.01 Hz. Consequently, a second damage was mimicked in the spring season (1st of April 2018) with a shift of 0.02 Hz. A third one equal to 0.03 Hz in the summer (1st of June 2018), and the last one (1st of August 2018) with a frequency shift of 0,04 Hz.

From both diagrams in **Fig. 8.21**(b) and **Fig. 8.22**(b), the clear bell-shapes of the probability appear in the correspondence of the simulated damages. Considering these results, a further investigation was performed in order to test the sensitivity of the implemented strategy applying small damages with identical amplitude (i.e., frequency drops of 0.02 Hz).

Thus, the model was subjected to further tests in order to verify if the effect caused by environmental factors on the natural frequency estimates can also reflect on the sensitivity of the model during different seasons. Therefore, this analysis was carried out on the frequency evolutions obtained in the same days as the previous analysis.

In **Fig. 8.23** and **Fig. 8.24**, the results obtained simulating different damages with a constant amplitude are reported. In particular, **Fig. 8.23** refers to the first natural frequency, and **Fig. 8.24** refers to the second frequency evolution.

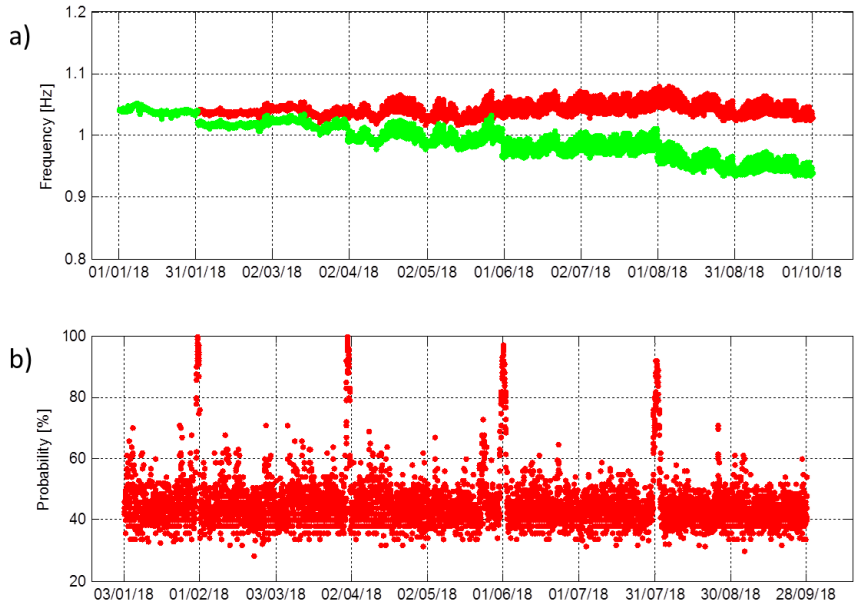

Fig. 8.23. Analysis of corrupted frequencies using a constant frequency shift: a) evolution of the first frequency estimates (red dots) and corrupted values (green dots); b) damage probability values obtained applying the CSA strategy

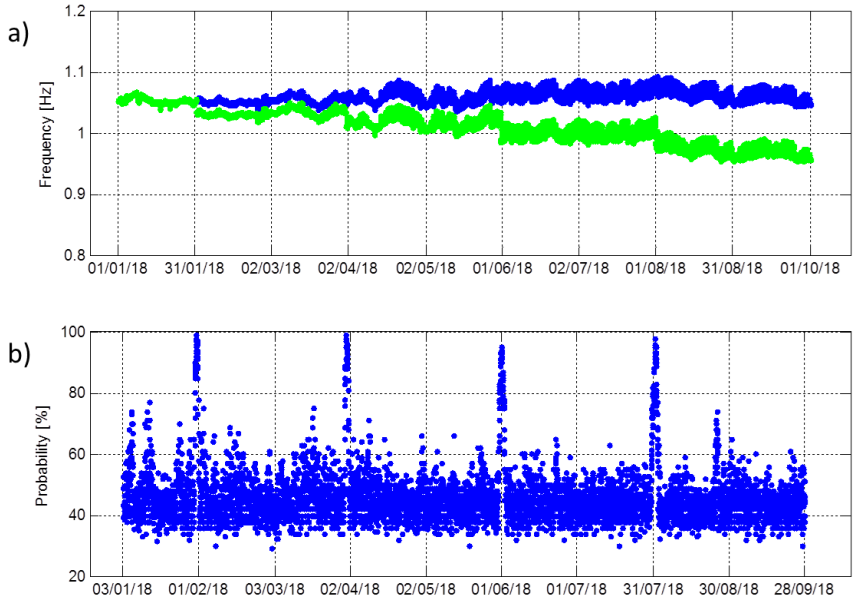

Fig. 8.24. Analysis of corrupted frequencies using a constant frequency shift: a) evolution of the first frequency estimates (blue dots) and corrupted values (green dots); b) damage probability values obtained applying the CSA strategy

From the inspections of the two diagrams, some considerations can be pointed out:

1) The algorithm is capable to recognize slight variations in the trend of the natural frequency during different seasonal periods of monitoring.
2) No relevant spurious peaks of the damage probability appear during the monitoring phase, demonstrating the robustness of the implemented methodology.
3) The effects of the environmental factors on the natural frequency estimates seem not to produce relevant issues in the detection of slight damages.
4) Different statistical characteristics of the input estimates (i.e., between the winter and summer period) could affect the damage detection strategy.
5) From the outputs obtained by the sensitivity analysis, it seems that the algorithm works better in the winter period than summer period. This is due to the different standard deviations of the input data provided to the algorithm in different periods of the year. This condition can be solved by varying the length of the input segments.

6) All analyses are carried out using a fixed length of each input segment equal to 48 elements. This parameter indicates that the occurred damage in the structure is fully identified with only two days of delay.

To conclude this paragraph, the author wants to point out the strict correlation between a high success rate in the identification process and the robustness of the implemented damage detection procedure. It is worth highlighting how the good performance of the implemented strategy has been obtained by simulating slight damages in the first and second frequency evolution, with a success rate close to 98% for both features. Meanwhile, for higher frequencies, the procedure could provide possible spurious peaks because of a loss of estimates. Moreover, to be critical, a simple averaging of all obtained accuracies related to all investigated structural modes might not be enough to provide a proper alarm, because of false positives caused by extreme variations in the environmental conditions. Hence, the use of pattern recognition models for SHM purposes deserves further investigation in order to avoid the comparison of false positives that do not depend only on structural conditions.

8.9 Conclusions

This Chapter describes the continuous dynamic monitoring of an historical bell-tower located in the center of Milan. The tower was built in the XIII century and it is part of the *San Gottardo in Corte Church.* After a brief description of this case study, the main results obtained by applying the developed OMA algorithm (i.e., 2D-MPE and MT tools) to the structural responses of the tower, collected during the first months of monitoring, are reported and commented in detail.

Subsequently, from the analysis of the data recorded during the dynamic test of the tower, eight structural modes have been detected. These modes have been selected as reference and used to perform two years of permanent monitoring of tower. The natural frequencies associated to the eight investigated modes are reported in detail, highlighting also the main

correlation between the identified frequencies and the main environmental factors (such as temperature and humidity).

The estimations of the natural frequencies were used as damage sensitive features for the continuous assessment of the structure. As expected, from the application of the alternative damage detection approach proposed in this Dissertation (the CSA strategy), the tower does not suffer any damages during its monitoring.

Subsequently, to demonstrate the robustness of the implemented novelty detection algorithm, a sensitivity analysis was carried out simulating some artificial damages in the evolution of the natural frequencies. As demonstrated, the algorithm is capable to recognize possible anomalies with a nominal amplitude of about 1% of the mean value of the tested frequency. The excellent results prove the robustness of the developed strategy in the permanent assessment of the ancient tower and demonstrate its promising future in the context of OMA-based SHM strategies without performing the removal of environmental effects on the damage sensitive features.

Chapter 9

CONCLUSIONS AND FUTURE DEVELOPMENTS

Contents

9.1 Conclusions

The present Dissertation focuses on the use of OMA in the context of vibration-based SHM of Cultural Heritage (CH) constructions and large structures.

This work includes the development, validation and application of algorithms and procedures aimed at automatically estimating the dynamic features of investigated structures, analyzing the output responses collected in operational conditions during a single test or in the context of permanent monitoring. Moreover, a damage detection approach is developed for the continuous assessment of the monitored structures without any removal of the masking (environmental and operational) effects on the identified modal estimates.

The Thesis starts with a brief overview of the most common OMA algorithms and continues with the implementation of four state-of-the-art identification techniques: Peak Picking and FDD methods, developed in the frequency domain, and the SSI-Cov and the SSI-Data methods, implemented in the time domain.

Subsequently, a description of the classical approach of OMA-based SHM is provided, emphasizing the use of the modal parameters (mainly natural frequencies). Moreover, a brief description of the methodologies and tools normally used to reduce the effects of the environmental and operational factors on natural frequencies is provided. It is worth noting that the classical SHM based on the monitoring of natural frequencies generally involves a relatively long training period for an accurate setting of regression models or output-only techniques to remove such effects and to consequently obtain proper indices for damage detection applications.

The main goals of the research project developed in this Dissertation are oriented to: a) increase the automation level in the methodologies adopted to extract the modal parameter estimates from the signals collected on the structures; b) perform the continuous assessment of the monitored structures avoiding the training periods used to

remove the external effects on the adopted sensitive features, and c) quickly obtain information about the structural integrity of the monitored structures with a significantly reduced delay in case of occurred damage.

To achieve these goals, automated OMA algorithms have been developed in order to mimic the choices performed by an expert analyst during the identification problem, follow the evolution in time of the modal features without any interaction and provide a proper alarm in case of structural anomalies. In particular, the following algorithms have been developed:

1) Modal Parameter Estimation (MPE) algorithm based on the automated interpretation of two-dimensional stabilization diagrams,
2) 3D Modal Parameter Estimation (3D-MPE) algorithm operating on tri-dimensional stabilization diagrams,
3) Modal tracking (MT) procedure aimed at ensuring the correct tracking of the structural modes also in case of closely-spaced modes with similar mode shapes,
4) Damage Detection algorithm aimed at providing a probability value associated to the occurred damage in the structure, working directly on the extracted modal features.

It is worth remarking that the developed tools (1)-(2) are mainly geared toward identification techniques based on parametric SSI methods, being particularly suited for automation because of their algebraic nature, which permits the evaluation of the modal parameters with higher levels of accuracy than the methods based on the frequency domain.

The first MPE algorithm is developed in order to extract the modal estimates from a single dataset collected during a dynamic test or continuous dynamic monitoring. This algorithm works on the outputs provided by any parametric method that involves the construction and the interpretation of stabilization diagrams. The original aspect of this tool consists of the sequence of three key-steps aimed at exerting a cleaning action on the stabilization diagram and at obtaining an accurate set of modal estimates with low

uncertainty. This procedure still requires an initial tuning of input parameters and the definition of pre-selected values for the processing of input data.

Important improvements have been achieved with the implementation of the second MPE algorithm. In fact, the 3D-MPE is based on the construction and the automatic interpretation of 3D stabilization diagrams and is aimed at providing a more accurate estimation of the modal features without any initial tuning of the input parameters, such as the maximum model order of the state-space model and the input parameter of the adopted SSI method (i.e. the time-lag value or the number of block-rows used by SSI-Cov and SSI-Data, respectively). Moreover, the use of the MACX criterion in the clustering process allows for the extension, and then generalization of the analysis also at modes with high complexity components.

Thirdly, a new automated Modal Tracking (MT) tool that allows the tracking of modal features in the context of continuous dynamic monitoring is given. The original aspects that characterize this tool consist of: a) the use of a very short period of time devoted to storing a minimum number of estimates to achieve the full automation of the monitoring process, b) the use of a dynamic reference list of modes adopted to perform the correct tracking between the estimates provided by the analysis of consecutive datasets, and c) the use of self-adaptive rejection thresholds together with an adaptive baseline reference list that are continuously updated during the monitoring phase ensuring a correct tracking of the modes and conceivably avoiding the appearance of outliers.

The set of implemented algorithms is completed by the development of a damage detection algorithm based on the application of pattern recognition models devoted to identifying the outset structural anomalies of the monitored constructions by the analysis of the extracted OMA features. The algorithm was firstly exploited by using the natural frequency evolutions provided by a simple academic structure and then validated by using experimental data collected on the *Gabbia Tower* (Mantua, Italy) during its monitoring process.

The work developed in this Dissertation has led to the achievement of the following main outcomes, already described in the partial conclusions at the end of each Chapter.

- The identification of the modal parameters performed with data collected during the AVT of a lively footbridge located in Seriate (Milan) pointed out the capability of the first MPE algorithm in the process of identification of closely-spaced and weakly excited modes of the structure. The obtained results were validated by a comparison with reference values previously identified using the commercial software ARTeMIS. Moreover, the presence of a further pair of closely-spaced modes and two weakly excited modes of the footbridge was pointed out, that had not been identified during the previous campaign. The modal analysis performed on data collected during a dynamic test of the *Olla* bridge made it possible to explore the accuracy of MPE also for weakly excited modes characterized by higher complexity of the mode shape components. In this case, too, the validation of the provided results was performed by the analysis carried out using a commercial software (ARTeMIS) highlighting the good match between the sets of extracted modes. The results previously described demonstrate the good performance of the developed strategy given by the three key-steps of the MPE algorithm. In particular, the third subroutine (i.e. post-processing) provides a more accurate identification of the stable alignments removing possible replications and outliers from the stabilization diagram and making the identification analysis less dependent on user sensitivity.
- In order to reduce the dependence of the automated algorithm on the analyst's sensitivity in the definition of the input parameters of the SSI methods, a further improvement was developed introducing the concept of tri-dimensional (3D) stabilization diagram. In this way, the initial tuning of the pre-selected input parameters is avoided entirely, improving the accuracy of the results by using a wide redundancy of estimates and removing the dependence in the selection of the structural modes on human interactions. In addition, to perform a more general investigation in case of complex modes, another improvement was developed in the clustering process using the MACX criterion instead the MAC value.

- The performance of the 3D-MPE algorithm was demonstrated by its application to the analysis of monitoring data collected on the *Infante D. Henrique Bridge*. The results highlight the identification of all relevant modes of the bridge. Furthermore, the extension of the investigated frequency interval to 5.5 Hz allowed for the identification of four further structural modes never investigated in the previous analysis. Moreover, the application of the 3D-MPE algorithm to data collected on the *San Michele Bridge* highlights the accuracy of the algorithm also in the identification of modes characterized by high complexity. As reported, 15 structural lateral modes of the bridge were identified with very low uncertainty. In both applications, the high success rate in the identification of the structural modes confirms the robust performance of the implemented algorithm in the identification process, carried out completely avoiding the initial tuning of the input parameters.
- As shown by several works present in literature, the correct tracking of the identified dynamic features plays a crucial role in the context of the SHM approach based on OMA parameters, because the evolution of modal parameters is generally used as input data for the continuous assessment of the structure. Despite this, a strategy to perform a fully automated modal tracking is still a changeling task. Thus, a novel approach for Modal Tracking (MT) was developed in this Dissertation. The MT procedure presented herein combines the use of the self-adaptive thresholds and reference values with a reduced *period of training* for the auto-setting of such values. The impact of this original aspect is pointed out by performing the continuous dynamic monitoring of two different case studies: the *Gabbia Tower*, an ancient masonry tower built in the XIII century in the city of Mantua, and the *San Michele Bridge*, already mentioned. These case studies have been selected because of their peculiar behavior in the reference monitoring period. In the first case, the natural frequency associated to the local mode of the tower drops from a nominal value of 10 Hz identified in the beginning of the monitoring phase (December 2012) to 8.3 Hz in the end of the monitoring period (July 2013). In the second case study, an intense temperature variation due to a heavy snowfall completely changed the dynamic response of the bridge for more than two weeks of monitoring. During such a period,

the combined variation of the natural frequencies and mode shapes associated to the structural modes generally involves a remarkable loss in identification rate, as highlighted by previous analyses. The improvements provided by the MT algorithm allowed for the correct tracking of all structural modes of the tower using a training period of only 4 days. Meanwhile, for the second case study, the efficiency of the MT procedure was highlighted by the fairly good identification rate of the modal parameters of the bridge, while subjected to extreme environmental conditions, adopting only 2 days for training.

- The damage detection strategy based on pattern recognition models developed in this Dissertation performs the continuous assessment of the structure, working directly on the evolution of the modal estimates provided by OMA algorithms (MPE and MT tools) without performing the removal of the environmental and operational effects. Mainly, the algorithm involves the use of Support Vector Machine (SVM) models in the classification of the input data in order to automatically recognize the occurrence of structural deficiencies in the "normal" behavior of the structure during its monitoring. In more details, the algorithm is forced to perform the classification of the provided estimates into two different classes (Class I and Class II) associated to two structural conditions: undamaged and damaged scenario. This approach was developed with two different strategies: 1) the Continuous Segment Analysis (CSA) strategy, in which the data input are organized into two consecutive segments that are continuously updated after each run of the identification algorithm, 2) the Separate Segment Analysis (SSA) strategy, which is composed by two separate data segments, the first one being fixed and representing the reference undamaged state. Both strategies provide probability values, associated to the accuracy of the model, that in case of occurred damage should reach a peak value of 100% (perfect separation of the data into two classes). The maximum value is reached when the damage is exactly in the middle of the provided dataset. The algorithm was exploited analyzing numerical accelerations generated using a simple five DOFs system and consecutively corrupted by simulating structural damages. Afterwards, this strategy was successfully validated

by its application to the monitoring data collected on the *Gabbia Tower*, highlighting the occurrence of a structural damage to the tower due to a far-filed earthquake.

- Finally, the implemented algorithms were used to perform the SHM of the *San Gottardo* masonry tower. The monitoring system has been in place since the end of October 2016, and the output responses have been processed by using all implemented tools. In fact, the MPE and the MT algorithms have been adopted for the automatic identification and tracking of the modal parameters of the tower for over two years. Thus, the damage detection (CSA) strategy is applied to natural frequency evolutions to perform the structural assessment of the ancient construction. As proved, the tower has not suffered any damages during the investigated period.
- To complete this Dissertation a sensitivity analysis was carried out to test the robustness of the damage detection approach in the identification of simulated damages to the structure though frequency shifts in the obtained frequency evolutions. As reported, the algorithm recognizes very small drops in the frequency evolution (i.e., 0.01-0.02 Hz) providing a clear peak in the probability value associated to the occurred damage.

9.2 Future developments

The work presented in this Dissertation includes the development of important tools used to transform the signals collected by the installed monitoring system in useful information about the structural behavior of the monitored construction. In this way, the present developments could be the starting point for several new implementations to make the continuous dynamic monitoring process and the structural health monitoring process more strategic, accurate and advantageous for the maintenance of the structural integrity of ancient constructions and large infrastructures. However, some new developments could be implemented to make dynamic testing and monitoring even more advantageous.

Therefore, some research topics in line with the developed work are suggested below:

- Implementation of further robust routines to automatically process data collected during Ambient Vibration Testing of large infrastructures generally performed in multi-setups configuration. The automatic management and reconstruction of the mode shapes obtained by analyzing each setup of the dynamic test. Test and validation of the new implementation using numerical data and full-scale tests to understand how the non-stationarity conditions can affect the estimates and, consequently, the efficiency of the algorithm.
- Emphasize the useful information provided by the complexity indices associated to the mode shapes estimates in the context of continuous dynamic monitoring of ancient buildings and, in more general cases, poorly maintained constructions in which the high degradation of the mechanical properties could be provided by further criteria based on the monitoring of the complexity indices.
- Adapt the second damage detection algorithm (SSA strategy) implemented in this work for the continuous assessment purposes operating on frequency estimates after the removal of the environmental effect. Test the efficiency of the new implementation defining the influence of temperature and other external factors in the masking of small damages. Compare the effective advantages (or disadvantages) of both strategies in terms of economic costs and safety of the whole process, with or without performing the post-processing on OMA outputs (removal of external effects).
- Since the mode shapes are less affected by environmental effects, a further implementation dedicated to a mode-shape-variation-based SHM devoted to performing the monitoring of the health condition based only on the mode shape variation or on the variation of the complexity component of the investigated structural modes. This kind of approach should be really profitable for SHM purposes of large infrastructures with widespread dynamic systems.
- The database created with the collected data in the monitoring project of the *San Gottardo* bell-tower is useful for performing benchmark studies to evaluate the

implementation and the efficiency of further algorithms for automatic identification, to remove the effects of the environmental factors and to validate further damage detection strategies with the goal of obtaining a proper alarm in case of occurred anomalies.

- Integrate the automated algorithms and approaches implemented in this Dissertation in a unique software package. Make the software user-friendly, flexible and adaptive to different monitoring applications, developing an intuitive and accurate graphic interface paying particular attention also to graphic results. Customize the software based on the requests of the infrastructure designer or owner and forecast the storing of collected data and the corresponding results from different structures that could be connected in an easy access network.

REFERENCES

Adhikari, S., (2004), *Optimal complex modes and an index of damping non-proportionality*, Mechanical Systems and Signal Processing 18: 1-27.

Adhikari, S., Woodhouse, J., (2001), *Identification of damping: part2, non-viscous damping*, Journal of Sound and Vibration 243: 63-88.

Ahmida, K. M., Arruda, J. R. F., (2002), *On the relation between complex modes and wave propagation phenomena*, Journal of Sound and Vibration 255(4): 663-684.

Akaike, H., (1975), *Markovian representation of stochastic processes by canonical variables*, Journal on Control and Optimization, 13(1): 162-173.

Allemang, R.J., Brown, D.L., (1983), *Correlation coefficient for modal vector analysis*, in Proceedings. of IMAC I, Orlando, Florida USA.

Allemang, R.J., (2003), *The modal assurance criterion - Twenty years of use and abuse*, Sound and Vibration 37(8), 14-21.

Alvandi, A., Cremona, C., (2006), *Assessment of vibration-based damage identification techniques*, Journal of Sound and Vibration 292: 179–202.

Andersen, P., (1997), *Identification of civil engineering structures using vector ARMA models*, PhD Thesis, Aalborg University, Denmark.

Andersen, P., Brincker, R., Goursat, M., Mevel, L., (2007), *Automated Modal Parameter Estimation for Operational Modal Analysis of Large Systems*. in Proceedings of the 2nd International Operational Modal Analysis Conference, 299–308.

Antoni, J., (2009), *Cyclostationarity by example*, Mechanical Systems and Signal Processing 23: 987–1036.

Asmussen, J. C., (1997), *Modal analysis based on random decrement technique - application to civil engineering structures*, PhD Thesis, Aalborg University, Denmark.

Au., S. K., Zhang, F. L., Ni, Y. C., (2013), *Bayesian operational modal analysis: theory, computation, practice*, Computers & Structures 126: 3-14.

Azzara, R.M., De Roeck, G., Girardi, M., Padovani, C., Pellegrini, D., Reynders, E., (2018), *The influence of environmental parameters on the dynamic behaviour of the San Frediano bell tower in Lucca*, Engineering Structures 156, 175-187.

Basseville, M., Bourquin, F., Mevel, L., Nasser, H., Treyssède, F., (2010), *Handling the temperature effect in vibration monitoring: two subspace-based analytical approaches*, Journal of Engineering Mechanics 136(3): 367-378.

Bendat, J. S., Piersol, A. G., (1980), *Engineering applications of correlation and spectral analysis 2nd ed.*, John Wiley & Sons, New York, USA.

Benedettini, F., Gentile C., (2011), *Operational modal testing and FE model tuning of a cable-stayed bridge*, Engineering Structures 33: 2063-2073.

Bennati, S., Nardini L., Salvatore, W., (2005), *Dynamic behavior of a medieval masonry bell tower. II: measurement and modelling of the tower motion*, Journal of Structural Engineering 131(11): 1656-1664.

Bernal, D., (2008), *A state space approach to system identification*, Modern Testing for Structural Systems (CISM) 502: 97-129.

Bernal, D., Gunes, B., (2004), *A flexibility-based approach for the localization and quantification of damage: A benchmark application*, Journal of Engineering Mechanics 130: 61-70.

Bernal, D., (2011), *The zero-order hold in time domain identification: an unnecessary operating premise*, Structural Control and Health Monitoring 18: 510-518.

Bishop C. M., (2006), *Pattern recognition and machine learning*, Ed. Springer.

Boller, C., Chang, F.K., Fujino, Y., (2009), *Encyclopedia of Structural Health Monitoring*, John Wiley & Sons: New York, USA.

Borlenghi. P., Saisi, A., Gentile, C., Carmelo, (2019), *Preliminary Structural Assessment of a Multi-span Masonry Arch Bridge*, in Proceedings of ARCH 2019, October 2-4, Porto, Portugal.

Branden, B., Peeters, B., De Roeck, G., (1999), *Introduction to Macec*, Technical Report, K. U. Leuven.

Brandt, A., Lagö, T., Ahlin, K. (2004). *Summary of Spectrum Estimators for Vibration Signals and Their Errors*. Proc of 22nd International Modal Analysis Conference, Dearborn, Michigan, USA.

Brandt, A., (2010), *Noise and vibration analysis: signal analysis and experimental procedures*, John Wiley & Sons.

Brencich, A., Sabia, D., (2008), *Experimental identification of a multi-span masonry bridge: the Tanaro Bridge*, Construction and Building Materials 22: 2087-2099.

Brinker, R., Zhang, L., Andersen, P., (2000) *Modal Identification from Ambient Responses Using Frequency Domain Decomposition*, in Proceedings of 18th Modal Analysis Conference IMAC-XVIII, San Antonio, USA.

Brincker, R., Zhang, L., Andersen, P., (2001), *Modal identification of output-only systems using frequency domain decomposition*, Smart Materials and Structures 10(3): 441-445.

Brincker, R., Zhang, L., (2009), *Frequency Domain Decomposition Revisited*, in Proceedings of IOMAC 2009 (483-490), May 4-6, Portonovo, Italy.

Brownjohn, J. M. W., Xia, P. Q., Hao, H., Xia, Y., (2001), *Civil structure condition assessment by FE model updating: methodology and case studies*, Finite Elements in Analysis and Design 37: 761-775.

Brownjohn, J. M. W., De Stefano, A., Xu, Y. L., Wenzel, H., Aktan, A. E., (2011), *Vibration-based monitoring of civil infrastructures: challenges and successes*, Journal of Civil Structural Health Monitoring 1(3-4): 79-95.

Brownjohn, J. M. W., Koo, K.-Y., (2013), *Structural Health Monitoring of Sheffield University arts tower during retrofit*, Earthquakes and Health Monitoring of Civil Structures, 149-166.

Bucher, I., (2004), *Estimating the ratio between travelling and standing vibration waves under nonstationary conditions*, Journal of Sound and Vibration 270: 341-359.

Busatta, F., (2012), *Dynamic monitoring and automated modal analysis of large structures: methodological aspects and application to a historic iron bridge*, Phd Thesis, Politecnico di Milano, Italy.

Busatta, F., Gentile, C., Saisi, A., (2012), *Structural health monitoring of a centenary iron arch bridge*, in Proceedings of IALCCE 2012, October 3-6, Vienna, Austria.

Cabboi, A., Gentile, C., Saisi, A., (2013), *Frequency tracking and F.E. model identification of a masonry tower*, in Proceedings of IOMAC 2013, May 14-15, Guimarães, Portugal.

Cabboi, A., Gentile, C., Saisi, A., (2014), *Vibration-based SHM of a centenary bridge: a comparative study between two different automated OMA techniques*, in Proceedings of EURODYN 2014, June 30 - July 2, Porto, Portugal.

Cabboi, A., (2013), *Automatic operational modal analysis; challenges and applications to historic structure and infrastructures*, PhD Thesis, University of Cagliari, Italy.

Cabboi, A., Magalhães, F., Gentile, C., Cunha, Á., (2013), *Automatic operational modal analysis: Challenges and practical application to a historic bridge*, in Proceedings of SMART 2013, June 24-26, Torino, Italy.

Cabboi, A., Magalhães, F., Gentile, C., Cunha, A., (2017), *Automated modal identification and tracking: Application to an iron arch bridge*, Structural Control and Health Monitoring, 24(1) e1854.

Calçada, R., Cunha, Á., Delgado, R., (2002), *Dynamic Analysis of Metallic Arch Railway Bridge*, Journal of Bridge Engineering 7(4): 214-222.

Cantieni, R., (2005), *Experimental methods used in system identification of civil engineering structures*, in Proceedings of IOMAC 2005, April 25-27, Copenhagen, Denmark.

Casarin, F., Lorenzoni, F., Islami, K., Modena, C., (2011), *Dynamic identification and monitoring of the churches of St. Biagio and St. Giuseppe in L'Aquila*, in Proceedings of EVACES 2011, October 3-5, Varenna, Italy.

Casarin, F., Modena, C., (2008), *Seismic assessment of complex historical buildings: application to Reggio Emilia Cathedral, Italy*, International Journal of Architectural Heritage 2(3): 304-327.

Casarin, F., Valluzzi, M. R., da Porto, F., Modena, C., (2008), *Structural monitoring for the evaluation of the dynamic response of historical monuments*, in Proceedings of SACoMaTiS 2008, Varenna, Italy, 483-490.

Cauberghe, P., (2004), *Applied frequency-domain system identification in the field of experimental and operational modal analysis*, PhD Thesis, Vrije Universitei Brussel, Belgium.

Chesné, S., Deraemaeker, A., (2013), *Damage localization using transmissibility functions: a critical review*, Mechanical Systems and Signal Processing 38: 569–584.

Chun, X., Qu, W., Tan, D., (2005), *An application of data fusion technology in structural health monitoring and damage identification*, Proceedings of the Smart Sensors Technology and Measurement Systems, Belgium, 451-461.

Clough, R. W., Penzien, J., (1993), *Dynamics of Structures 2nd ed.*, McGraw Hill, New York, USA.

Comanducci, G., Ubertini, F., Materazzi, A.L., (2015), *Structural health monitoring of suspension bridges with features affected by changing wind speed*, Journal of Wind Engineering and Industrial Aerodynamics 141, 12-26.

Comanducci, G., Magalhães, F., Ubertini, F., Cunha, Á., (2016), *On vibration-based damage detection by multivariate statistical techniques: Application to a long-span arch bridge*, Structural Health Monitoring 15(5), 505-524

Cross, E.J., Koo, K.Y., Brownjohn, J.M.W., Worden, K., (2013), *Long-term monitoring and data analysis of the Tamar Bridge*, Mechanical Systems and Signal Processing 35: 16-34.

Cunha, Á., Caetano, E., Magalhães, F., Moutinho, C., (2013), *Recent perspectives in dynamic testing and monitoring of bridges*, Structural Control and Health Monitoring 20: 853-877.

Curti, E., Podestà, S., Scandolo, L., (2012), *Simplified mechanical model for the seismic vulnerability evaluation of belfries*, International Journal of Architectural Heritage 6(6): 605-625.

Cury, A., Cremona, C., Dumoulin, J., (2012), *Long-term monitoring of a PSC box girder bridge: operational modal analysis, data normalization and structural modification assessment*, Mechanical Systems and Signal Processing 33: 13-37.

Cury A., and Cremona, C., (2012) *Pattern recognition of structural behaviors based on learning algorithms and symbolic data concepts*, Structural Control and health monitoring 19: 161-186.

Darbre, G.R., Proulx, J., (2002) C*ontinuous ambient-vibration monitoring of the arch dam of Mauvoisin*, Earthquake Engineering and Structural Dynamics, 31: 475-480.

De Matteis, G., Mazzolani F. M., (2010), *The Fossanova Church: Seismic Vulnerability Assessment by Numeric and Physical Testing*, International Journal of Architectural Heritage 4(3): 222-245.

Deraemaeker, A., Reynders, E., De Roeck, G., Kullaa, J., (2008), *Vibration-based Structural Health Monitoring using output-only measurements under changing environment*, Mechanical Systems and Signal Processing, 22(1), 34-56.

Devriendt, C., De Sitter, G., Vanlanduit, S., Guillaume, P., (2009), *Operational modal analysis in the presence of harmonic excitations by the use of transmissibility measurements*, Mechanical Systems and Signal Processing 23(3): 621-635.

Devriendt, C., Guillaume, P., (2008), *Identification of modal parameters from transmissibility measurements*, Journal of Sound and Vibration 314(1-2): 343-356.

Devriendt, C., De Troyer, T., De Sitter, G., Guillaume, P., (2011) *On the use of transmissibility functions in an OMAX framework for flight flutter testing*, in Proceedings of 8th International Conference on Structural Dynamics, EURODYN 2011, July 4-6, Leuven, Belgium.

Devriendt, C., Magalhães, F., El Kafaly, M., De Sitter, G., Cunha, Á., Guillaume, P., (2013), *Long term dynamic monitoring of an offshore wind turbine*, in Proceedings of IMAC-XXX1 2013, February 11-14, Garden Grove, California USA.

Diday, E., Noirhomme-Fraiture, M. (Editors). (2008), *Symbolic Data Analysis and the SODAS Software*, John Wiley & Sons.

Dion, J. L., Tawfiq, I., Chevallier, G., (2012), *Harmonic component detection: optimized spectral kurtosis for operational modal analysis*, Mechanical Systems and Signal Processing 26: 24-33.

Döhler, M., Hille, F., Mevel, L., Rücker, W., (2014), *Structural health monitoring with statistical methods during progressive damage test of S101 Bridge*, Engineering Structures 69, 183-193.

Elyamani, A., Caselles, O., Roca, P., Clapes, J., (2017), *Dynamic investigation of large historical cathedral*, Structural Control and Health Monitoring 24(3), 1-25.

Ewins, D. J., (2000), *Modal Testing: theory and practice*, Research Studies Press, U.K.

Fan, W., Qiao, P., (2011), *Vibration-based damage identification methods: a review and comparative study*, Structural Health Monitoring 10: 83-111.

Farrar, C. R., Doebling, S. W., Cornwell, P. J., Straser, E. G., (1997), *Variability of Modal Parameters Measured on the Alamosa Canyon Bridge*, In Proceedings of IMAC 15, International Modal Analysis Conference, Orlando, Florida, USA.

Felber, A. J., (1993), *Development of a hybrid bridge evaluation system*, Ph.D. Thesis, University of British Columbia, Canada.

Felber, A. J., Cantieni, R., (1996), *Introduction of a new Ambient Vibration Testing System: Description of the System and Seven Bridges Tests*, Technical Report N° 156'521, EMPA, Dubendorf, Switzerland.

Feldman, M., (2011), *Hilbert transform in vibration analysis*, Mechanical Systems and Signal Processing 25: 735–802.

Fritzen, C. P., (2005), *Vibration-based Structural Health Monitoring - concepts and applications*, Key Engineering Materials 293-294: 3-20.

Gawronski, W. K., (1998), *Dynamics and control of structures - a model approach*, Springer.

Gentile C., Saisi, A., Busatta, F., (2011), *Dynamic testing and permanent monitoring of an historic iron arch bridge*, in Proceedings of EURODYN 2011, July 4-6, Leuven, Belgium.

Gentile, C., Saisi A., Cabboi A., (2012), *Dynamic monitoring of a masonry tower*, Proc. of SAHC 2012, October 15-17, Wroclaw, Poland.

Gentile, C., Saisi, A., (2011), *Ambient vibration testing and condition assessment of the Paderno iron arch bridge (1889)*, Construction and Building Materials 25: 3709-3720.

Gentile, C., Saisi, A., (2007), *Ambient vibration testing of historic masonry towers for structural identification and damage assessment*, Construction and Building Materials 21(6): 1311-1321.

Gentile, C., Saisi, A., Cabboi, A., (2015), *Structural identification of a masonry tower based on operational modal analysis*, International Journal of Architectural Heritage, 9:2, 98-110.

Gentile, C., Saisi, A., (2013), *Operational modal testing of historic structures at different levels of excitation*, Construction and Building Materials 48: 1273-1285.

Gentile, C., Saisi, A., (2015), *Continuous dynamic monitoring of a centenary iron bridge for structural modification assessment*, Frontiers of Structural and Civil Engineering 9: 26-41.

Gentile, C., Guidobaldi, M., Saisi, A., (2016), *One-year dynamic monitoring of a historic tower: damage detection under changing environment*, Meccanica 51: 2873–2889.

Goethals, I. De Moor, B., (2002), *Model reduction and energy analysis as a tool to detect spurious modes*, in Proceedings of ISMA 2002, Leuven, Belgium.

Goethals, I., Vanluyten, B., De Moor, B., (2004), *Reliable spurious mode rejection using self-learning algorithms*, in Proceedings of ISMA 2004, Leuven, Belgium.

Guidobaldi M., (2016), *Vibration-based structural health monitoring for historic masonry towers*, Ph.D. Thesis, Politecnico di Milano, Italy.

Guillaume, P., Hermans, L., Van der Auweraer, H., (1999), *Maximum likelihood identification of modal parameters from operational data*, in Proceedings of IMAC XVII 1999, February 8-11, Kissimmee, Florida, USA.

Guillaume, P., Verboven, P., Vanlanduit, S., Van der Auweraer, H., Peeters, B., (2003), *A Polyreference implementation of the least-squares complex frequency-domain estimator*, in Proceedings of IMAC XXI 2003, February 3-6, Kissimmee, Florida, USA.

Guillaume, P., De Troyer, T., Devriendt, C., De Sitter, G., (2007) *OMAX - Operational Modal Analysis in presence of eXogenous inputs*, in Proceedings of 25th Conference and Exposition on Structural Dynamics 2007, IMAC-XXV 2007, February 19-22, 2Orlando, Florida, USA

Guo, H.Y., (2006), *Structural damage detection using information fusion technique*, Mechanical Systems and Signal Processing 20: 1173–1188.

Hammond, J. K., White, P. R., (1996), *The analysis of non-stationarity signals using time-frequency methods*, Journal of Sound and Vibration 190(3): 419–447.

Heylen, W., Lammens, S., Sas, P., (2007), *Modal Analysis: Theory and Testing*, KU Leuven, Belgium.

Hong, A. L, Ubertini, F., Betti, R., (2011), *Wind analysis of a suspension bridge: identification and finite-element model simulation*, Journal of Structural Engineering 137(1): 133–42.

Hu W., Liao Y., Vemori V., (2003), *Robust anomaly detection using support vector machines*, Proc. of the International Conference on Machine Learning, 282-289.

Hu, W.-H., Moutinho, C., Caetano, E., Magalhães, F., Cunha, A., (2012), *Continuous dynamic monitoring of a lively footbridge for serviceability assessment and damage detection*, Mechanical Systems and Signal Processing 33, 38-55.

Hu, W.-H., Said, S., Rohrmann, R.G., Rücker, W., Cunha, Á., Rogge, A., (2015), *Vibration-based structural health monitoring of a highway bridge based on continuous dynamic measurements during 14 years*, in Proceeding of 7th SHMII 2015; July 1-3, Torino; Italy.

Hu, W.-H, Said, S., Rohrmann, R.G., Cunha, Á., Teng, J., (2018), *Continuous dynamic monitoring of a prestressed concrete bridge based on strain, inclination and crack measurements over a 14-year span*, Structural Health Monitoring17(5), 1073-1094.

Hu, W., Moutinho, C., Caetano, E., Magalhães, F., Cunha, A., (2012), *Continuous dynamic monitoring of a lively footbridge for serviceability assessment and damage detection*, Mechanical Systems and Signal Processing 33: 38-55.

Ibrahim, S. R., (1977), *Random Decrement Technique for Modal Identification of Structures*, Journal of Spacecraft and Rockets, 14: 696-700.

Imregun, M., Ewins, D. J., (1995), *Complex modes - origin and limits*, in Proceedings of IMAC XIII 1995, February 13-16, Nashville, Tennessee USA.

Inman, D., (2006), *Vibration with control*, John Wiley & Sons.

Ivorra, S., Pallares, F. J., (2006), *Dynamic investigation on a masonry bell tower*, Engineering Structures 25(5): 660-667.

Iwasaki A., Todoroki A., Shimamura Y., Kobayashi H., (2004), *An unsupervised statistical damage detection method for structural health monitoring*, Smart Material and Structures 13: 80-85.

James, G. H., Carne, T. G., Lauffer, J. P., Nard, A. R., (1992), *Modal testing using natural excitation*, in Proceedings IMAC X 1992, February 3-7, San Diego, USA.

Johnson, R. A.; Wichern, D. W. (1992) *Applied Multivariate Statistical Analysis*. Prentice Hall.

Juang, J. N., (1994), *Applied system identification*, Prentice Hall.

Juang, J. N., Pappa, R. S., (1985), *An Eigensystem Realization Algorithm for modal parameter identification and modal reduction*, Journal of Guidance, Control, and Dynamics 8(5): 620-627.

Katsuchi, H., Jones, N.P., Scanlan, R.H., Akiyama, H., (1998), *Multi-mode flutter and buffeting analysis of the Akashi-Kaikyo bridge*, Journal of Wind Engineering and Industrial Aerodynamics 77-78: 431-44.

Ko, J. M., Ni, Y. Q., (2005), *Technology developments in Structural Health Monitoring of largescale bridges*, Engineering Structures 27: 1715-1725.

Kohavi R., (1995), *A study of cross-validation and bootstrap for accuracy estimation and model selection*, in Proceeding of International Joint Conference on Artificially Intelligent 14: 1137-1145.

Koo, K. Y., Brownjohn, J. M. W., List, D. I., Cole, R., (2012), *Structural health monitoring of the Tamar suspension bridge*, Structural Control and Health Monitoring 20: 609-625.

Kullaa, J., (2009), *Eliminating environmental or operational influences in Structural Health Monitoring using the missing data analysis*, Journal of Intelligent Material Systems and Structures 20: 1381-1390.

Kung, S. Y., (1978), *A new identification and Model Reduction Algorithm via Singular Value Decomposition*, in Proceedings of 12th Asilomar Conference on Circuits, Systems and Computers, USA.

Lai, E., Gentile, C. Mulas, M. G., (2017), *Experimental and numerical serviceability assessment of a steel suspension footbridge*, Journal of Constructional Steel Research 132: 16–28, 2017.

Le T., Tran D., Ma W., Sharma D., (2011), *Multiple distribution data description learning algorithm for novelty detection*, Knowledge Discovery and Data Mining 6635: 246-257.

Li, Y., (2008), *A surface representation approach for novelty detection*, in: Proceedings of the International Conference on Information and Automation (ICIA), IEEE, 2008, 1464–1468.

Li, G., Wen, C., Li, Z., (2011), *A new online learning with kernels method in novelty detection*, in Proceedings of the 37th Annual Conference on IEEE Industrial Electronics Society (IECON), IEEE, 2011, 2311–2316.

Ljung, L., (1999), *System identification: theory for the user*, Prentice Hall.

Luzi, l., Pacor, F., Ameri, G.,Puglia, R., Burrato, P., Massa, M.,Augliera, P., Franceschina, G., Lovati, S., Castro, R., (2013), *Overview of the strong-motion data recorded during the May-June 2012 Emilia seismic sequence*, Seismol Res Lett 84(4): 629-644.

Lorenzoni, F., Casarin, F., Caldon, M., Islami, K., Modena, C., (2016), *Uncertainty quantification in structural health Monitoring: Application on Cultural Heritage buildings*, Mechanical Systems and Signal Processing, 66-67, 268-281.

Magalhães, F., Cunha, Á., Caetano, E., (2008), *Dynamic Monitoring of a Long Span Arch Bridge*, Engineering Structures 30: 3034–3044.

Magalhães, F., Cunha, Á., Caetano, E., (2009), *Online automatic identification of the modal parameters of a long span arch bridge*, Mechanical Systems and Signal Processing 23: 316–329.

Magalhães, F., Cunha, Á., Caetano, E., Brincker, R., (2010), *Damping estimation using free decays and ambient vibration tests*, Mechanical Systems and Signal Processing 24: 1274–1290.

Magalhães, F., (2010), *Operational modal analysis for testing and monitoring of bridges and special structures*, Ph.D. Thesis, Faculty of Engineering of Porto, Portugal.

Magalhães, F., Cunha, Á., (2011), *Explaining operational modal analysis with data from an arch bridge*, Mechanical Systems and Signal Processing 25: 1431–1450.

Magalhães, F., Reynders, E., Cunha, Á., De Roeck, G., (2009), *Online automatic identification of modal parameters of a bridge using p-LSCF method*, in Proceedings of IOMAC 2009, May 4-6, Portonovo, Italy.

Magalhães, F., Cunha, A., Caetano, E., (2012), *Vibration based structural health monitoring of an arch bridge: From automated OMA to damage detection*, Mechanical Systems and Signal Processing 28: 212-228.

Maia, N. M., Silva, J. M., (1997), *Theoretical and experimental modal analysis*, John Wiley & Sons.

Manevitz, L., and Yousef, M., (2001), *One-class SVMs for document classification* Journal of machine Learning research 2, 139-154

Marrongelli, G., Magalhães, F., Cunha, Á., (2017), *Automated Operational Modal Analysis of an arch bridge considering the influence of the parametric methods inputs*, Procedia Engineering 199: 2172-2177.

Marrongelli, G., Gentile, C., Saisi, A., (2018a), *Automated modal identification of a historic bell tower*, In Proceeding of 10th 10th IMC, July 8-10, Milan, Italy.

Marrongelli, G., Finotti, R., Gentile, C., Barbosa, F., (2018b), *An artificial intelligence strategy to detect damage from response measurements: application on an ancient tower*, MATEC Web of Conferences 211, 21002, Lisbon, Portugal.

Marrongelli, G., and Gentile, C., (2018) *A new automated procedure of modal identification in operational conditions*, MATEC Web of Conferences 211, 21003, Lisbon, Portugal.

Marrongelli, G., Magalhães, F., Gentile, C., Cunha Á., (2018c) *Automated modal identification in operational conditions using 3D stabilization diagrams*. In Proceedings of ISMA 2018, September 9-11, Leuven, Belgium.

Marrongelli, G., Gentile, C., Saisi, A., (2019a), *Development and application of automated OMA algorithms*, In Proceeding of IOMAC 2019, May 13-15 Copenhagen, Denmark.

Marrongelli, G., Gentile, G., Saisi, A., (2019b), *Anomaly Detection Based on Automated OMA and Mode Shape Changes: Application on a Historic Arch Bridge*, in Proceedings of ARCH 2019, October 2-4, Porto, Portugal.

Montgomery, D. (2005) *Introduction to Statistical Quality Control*. John Wiley & Sons.

Moutinho, C., Cunha, Á., Caetano, E., (2011), *Analysis and Control of Vibrations in a Stress-ribbon Footbridge*, Structural Control and Health Monitoring 18: 619–634, 2011.

Moser, P., Moaveni, B., (2013), *Design and deployment of a continuous monitoring system for the Dowling Hall footbridge*, Experimental Techniques 37(1): 15-26.

Moser, P., Moaveni, B., (2011), *Environmental effects on the identified natural frequencies of the Dowling Hall Footbridge*, Mechanical Systems and Signal Processing 25: 2336-2357.

Ni, Y. Q., Hua, X. G., Fan, K. Q., Ko, J. M., (2005), *Correlating modal properties with temperature using long-term monitoring data and support vector machine technique*, Engineering Structures 27: 1762-1773.

Oppenheim, A. V., Schafer, R. V., (1975), *Digital Signal Processing*, Prentice-Hall.

Pappa, R. S., Elliott, K. B., Schenk, A., (1993), *Consistent mode indicator for the eigensystem realization algorithm*, Journal of Guidance, Control and Dynamics 16(5): 852–858.

Pappa, R., James III, G., Zimmerman, D., (1998), *Autonomous Modal Identification of the Space Shuttle Tail Rudder*, Journal of Spacecraft and Rockects, 35(2), 163-169.

Pappa, R.; James III, G.; Zimmerman, D. (1998) *Autonomous Modal Identification of the Space Shuttle Tail Rudder*, Journal of Spacecraft and Rockects, 35(2), 163-169.

Pau, A., Vestroni, F., (2008), *Vibration analysis and dynamic characterization of the Colosseum*, Structural Control and Health Monitoring 15(8): 1105-1121.

Peeters, B., De Roeck, G., Andersen, P., (1999), *Reference-based Stochastic Subspace Identification for Output-only Modal Analysis*, Mechanical Systems and Signal Processing 13: 855–878.

Peeters, B., De Roeck, G., (2001), *One-year monitoring of the Z24-Bridge: environmental effects versus damage events*, Earthquake Engineering and Structural Systems 30: 149-171.

Peeters, B., (2000), *System identification and damage detection in civil engineering structures*, PhD Thesis, K. U. Leuven, Belgium.

Peeters, B., Van der Auweraer, H., Guillaume, P., Leuridan, J., (2004), *The Poly-MAX frequency domain method: a new standard for modal parameter estimation?*, Shock and Vibration 11: 395-409.

Peeters, B., Van Der Auweraer, H., *PolyMax: a revolution in operational modal analysis*, in Proceedings of IOMAC 2005, April 25-27, Copenhagen, Denmark.

Peeters, B., Couvreur, G., Razinkov, O., Kündig, C., Van der Auweraer, H., de Roeck, G. (2009), *Continuous Monitoring of the Øresund Bridge: System and Data Analysis*, Structure and Infrastructure Engineering 5, 395–405.

Peña, F., Lourenço, P.B., Mendes, N., Oliveira, D.V., *Numerical models for the seismic assessment of an old masonry tower*, Engineering Structures 32(5): 1466-1478, 2010.

Pintelon, R., Peeters, B., Guillaume, P., (2008), *Continuous-time operational modal analysis in the presence of harmonic disturbances*, Mechanical Systems and Signal Processing 22(5): 1017-1035.

Prells, U., Friswell, M. I., (2000), *A measure of non-proportional damping*, Mechanical Systems and Signal Processing 14(2): 125-137.

Pevosto, M., *Algorithmes d'Identification des Caractéristiques Vibratoires de Structures Mécaniques Complexes*, Ph. D. Thesis. Université de Rennes I, Rennes, France.

Pridham, B. A., Wilson, J. C., (2005), *A reassessment of dynamic characteristics of the Quincy bay bridge using output-only identification techniques*, Earthquake Engineering and Structural Dynamics 34: 787–805.

Rainieri, C., Fabbrocino, G., (2010), *Automated output-only dynamic identification of civil engineering structures*, Mechanical Systems and Signal Processing 24(3): 678–695.

Ramos, L. F., Aguilar, R., Lourenço, P. B., Morerira, S., (2013), *Dynamic Structural Health Monitoring of Saint Torcato church*, Mechanical Systems and Signal Processing 35(1-2): 1- 15.

Ramos, L. F., Marques, L., Lourenço, P. B., De Roeck, G., Campos-Costa A., Roque J., (2010), *Monitoring historical masonry structures with operational modal analysis: two case studies*, Mechanical Systems and Signal Processing 24: 1291-1305.

Ramos, L.F., Aguilar, R., Lourenco, P.B., Moreira, S., (2013), *Dynamic structural health monitoring of Saint Torcato Church*, Mechanical Systems and Signal Processing 35, 1-15.

Randall, R. B., Manzato, S., Peeters, B., Antoni, J., Smith, W., (2013), *New applications of the cepstrum in OMA*, in Proceedings of IOMAC 2013, May 14-15, Guimarães, Portugal.

Ren, W., De Roeck, G., (2002), *Structural damage identification using modal data. I: simulation verification*, Journal of Structural Engineering 128(1):87-95.

Ren, W., De Roeck, G., (2002), *Structural damage identification using modal data. II: test verification*, Journal of Structural Engineering 128(1):96-104.

Reynders, E., De Roeck, G., (2008), *Reference-based combined deterministic–stochastic subspace identification for experimental and operational modal analysis*, Mechanical Systems and Signal Processing 22: 617–637.

Reynders, E., Pintelon, R., De Roeck, G., (2008a), *Uncertainty bounds on modal parameters obtained from stochastic subspace identification*, Mechanical Systems and Signal Processing 22: 948–969.

Reynders, E., Schevenels, M., De Roeck, G., (2008b), *MACEC: A Matlab toolbox for experimental and operational analysis* Department of Civil Engineering, K. U. Leuven.

Reynders, E., (2009), *System Identification and Modal Analysis in Structural Mechanics*, PhD Thesis, K.U. Leuven.

Reynders, E., François, S., De Roeck, G., (2009a) *Operational modal analysis using ambient support excitation: An OMAX approach*, in Proceedings of 3rd International Operational Modal Analysis Conference, IOMAC 2009, 4 May 4-6 Portonovo; Italy.

Reynders, E., Magalhães, F., De Roeck, G., Cunha, Á., (2009b), *Merging Strategies for Multi-Setup Operational Modal Analysis: Application to the Luiz I steel Arch Bridge*, in

Proceedings of IMAC XXVII, International Modal Analysis Conference, Orlando, Florida, USA.

Reynders, E., Degrauwe, D., Schevenels, M., De Roeck, G., Van Den Broeck, P., Deckers, K., Guillaume, P., (2011), *OMAX testing of a steel bowstring footbridge*, in Proceedings of 29th IMAC, a Conference on Structural Dynamics, January 31-February 3, Jacksonville, Florida, USA.

Reynders, E., Wursten, G., De Roeck, G., (2012), *Non-linear system identification for vibration based Structural Health Monitoring*, in Proceedings of the National Congress on Theoretical and Applied Mechanics, May 9-11, Brussels, Belgium.

Reynders, E., Houbrechts, J., De Roeck, G., (2012), *Fully automated (operational) modal analysis*, Mechanical Systems and Signal Processing 29: 228–250.

Rohrmann, R. G., Baessler, M., Said, S., Schmid, W., Ruecker, W. F., (2000), *Structural causes of temperature affected modal data of civil structures obtained by long time monitoring*, in Proceedings of IMAC-XVIII (1-7), February 7-10, San Antonio, Texas USA.

Rohrmann, R. G., Said, S., Schmid, W., Thöns, S., Bicker, S., Ruecker, W. F., (2011), *Results from monitoring and assessment of offshore wind turbines*, Proceedings of EURODYN 2011 (3450-3456), July 4-6, Leuven, Belgium.

Saisi A. and Gentile C., (2015), *Post-earthquake diagnostic investigation of a historic masonry tower*, Journal of Cultural Heritage 16: 602-609.

Saisi, A., Gentile, C., Guidobaldi, M., (2015), *Post-Earthquake Continuous Dynamic Monitoring of the Gabbia Tower in Mantua, Italy*, Construction and Building Materials 81: 101–112.

Santos, J. P., Cremona, C., Orcesi, D. A., Silveira, P., (2013), *Multivariate statistical analysis for early damage detection*, Engineering Structures 56: 273-285.

Schölkopf, B., Williamson, R., Smola A., Shawe-Taylor, J., Platt J., (2000), *Support vector method for novelty detection*, Neural Information Processing Systems, 582-588.

Silva, M., Santos, A., Santos, R., Figueiredo, E., Sales, C., Costa, J. C. W. A., (2017), *Agglomerative Concentric Hypersphere Clustering Applied to Structural Damage Detection*, Mechanical Systems and Signal Processing 92: 196-212.

Sharma, S., (1995), *Applied Multivariate Techniques*, John Wiley & Sons, Inc.

Shih, C.Y., Tsuei, Y.G., Allemang, R.J., Brown, D.L., (1989), *Complex Mode Indicator Function and its Applications to Spatial Domain Parameter Estimation*, Mechanical Systems and Signal Processing 2(4), 367-377.

Scionti, M., Lanslots, J., Goethals, I., Vecchio, A., Van der Auweraer, H., Peeters, B., De Moor, B., (2003), *Tool to Improve detection of Structural changes from In-Flight Flutter Data*. In Proceedings of 8th International Conference on recent advances in Structural Dynamics, Southampton, UK.

Scionti, M., Lanslots, J. P., (2005), *Stabilization diagrams: Pole identification using fuzzy clustering technique*, Advances in Engineering Software 36(11-12), 768-779.

Sohn, H.; Farrar, R.; Hemez, M.; Czarnecki, J.; Shunk, D.; Stinemates, W.; Nadler, R. (2002) *A review of Structural Health Monitoring Literature: 1996-2001*. Los Alamos National Laboratory, Los Alamos.

Sohn, H., Worden, K., Farrar, C. R., (2003), *Statistical damage classification under changing environmental and operational conditions*, Journal of Intelligent Material Systems and Structures 13(9), 561-574.

Sotiris, V., Tse, P., Pecht, M., (2010.), *Anomaly detection through a Bayesian support vector machine*, IEEE Trans. Reliab., 59 (2): 277-286.

Spencer Jr., B. F., Nagarajaiah, S., (2003), *State of the art of structural control*, Journal of Structural Engineering 129(7): 845-856.

SVS (2012) ARTeMIS Extractor 2010 release 5.3, http://www.svibs.com.

Tax D. and Duin R., (1999), *Support vector domain description*, Pattern recognition letters 20(11): 1191-1199.

Trendafilova, I., and Heylen, W., (2003), *Categorization and pattern recognition methods for damage localization from vibration measurements*, Mechanical Systems and Signal Processing 17(4), 825–836.

Ubertini, F., Gentile, C., Materazzi, A. L., (2013), *Automated modal identification in operational conditions and its application to bridges*, Engineering Structures 46: 264-278.

Ubertini, F., Gentile, C., Materazzi, A. L., (2013), *Time-frequency analysis of dispersive phenomena in bridges*, in Proceedings of IOMAC 2013, May 14-15, Guimarães, Portugal.

Ubertini, F., Comanducci, G., Cavalagli, N., (2016), *Vibration-Based Structural Health Monitoring of a Historic Bell-Tower using Output-only Measurements and Multivariate Statistical Analysis*. Structural Health Monitoring 15, 438-457.

Ubertini, F., Comanducci, G., Cavalagli, N., Pisello, A.L., Materazzi, A.L., Cotana, F., (2017), *Environmental effects on natural frequencies of the San Pietro bell tower in Perugia, Italy, and their removal for structural performance assessment*, Mechanical Systems and Signal Processing 82, 307-322.

Ubertini, F., Cavalagli, N., Kita, A., Comanducci, G., (2018), *Assessment of a monumental masonry bell-tower after 2016 Central Italy seismic sequence by long-term SHM*, Bulletin of Earthquake Engineering 16(2), 775-801.

Vacher, P., Jacquier, B., Bucharles, A., (2010), *Extensions of the MAC criterion to complex modes*, in Proceedings of ISMA 2010, September 20-22, Leuven, Belgium.

Van Overschee P., De Moor B., (1996), *Subspace identification for linear systems: Theory, implementation, applications*, Kluwer Academic Publishers, Belgium.

Vanlanduit, S., Verboven, P., Guillaume, P., Schoukens, J., (2003), *An automatic frequency domain modal parameter estimation algorithm*, Journal of Sound and Vibration 265: 647-661.

Verboven, P., Parloo, E., Guillaume, P. Van Overmeire, M., (2010), Autonomous Modal parameter Estimation based on Statistical Frequency Domain Maximum Likelihood approach. In Proceedings of IMAC 19, Kissimmee, Florida, USA.

Verboven, P., Parloo, E., Guillaume, P., Van Overmeire, M., (2002), *Autonomous Structural Health Monitoring - part 1: modal parameter estimation and tracking*, Mechanical Systems and Signal Processing 16(4): 637-657.

Vitberg, M., (1995), *Subspace-based methods for the identification of linear time-invariant systems*, Automatica 31(12): 1835-1851.

Weng, J, Loh, C., (2010), *Structural Health Monitoring of arch dam from dynamic measurements*, Earth and Space: 2518-2534.

Welch, P. D., (1967), *The use of Fast Fourier Transform for the Estimation of Power Spectra: A Method Based on Time Averaging over short Modified Periodograms*, IEEE Transactions on Audio Electro-Acoustics, AU-15(2), 70-73.

Wenzel, H. (2009). *Health monitoring of bridges*. John Wiley & Sons.

Wong, K. Y., (2004), *Instrumentation and health monitoring of cable-supported bridges*, Structural Control and Health Monitoring 11: 91-124.

Wu M., Ye J., *A small sphere and large margin approach for novelty detection using training data with outliers*, IEEE Transactions on Pattern Analysis and Machine Intelligence 31(11): 2088-2092, 2009.

Xia, Y., Chen, B., Zhou, X., Xu, Y., (2013), *Field monitoring and numerical analysis of Tsing Ma suspension bridge temperature behaviour*, Structural Control and Health Monitoring 20: 560-575.

Yan, A. M., Kerschen, G., De Boe, P., Golinval, J. C., (2005), *Structural damage diagnosis under varying environmental conditions - part I: a linear analysis*, Mechanical Systems and Signal Processing 19: 847-864.

Yan, A. M., Kerschen, G., De Boe, P., Golinval, J. C., (2005) *Structural damage diagnosis undervarying environmental conditions - part II: local PCA for non linear analysis*, Mechanical Systems and Signal Processing 19: 865-880.

Yan, Y. J., Cheng, L., Wu, Z.Y., Yam, L.H., (2007), *Development in vibration-based structural damage detection technique*, Mechanical Systems and Signal Processing 21: 2198–2211.

Yuen, K. V., Kuok, S. C., (2011), *Bayesian methods for updating dynamic models*, Applied Mechanics Reviews 64(1): doi:10.1115/1.4004479.

Zabel, V., Magalhães, F., Bucher, C., (2016), *The influence of parameter choice in Operational Modal Analysis: A case study*, IMAC in Mains M. (eds) Topics in Modal Analysis & Testing 10, in Proceedings of the Society for Experimental Mechanics Series Conference, Springer.

Zhang, Q. W., (2007), *Statistical damage identification for bridges using ambient vibration data*, Computers and Structures: 476-485.

Zonno, G., Aguilar, R., Boroschek, R., Lourenço, P. B., (2018), *Automated long-term dynamic monitoring using hierarchical clustering and adaptive modal tracking: validation and applications*, Journal of Civil Structural Health Monitoring 8(5), 791-808.